Cape Peninsula
University of Technology

Synthesis of fly ash-based zeolites for use as catalysts in the transesterification of waste-derived maggot oil for biodiesel production

by

Juvet Malonda Shabani

Thesis submission in fulfillment of the requirements for the Degree of

Doctorate of Engineering: Chemical Engineering

In the Faculty of Engineering and Built Environment

At the Cape Peninsula University of Technology

Supervisor: Dr Omotola Babajide

Co-Supervisors: Prof. Oluwaseun Oyekola; Prof Leslie Petrik

Bellville campus

2020-2021

Declaration

I, Juvet Malonda Shabani, declare that the contents of this dissertation/thesis represent my own unaided work, and that the dissertation/thesis has not previously been submitted for academic examination towards any qualification. Furthermore, it represents my own opinions and not necessarily those of the Cape Peninsula University of Technology.

Signed **Date**

Abstract

From nearly a century, biodiesel production has demonstrated its potential as an alternative to petroleum diesel mainly due to environmental and energy security. The principal biodiesel production route from different oil feedstocks is dependent on catalysts, of which solid catalysts have attracted attention for greener production. Fly ash solid waste derived from coal power station is identified as a suitable and cheaper catalyst feedstock. In spite of escalating market, biodiesel industry has been faced with the challenge of overall production cost, owing to conventional vegetable oil feedstocks high cost of most solid catalysts derived from conventional feedstocks and synthesis routes**.** This study therefore introduces and explores the use of maggot oil as a novel waste-derived feedstock for biodiesel production, aims to develop cheaper solid catalysts by various routes using coal fly ash, in bid to make biodiesel production more economical.

The characterisation of physicochemical properties was employed on the as-received oil feedstock. These include free fatty acid (FFA) analysis via a gas chromatogram (GC); titrimetric determination of acid value (AV) and saponification value (SV); test for Iodine value (IV) by Wij's method; density, viscosity and refractive index using appropriate equipment. Further oil feedstock characteristic was carried out via screening transesterification tests using conventional homogeneous catalysts. Maggot oil revealed to contain triglyceride characteristic components and was found to be highly saturated (SFAs) with lauric acid in major proportion (40 %). The oil exhibited a high acid value ranging between 7-10 mg KOH/g oil, a low-density value (0.883 g/cm^3) and viscosity (43.16 mm^2/s) suitable for biodiesel feedstock characteristics. An iodine value of 44.27 g I_2/g of the oil was reported as reflective of oil good reactive characteristic. Based on these, maggot oil demonstrated potential by feedstock converting to fatty acid methyl esters (FAMEs) with high yield (65.50-70.02 %) and quality-compliant biodiesel over homogeneous catalysts.

Catalyst characterisation employed on the prepared and modified catalyst samples included X-Ray diffraction (XRD), Fourier transform infrared (FT-IR), Scanning electron microscopy (SEM) coupled with energy-dispersive spectroscopy (EDS), and the Brunauer–Emmett–Teller (BET) coupled with the Barret-Joyner-Halenda (BJH) measurement. In exception to BET, the above characterisations were also conducted on the as-received Arnot coal fly ash. Characterisation and analytics employed for biodiesel products were as similar as those used for the feedstock oil. Coal fly ash showed inherent material characteristic in terms of

mineralogical composition, structural configuration, and the material showed compositionally characteristic of class F type fly ash. Zeolite samples were hydrothermally prepared from coal fly ash via the direct method and fusion-assisted synthesis route. The effect of pre-synthesis chemical and physical parameters, followed by the actual hydrothermal synthesis time and temperature, were investigated for the direct method synthesis route. Fusion-assisted synthesis route, based on optimum conditions from the direct method, was achieved by investigation of hydrothermal synthesis time. Zeolite was successfully produced from coal fly ash by both the direct and the fusion-assisted hydrothermal method. The direct method synthesis revealed the formation of HS-zeolite from as low as 11-20 % to 100 % phase crystallinity, induced majorly by increase in hydrothermal synthesis time. Established optimum presynthesis conditions obtained were water-to-coal fly ratio mixture of 5:1, ageing at 60 °C for 1.5 hours, NaOH-to-coal fly ratio of 1.2:1, and hydrothermal synthesis time of 72 hours at 140 °C; including an extended synthesis time of 144 hour at 100 °C. The resultant sample (HS-72) demonstrated a considerably purer phase HS zeolite by 85 %, and this was extended to 91 % with the decreased temperature at extended synthesis time (HS-144(100°C)).. The fusion-assisted synthesis route comparably resulted to samples of low phase crystallinity range (< 30 %), with 52 % optimum crystallinity and 80 % phase purity HS zeolite obtained at 144-hour extended synthesis time at 100°C. The derived sample at the optimum condition (HSF-144) exhibited similar hexagonal cubic crystal morphology as those obtained via the direct method, and showed a comparably higher surface area and pore volume characteristic (44.98 m^2/g and 0.148 cm^3/g). The direct method synthesis resulted as a more energy efficiency approach, thus, was deemed as an economic and more feasible route for upscale synthesis of overall high quality HS zeolite. Selected prepared catalysts were modified by ion exchange method using potassium hydroxide (KOH) and by bifunctional method, to boost their characteristic properties and activity in biodiesel production in this work. Sample modification by both methods, demonstrated no effect on the phase identity of HS, neither considerably impacted on its crystal morphology. Both modification methods, caused a decrease in sample crystallinity to below 30 %, decrease in crystal sizes, and accounted for minor induction of basic properties.

The catalytic activity of the synthesised HS zeolite samples on the transesterification of maggot oil, was investigated on a batch production unit at fixed pre-optimised conditions (1.5 hour, 60 ^{o}C, 15:1 MeOH/oil ratio). Activity tests using the prepared samples were also carried out on sunflower oil for comparison. The above was followed by process optimisation of maggot oil transesterification using the design of central composite (CCD) for research methodology

studies (RSM), where the influence of methanol-to-oil ratio, agitation rate and reaction time on the yield of biodiesel, was investigated. HS zeolite obtained via the fusion hydrothermal method led to high activity with regard to a higher biodiesel yield (84.10 %), a higher FAME content (64.95 %) and an overall more compliant biodiesel quality, compared to catalyst samples obtained via the direct method. The high activity majorly owed to larger surface area, higher mesoporosity and a possibly better acidity shown by the fusion-assisted HS zeolite catalyst. The catalyst showed a greater activity in the transesterification of sunflower oil (biodiesel yield, 89.70 %; FAME content, 90.93 %), and gave the RSM optimum conditions of MeOH/oil ratio of 6:1, agitation rate of 400 rpm and reaction time of 1.5 hour. Under these conditions, maggot oil-derived biodiesel yield and FAME content were as highest as 85.47 % and 84.76 % respectively, and the obtained biodiesel complied with the standard specifications.

Kinetic study for the transesterification of maggot oil was conducted to predict the yield of biodiesel with reaction time, using the pseudo first-order mechanism. The mechanism held true for reaction time below 1.5 hour and revealed that a higher biodiesel yield could have been achieved from a shorter reaction time of 0.25 hour. A liner kinetic model resulted and was associated with a considerable reaction rate constant of 1.15×10^{-3} min^{-1} and gradual increase in the rate of reaction (5.37×10^{-6} - 6.13×10-6 $mol/cm^3.min$) with an increase in reaction time. This study has guaranteed feasibility for upscale production of HS as a novel heterogeneous catalyst and an economic approach of biodiesel production using both coal fly ash and maggot oil as industrial waste-derived feedstocks. The study recommends improving major qualities associated with enhanced catalyst activity of produced zeolites and further RSM optimisation of biodiesel production to enhance the FAME yield of biodiesel.

Dedication

My father Malonda Masinga and family in DRC

To Melanie Smuts, Julian Grieve, Stuart P. Denoon, Shen tian, Abu Addae, Sadiq Addae, Peter Chingoma, Malik H.,...

Magdaleen Smuts, the late mother to Melanie Smuts

Cape Peninsula University of Technology and the CPUT community

Alex Van Ster and Family

The Ark City of Refuge

Acknowledgments

- My acknowledgement foremost goes to God, whom has helped and made my journey towards this degree possible. I was kept and motivated regularly by the biblical teaching of faith and possibility, I testify of the manifestation of faith and God's spiritual power beyond my capabilities through this project

- **Doctor Omotola Babajide:** My main supervisor to this project, who took the initiative and risk in working with me; believed and was patient with me, she kept on holding me up to complete work and meet deadlines. The mother figure I have perceived in her, and the image she enforced me that women can do and are an important drive to gear me up in life. Lastly, she has inspired me through in her role as an entrepreneur, that one can utilize her educational platform to expand herself into various profitable adventures.

- **Department of Chemical engineering, Cape Peninsula University of Technology**
  - **Prof Oluwaseun Oyekola:** My co-supervisor to the PhD project; to have set foundation for me to build on this project. Over time, he had natured in me as a role model. Dedication, discipline and hardworking was sown in me through him as I become the productive and accomplishing person I saw of him.
  - **Prof Ntwampe Karabo:** The former Head of Chemical Engineering Department in the year 2019
  - **Mr Taffi Madzimbamutho:** My mentor to lecturing B. Tech Design part-time (PQD400S), Chemical Process Design Principles 3 (CPD300S) & Process Design Principles 2: Safety and Loss Prevention (PSL260S). His great support in taking up the whole semester lecture classes for PQD400S and continually assisting me with any Design subject queries and assessment moderations
  - **Dr Narsingh Udi:** My internal supervisor for being supportive to the administrative requirements of my work.
  - **Siya Nqwazi:** Chemical Engineering Assistant Secretary
  - **Nomava Mti:** Former coordinator of work-integrated programme at the department. She entrusted me with assisting students who did not have in-service training.
  - **Sindiswa Booi:** Her motivation and thought to seeking for my best, both in academic and personal well-being. She continually sought after opportunities for me to keep being part of the department, and engaged me as a tutor for her subject both in 2020 and 2021.

- **Ntombie Futhi and Derrick Dlamini:** Their continual supports and motivation towards my academic, career and personal life. They always sought the best for me and would not let any opportunity pass without informing me. Yours very gratefully.

➢ **Environment Nanoscience Group (ENS) at UWC**

- **Prof Leslie:** The ENS group leader and my co-supervisor to the PhD project. To have warmly and heartedly opened door for me to be part of ENS group. To have entrusted, believed in me, motivated me and even supported me financially through stipends from the group. For the collaboration set with Agriprotein to carry out the project, to have walked with me through every step of the PhD programme (experimental work, journal drafting and corrections, thesis compilation and corrections) and her continual patience and support; and to have further played a role as a mother to me (beyond the academics). Thank you God to have sent you my way, I am forever grateful.
- Dr Roland Missengue: PhD graduate from UWC. His guidance and supply of the maggot oil sample for use in the project.
- Emmanuel Ameh: His support to always will to assist in both experimental work, his guidance into the various softwares needed for data interpretation and to have provided his guidance towards the compilation of my thesis
- My addition acknowledgment goes to Maman Vanessa Kellerman (administration); Ilse Wells (administration); Denzil (administration); Dr Chris (Data interpretation software; Mero-lee (thesis write up guidance) and Mr Timothy Lesch (kindly provided schedules and access to FT-IR facility usage)

➢ **AgriProtein:** For the collaborative opportunity granted by supplying the maggot oil feedstock of interest in the thesis study. For also open information and access of visit to the company

➢ **Department of Food Technology (Agrifood station)**

- **Mr Ndumiso Mschieli:** You kindly went beyond the authorization to organizing with Agrifood Department that I do make me use of the GC facility at the Food technology (Agrifood station) Department. I forever appreaciate you kindness, patience and the discount to cost of analyses.
- **Bongisiwe Zozo**: Her welcoming and assistance in my experimental work (fatty analysis and GC operation) at Agrifood lab

- **Christa Van Schalkwyk:** To have assisted with access and operation to viscometer facility at Agrifood station.
- **Zolelwa and Mr Vuyisani: For** their welcoming and hospitality at Agrifood station, at their office space and labs

➢ **Family and mentors / Friends**

- **Melanie Smuts** and her late mother Magdaleen Smuts, Stuart Du Noon, Julien Grieve, Shen Tian, Peter Chingoma, Abu Addae, Sadiq Addae, Malik H. The God's sent to me. Sponsors and mentors. I am forever greatful to have had you to my rescue.
- **J.W Malonda Masinga**: my biological Father in the D.R.C Congo. Your support and motivation from far distance away, both in prayer and spiritually, financially, caring, affection and playing his true role as a parent and dad.
- **Papa Jeannot Mangonda and his family:** catered for my initial stay in Cape Town, South Africa.
- **Alex Van Ster**, Rene Witbooie and Van Ster Family: To have proudly and supportively taken me in as one of their own in their own, and given me a home and family away from home, when I did not have
- The **Ark City of Refuge:** The refuge shelter for homeless that hosted and catered for me during my early years in Cape Town.

➢ **Faculty of Engineering (CPUT)**

- **Prof Mellet Moll:** The Dean of Engineering
- **Taylia Green:** To have assisted me throughout the HDC administration and submission requirements of the thesis (both masters and PhD). Her support and advice similar to a parent.
- **Prof Tunde Ojumu:** His assistance towards obtaining Confcom funding has enabled me attend conferences required for accreditation of my PhD work.
- **The Confcom commuty:** For granting me the necessary funding to attend two international conferences in Johannesburg (South Africa), where I had the opportunity to present and share my research findings to academic and industrial audience.

➢ **Centre for Postgraduate Studies (CPGS)**

- Dr Connie Urys: Her role to landing me on CPUT postgraduate bursary grant during the completion years of my PhD programme.

- **University of the Western Cape (UWC)**

  - **Department of Physics:** To have granted me the facility for SEM/EDS sample characterisation
  - **South African Institute for Advanced Materials Chemistry (SAAIMEC)**, specifically to Ebrahim Mohiuddin: His assistance free of charge to analyse samples for BET and BJH textual properties, etc.

- **Pastor Mike Ayeni:** Through Harvest House Ministry on campus since 2012. The empowerment, motivation and spiritual growth I obtained through his teaching and ministration throughout my years at CPUT.

- **Collegues, friends and others**

  - **CPUT Bellville Housing Department** and Mr Lizo Mankayi (Former Heroes House Residence Coordinator) - In Support to my appointment as a Residence Student Assistant for 2013 and 2014.
  - **Thapelo Lekone:** His contribution towards my 2016 academic fee and to have been a friend through his outmost means.
  - **Busi Gcobo:** For formal and continual support during my year at CPUT
  - **Tunde Oladipo:** A God's sent to me, and who helped me in understanding and carrying out my experimental work (right when I was stuck). He gave out his time, energy to attend to me in the lab, provided me with mentorship on publications matters and went as far as sharing his published papers for me to use as guidance to my write up.
  - **Yvonne Maphosa:** She came through for me on the third attempt of my proposal presentation in 2018 (after two failed attempts), restructured the presentation both in power point and through oral practice. Role model as a young lady and the impact she has had through philanthropic work in the community.
  - **Oluwatimilehin George:** A flatmate during 2018-2021, for his continual motivation, hospitality and kindness during our stay together between 2019 till early 2021
  - **Tabisa Nose:** To have once been a friend and portrayed sisterhood to me

Table of contents

List of Figures

Appendix 1 & 2

List of Tables

Appendix 1& 2

Keywords and concepts

Maggot oil; coal fly ash; zeolite; direct hydrothermal method; fusion hydrothermal method; transesterification; catalyst; hydroxy sodalite (HS); ion exchange-modification; bifunctional; biodiesel; FAME; yield; optimisation, response surface methodology; pseudo first-order kinetic

List of abbreviations / Nomenclature

AV	**:**	Acid value
BET and BJH	**:**	Brunauer–Emmett–Teller coupled with/and the Barret-Joyner-Halenda measurement
CCD	**:**	Central composite design of experiment
CFA	**:**	Coal fly ash
HM	**:**	Hydrothermal method
DHM	**:**	Direct hydrothermal method
FAME	**:**	Fatty acid methyl ester in %
FFA	**:**	Free fatty acid in %
MUFA	**:**	Mono unsaturated fatty acids
PUFA	**:**	Poly unsaturated fatty acids
SFA	**:**	Saturated fatty acids
FHM	**:**	Fusion-assisted hydrothermal method
FT-IR	**:**	Fourier transform infrared
IZA	**:**	International Zeolite Association
MagOil and MagOil$^{(b)}$	**:**	Maggot oil (oil feedstock of interest for biodiesel production in this work)
MeOH	**:**	Methanol
MeOH/oi ratio	**:**	Methanol-to-oil molar ratio (n/n)
Na-X	**:**	zeolite X derived from NaOH as the alkali content (i.e. Na-X zeolite)
NaOH/CFA ratio	**:**	The mass ratio of NaOH-to-CFA (also referred to as NaOH concentration) in the zeolite synthesis mixture
Water/CFA ratio	**:**	The mass ratio of water-to-fly ash (also referred to as water content) in the zeolite synthesis mixture

NH_3-TPD or CO_2-TPD	**:**	Ammonia or CO_2 Temperature-programmed desorption for acidity measurement of catalytic materials
RSM	**:**	Response surface methodology studies
SEM and EDS	**:**	Scanning electron microscopy coupled with/ and the energy-dispersive spectroscopy (EDS)
TEM	**:**	Transmission electron microscopy
TG or TGA	**:**	Triglyceride
T–O (T = Si or Al)	**:**	Referred to as Si–O–Al , Si-O or Al-O units in a zeolite framework unit
Trans.	**:**	Transesterication
SV	**:**	Saponification value
XRD	**:**	X-ray diffraction patter

Glossary of terms

Acid density	**:**	Frequency or number of acidic (active) sites onto the surface of a catalyst sample
Biodiesel	**:**	Quality of biodiesel – evaluated in terms of physicochemical properties (FAME content as the major)
Conversion	**:**	Conversion rate or efficiency
low conversion	**:**	Could be referred to as poor nucleation and growth of HS zeolite
Crystallinity	**:**	***Phase crystallinity*** - Referred to as the degree of nucleation or crystal growth of HS zeolite phase of interest and is a **relative crystallinity** (in %) in this work
Direct hydrothermal method	**:**	Conventional hydrothermal (alkaline activation), or one-step process for the synthesis of zeolite
Direct hydrothermal products	**:**	Direct method-derived samples or samples obtained via the direct hydrothermal method
Fusion-assisted method:	**:**	Fusion method, indirect fusion method, alkaline treatment of fly ash by fusion at high temperature, followed hydrothermal synthesis
FAME	**:**	Methyl ester content of feedstock or biodiesel products, also referred to as ***ester content*** obtained from GC characterisation of biodiesel samples, or FAME yield (unlike biodiesel yield).

Framework Si/Al ratio	**:**	The major elemental composition of Silicon and Aluminium that constitute the structural framework of a zeolite
Fusion product	**:**	Fusion-derived sample
HS phase purity	**:**	Also referred to as concentration , selectivity or mineralogical purity of HS phase in a product sample
HS zeolite	**:**	***zeolite structures*** – zeolite framework types
Mixed phase HS zeolite		HS zeolite sample with co-existing phases of zeolite X and P
Magmeal	**:**	The natural protein product, derived from the remainder dry insect body after the oil has been extracted
Phase purity	**:**	% of crystalline phase HS or can be referred to as the degree of selectivity of HS phase in obtained products. Referred as merely crystallinity by Du Plessis (2014).
Water content	**:**	Mostly referred to as in terms of the ratio of water-to-fly ash

Research outputs and conference presentations

Publications: DHET accredited Journal(s) and Academic Books

- Malonda Shabani, J., Babajide, O., Oyekola, O. & Petrik, l. 2019. Synthesis of Hydroxy Sodalite from Coal Fly Ash for Biodiesel Production from Waste-Derived Maggot Oil. Catalysts, 9 (12), 1052. https://doi.org/10.3390/catal9121052
- Shabani, J., Babajide, O. & Oyekola, O. 2020. An Investigation into the Potential of Maggot Oil as a Feedstock for Biodiesel Production. Valorization of Biomass to Value-Added Commodities. Springer, 285-301. doi: 10.1007/978-3-030-38032-8_14

To be submitted for publications in 2021 (currently pending due to disclosure agreement with industry)

- Malonda Shabani, J., Babajide, O., Oyekola, O. & Petrik, l. 2021. Investigation of hydrothermal synthesis methods on the synthesis of hydroxy sodalite zeolite from fly ash
- Malonda Shabani, J., Babajide, O., Oyekola, O. & Petrik, l. 2021. Biodiesel production from waste-derived maggot oil over fusion-assisted hydrothermally and ion-exchanged produced hydroxy sodalite catalyst
- **NB:** Additional publications from the content of the thesis have been currently put on hold due to disclosure agreement set with industry via the technology transfer office (TTO) of the University of the Western Cape (UWC).

Conference presentations (attendance)

- DST-UNESCO engineering student conference, Cape Town (Cape Peninsula University of Technology), South Africa, 17 September 2018. **Oral presentation**: Synthesis of hydroxy sodalite from coal fly ash for biodiesel production

- The 7th International Conference on Biorefinery 2019 (ICB 2019), Johannesburg, South Africa, 18-21 August 2019. **Oral presentation**: Hydroxy sodalite zeolite synthesised from coal fly ash as a heterogeneous catalyst in biodiesel production

- 17th Johannesburg Internal Conference on Science, Engineering, Technology and Waste Management (SETWM-19), Johannesburg, South Africa, 18-19 November 2019. **Paper presented/ Oral presentation** : Synthesis and Characterisation of Hydroxy sodalite zeolite from coal fly ash: Investigation of Pre-synthesis and Hydrothermal synthesis conditions and methods on Quality of Product

Chapter One
Introduction

1.1 Background

The history of biodiesel production dates from late in the 19th century and its commercial production in the 20th century was due to its potential as an alternative fuel to petroleum diesel for economic, environmental and energy security (Junaid, 2014, Zhou and Thomson, 2009). To date, biodiesel production has emerged as one of the potential sources of energy, a renewable and sustainable energy source mainly required for transportation purposes (Lam et al., 2010). According to research, biodiesel production has proven to be the fastest-growing industry worldwide and has increasingly made a contribution of over 10 % to world energy by renewable technologies (Hajjari et al., 2017, Lam et al., 2010, Ho et al., 2014, Agency and Birol, 2013, IEA, 2006). Within the past decade, the rise in global biodiesel production, triggered by the required escalating demand, has more than tripled from a figure of 6.5 billion litres in 2006 to 35 billion litres of production by the end of 2016 (Nyale et al., 2014, Raturi, 2016). Figure 1.1 shows the trend of global biodiesel production over ten years and has further projected that this trend for world energy contribution, will continue to escalate and remain the fastest growing in the coming decades (Saifuddin et al., 2015, Martinot et al., 2007).

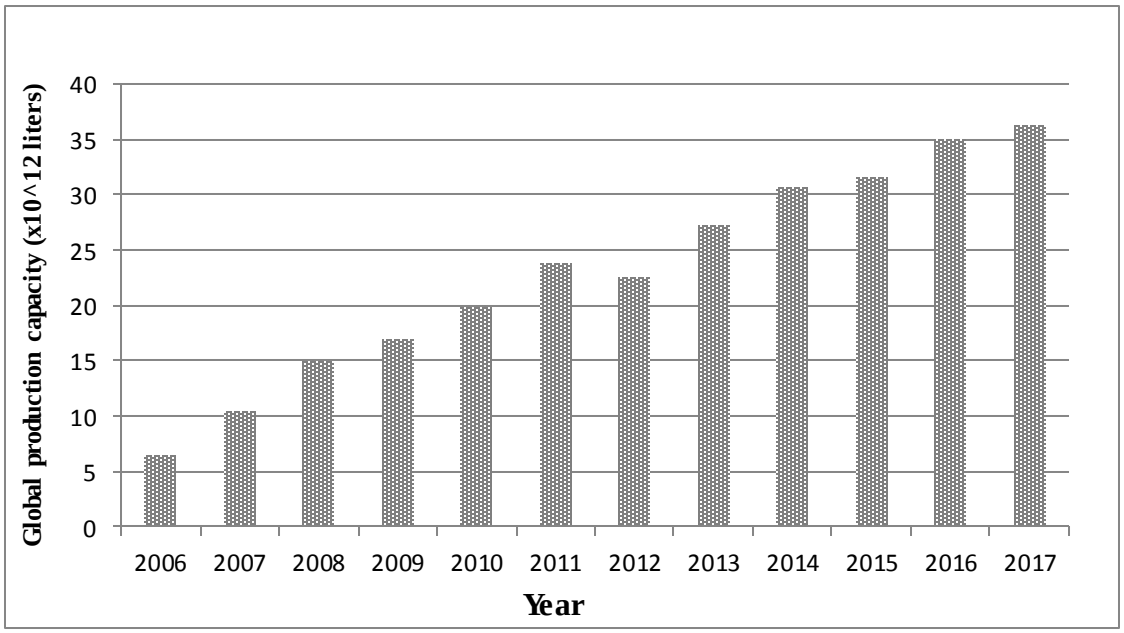

Figure 1. 1: Rise in global biodiesel production from 2006 to 2017 (Nyale et al., 2014, Lam et al., 2010, Ho et al., 2014, Raturi, 2016).

Biodiesel synthesis from different feedstock is dependent on the type of catalysts used, of which liquid and solid catalysts are predominant. Due to waste generation encountered during the use of homogenous catalysts, current focus and development in biodiesel production have been geared towards using solid catalysts (Tshizanga et al., 2017, Jacobson et al., 2008). Coal fly ash (CFA) is one of the materials identified and proven useful for the development of potential solid catalysts required for biodiesel production (Babajide et al., 2012). CFA is a waste residue generated from burning coal in power stations, and over 30 million tonnes (Mt) is generated yearly in South Africa (Sheqafrica.com, 2018).

1.2 Problem statement

The use of biomass sources for biodiesel production is considered an alternative to fossil fuels due to the increased emission of greenhouse gases encountered in processing fossil fuels. The depletion of fossil fuel from global natural reserves and the imposition of their us on growing environmental pollution and energy crisis (since energy mainly derives from fossil fuels), sets the long term independence of fossil fuels (Lam et al., 2010, Musa, 2016, Saifuddin et al., 2015, IEA, 2006). This dependence, in turn, motivates the search for biomass renewable sources of energy, which presents a clean and sustainable source of energy.

Currently, refined vegetable oils are predominant biomass feedstock sources employed in biodiesel production. Due to their priority as food resources against their demand in biofuel production, these oils have resulted in competitive pricing and are expensive (Gonfa Keneni et al., 2017). Research shows that the conventional biodiesel feedstocks alone, make up over 80 % of the overall biodiesel production cost (Lam et al., 2010, Gonfa Keneni et al., 2017, Lam et al., 2009). In a bid to reduce production costs, this research study seeks to explore the use of much cheaper and sustainable waste-derived maggot oil as source for biodiesel production.

Coal fly ash presents itself as solid waste and a vast pollutant (Zielke-Olivier and Vermeulen, 2016); thus, coal fly ash waste beneficiation is essential for environmental preservation and environmental remediation. This research work, therefore, aims to utilize coal fly ash as feedstock for the synthesis of suitable catalysts required in biodiesel production.

1.3 Research motivation

Biodiesel production from suitable biomass could produce a fuel that is biodegradable, non-toxic and a cleaner fuel that is associated with low emission of greenhouse gases, as well as better fuel properties than those obtained from fossil fuel sources (Saifuddin et al., 2015). The above are the proven advantages of biodiesel as a substitute for petroleum diesel (fossil fuel-derived).

Waste-derived maggot oil (simply referred to as maggot oil) is a biomass fat extruded from black soldier fly insects, is primarily a product of bioconversion of organic food waste on which the insects feed. Currently, an estimate of over 1300 tonnes of maggot oil is produced yearly in South Africa; making this a promisingly renewable and sustainable feedstock (John, 2009, Agriprotein, 2017). Maggot oil, a material with a low market value and discarded as a waste. Thus is a far cheaper feedstock and can be obtained at a cost that is over three times less than refined vegetable oils (Agriprotein, 2017). The feedstock, which has not escalated into a market competition, offers advantageous inherent characteristics and could be deemed an alternative for biodiesel production. This research work explores the potential use of the maggoil as feedstock in a bid to reduce biodiesel production costs significantly.

Catalysis in biodiesel production is an essential factor to consider for dynamics and energy efficiency in the transesterification reaction process (Syamsiro et al., 2014). Coal fly ash possesses basic catalytic properties due to its alkali content, that means it can be easily converted to zeolites (Babajide, 2011). Besides serving as a disposal management strategy, the abundant availability and utilisation of coal fly ash for zeolite production will also promote the economic beneficiation of the waste. These could simultaneously result in a lower cost of producing zeolites (compared to prices charged by global commercial catalyst suppliers). The use of zeolites in biodiesel production is limited due to the high costs of commercial reagents required for their synthesis (Musyoka et al., 2014, Wang et al., 2007). This study, hence, couples the use of maggot oil as biodiesel feedstock with low cost coal fly ash for the catalyst synthesis.

This research study stands on the premise that two major industrial wastes (coal fly ash and maggot oil), are thoroughly explored as cheap feedstocks respectively,

1) in the exploration, development and synthesis of coal fly ash-derived hydroxy sodalite (HS) zeolites.
2) for biodiesel production

1.4 Research questions

1. Will waste-derived maggot oil present itself as a renewable, sustainable and economical feedstock for biodiesel production?
2. Does maggot oil contain significant amounts of free fatty acids (FFA) and how will its composition influence the catalytic activity of fly ash-derived catalyst during transesterification?
3. Will ion exchange and bifunctional modification of the coal fly ash-based catalyst materials influence the yield of biodiesel production?
4. How do the properties of coal fly ash-based zeolites (HS) correspond to their performance in biodiesel production?
5. Will the maggot oil-derived biodiesel meet suitable international specification standards?

1.5 Project aim and objectives

This study aims to synthesise zeolite catalysts from waste coal fly ash and will then utilise the catalysts in the production of biodiesel from maggot oil feedstock. The following objectives proposed for the project include:

1. Synthesise hydroxy sodalite (HS) and zeolite X (Na-X) from coal fly ash.
2. Carry out characterisation studies on the produced catalysts.
3. Investigate the effect of zeolite synthesis parameters upon product characteristics and yields
4. Investigate the effect of alkali-exchange and bifunctional modification on catalytic properties
5. Carry out characterisation of maggot oil to determine its potential as a feedstock for biodiesel production

- 6. Study the activity of the produced zeolites on transesterification of maggot oil, and compare this to virgin vegetable oil.
- 7. Establish the optimum process conditions for the transesterification of maggot oil using the response surface methodology approach.
- 8. Evaluate the kinetics of transesterification of maggot oil
- 9. To characterise the biodiesel produced.

1.5 Research hypotheses

- Maggot oil will convert to biodiesel via transesterification reaction when used as a feedstock.
- Due to high temperature fusion step, the fusion-assisted method will result in high quality zeolite within a short hydrothermal synthesis time (or less intense hydrothermal conditions).
- Hydroxy sodalite (HS) is an active catalyst for transesterification of maggot oil based on its basic property and large external surface area
- Transesterification of maggot oil over the optimum fly ash-based zeolite can yield biodiesel at significant reaction kinetics.
- Coal fly ash-based zeolites are suitable catalysts for the transesterification of maggot oil for higher biodiesel yields and quality.

1.7 Importance of the research

1.7.1 Energy security, efficiency and greenhouse emission

Improvement in energy efficiency and affordability for every individual is among the strategies set by the South African Department of Mineral Resources and Energy (DMRE) (Minerals and Energy, 2009). From 2002-2009, the DMRE, Department of Environment and Tourism (DET) and all major departments in the South African government, acceded to the Kyoto protocol aiming to reduce the emission of greenhouse gas and adverse effects of energy usage upon the health of its citizenry and the environment. In alignment to the above, this research work introduces an alternative biomass renewable source of energy, so as to minimise the dependence of the use of fossil fuels and promote energy efficiency. Biodiesel production from

waste and much cheaper feedstock materials in this work would allow the reduction in price of the actual fuel product and consequently will make energy affordable to all and bestow energy security. Furthermore, biodiesel of interest in this research as a carbon-neutral fuel, is associated with low greenhouse emission, enforcing a cleaner environment with use. Thus, this research aims to embrace the national policy of Green Technology while ensuring the proposed recognition of biofuels in South Africa is realised.

1.7.2 Waste and environmental management

In open literature, very limited information on the use of two major industrial wastes, one as feedstock for biodiesel production and other as a catalyst precursor for the process, was reported. These particularly with reference to the maggot oil by-product from bioconversion of organic waste and coal fly ash waste generated in large amounts from coal power stations. This study is of academic significance and adds technical knowledge in the application of these feedstocks for biodiesel production. The study also conducts a waste beneficiation process for the coal fly ash into valuable products and offers an appropriate disposal method (or waste management practice) (Zielke-Olivier and Vermeulen, 2016, Shumba et al., 2011). The research, thus, promotes the South African National Environment Management act (Air Quality Act no.39 of 2004), which stresses air quality and environment protection.

The abundant generation of coal-fired power leads to the availability of CFA in South Africa of over 35 tonnes per annum with 95 % unutilised (Zielke-Olivier and Vermeulen, 2016). Finding new uses, could go a long way in boosting economic growth when waste is utilised in the production of value-added products. This research hence leads towards developing appropriate techniques to make valuable catalysts with potential application in producing biodiesel. Besides energy, this research also has an influence in other industrial applications where the waste-derived zeolite product is critical for other applications like water treatment and gas purification applications.

This research study is important in proposing a pilot plant set-up for the conversion of coal fly ash and maggot oil to respective intermediate/end products, which could lead to a continuous process at larger scale.

1.8 Thesis Format

This thesis consists of seven chapters.

Research in biofuel and particular biodiesel has gained much attention due to the detrimental effects of fossil fuel sources and uncertainty in their long-term supply. The high cost of conventional feedstocks challenges the modern biodiesel production; consequently, this has led the current biodiesel market price to be higher than the price of petroleum diesel. For this reason, this work introduces a cheaper feedstock to minimise and make biodiesel production more economical.

Chapter 1 discusses the use of maggot oil and the beneficiation of fly ash via techniques to obtain (intermediate) value-added catalysts and final biodiesel products.

Chapter 2 covers the literature review, in which the first section gives an overview of energy in general, energy dependence on fossil fuels and the emerging of biofuels vis-à-vis fossil fuels. With biodiesel being the biofuel of interest, the (second) section further reviews biodiesel feedstocks, revealing current associated challenges in biodiesel production. The section concludes by suggesting maggot oil as a more economical potential feedstock, due to its availability as waste from large-scale supply and its inherent characteristics. The third section of the literature reviews the secondary coal fly ash feedstock required for the biodiesel production catalysts. This section explores the availability and inherent properties of coal fly ash as feedstock for catalyst development. Fourth section covers zeolites, the catalysts of interest (particularly HS zeolite), their general properties and existing applications, including as catalysts in biodiesel production. The fifth and sixth section of the literature review thoroughly reports on zeolite synthesis from coal fly ash concerning methods and parameters involved, as well as possible subsequent modifications as catalysts for biodiesel production. The seventh section reviews transesterification method and corresponding influential parameters with the view of process optimisation. Concerning the objective set for product analysis in this work, this section further highlights the required biodiesel specifications as per EN and ASTMD standards. Kinetic studies of the process, in view of another set objective, are also unveiled with a precise mechanism adopted from literature. The last section (8th section) of the literature review summarises the gap that this work has to cover in the space of research and particularly in the area of biodiesel production.

Chapter 3 reports on the materials and equipment required for the analysis of feedstock oil, catalyst preparation/modification and application in the biodiesel synthesis stage. The above is

accompanied by thorough experimental procedures to achieve each objective. A presentation of various catalyst characterisation techniques and corresponding procedures attached to catalyst preparation and modification is made in this section, as well as product characterisation techniques and the procedures taken attached to catalyst application.

Chapter 4 reports on the result and findings of the first stage of the investigation on (maggot oil) feedstock analysis. Physicochemical characteristics of maggot oil (determined from the experimental work) are thoroughly reported and discussed in this chapter, with the view to substantiate its technical feasibility as a potential feedstock for biodiesel production.

The outcome properties of catalyst synthesis from coal fly ash; synthesised via the direct method, fusion-assisted hydrothermal method, and subjected to modifications; are reported in Chapter 5. The first section of chapter 5 (denoted as 5.1) reports on catalytic properties of synthesised samples via the direct hydrothermal method, whereby these are evaluated in terms of varying chemical parameters, ageing (pre-synthesis physical) parameters, and actual hydrothermal synthesis time and temperature (physical) parameters. In the second section of chapter 5 (5.2), the properties of samples synthesised via the fusion-assisted hydrothermal method were mainly evaluated or discussed in terms of varying synthesis time parameter. The above sections are summarised as section 5.3, which also compares the properties of best HS zeolite samples obtained from both hydrothermal methods and selecting appropriate samples as catalysts for biodiesel production.

The catalytic evaluation of selected synthesised samples based on finding in chapter 5, is reported in the first section (6.1) of Chapter 6. The performances of the catalysts presented under this section are evaluated in terms of yield of biodiesel and FAME content, and physicochemical properties. The second section (6.2) reports on process optimisation of biodiesel production via RSM using the catalyst with best performance from section 6.1. The final section of chapter 6 (6.3), reports on kinetics evaluation of the biodiesel production process, using the previously best selected catalyst at single factor-optimised biodiesel production conditions.

Chapter 7 is the concluding chapter and includes highlights of the novelty findings of the thesis as well as a recommendation section for unattended and future objectives and studies.

Chapter Two

Literature review

Biodiesel production is a process to make fuel from vegetable and animal fats. This process to date is known to be achievable via four main routes (Zhang et al., 2010, Leung et al., 2010); the direct use and blending of biodiesel with diesel, biodiesel production by pyrolysis or thermal catalytic cracking, biodiesel production by microemulsions of oil or fats with solvents (such as short-chain alcohols), and biodiesel production via the transesterification reaction.

Transesterification is the conventional biodiesel production technique achieved by chemical and catalytic approaches. This method has been commercialised worldwide and is the most commonly employed and commercially known biodiesel production method worldwide. (Saifuddin et al., 2015). Biodiesel was discovered over a century ago when triglycerides of vegetable oils were reacted with short-chain alcohols (methanol in particular) over potassium hydroxide resulting in the formation of free glycerol and Fatty Acid Methyl Esters (FAME) (El Banna and El Deen, 2004, Mittelbach and Remschmidt, 2004). Towards the mid-19th century, the method of transesterification was frequently employed for soap production. Within the same period, the procedure gained its reference for biodiesel production through a Belgian patent.

The catalysed transesterification of oil or fats with short-chain alcohols stated above, is a relatively cheaper method, as it is less energy-intensive (based on lower energy requirement), a simple method that produces fuels with better properties than those obtained by other routes (afore-mentioned); a method that does not result in side products of no commercial value, and consequently generates fuels that are not as problematic in diesel engine application (Leung et al., 2010, Lam et al., 2010, Sharma et al., 2011).

Moreover, the transesterification method is diversified with various intensification technologies such as ultrasound, microwave and the non-catalytic transesterification using alcohol at supercritical conditions (Saifuddin et al., 2015). Research on these technologies, however, may only be considered for process optimisation purposes.

The above reasons are the key to the selection of the transesterification method/route for biodiesel production in this research.

2.1 Review on energy and biofuels

From the beginning of time, almost every human activity about sustaining life depended on the use of energy. The activities include agriculture, industries for chemical and food production, electricity generation and transportation activity (Saifuddin et al., 2015, Silitonga et al., 2011). It is reported that over 80 % of the world energy required to drive various human activities are derived from fossil fuel sources (Ho et al., 2014). Around 57 % of this energy derived from conventional fuels, caters for transportation (Lam et al., 2010, IEA, 2006). There is, however, a concern regarding the world's continual reliance on fossil fuels as energy sources. Fossil fuels have been utilised at a very much faster rate than they are produced naturally. As a result, global natural reserves have been undergoing depletion and the World Energy Forum (WEF) has made predictions of their complete depletion within the next 10 decades (Lam et al., 2010, Sharma et al., 2011).

The processing and utilisation of fossil fuels for energy production have also been identified as the source of greenhouse emissions (Gonfa Keneni et al., 2017), serving in connection to currently experienced global environmental pollution. Moreover, the ever-increasing human population and human activities have impacted on increased demand for energy. Hence, failure to meet this demand and significant dependence on fossil fuels has been a trigger to an energy crisis. For this reason, alternative sources of energy have been explored in research to overcome the above challenges (dependence on fossil fuels; environmental pollution, energy crisis). Biomass alternatives and transformation to biofuels are believed to be the most promising in this regard. Biomass-derived fuels (biofuels) have proven to possess the same properties as those from fossil fuel-derived technologies, with the advantages of being easily transformed to meet targets, and reduce dependency on fossil-derived fuels (Yue et al., 2014).

2.1.1 Biofuels and trends

Over the past decade, national and global energy supplies from renewable biofuels have shown an increasing and promising trend; although to date fossil fuels still mainly cater for the energy demand (Jensen et al., 2017, IEA, 2006). The global energy distribution by source is presented in Figure 2.1. This distribution corresponds to the South African energy distribution.

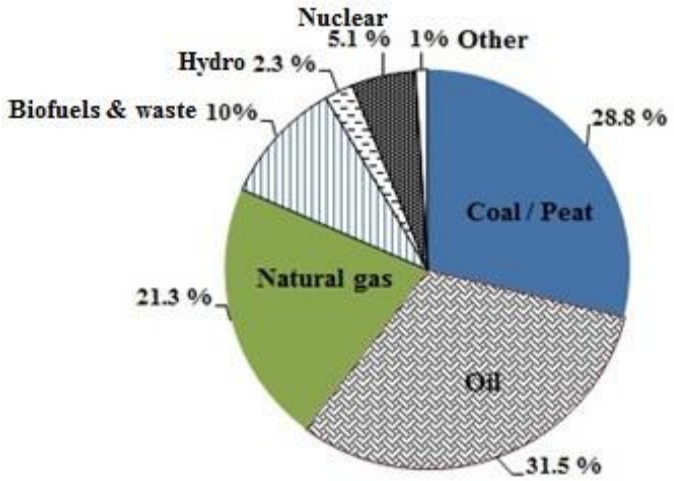

Figure 2. 1. World energy distribution by source and biofuel energy supply distribution in 2011 (Ho et al., 2014, Agency and Birol, 2013, Minerals and Energy, 2009).

Biofuels refer to fuels obtained from renewable biomass sources and have been currently and intensively explored by many researchers (Ho et al., 2014). Biofuels, as obtained from biomass, are renewable, sustainable and cleaner alternative fuels (Yue et al., 2014). Biodiesel being the proposed biofuel in this work, is non-toxic, biodegradable, and is one of the technically and economically feasible options to tackle the fast depletion of fossil fuels and environmental pollution. Besides, biodiesel has proven to possess better properties than fossil-derived diesel (Zhang et al., 2010, Gonfa Keneni et al., 2017, Saifuddin et al., 2015).

The transformation of a biomass resource has been proposed towards biodiesel–production, of which oil-based crops (e.g. vegetable oil) and animal fats are the predominant biomass in this regard.

2.2 Review on biodiesel oil feedstocks and proposed feedstock

Biodiesel feedstocks exist in vast diversity in such that these have been classified into three major groups namely: the first generation feedstocks, second generation and the new third-generation biodiesel feedstocks (Gonfa Keneni et al., 2017, Manzano-Agugliaro et al., 2012).

First-generation feedstocks are majorly crop-based edible oils, which are famously known as vegetable oils such as soybean, palm oil, rapeseed, corn, sunflower, groundnut, coconut,

cottonseed, etc. (Lam et al., 2010, Gonfa Keneni et al., 2017). Non-edible oils (crop-based) are also inclusive as first-generation biodiesel feedstocks of which one of the most prominent examples include Jatropha and linseed oils (Yang et al., 2014, Gonfa Keneni et al., 2017). Animal oils and fats are also inclusive with examples such as tallow, grease, fish oil. (da Cunha et al., 2009).

Vegetable oils are the main feedstocks for biodiesel production, as such, they contribute to nearly 75 % of the world's biodiesel production (Lam et al., 2010, Naylor and Higgins, 2017) (Table 2.2, section 2.2.2).

The challenge of using vegetable oils as feedstocks for biodiesel production is due to the high demand that has gradually posed market competition between (biodiesel) fuel and food industries (Gonfa Keneni et al., 2017). The use of vegetable oils alone as a feedstock contributes to nearly 80 % of the overall biodiesel production cost (Lam et al., 2009, Gonfa Keneni et al., 2017). The focus of biodiesel manufacture has been directed to the use of various other feedstocks to overcome the above limitation on cost. Waste cooking vegetable oils (WVO), which are far less expensive than refined vegetable oils, are the most common low-cost feedstock for this purpose (Lam et al., 2010, Gui et al., 2008). These are generated in large amounts that increase their opportunity to be used for biodiesel production (second-generation biodiesel), or otherwise would contaminate the environment if not appropriately disposed of. The use of waste vegetable oils for biodiesel production, therefore, compensates for their availability and disposal and this, in turn, saves the environment from possible contamination.

Research has also been geared towards the use of non-edible biomass feedstocks, as alternatives to refined vegetable oil for the production of second and third generation biodiesel. Examples of biodiesel second-generation non-edible feedstocks are jatropha oil, oil grease, castor oil, and algae oil being a third-generation feedstock (Bhuiya et al., 2014, Halim et al., 2011). In addition to the above known traditional feedstocks, this research introduces the novel use of non-edible waste-derived maggot oil as a feedstock for biodiesel production. The feedstock in question is deemed to meet the need of a more available and sustainable oil feedstock derived from waste, with the implication of lowering the overall production cost of biodiesel.

2.2.1 The emerging of waste-derived maggot oil for biodiesel production

Maggot oil is a natural fat extruded from dry larvae of Black Soldier Flies (BSF) and harvested during their larval or pupation stage. Biologically known as *Hermatia illucens*, the oil is obtainable as a product of digestion and breakdown of organic waste materials upon which BSF feed (Oonincx et al., 2015, John, 2009). The dried and defatted insect is a protein-rich product (commercially known as Magmeal) that is useful for animal farming and agricultural industry (Douglas, 2012). Food organic wastes, followed by paper waste, constitute the largest of the global municipal wastes (Demirbas, 2004). Owing to their abundance and increase in their disposal on landfills across the world over time, continual cultivation (mass cultivation) of BSF and hence feasible generation and renewability of the derived-oil biomass, is guaranteed. Thus, this study also promotes waste management practise for such huge volumes of organic municipal wastes.

Currently, there are only two corporates known globally for commercially mass production of BSF, majorly for the interest of natural protein (MagMeal) obtainable from the insect (Surendra et al., 2016). AgriProtein, a South African-based company in Cape Town, is the world's leading manufacturer of Magmeal (the natural protein feed) (Agriprotein, 2017). Recently, an American corporate company (Ecosystem (Ltd), located in the United States) also emerged for a mass of production of Magmeal and the derived-oil (magOil) (Manzano-Agugliaro et al., 2012). AgriProtein has produced an estimate of about 2000 tonnes of Magmeal annually since the year of their emergence in 2016 (Agriprotein, 2017). An estimation of 40 % oil content by the average in the biomass insect (Ushakova et al., 2016, Leong et al., 2016), accounts for about 1 300 tonnes of the maggot oil by-product produced annually.

Ecosystem Corp, on the other hand, envisioned to produce about 700 tonnes of maggot oil yearly (John, 2009, Ecosystem, 2010). The oil, therefore, as a waste-derived produced at such industrial significant quantity, guarantees sustainability for its use as a feedstock for biodiesel production. Moreover, based on the continual and estimated increase in market demand of Magmeal with time, increased and sustainable production of maggot oil is also guaranteed (Douglas, 2012). According to the best of this author's knowledge, this is the first of its kind in which an industrially produced volume of waste-derived oil is extensively explored for biodiesel production.

To date, no remarkable and beneficial use of maggot oil has been identified from open literature, and neither has the oil been openly identified or reported healthy for human consumption (non-edible) (Wang and Shelomi, 2017). The oil instead, has only been exclusively accounted for low-valuable application as a flavouring additive to animal feed (poultry, fish and pet diets) (Agriprotein, 2017, Manzano-Agugliaro et al., 2012).

Based on the abundant generation with limited application, the oil has presented itself as a waste that could generate a return to the company when sold or supplied at a cheaper cost. Apparently, maggot oil is even less expensive than waste cooking oil (assumption based on application and demand), and comparably a far cheaper feedstock than conventional vegetable oils for biodiesel production (Lam et al., 2010). The selection of maggot oil and its local supply from Agriprotein in this work, is a great way to address the challenge associated with the cost of conventional feedstock oils of biodiesel production (Gonfa Keneni et al., 2017).

Maggot oil considered a waste-derived and a low-cost feedstock extruded from BSL insects can be categorised as a feedstock of the same generation as waste cooking oil (WCO) and animal oil/ fat. Compared to the first generation, second-generation feedstocks such as WCO and animal fats, are low-cost feedstocks as they do not require arable land and neither compete with food edible oil for their generation (Bhuiya et al., 2014). These, however, are generally generated in limited supply and hence have limited availability to satisfy a large scale or global demand (Gonfa Keneni et al., 2017). For this reason, waste-derived maggot oil being a more abundant and available second-generation feedstock, is being introduced in this study to bridge the gap associated with second-generation feedstocks. The growing market of magMeal and maggot oil, promises a sustainable supply to meet large-scale demand for biodiesel production. (Agriprotein, 2017). Classification of biodiesel feedstocks, their production and prospects as well as their contribution to global biodiesel production are reported in Table 2.1.

2.2.2 Characteristic potential of waste-derived maggot oil as a feedstock in biodiesel production

Maggot oil, referred to as lipid of black soldier fly (BSF), is reported to consist of similar components as any other triglyceride containing oil known in literature (Gonfa Keneni et al., 2017, Lam et al., 2010). These include lauric acid, palmitic acid, stearic acid, oleic acid and linoleic acid (Table 2.1).

The proportional concentration of the respective fatty acids content marks the only difference between maggot oil and conventional oils (Table 2.1). Maggot oil majorly constitutes of saturated fatty acids (SFA), among which lauric acid has been identified to have the highest concentration from the few literature studies (Leong et al., 2016, Ushakova et al., 2016). Thus far, based on similarity in triglyceride compositional characteristics, maggot oil can be potentially predicted as a suitable feedstock for biodiesel production. Leong et al. (2016) conducted three technical feasibility tests of maggot oil's conversion to biodiesel in a sulphuric acid medium via ultrasonic aided in-situ transesterification, and results showed FAME yields of 48.46 %. In another study by Li et al. (2011), a two-step transesterification of maggot oil in sulphuric acid and sodium hydroxide (NaOH) homogeneous-catalysed reaction, was reported with an estimated biodiesel yield of 77 %. To the best of the author's knowledge, the potential conversion of maggot oil to biodiesel is limited to the reports described above. In this study, the catalytic activity of synthesised heterogeneous catalysts used for transesterification reactions using maggot oil, will be investigated to ascertain the oil's conversion over an heterogeneous catalyst and to bridge the gap of a more simple, cheaper and cleaner approach to produce biodiesel from maggot oil.

Table 2.1 further reports on the fatty acid composition of maggot oil and other biodiesel feedstocks.

Table 2. 1. Classification, production prospect and characteristic fatty acid composition of biodiesel feedstocks

	First generation edible oil sources			Second generation non-edible oil sources					
	Soybean	**Rapeseed**	**Palm oil**	**Castor oil**	**Linseed**	**[a]WCO**	**[b]Beef tallow**	***Maggot oil**	**Reference**
[c]Oil yield (L/ha/year)	**446**	1190	**5950**	1413	**478**	n/a	**n/a**	**~215× 10^4**	Hajjari et al. (2017), Ziolkowska (2014)
Cost/ kg ($)	[a] 0.87-1.3/kg	[a] 0.9-1.3/kg	[a] 0.7-1 /kg	-	-	0.5$/ kg	-	-	IndexMundi (2019)
[d]Contribution to global *BD production (%)	28 %	23.7 %	17.6 %	-	-	10.6	7.9-11 %	-	Ho et al. (2014), Naylor and Higgins (2017)
[e]Oil content (wt. %)	-	-	-	-	-	-	-	40 %	Wang and Shelomi (2017)
Fatty acid (wt. %)	**[f](wt. %)**								
Lauric acid (C12:0)	0.1	-	0.1	-	-	-	-	35.6	Lam et al. (2010),
Myristic acid (C14:0)	0.1	-	48.9	-	-	-	2.72	5.77	Gonfa Keneni et al. (2017),
Palmitic acid (C16:0)	0.2	-	18.8	1.1	5.1	-	25.33	15.6	Zhang et al. (2010),
Stearic acid (C18:0)	3.7	0.85	10.2	3.1	2.5	-	34.7	2.76	da Cunha et al. (2009),
Oleic acid (C18:1)	22.8	64.4	17.0	4.9	18.9	-	29.87	18.2	Marchetti (2012),
Linoleic acid (C18:2)	53.7	22.3	2.2	1.3	18.10	-	0.75	14.3	Verma and Sharma (2016),
Linolenic acid (C18:3)	8.6	8.23	-	-	55.10	-	-	0.99	Borugadda and Goud (2012),
*Others (minor)		3.49	-	*89.9	0.3	-	6.65	6.92	Demirbas (2009), Agriprotein (2017)

[a] WCO: Waste cooking oil [b] representative of all animal fat [c] Estimate commercial amount generated [d] Estimate contribution [e] Utmost average oil content in BSF larva maggot [f] Weight % of fatty acid components in respective oil *Maggot oil of interest in this work *BD: biodiesel *Others: Other fatty acids not reported or unaccounted

2.3 Production prospect overview of coal fly ash

Coal fly ash (CFA) is the solid residual by-product (from coal) generated during coal burning and gasification at power stations (Zielke-Olivier and Vermeulen, 2016). The fly ash material is usually collected using filters, electrostatic precipitators, electro-magnetic precipitators and/or by simple ejection into the atmosphere (Ram et al., 2010). A typical coal combustion process, displaying fly ash collection in a precipitator is presented in Figure 2.2.

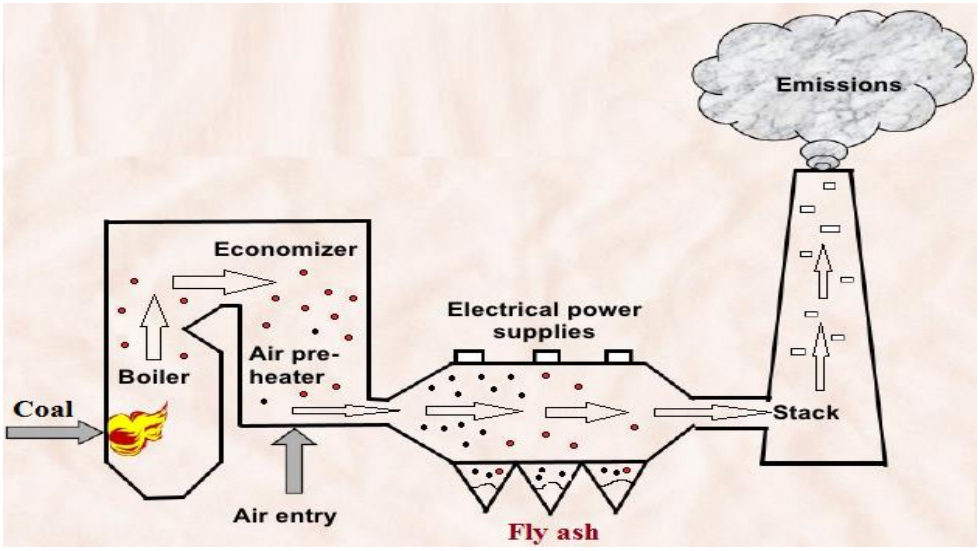

Figure 2.2. Fly ash generation from a coal combustion process (Toniolo, 2018).

Burning of coal within the past decades has made up to about half of the electricity generated globally (Bukhari et al., 2014). This has resulted in the generation of fly ash; consequently imposing safe and long-term storage requirements thereof.

An estimate of over 800 million tonnes of fly ash is produced yearly worldwide within the past decade (Shumba et al., 2011). According to the 2017 estimate prospect of fly ash generation, South Africa ranks as the fifth-largest producer with over 35 million tonnes (Mt) of fly ash generated annually (Zielke-Olivier and Vermeulen, 2016, Usmani and Kumar, 2017) (Figure 2.3). According to Figure 2.3, on average nearly half (given a figure of 52.6 %) of the amount of fly ash generated globally, is recycled for use in the manufacturing of cement and concrete ceramics (Querol et al., 2002, Bukhari et al., 2014). The rest is disposed to ponds, dams and most commonly to landfills as solid waste.

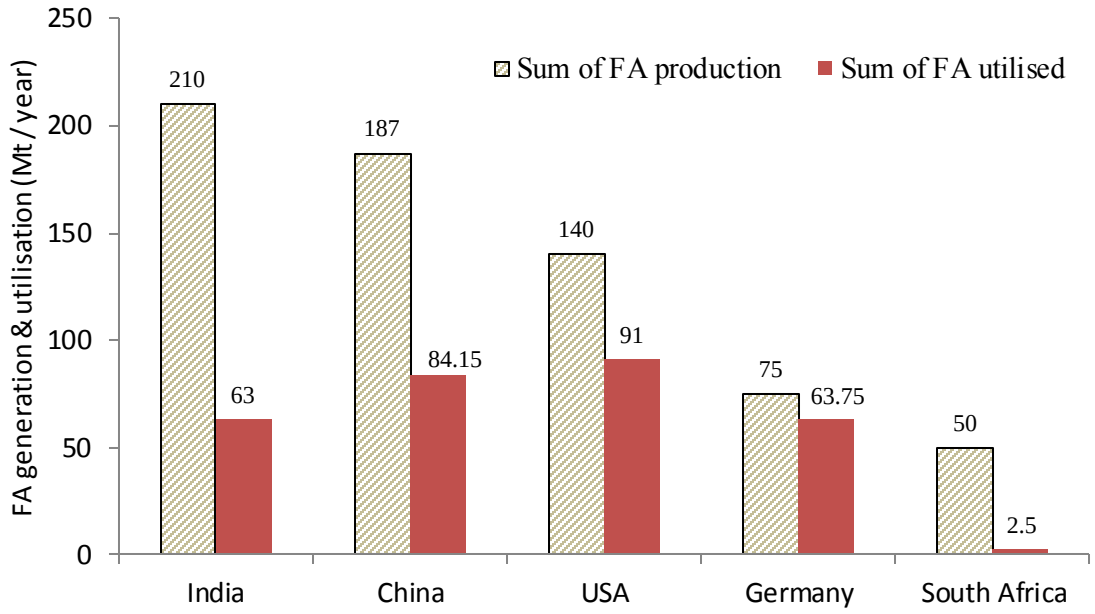

Figure 2.3. 2017 estimate prospect of fly ash generation and utilisation in South Africa and various countries worldwide (Usmani and Kumar, 2017, Reynolds-Clausen and Singh, 2017).

While this drives the necessity to secure land for landfills, fly ash has been a threat and pollutant to the environment. Other than (ceramic) building materials, utilising fly ash for the manufacturing of other value-added products could be one of the ways to remediate its impact on the environment. Coal fly ash, based on thorough research within the past 40 years, is sufficient for the manufacturing of zeolites (Murayama et al., 2002, Henmi, 1987). Although zeolites only utilise a minor amount of the CFA generated, zeolites have drawn much interest in research (Querol et al., 2002).

2.3.1 Properties and application of coal fly ash

The physical and chemical properties of CFA vary depending on the source from which it is obtained, the coal burning processes and the degree of coal pulverization at power stations. Coal fly ash generally consists of smooth, glassy, hollow and microspherical particles of low density and size that typically range between 30 and 100 µm (Musyoka et al., 2014, Murayama et al., 2002, dos Santos et al., 2014). The material is mostly glassy, as it generally consists of an aluminium-silicate matrix and calcium aluminosilicate glasses (Aughenbaugh et al., 2016). In other words, the material is an aluminosilicate that mainly consists of SiO_2, Al_2O_3, Fe_2O_3

and CaO (Zielke-Olivier and Vermeulen, 2016, Toniolo, 2018). Aughenbaugh et al. (2016), further on reported that fly ash comprises between 50 and 90 % of the amorphous glassy phase while the remaining crystalline mineral phases include quartz, mullite, calcite, hematite and magnetite (Musyoka et al., 2011, Steenbruggen and Hollman, 1998).

Table 2.2 reports the chemical composition proportion of CFA obtained from various power station sources.

Table 2.2: Chemical composition of coal fly ash obtained from different sources (Musyoka et al., 2011, Volli and Purkait, 2015, Brassell, 2017).

Major oxides (wt. %)	**Fly ash source**		
	SA- Matla Pw. station	SA-Arnot power station	India -SARACA laboratories[(a)]
SiO_2	50.91	53.6	56.61
Al_2O_3	30.91	25.44	23.21
Fe_2O_3	3.46	5.56	5.89
CaO	6.2	5.23	7.93
Na_2O	0.1	0	0.28
MgO	1.48	1.54	1.53
K_2O	0.6	0.55	1.39
TiO_2	1.65	1.58	1.35
MnO	0.02	0.05	0.05
P_2O_5	0.56	0.35	0.27
SO_3	0.24	-	0.53
LOI	3.85	6.76	-
SiO_2/Al_2O_3 (w/w)	1.65	2.11	2.44
Reference	Musyoka et al. (2011)	Brassell (2017)	Volli (2015)

[(a)] M/s SARACA laboratories limited (Ltd), Andhra Pradesh, India

2.3.2 Classification of fly ash (Class C, D and F)

Fly ash materials are classified into three major categories: Class A, C and Class F. The above classification is based on proportions of major chemical composition such as silica, alumina, iron and calcium. Class C fly ash is the type that results from the burning of lignite and sub-bituminous coal and contains more than 20 % lime (CaO) and higher proportions of alkali and

sulphate content (Dwivedi and Jain, 2014). Consequently, Class C fly ash possesses self-cementing properties (Dwivedi and Jain, 2014). Unlike Class C, Class F fly ash is the type that results from the burning of older and bituminous coal, contains less than 10 % lime and does not exhibit cementing properties (unless activated with a cementing agent).

Based on the reported properties, fly ash has been widely employed in various environmental and construction applications. These include land stabilisation in mining areas; wastewater purification as a sorbent and adsorption agent; flue gas desulphurisation (Janoš et al., 2003); a fill-in low-lying area and; an additive in ceramic, brick, cement and concrete preparation (dos Santos et al., 2014, Dwivedi and Jain, 2014, Queralt et al., 1997). Fly ash has also been employed in the synthesis of zeolites as the main raw material (Volli and Purkait, 2015, Musyoka et al., 2011, Querol et al., 2002).

2.4 Zeolites: properties, classification and application

Zeolites are crystalline, microporous and hydrated aluminium–silicates of alkali or alkali earth metals (Gougazeh and Buhl, 2014). Zeolites are formed under hydrothermal conditions, either naturally from volcanic rocks or synthetically from a variety of aluminosilicate materials such as clay minerals, natural and synthetic glasses, aluminosilicate gels, and coal fly ash (Chantawong and Harvey, 2003). The general chemical formula of zeolites is presented in equation 2.1 (Weitkamp, 2000, Musyoka, 2009).

$$M^{n+}_{x/n}O[(AlO_2)x.(SiO_2)y].wH_2O \qquad (2.1)$$

Where M is the exchangeable cation with the charge or valence of n

w is the number of water molecules

y/x is the stoichiometric factor of between 1-5 depending upon the structure

(x+y) is the total number of tetrahedral in the unit cell

Zeolites consist of a three-dimensional framework or channels of tetrahedral structures of $[SiO_4]^{4-}$ and $[AlO_4]^{5-}$ that are linked to each other by sharing on their oxygens (Querol et al., 2002, Frising and Leflaive, 2008). The framework of zeolites as observed in Figure 2.4, possess open spaces in their structures, which can accommodate a wide variety of charge balancing cations such as Na^+, Ca^{2+}, Mg^{2+} and K^+ (Chouhan and Sarma, 2011, Weitkamp, 2000). As a result, special properties emerge such as effective adsorption of molecules in the framework's

internal channels, high CEC due to the basic alkaline cations that are held loosely and readily can be exchanged with other cations in a contact solution (Shumba et al., 2011, Chantawong and Harvey, 2003).

The general structure of zeolites, including those investigated in this work (sodalite and faujasite) are presented in Figure 2.4.

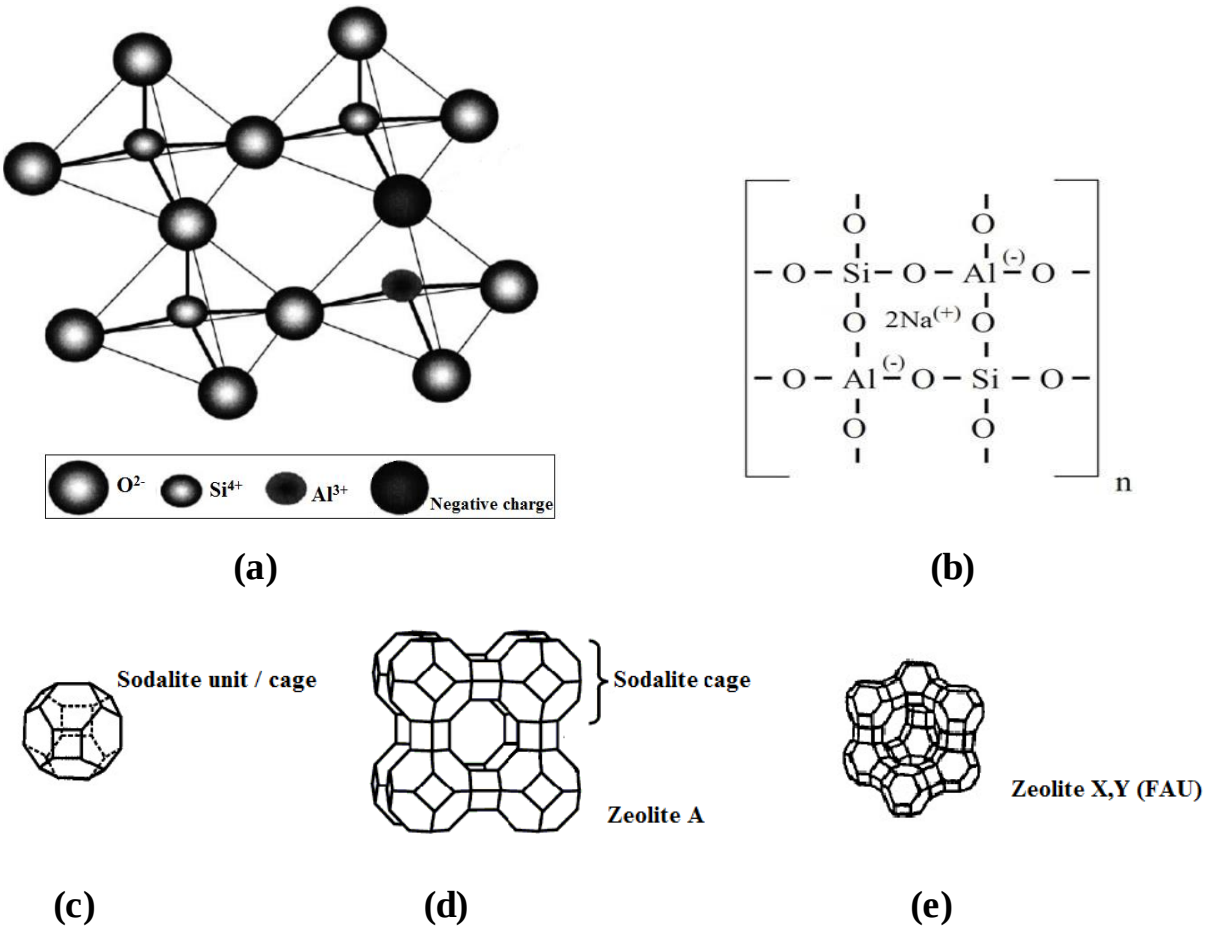

Figure 2. 4. Structure of zeolites

(a) Structure of Zeolite Framework with tetrahedral $[SiO_4]^{4-}$ and $[AlO_4]^{5-}$ (Querol et al., 2002).

(b) The one-dimensional basic structure of zeolite with Na^+ ion tightly held in the porous structure (Cheresources.com, 2011, Breck, 1984).

(c) Unit structure of sodalite (Weitkamp, 2000).

(d) The surface structure of Zeolite A (Baerlocher et al., 2007).

(e) Structure of faujasite (Weitkamp, 2000).

Zeolites are materials with a high degree/concentration of surface acidity and high thermal stability property of 1000 °C (Shu et al., 2007); having their unique channel structure (mentioned above) that enables size and shape-selective features - known as shape-selective materials (Silva et al., 2013). As a result, this allows their application in sorption and catalysis (Khatamian and Irani, 2009).

2.4.1 Properties of hydroxy sodalite and zeolite X

Hydroxy sodalite (HS) is a hydrophilic zeolite that belongs to the clathrasils group and possesses a sodalite cage made of a cubic array of β-cages (Nanganoa et al., 2016). The cages are held by the alumina-silicate framework and are interconnected by small 4-membered rings and 6-membered rings (Musyoka et al., 2011) (Figure 2.5). The interconnection is in such a way that does not allow distinct pore channels between the cages. Consequently, HS structurally consist of no distinct pores or small pore sizes of about 2.3 Å (2.2-2.8 Å). Due to this phenomenon, HS has a low molecular sieving potential and low ion exchange capacity (IEC) (Querol et al., 2002, Nabavi et al., 2014). The structure of HS as described above is depicted in Figure 2.5.

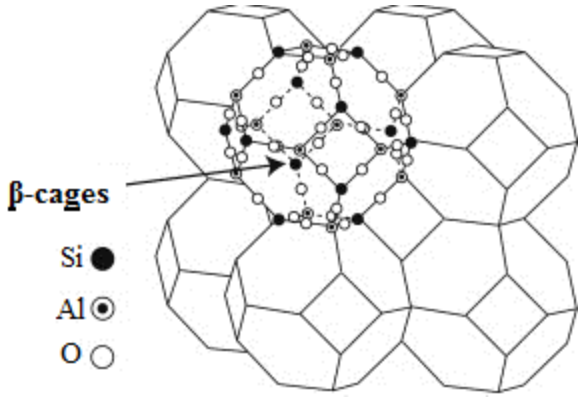

Figure 2. 5. Illustrative structure of hydroxy sodalite (HS)

HS is a hydrophilic zeolite that possesses a similar framework structure as sodalite (Musyoka et al., 2011, Nanganoa et al., 2016, Henmi, 1987). It may also be referred to as the hydrated form of sodalite, chemically represented by equation 2.2 (Musyoka et al., 2011). Sodalite on

the other hand as chemically shown by equation 2.3 is the non-hydrated form containing chloride molecules in place of water molecules.

Hydroxy Sodalite $Na_{1.08}Al_2\,Si_{1.68}O_{7.44}\ 1.8\ H_20$ (2. 2)

Sodalite $Na_8[(AlO_2)_6\ (SiO_2)_6Cl_2$ (2. 3)

Unlike sodalite, Zeolite X of Faujasite structure consists of relatively large pore size (7 Å) based on which this zeolite possesses high ion exchange capacity and high molecular sieving potential (Musyoka et al., 2011). Zeolite Na-X as reported by Querol et al. (2002) is chemically represented by the general formula in equation 2.4.

Zeolites Na-X $Na_2Al_2\,Si_{3.3}O_{8.8}\cdot\ 6.7\ H_20$ (2. 4)

According to Frising and Leflaive (2008), Faujasites are classified into zeolite X and zeolite Y; and this classification is defined based on the ratio of Si/Al content present in the respective product. The Si/Al ratio for zeolite X ranges between 1-1.5 whereas that of zeolite Y ranges above 1.5. The above is reflected in their respective following chemical equations (Querol et al., 2002).

Zeolites X $NaAlSi_{1.23}O_{4.46}\cdot 3.07\ H_20$ (2. 5)

Zeolites Y $NaAlSi_{2.43}\ O_{6.86}\cdot 4.46\ H_20$ (2. 6)

The Si/Al range given as a range further reveals that faujasites possess a tuneable acidic property, and are most likely classified as base heterogeneous zeolites when treated with an alkaline solution. Unlike zeolite X, zeolite Y has been identified to be acidic (Chouhan and Sarma, 2011); for which reason, it has been typically categorised in Figure 2.4 as an acid heterogeneous zeolite (Brito et al., 2007). The larger pore size of faujasites, precisely zeolite X as compared to hydroxy sodalite, induces both a high molecular sieving potential and a high ion exchange capacity of the material (Querol et al., 2002, Frising and Leflaive, 2008).

Consequently, the exchange of faujasite zeolites with different cations has been successfully achieved and extensively studied over the past 50 years due to their commercial applications for separation and catalysis engineering in petrochemical industries (Frising and Leflaive, 2008). Moreover, faujasites when alkaline treated (inducing basic property), have proven to

have outstanding potential and successful application in biodiesel production (Babajide et al., 2012). Consequently, faujasites have been continually adapted by several researchers (Babajide et al., 2012, Pandiangan et al., 2017, Volli and Purkait, 2015) and thus the case is for zeolite-X in this work.

In catalytic applications, additional properties of the above-mentioned zeolite of interest such as specific surface area, base strength and base site concentration, are deemed determinant or a relevant parameter of their activity or behaviour in catalytic applications (Refaat, 2011). Therefore, a high degree of each of the above properties for example in biodiesel production should be associated with an active transesterification reaction.

The properties of hydroxy sodalite (HS) and zeolite-X, as well as those of common zeolites successfully applied in biodiesel production synthesis is highlighted in Table 2.3.

Table 2. 3. Physicochemical properties of zeolites HS and Na-X (other zeolites)

Zeolite structure	**Surface area,** $S_{BET}(m^2/g)$	**Pore size** (Å)	**Pore volume**, $P_V\ (mL/g)$	**Micropore surface** (m^2/g)	**Si/Al ratio**[a]	**CEC** $(meq/100g)$ [b]	**Reference**
CFA	2[c] -13.87		0.00292	5.542		11	Babajide et al. (2012), Golbad et al. (2017)
Sodalite[d]	11[e]	2.8	0.002128[f]	-	~ 1	30	Shirani Lapari et al. (2015), Querol et al. (2002)
HS[g]	43.6	-	0.0048	9.62	0.84	320	Golbad et al. (2017), Querol et al. (2002)
HS[h]	46.23	-	0.21[f]	-		203.06	Nanganoa et al. (2016)
Na-X[i]	320	7.3	1.40	-	~ 1.23	352.7	Babajide et al. (2012), Volli and Purkait (2015), Querol et al. (2002)
Na-X[Com][j]	802	-	3.62	-		-	
Con-ZSM-5[k]	338	32	0.18	-	16-40[l]	-	Rownaghi et al. (2011), Ferreira Madeira et al. (2012)

[a] Si/Al ratio estimated based on the chemical equation
[b] Cation exchange capacity (CEC), which may vary from one zeolite to another as it is a function of NaOH or alkali substance concentration (Volli and Purkait, 2015)
[c] Surface area of South African class F fly ash
[d] sodalite synthesised from commercial conventional chemical reagents
[e] Single point Measurement
[f] Total pore volume
[g] Synthesised from fly ash
[h] Synthesised from fine fractions of sandy loam
[i] Synthesised from fly ash
[j] Commercially synthesised zeolite-X
[k] Conventional ZSM-5 zeolite derived from commercial chemical reagents
[l] The most common range synthesised in literature. The range of Si/Al ratio of ZSM-5 goes to as far as 140 to 500.

2.4.2 Classification and application of zeolites: General and in biodiesel production

Many varieties of zeolites are of interest in catalysis, and their general classification is mostly based on their structure. According to literature, 126 zeolites approved structures were identified by the International Zeolite Association (IZA) at the end of 1999 and additional 50 by 2007 (Weitkamp, 2000, Treacy and Higgins, 2007, Baerlocher et al., 2007). See Table 2.4 for common zeolite structures.

Table 2.4. Common zeolite structures identified by IZA (Weitkamp, 2000, Musyoka, 2009, Baerlocher et al., 2007).

Zeolite structure	CODE[(a)]	Example of zeolite products
Faujasite	FAU	Zeolite X; Zeolite Y
Mordenite Framework Inverted	MFI	ZSM-5; ZRP-5
	BEA	Beta zeolite
Linde Type A	LTA	Zeolite A
Gismondine	GIS	Zeolite P
Mordernite	MOR	Mordenite
Gmelinite	GME	-
	EMT	EMC-2
	MTW	ZSM-12
	TON	ZSM-22; Theta-1
	M41S	MCM-41
	EUO	EU-1

[(a)] assigned three-letter code of the zeolites by IZA

Zeolites are known as molecular sieves, as their first commercial application was in adsorption (Chantawong V., 2003). The high cation exchange capacity (CEC) of zeolites, inherent in their structures due to distribution of charge balancing cations associated with their structures, accounts for their application as good ion exchangers or adsorbents (Frising and Leflaive, 2008, Querol et al., 2002). Moreover, the basic nature of zeolite attributed by the cations present in their structures, including their shape-selectivity property, makes them highly selective and active in many catalytic processes (Chouhan and Sarma, 2011). The common industrialcatalytic applications of zeolites in question include isomerisation, oligomerisation,

alkylation, aromatisation and cracking (Silva et al., 2013, Shen et al., 2006). General applications of biodiesel, based on the various properties as highlighted above, are presented in Table 2.5.

Table 2.5. General application of zeolites

Zeolites	Properties	Application	Reference
Sodalite	- Molecular sieve : Small pore size_*Adsorption*	- Water treatment (Removal of heavy metal) - Gas separation process (H_2 from syngas, membrane[a]) - NOx reduction	Luo et al. (2016), Golbad et al. (2017), Shumba et al. (2011), Nabavi et al. (2014), Kim et al. (2013).
Zeolite-A Fe/Z-A[b]	- Ion Exchange Capacity (IEC or CEC)_*Adsorption*	- Removal of ion species, heavy metals, organic compounds (e.g. Ammonium & Phosphate) in Aqueous media or environmental engineering	Kim et al. (2013), Steenbruggen and Hollman (1998).
ZSM-5	- Framework - Pore structure (size, shape) - Shape/size selectivity	- Catalysis in petroleum Cracking - Catalysis in biodiesel production	Corma et al. (2012)
H-ZSM-5	- Acidity/ basicity	Catalysis in the synthesis of gasoline-range hydrocarbons	Inaba et al. (2006)

[a] Gas separation membrane Z-A: denotes zeolite-A

The use of zeolites in biodiesel production over the past decade has attracted attention all over the world. According to Sivasamy et al. (2009), "zeolites are probably the most investigated inorganic solid catalysts for the production of biodiesel by transesterification". Several zeolite structures have been reported for catalytic application in biodiesel production. These, among those listed in Table 2.5, include faujasite (FAU), LTA, MFI, Beta (BEA), Mordenite (MOR), Ultra Stable Y (USY), ZRP-5, etc. (Sun et al., 2015, Leung et al., 2010, Ramos et al., 2008). This research, however, focuses on hydroxy Sodalite (HS) and faujasite (zeolite-X) zeolite

type, which from limited reported research, have shown a potential for biodiesel production (Volli and Purkait, 2015, Makgaba and Daramola, 2015). The application of the various zeolites in biodiesel production, including few on the above of interest, is reported in section 2.7.1 (Table 2.6).

Catalysts in biodiesel production are classified into majorly two groups; homogeneous and heterogeneous catalysts and then further subdivided into three groups; The acids/bases of both homogeneous and heterogeneous catalysts and the enzyme of the heterogeneous catalysts (Fjerbaek et al., 2009, Haas et al., 2006, Meher et al., 2006). The controllable acidic property of zeolites generally classifies zeolites as either base or acid heterogeneous catalysts (Saifuddin et al., 2015). Classification of catalysts used in biodiesel production is schematically represented in Figure 2.6.

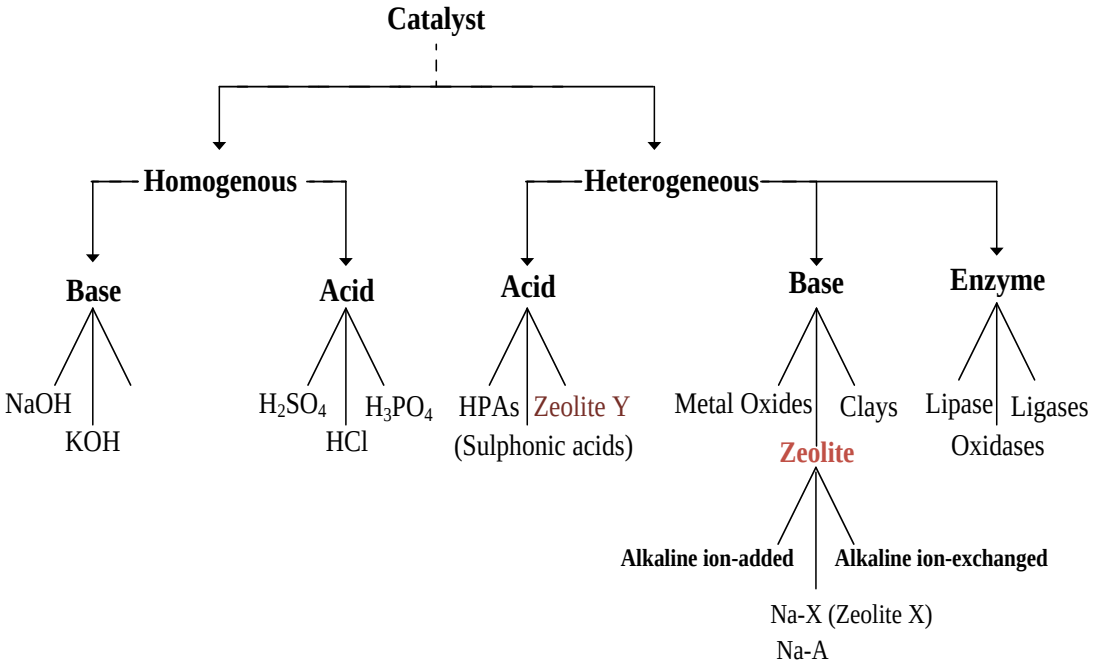

Figure 2.6. Classification and examples of catalysts in biodiesel production (Chouhan and Sarma, 2011, Saifuddin et al., 2015, Fjerbaek et al., 2009).

2.5 Synthesis of zeolites from coal fly ash

The alumino-silica content in fly ash as shown in Table 2.1 is also predominant in zeolites, making fly ash a suitable substrate feedstock for zeolites synthesis (Querol et al., 2002, Steenbruggen and Hollman, 1998). According to Babajide (2011), the fly ash itself prior to synthesis or modification, has demonstrated a minimum catalytic potential in biodiesel production. Currently, the use of fly ash (CFA) for zeolite synthesis accounts for only a minor proportion of the total amount generated as solid waste at power stations (Querol et al., 2002). In addition to zeolite synthesis, fly ash has also proven to be convertible to other value-added products, majorly such as those used in construction and ceramic applications (Zielke-Olivier and Vermeulen, 2016, Dwivedi and Jain, 2014). For decades, zeolite synthesis is prominently achieved via hydrothermal reactions (Cundy and Cox, 2003, Shumba et al., 2011). The reaction involves the dissolution of alumino-silicate content in fly ash in an alkali solution, followed by conversion to zeolite crystals (Murayama et al., 2002, Shumba et al., 2011). Murayama et al. (2002), Musyoka (2009) and Brassell (2017) gave a simple classification of the synthesis reaction into three primary mechanisms: the dissolution process, the condensation stage and the actual crystallisation stage of the synthesis.

During the first stage, the alumina-silicate matrix in fly ash dissolves in alkali solution, resulting in monomers and oligomers (Musyoka, 2009). In the second stage, the latter condense into specific precursor structures, as organised extended structures in the solution to form an alumino-silicate gel deposit. The stage path, as described, is also referred to as condensation gelation and additionally involves heterogeneous nucleation, followed by the formation of metal-oxygen bonds in zeolite structure (Cundy and Cox, 2003). The third step of crystallisation involves crystal growth from the formed gel, which then undergoes a hydrothermal process. This step consists of a series of depolymerisation and polymerization reactions under high-temperature conditions to yield the crystalline zeolite (Cundy and Cox, 2003). Cundy and Cox (2003) further mentioned that this step is known to be catalysed by an excess amount of hydroxyl ion. Figure 2.7 shows an illustrative mechanism of hydrothermal synthesis described above.

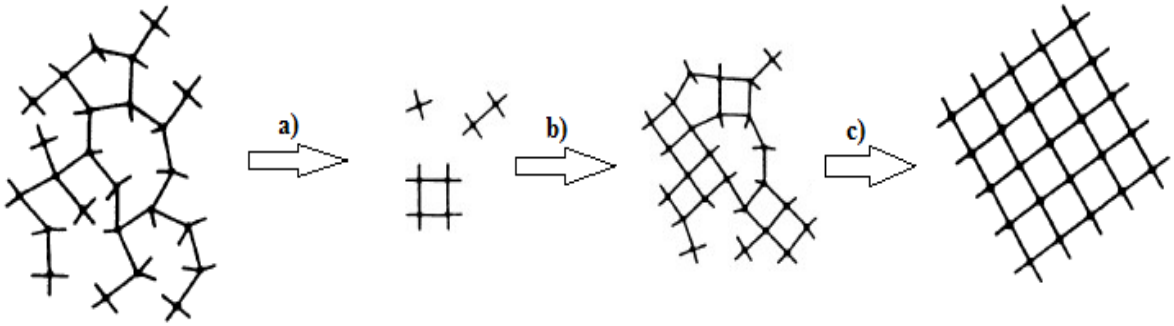

Figure 2. 7. Mechanism of hydrothermal synthesis; (a) Dissolution, (b) Condensation gelation and (c) Crystallisation (Cundy and Cox, 2003).

2.5.1 Influential parameters for zeolite synthesis

Controlled and optimum synthesis of zeolites from fly ash (CFA) by the hydrothermal method, as extensively reported in the literature to date (Querol et al., 2002, Steenbruggen and Hollman, 1998) is based on several parameters. These include the following:

(i) the type and concentration of the alkali source substance for the activation of fly ash (CFA);
(ii) the ratio of alkali activation solution to fly ash;
(iii) the aluminium-silicate content of the fly ash starting material; and
(iv) the mixing intensity and temperature of the alkali-fly ash solution in the first step of dissolution
(v) The hydrothermal reaction temperature and conversion time (third step of crystallisation).
(vi) The aluminium-silicate content of the CFA, as discussed later in this section, is a parameter that influences other parameters in either of the three mechanism steps of zeolite synthesis.

According to Murayama et al. (2002), the reaction mechanism of hydrothermal synthesis is not clarified adequately. The mechanism may vary depending on the type, yield or zeolite of interest. Nonetheless, a range of each of the parameters mentioned above for general zeolite synthesis (from fly ash) has been deduced from various literature. This may serve as the basis for zeolite synthesis in the present work. The details of each of the above parameters concerning hydrothermal processing are discussed in the following section.

2.5.1.1 Alkali source and concentration of alkali solution

Sodium hydroxide (NaOH) is the most common alkali source used for zeolites synthesis, compared to other sources in literature such as sodium carbonate (Na_2CO_3) and potassium hydroxide (KOH) (Querol et al., 2002). NaOH contains sodium ion (Na^+) whose concentration, unlike that of K^+, has been found to favourably control the rate of crystallisation during the hydrothermal reaction and has been reported to be the predominant factor for the entire reaction rate of zeolite formation (Murayama et al., 2002). Compared to sodium carbonate (Na_2CO_3), NaOH contains the peculiar hydroxide ion (OH^-) of which the concentration has been reported to favourably enhance the dissolution rate of fly ash during the dissolution step (Murayama et al., 2002). Further, increased dissolution and zeolite crystallization rate, lead to a decrease in the reaction time required for the crystallization process.

The concentration of the alkali solution is another parameter that influences the dissolution process during zeolite synthesis. Sodium hydroxide (NaOH) being preferred as distinguished above, has been reported by several researchers for dissolution of fly ah over a concentration range of between 1-5 M (Steenbruggen and Hollman, 1998, Querol et al., 2002, Murayama et al., 2002). The concentration parameter for zeolite or optimal zeolite synthesis can be a rate-determining step for crystallisation period and hence dictates the crystallisation temperature and type of zeolite to be produced (Querol et al., 2002). In order words, the selection of a particular alkali concentration is co-dependent upon the crystallisation temperature and time set for a particular zeolite type.

2.5.1.2 The ratio of alkali solution or water-to-fly ash ratio

Apart from the alkali NaOH concentration, zeolite synthesis is also influenced by the ratio of alkali solution to fly ash (e.g. NaOH/CFA) required for the dissolution step. Other than the alkali solution, many researchers have commonly used water instead and water content (which makes up the mentioned solution) can be interchangeably used to quantify the alkali solution required for the dissolution of fly ash. According to Brassell (2017) & Querol et al. (2002), an increase in water content when utilising fly ash for synthesis increases the rate of dissolution of both amorphous and crystalline components of fly ash. This consequently would result to increase in zeolite yield.

The selection of water to fly ash ratio (or alkaline solution) in the range of between 1-20 mL of the alkaline solution per gram of fly ash (water/CFA), has been reported and generally observed for zeolite synthesis from fly ash (Murayama et al., 2002, Querol et al., 2002, Volli, 2015).

The ratio of water/CFA required for zeolite synthesis nonetheless depends on the aluminium-silicate content of the fly ash starting material. Fly ash with high aluminium-silicate content will require a relatively low amount of water (i.e. the high ratio of alkali solution / CFA) to attain an optimal dissolution rate (Querol et al., 2002). This conversely applies to fly ash with high aluminium-silicate content; as it would only require a relatively low amount of water (alkali solution) for dissolution or extraction of aluminium-silicate content from fly ash.

2.5.1.3 The aluminium-silicate content of fly ash

The aluminium-silicate content of fly ash, commonly reported in the form of a silicon-to-aluminium ratio (Si/Al ratio), is another essential parameter that describes the properties of a resultant zeolite product (Sun et al., 2009). Si and Al content in fly ash, as reported in Figure 2.4 (section 2.4 of literature), make up the oxygen tetrahedral units and as a result, this parameter is a dictating agent for the microscopic structure of a zeolite product (Querol et al., 2002). The framework Si/Al ratio as also referred to (i.e. tetrahedral structures coordinated by aluminium-silicate content) in the literature (Ferreira Madeira et al., 2012), governs the acidity of a zeolite product and influences the cation exchange capacity (CEC) of both CFA starting material and the resultant zeolite product (Ferreira Madeira et al., 2012, Viswanadham et al., 2012, Querol et al., 2002). Consequently, the aluminium-silicate content (Si/Al ratio) as described, has an influence on the activation period required for coal fly ash conversion to a zeolite product (Querol et al., 2002).

2.5.1.4 Hydrothermal synthesis time

The hydrothermal reaction for zeolite synthesis is further influenced by the crystallisation temperature and conversion time.

Hydrothermal crystallisation time depends on several factors, among which Si/Al ratio has been mentioned earlier and further including the mineralogical composition of fly ash; and the

degree of dissolution step before crystallisation. However, crystallisation time for zeolite synthesis, in general, has been reported between the range of 6 and 48 hours (Murayama et al., 2002:3). For example, with the mineralogical content, a longer crystallisation period of between 24-48 hours is usually required for fly ash with high mineralogical (crystalline) content and conversely a shorter crystallisation period of between 6 to 12 hours for fly ash with low mineralogical content (Querol et al., 2002).

In contrast to mineralogical content and based on the disproportionality in the amount of mineralogical and aluminium-silica content observed in fly ash (Musyoka et al., 2011, Steenbruggen and Hollman, 1998), it is deduced that longer activation time is required for fly ash with low (amorphous) aluminium-silica content and vice versa. Based on the above discussed and as also deduced by Querol et al. (2002), the range of between 12 and 24 hours activation time would, therefore, be the average for general zeolite synthesis in favour to complete dissolution of mineralogical content of fly ash of any given aluminium-silica content. Other than the composition of fly ash starting material, crystallisation time for zeolite synthesis (under fixed conditions) is a dictating factor when targeting a particular zeolite type; as zeolites are distinguishable on basis of their phase density. Most zeolites are metastable and an increase in hydrothermal crystallisation time in the zeolitic phase, according to the Ostwald ripening theory will coarsen the sample into a denser or a more stable phase (Baldan, 2002, Brassell, 2017). It has been affirmed that the denser a zeolite phase, the smaller its pore size and the heavier the sample is more likely to be (Du Plessis, 2014, Querol et al., 2002). This is proven by the example of HS having a relatively smaller pore size than zeolite X (2.3 Å < 7.3 Å) and yet coherently denser than zeolite X (Querol et al., 2002, Brassell, 2017). This difference over a range of zeolites brings about increased stability and an increased hydrothermal synthesis time (under fixed standard conditions) (Brassell, 2017, Boycheva et al., 2015).

Linde F → Zeolite A → Faujasite (Zeolite X or Y) → Chabazite → NaP_1 → hydroxy sodalite.

It can be observed from the above trend that sodalite is denser (heavier and less porous) than zeolite X and hence an increase in hydrothermal reaction time over a duo-phase sample of sodalite-zeolite X, conforms to the Ostwald ripening theory whereby the precursor species condenses into a more dense sodalite phase (Baldan, 2002). Conversely, reduction in reaction time will promote the precursor species in the reaction mixture into the less dense zeolite X (Brassell, 2017).

2.5.1.5 Hydrothermal reaction temperature

A direct correlation between reaction time and temperature exists based on metastable behaviour of zeolites. Like crystallisation time, it is reported (Brassell, 2017, Belviso et al., 2010, Boycheva et al., 2015, Musyoka, 2009) that an increase in crystallisation temperature also favours the synthesis of a more dense phase zeolite in a precursor reaction mixture and vice versa (Belviso et al., 2009). For example, for a duo-phase mixture that competitively consists of zeolite X and hydroxysodalite of interest in this work, an increase in crystallisation temperature would favour the denser phase hydroxysodalite whereas the phase of the less dense zeolite X will become dominant at lower synthesis temperature.

In correlation to phase density, it is deduced that an increase in crystallisation temperature will result in a zeolite product with large particles (Molina and Poole, 2004). Further, high crystallisation temperature enhances the Si/Al ratio and based on this property, the crystallisation temperature is determinant of a particular zeolite type. The temperature range of 90-200 °C has been the generally reported for variety of synthesised zeolites (Steenbruggen and Hollman, 1998, Musyoka et al., 2011, Volli and Purkait, 2015). Based on the temperature classification for zeolite synthesis, this range is comprised of the low, and moderate temperature range of 90-120 °C and 120-180 °C, respectively. Below this range, is the ambient temperature range of between 25-60 °C and above is the high temperature range for zeolite synthesis of 250 °C and above (Musyoka, 2009). Synthesis of hydroxy sodalite to date, has been mostly reported within the moderate temperature range (Musyoka et al., 2011, Querol et al., 2002) whereas Zeolite X has been synthesised mostly within the low temperature (Volli and Purkait, 2015, Brassell, 2017).

Like hydrothermal synthesis time and as discussed above, the order of phase density or stability of zeolites with an increase in synthesis temperature has been generally deduced in the following order: Zeolite A (≤90 °C) → Zeolite X (90-120 °C) → NaP1 (90-150 °C) → HS (150-200 °C).

2.5.2 Zeolites hydrothermal synthesis methods

The various methods utilised for the conversion of fly ash to zeolites include the hydrothermal conversion method and the molten salt liquid free method. The hydrothermal method (HM), being the principle and most commonly method, is further subdivided into direct, fusion indirect (prior to HM) (also known as fusion-assisted), and two-step hydrothermal method (Bukhari et al., 2014).

The two-step hydrothermal method is a relatively longer synthesis approach whereby most commonly (either) the filtrate (or solid residue) of the solution of the alkaline-treated fly ash (obtained from either the direct or fusion method) is further hydrothermally treated. Zeolites synthesised from other methods have been generally reported to contain unreacted fly ash (far less than 100 % conversion). The two-step method has been introduced with the aim to obtain purer or maximally pure zeolite products (Hollman et al., 1999). In spite of high quality zeolite obtained, the two-step method is more likely to be energy intensive and required longer time and the method is usually associated with poor zeolite yield. For these reasons, the fusion-assisted and direct methods are deemed most useful for application in this research.

The fusion-assisted method of conversion involves the fusion of dry NaOH with fly ash at high temperature prior to hydrothermal treatment; whereas the direct method is a single- step hydrothermal treatment of fly ash with alkaline solution. Apparently, the fusion method is a more effective approach with regard to boosting the extraction of both silicon and aluminium from fly ash; while the direct method in most cases has rather proven to extract a considerable amount of silicon as compared to aluminium (Bukhari et al., 2014, Brassell, 2017, Mezni et al., 2011). Furthermore, the direct method involving leaching or dissolution of silicon and aluminum into the alkaline solution, apparently can result in zeolite products with a relatively high degree of purity, compared to fusion-obtained zeolites (Bukhari et al., 2014).

Zeolite X, as observed and generally reported by many researchers, has been primarily obtained by the fusion-assisted hydrothermal method (Volli and Purkait, 2015, Brassell, 2017). The fusion method is a more energy intensive approach (Musyoka et al., 2014); which further motivates this research to rather seek for an alternative (low siliceous) zeolite (with as much potential as zeolite X in biodiesel production), that can be rather obtained by a direct method from fly ash. Hydroxy sodalite is introduced in this regard as the alternative in question.

From literature, the synthesis of HS both from fly ash and from commercial chemical reagents has been mainly achieved via the direct hydrothermal method (Golbad et al., 2017, Henmi, 1987, Musyoka et al., 2011).

2.6. Modification of zeolite as catalyst for biodiesel

Heterogeneous catalysts possess a wide range of compositions, which allow them to be susceptible to high possibility of modification and reconstruction (Fernandes Machado et al., 2006). These features have allowed solid catalysts such as zeolites to be considered as excellent gas and liquid phase catalysts and as catalyst supports. Modification of heterogeneous catalysts in various studies have been intended to enhance their properties in view of a particular application (Machado et al., 2005)

For many decades, researchers have employed various modification routes for preparation of heterogeneous catalysts in biodiesel productions (Volli and Purkait, 2015, Babajide et al., 2012, Ramli et al., 2017). The most common approaches include the ion-exchange modification method, the incipient wetness impregnation (IWI) method, the bifunctional method, and the co-precipitation method (Chouhan and Sarma, 2011, Thangaraj et al., 2019, Ramli et al., 2017, Peternele et al., 2014).

Chouhan et al. and Babajide et al. in separate studies, reported the ion-exchange modification of Na-X with K^+ (derived from KOH) with the view to enhance the basicity of the catalyst for improved activity in biodiesel production (Chouhan and Sarma, 2011, Babajide et al., 2012). For the above modification the most effective cation is K^+ (potassium ion) due to its size and exchange capacity compared to other alkali earth metals (Babajide et al., 2012, Frising and Leflaive, 2008).

Catalyst modification by IWI, as per Babajide et al. (2012), was similarly identified as a potential approach for basicity enhancement of the catalyst. This method as reported by Aqliliriana et al. (2015) was employed on MgO catalyst (MgO impregnated with KOH) and resulted in more than 98 % biodiesel yield in the space of 20 minutes. The above modification approach has also been demonstrated on the prominent ZSM-5 zeolite-type with respect to several other applications (Silva et al., 2013).

The bifunctional method appears to be a most recent concept for modification of heterogeneous catalyst in biodiesel production. Heterogeneous catalysts to date have attracted global attention in research and progressively with time, have been considered as best candidates for biodiesel production (Ramli et al., 2017, Chouhan and Sarma, 2011). Nonetheless, to compensation for challenge experienced by use of low-cost feedstocks (such as FFA content) it is necessary to develop the heterogeneous catalysts further, so that it has the ability to simultaneously achieve esterification (FFA reduction) and transesterication (Lam et al., 2010). Bifunctional catalysts possess a duo acid-base characteristic. This aspect will be introduced in this work for the above purpose (Ramli et al., 2017).

2.7. Biodiesel production process (transesterification): method, chemistry and influential factors

The transesterification reaction, as introduced earlier, is the most common and effective method for producing biodiesel from biomass-derived oil (vegetable oils, animal fat, grease, etc.). In the course of the transesterification reaction, the triglyceride content in oil reacts with an alcohol (typically a short-chain alcohol such as methanol or ethanol) in the presence of a catalyst, to yield a mixture of fatty acid alkyl esters and glycerol (Volli, 2015). The former is commercially known as biodiesel. The chemistry of the reaction is presented in Figure 2.8.

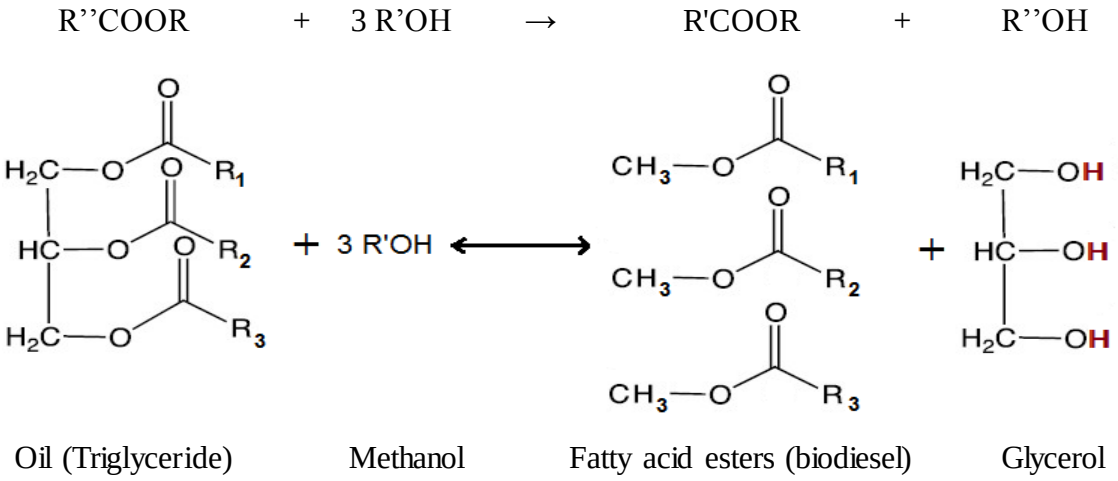

Figure 2.8. Chemistry of transesterification reaction for biodiesel production (Leung et al., 2010, Lam et al., 2010).

The triglyceride content in oil are esters constituting of 1 mol of glycerol and 3 moles of long-chain fatty acids (Lam et al., 2010). During transesterification, the triglycerides (TG) in question are converted stepwise to diglyceride (DG), monoglyceride (MG) and finally to glycerol; releasing 1 mole of fatty acid in the course of each step (Leung et al., 2010).

Methanol as depicted in Figure 2.7, is the preferred and most recommended alcohol because of its availability and low cost compared to ethanol and longer-chains alcohols (Leung et al., 2010, Saifuddin et al., 2015). Saifuddin et al. (2015) further reported that methanol in excess amount in the reaction mixture drives the movement of the transesterification reaction in the forward direction.

Other methods of biodiesel production reported earlier in this chapter 2 are mainly pyrolysis and microemulsions of oil or fats with solvents (Saifuddin et al., 2015). Biodiesel obtained via the transesterification method possesses several advantages over the other methods: higher cetane number, higher combustion efficiency (caloric value), lower carbon residue (greenhouse gases emissions) and lower viscosity (Leung et al., 2010). The reduced viscosity is indirectly observed in Figure 2.8, relating to the fact that the converted oil exhibits a smaller molecular structure corresponding to the size of regular diesel. The above-mentioned properties of biodiesel and their required specification values are listed in Table 2.7 (Section 2.7.2).

2.7.1 Operating conditions and their influence on the yield of biodiesel

In the open literature, five main parameters have been identified to have influence on the yield and quality of biodiesel. These include: free fatty acid (FFA) content in the oil feedstock; the type of alcohol and the alcohol molar ratio to oil; the nature and weight of catalyst in the reaction; the reaction temperature and time (Verma and Sharma, 2016).

2.7.1.1 Fatty acids in oil feedstock

Fatty acids content in natural vegetable oils and animal fats are regarded as impurities since these are obtained in crude form, by either solvent extraction or mechanical pressing (Lam et al., 2010). Fatty acids are responsible for soap formation during transesterification, and as a result interfere with separation of biodiesel from glycerol during washing. Many treatment methods have been proposed to reduce fatty acid contents in oils and these include steam

distillation, or fatty acid extraction by alcohol and esterification of the oil by acid catalysis (Leung et al., 2010). The latter being one of the methods, indirectly signifies that base catalysts are the most sensitive to fatty acid in oils. Esterification by acid catalysis prior to transesterification is the most feasible means of fatty acid reduction, as it retains and transforms fatty acid into biodiesel. It is deduced from Table 2.1 (section 2.2 of literature) that maggot oil (magOil) feedstock in this work contains a high concentration of Fatty acid (FFA), which will therefore pose a difficulty in handling and is surely considered as one of the influential parameters towards biodiesel yield in this work. To avoid this, generally FFA content in oil of less than 0.5-2 % has been recommended for base catalysts by various researchers (Ma and Hanna, 1999, Ramadhas et al., 2005, Lam et al., 2010).

2.7.1.2 Alcohol type and ratio

Methanol and ethanol are the most frequently used alcohols for transesterification (Reyero et al., 2015). Methanol however is preferred due to its relatively fast reactivity with oil and high dissolving power compared to ethanol (Ma and Hanna, 1999). The above properties have an impact on the reaction kinetics and as a result influence the yield of biodiesel. The molar ratio of alcohol to oil is another factor that has been reported to have an impact on the yield of biodiesel (Freedman et al., 1986, Leung et al., 2010). The minimum molar ratio of alcohol to oil is 3:1, which is the stoichiometric proportion of these two as reactants in the balanced chemical equation in Figure 2.4. However, since transesterification reaction is naturally reversible, an excess amount of alcohol is required to keep the reaction in the forward direction to obtain complete conversion of oil, increasing the yield of biodiesel (Leung and Guo, 2006). According to Leung et al. (2010), the excess amount of alcohol-oil molar ratio of 6:1 has been the mostly investigated in literature. Depending on the type of catalyst and FFA content in oil, such as base heterogeneous catalysts proposed in this work and as the most sensitive to FFA, the MeOH-oil molar ratio in such a case can even be adjusted to as high as 10:1.

2.7.1.3 Reaction temperature

Reaction temperature and time are other factors which generally are known to have an impact on the yield of biodiesel. An increase in reaction temperature normally increases the biodiesel yield. Raising the temperature decreases the viscosity of oil, enhancing the solubility of oil in

alcohol for the reaction, and enhancing the separation of FAME biodiesel from glycerol after the reaction (Verma and Sharma, 2016, Canakci and Van Gerpen, 1999, Nelson et al., 1996). Various researchers have reported on the temperature range from 50-60 °C as being the optimum for biodiesel yield (Leung and Guo, 2006, Ma and Hanna, 1999, Freedman et al., 1986). This however also depends on the properties of oil used, as for example in a study conducted by Vujicic et al. (2010) and Yunus et al. (2004) respectively, sunflower and palm oil resulted in optimum biodiesel yield at 80 °C (80 % and 98 % yield respectively). In contrast, in a study conducted by Darnoko and Cheryan (2000), a biodiesel yield of 98.8 % was attained at 55 °C for palm oil, which is within the optimum temperature range of 55-60 °C reported above.

2.7.1.4 Reaction time

Biodiesel yield increases typically with an increase in reaction time (Freedman et al., 1986). Unlike acid catalysts that have just been discussed above, base heterogeneous catalysts have been reported where the optimum reaction time was 2 hour (Verma and Sharma, 2016). In several other studies (Alamu et al., 2008)(Alamu et al., 2007; Leung et al., 2006), an optimum reaction time of even less than 1.5 hour has been reported for transesterification. Reaction time is also mainly dependent on the effect of temperature in reducing the viscosity of oil, or indirectly on the type of oil (Verma et al., 2016). The more the oil thickness is reduced, the more the solubility of the catalyst is enhanced in oil, and the shorter the reaction time required for transesterification.

2.7.1.5 Catalyst and catalyst loading

The presence of a catalyst is definitely crucial toward biodiesel yield, this being the area pursued by various researches and the main concern of catalyst development in this work. Catalysts that are used for biodiesel production through transesterification are classified as alkali, acid and enzyme catalysts (Meher et al., 2006). Alkali (base) catalysts to date have been found to be the most effective/active for transesterification (in terms of activity); of which sodium hydroxide (NaOH) is the most commonly used, inexpensive and generally the most

effective for transesterification as compared to potassium hydroxide (KOH), sodium methoxide (CH_3ONa) and calcium oxide (CaO) / metal oxides (Verma and Sharma, 2016).

The yield of biodiesel normally increases with an increase in catalyst weight or concentration, as most commonly applied for base heterogeneous catalysts (Leung et al., 2010, Verma and Sharma, 2016). However, for a typical homogenous base catalyst with the trend similar to that of other parameters, an increase in catalyst weight beyond the optimal concentration leads to a decrease in biodiesel yield (Verma and Sharma, 2016). The optimum range for NaOH is generally reported to be between 1 to 1.5 % (Leung et al., 2010, Verma and Sharma, 2016). Base catalysts as generally studied; have been reported to be used in the catalyst concentration range of 0.5 to 2.5 %. Nonetheless, several other studies to date have been conducted using up to 3, 5 and 10 % catalyst concentration, leading to over 95 % biodiesel yield (Viriya-empikul et al., 2010, Wei et al., 2009).

Acid catalysts, such as sulphuric (H_2SO_4), hydrochloric (HCl), phosphoric (H_3PO_4) and organic sulphonic acid are respectively the most investigated for transesterification. Their application is suitable for reducing fatty acid in oil and oil containing water, however with the disadvantage that these exhibit very slow reaction rates, require longer reaction times and more intense energy to achieve high biodiesel production yield. Moreover, a higher alcohol to oil ratio, as well as a higher catalyst concentration is required when using acid catalysts (Jacobson et al., 2008, Lam et al., 2010). Under such conditions, for example such as a temperature between 70 and 90 °C, MeOH/oil ratio of 20:1 to 245:1, catalyst loading of 4 to 42 % and 4 to 20-hour reaction time, Wang et al. (2006) and Zheng et al. (2006) reported that sulphuric acid typically reaches over 90 to 99 % biodiesel yield.

The application of HS and various zeolites in biodiesel production, the corresponding transesterification conditions and yield from various feedstocks, are reported in Table 2.6. The novel attention to HS as the catalyst from fly ash, in conjunction to maggot oil feedstock, is highlighted therein.

Table 2. 6. The use of HS (zeolite-X) and various zeolites in biodiesel production and operating conditions

Zeolites	Synthesis method	Source (Catalyst)	Feedstock	Yield (%)	Time (hr)	Temp.	CT loading (%)	MeOH/oil (n/n)	Reference
Na-X	Commercially obtained	Commercial obtained[(a)] (Fluka)	Sunflower	1.6%	7	60	10	6:1	Ramos et al. (2008)
Na-X	Not reported	Commercial reagents	Soybean	6.8	24	60	10	6:1	Di Serio et al. (2008), Babajide et al. (2011)
Na-X	Direct	Commercial reagents (Rice husk & Al metal)	Palm oil	-	2	70	~ 14 [(b)]	~47:1[(c)]	Pandiangan et al. (2017)
Na-X	Comm. obtained	Commercial obtained (*CWK, Bad Köstritz)	Sunflower	17.5	8	65	3%	6:1	Babajide et al. (2012)
Na-X	Not reported -	Coal fly ash	Sunflower	65.35	24	65	3%	6:1	Babajide et al., 2012
K/ Na-X[(d)]	Ion exchange -	-	Soybean	85.6	8	65	3%	10:1	Di Serio et al., 2008, Chouhan et al., 2010, Babajide (2011)
K/ Na-X	Fusion	Coal fly ash	Mustard oil	84.6	7	65	5	12:1	Volli (2015)
K/ Na-X[(d)]	Ion exchange -	Coal fly ash	Sunflower	85.1	24	65	3%	6:1	Babajide et al. (2012)
3Na-X[(e)]	Modified by IWI[(f)]	Commercial reagents	Sunflower	95.1	7	60	10	6:1	Ramos et al. (2008)
Na-HS	Direct hydrothermal	Commercial reagents	*WCO	-	6	60	3%	7.5:1	Makgaba et al. (2015)
Na-HS Na-X	Direct, fusion hydrothermal	Coal fly ash	Waste maggot oil	**Under investigation and optimisation**					**Proposed in this study**

[(a)] Chemicals commercially obtained (from Fluka). [(b)] Reported as 2.5 g/20 mL oil. [(c)] reported as 50 mL MeOH/25 mL of (palm) oil, where meOH and oil density are 0.792 and 0.893 g/mL respectively. [(d)] Na-X ion-exchanged with 10 % KOH loading. [(e)] Impregnated Na-X sample or Na-X loaded with 3 % excess Na per supercage. [(f)] Incipient Wetness Impregnation *Chemiewerk, German company that manufactures and sells chemicals *Waste cooking oil

2.7.2 Biodiesel properties and specification

In addition to the above, several other parameters that are used to account for the specification of biodiesel as obtained from oil are density, flash point, pour point, cloud point, acid value and heating value (Jaimasith and Phiyanalinmat, 2007).

In respect to the properties in question, biodiesel obtained by various researchers to date via transesterification, has proven to adhere to the international specification standards (ASTMD, EN). A typical example of biodiesel obtained from sunflower oil, in line with the required standards, is reported in Table 2.7.

Table 2.7. Physicochemical properties of biodiesel and required specification standards (Leung et al., 2010, Dias et al., 2009, Cooperation, 2009).

Properties	Sunflower		USA	Europe / S Afr.	Petroleum diesel
	Feedstock	Biodiesel	ASTMD 6751- 07b	EN14214:2003 / [c]SANS1935:2004	EN590:1999
	-	FAME[a]	FAEE[b]	FAME	DIESEL
Acid value (mg KOH/g)	-	-	0.8 max	0.5 max	-
Saponification value (mg KOH/g)		-	-	-	-
Iodine value (cg I / g)	132	142.7	-	120 max /140	-
Ester content (% m/m)	-	-	-	96.5 minimum	-
Density at 15℃– 20℃ (g/cm^3)	0.92	0.88	-	0.86-0.90	0.82-0.845
Kinematics viscosity at 40 ℃ (mm^2/s)	32.6	4.9	1.9-6.0	3.5-5.0	2.0-5.0
Refractive index	-	-	1.479	-	1.483
Pour point (℃)	-14	-	-	-16	-0.7
Cloud point (℃)	-	-	-	-	12.7
Cetane number (min)	-	49	47	51	51
Caloric heating value (MJ/kg)	-	45.3	-	38.4	42.9
Carbon residue (% m/m)	0.03	-	0.05 max	0.3 max	0.05
Flash point (℃)	272-274	-	130 minimum	101 min/120	76.7

[a] Fatty acid methyl ester; [b] Fatty acid ethyl ester; [c] South African National Standards

It is therefore crucial to identify the process parameters that are determinant in meeting the above biodiesel specifications through transesterification. The parameters in question are discussed in the following subsections.

2.7.3 Kinetics modelling of maggot oil transesterification

Biodiesel production in this work is mainly concerned with the utilisation potential of the waste-derived feedstock, coupled with the development of a suitable solid heterogeneous zeolite catalyst. Based on the nature of the catalysts to be employed, this work is further concerned with their on-going limitation of slow reaction rate (Chouhan and Sarma, 2011, Lam et al., 2010). According to literature, solid catalysts including those that are acidic nature, catalyse the transesterification reaction 400 times slower than conventional base homogeneous catalysts (Ramezani et al., 2010). Owing to the above, this work mainly seeks to evaluate and improve the kinetics of maggot oil transesterification over HS heterogeneous catalysts. By so, doing a kinetic model descriptive of the above reaction will be established. In literature, many researchers have reported on kinetic studies of various oil feedstocks, of which a typical feedstock includes soybean, castor oil and palm oil (Noureddini and Zhu, 1997b, Ramezani et al., 2010, Darnoko and Cheryan, 2000). There is however, no work to date that has been established on kinetics transesterification of maggot oil, which then is presented as a novelty from this work.

Transesterification reaction kinetics in this work is concerned with determining the rate of transesterification based on various kinetic parameters. In literature studies (Darnoko and Cheryan, 2000), it is been observed that evaluation and/or the effect of major variables that affect the rate of reaction; have usually been incorporated to support and define the kinetic parameters. Examples of above-mentioned variables include temperature, agitation mixing rate, oil feedstock composition, reaction time (conversion), etc.

With reference to Noureddini and Zhu (1997b), the kinetic parameters being explored in this work include the reaction rate constant and activation energy.

Various kinetic techniques can be used to evaluate the kinetic mechanism of transesterification. The commonly reported in literature include the pseudo-first order kinetics, pseudo second-

order kinetics and the first and second-order kinetics (Darnoko and Cheryan, 2000, Noureddini and Zhu, 1997b, Freedman et al., 1986).

The pseudo-first order kinetic mechanism is a simplified mechanism, which has been adopted for use in this work to assume a simple kinetic model. The mechanism, as reported in literature, has proven successful in defining the kinetics of the transesterification (Ramezani et al., 2010). The application of the above mechanism is however mainly applicable during the beginning periods of the reaction, with the assumption of reaction irreversibility and constant molar ratio of alcohol (due to an excess amount).

Many studies have revealed that transesterification, based on chemistry and as previously reported (section 2.7), is a non-elementary and reversible reaction (Lam et al., 2010, Noureddini and Zhu, 1997b). Stoichiometrically as depicted in Figure 2.7 (Section 2.7), the reaction of transesterification requires three moles of alcohol (methanol in this case) and one mole of the triglycerides. However in order to circumvent the reversibility of the reaction in favour of high conversion to methyl ester, the reaction often would require an excess supply of alcohol to drive the equilibrium forwards or toward the product (Leung et al., 2010). Hence, an excess alcohol beyond the stoichiometry, set to methanol-to-oil molar ratio of 6:1 and above, has often been required (Leung et al., 2010, Chouhan and Sarma, 2011). Based on such large (excess) proportion of methanol in relation to the oil, the assumption of constant molar concentration (negligible variation) of alcohol and irreversibility of the reaction has been made in attribution to the pseudo-first order kinetic mechanism (Ramezani et al., 2010). In other words, the pseudo-first order mechanism is founded on the assumption of reaction rate being mainly dependent on the triglyceride (TGA) concentration in the oil and negligible variation in alcohol concentration due at the beginning time of the reaction.

2.8 Gap analysis and research novelty

The current study involves the synthesis of hydroxy sodalite zeolites (HS) from fly ash in view of their use as heterogeneous catalysts in the transesterification of waste-derived maggot oil for biodiesel production.

First, this work exclusively highlights the use of two major industrial wastes, both serving as cheaper alternative feedstocks so as to alleviate the major challenge of high production costs

faced globally in the biodiesel industry (Gonfa Keneni et al., 2017, Lam et al., 2010). Many researchers have employed waste oil feedstocks (e.g. waste cooking/vegetable oil, waste animal oil) coupled with heterogeneous catalysts-derived from waste materials (Tshizanga et al., 2017), and these have certainly proven effective towards the yield, quality of biodiesel and reduction in the production cost. The challenge however still remains due to the fact that the feedstocks in question, tend to have a limited availability, unreliable supply (e.g. waste animal oil), and hence cannot be considered or recommended for either large scale or sustainable production of biodiesel. Unlike the above, the feedstocks of interest in this work (both maggot oil and fly ash) emerge with large availability (large industrial supply) and guarantee sustainability for scale up production.

Maggot oil extruded from black soldier fly (BSF) insects is commercially a waste-derived by-product which has only been produced from a limited number of established companies worldwide (Manzano-Agugliaro et al., 2012). From the leading waste-to-fly factory (AgriProtein, located in Cape Town, South Africa), the production of the protein meal being the main product, was escalated to over 2000 tonnes/year in less than two years (Agriprotein, 2017). The market demand of the main product has since then progressively risen and is predicted to continue to grow exponentially in the near future. This is coupled with rising production and supply of the by-product of interest, and consequently ensures sustainability of maggot oil as feedstock for biodiesel production. Fly ash on the other hand, being another major industrial by-product, accounts for a production of over 30 Mt tonnes annually in South Africa alone (Zielke-Olivier and Vermeulen, 2016). Of this, approximately 95 % is unutilised, which establishes its large availability as a feedstock for biodiesel value-added catalyst.

This work further, in addition to the catalyst being obtained from waste fly ash, considered both the synthesis and thorough optimisation of synthesis conditions with regard to obtaining a high quality HS zeolite or an optimally active for catalytic application in biodiesel production. It has been revealed through literature that synthesis conditions have an impact on the quality of a zeolite product (e.g. in catalytic properties) and its corresponding performance in a particular application (Ferreira Madeira et al., 2012). Several zeolites such as ZSM-5, Zeolite P, Zeolite A and most commonly Na-based Zeolite X are typically used (Ferreira Madeira et al., 2012, Murayama et al., 2002, Volli and Purkait, 2015). Volli and Purkait (2015) conducted a synthesis study based on Na-based Zeolite X and further optimised synthesis conditions with regard to CFA/NaOH ratio, pre-calcination fusion temperature and fusion synthesis time. The various conditions resulted to various qualities (e.g. crystallinity, CEC, and structure) of the

crystalline Na-X and corresponding performance in biodiesel production. Similarly, Zhang et al. (2013), also conducted a study on the synthesis optimisation of Na-X zeolite by varying the synthesis crystallisation time and temperature (Zhang et al., 2013). The above study however, was not conducted with respect to HS zeolite synthesis from coal fly ash. According to the author's knowledge, it is only a single study conducted by Nabavi et al. (2014) that demonstrated an optimisation synthesis attempt of HS by varying synthesis time and water molar ratio. The above study and the ultimately established conditions were prescribed exclusively for HS derived from non-fly ash conventional non-waste feedstock sources. Various other researchers have reported merely on the synthesis of the (HS) zeolite product at single particular prescribed or previously adopted conditions (Henmi, 1987, Luo et al., 2016, Golbad et al., 2017). This work therefore, presents itself as the only study, which could thoroughly optimise both the pre-synthesis and synthesis conditions of HS from waste fly ash material.

This work further investigates the synthesis and optimisation potential of HS zeolite via fusion-assisted hydrothermal method. The above method has not been reported with respect to HS synthesised from fly ash, and this is most probably due to the high energy requirement associated with calcination in the procedure (Musyoka et al., 2014), or because the method has been commonly applied upon zeolite (aluminosilicate-based) feedstocks that inherently possess a hard particulate nature (e.g. clay, rice husk) (Mezni et al., 2011, Nganoa et al., 2016, Pandiangan et al., 2017). This work by use of fly ash, presents itself as the only study that would possibly minimise the energy requirement imposed by the above synthesis route, by optimizing the synthesis time and temperature in conjunction to prepare a cost-effective and high quality HS product from fly ash. Consequently, this work further on, identifies itself as the first to establish a comparison study between the direct and fusion-assisted synthesis routes with respect to HS synthesis from fly ash.

Further to HS synthesis investigated in this work, the modification of the HS-zeolite by ion exchange with potassium (K) is also explored. To date, this approach in the open literature has been mainly effectuated on Na-X zeolite type (Babajide et al., 2012, Volli and Purkait, 2015, Di Serio et al., 2008) for biodiesel application, with the assumption that the zeolite in question possesses a high cation exchange capacity (CEC) (Querol et al., 2002). Nonetheless this work, in accord with the general view of zeolites' ability to accommodate a wide range of cations (Chouhan and Sarma, 2011), also presents itself as a novel study with respect to ion exchange modification of HS (fly ash-derived) for biodiesel production.

Further modification of the synthesised catalyst in this work, ought to involve the synthesis of bi-functional HS for improved catalytic application in biodiesel production. According to the author's best knowledge, the concept of bi-functional modification of catalysts in biodiesel production has been associated generally with heterogeneous catalysts (in general) (Ge et al., 1998, Ramli et al., 2017). The concept however, as from the open literature, seems not to have been yet reported with respect to zeolites (Ramli et al., 2017). This gap has motivated this work to further identify itself as the first (or among the few) to develop zeolite-based (precisely HS) bi-functional catalysts from the precursor synthesised catalysts.

Chapter Three
Materials and Methods

This chapter presents the detailed experimental methodologies and the materials employed in this study. These were carried out in order to achieve the objectives detailed in Chapter 1. The experimental approach includes feedstock oil analysis; catalyst preparation, modification and characterisation; and application of the prepared catalysts in the transesterification of maggot oil. This was coupled with characterisation of the produced biodiesel samples. The catalytic application stage of the experiment was extended to biodiesel production process optimisation and the kinetic evaluation of the process.

3.1 Material and Equipment

Coal fly ash (CFA) was obtained from Matla coal-fired power station located in the Mpumalanga province of South Africa (Figure 3.1). The coal fly ash was stored in an air-tight container and kept under dark conditions.

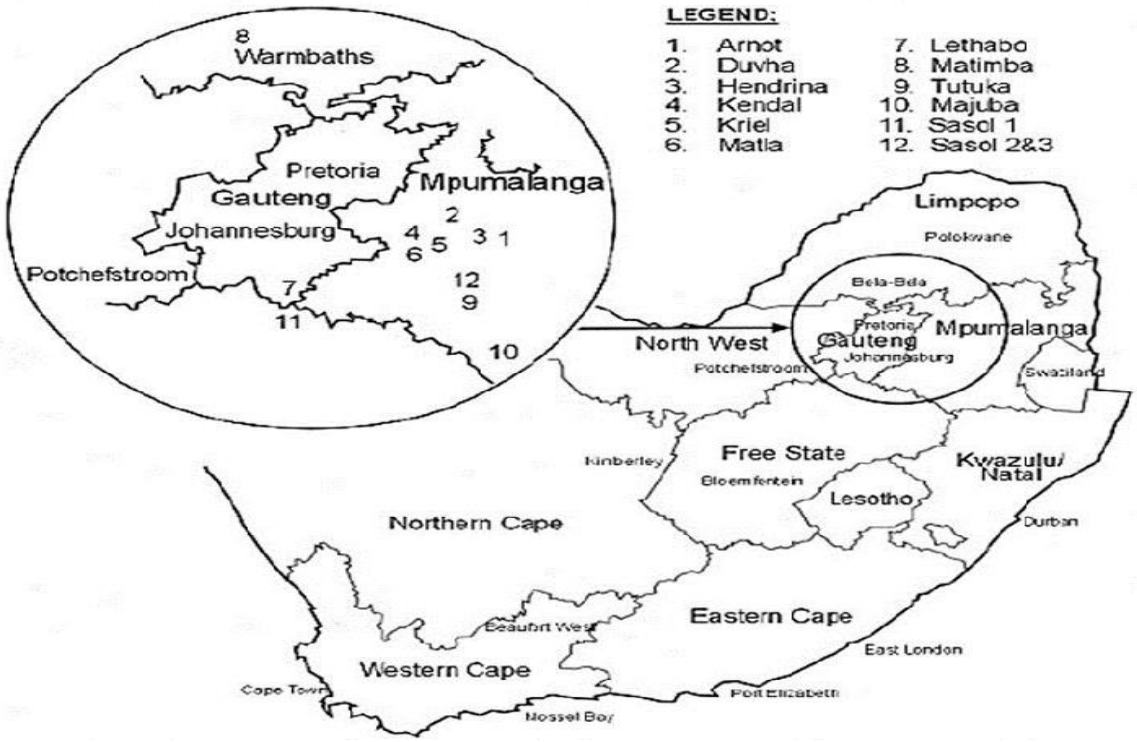

Figure 3. 1. Locations of Arnot and other various important coal power stations in South Africa (Krüger, 2003)

The in-house deionised water required in the synthesis of zeolite was obtained using laboratory water distillation equipment. Maggot oil, being the biodiesel feedstock of choice in this study, was obtained from AgriProtein Company, located in Cape Town, South Africa. The different reagents employed in the current study, their grades and sources, are listed in Table 3.1.

Table 3. 1. Material and reagents

Chemicals /reagents	Source	Grade / purity (%)
For Catalyst preparation		
Fly ash (CFA)	Arnot power station	-
Sodium hydroxide pellets	Kimix	98%
Potassium hydroxide pellets	Sigma Aldrich	85%
Sodium Aluminate	Sigma Aldrich	50-56 % Al_2O_3 & 40-45 % Na_2O
For oil analysis		
Ethanol	Science World	96%
Hydrochloric acid	Science world	32%
Diethyl Ether	Sigma Aldrich	99.0 - 99.8
Petroleum Ether	Merck	40-60 %
Chloroform	-	-
Sulphuric acid	Sigma Aldrich	98%
Toluene	-	-
Hexane	-	-
Isopropanol	CLEANSAFE	99.90%
Phenolphthalein indicator	Merck	1 % in ethanol
Iodine monochloride	Merck	-
Potassium Iodide	Merck	99%
Sodium Thiosulfate	CLEANSAFE	99%
Trichloroethane	-	-
Acetic acid glacial	CLEANSAFE	98%
For biodiesel production		
Maggot Oil	Agriprotein	Non-refined & refined
Sunflower oil (SFO)	Local Stores	Refined
Methanol	Science World	99.50%
		-

[a] (-) not recorded

3.2 Oil feedstock characterisation (oil analysis)

Free fatty acid (FFA) composition, acid value, saponification value, density and viscosity of maggot oil feedstock were determined so to assess its suitability as a feedstock for biodiesel production.

3.2.1 Sample preparation for free fatty acid characterisation

Fatty acid content of maggot oil (magOil) was determined according to the standard method developed by Agrifood analysis station. This was carried out in three stages, namely, digestion, extraction and methylation. In the first stage, 0.2 g of oil sample was placed in a 100 mL test-tube, and to it 2 mL of internal standard (undecanoic acid), 2 mL of ethanol and 10 mL of 32 % HCl were added. The obtained mixture was tightly sealed in the tube and transferred into a water bath where it was heated for fatty acid digestion (80 ºC; 40 minutes). The heated mixture was then allowed to cool at room temperature. In the second stage, 25 mL of diethyl ether and 25 mL of petroleum ether were added separately to the cooled mixture, and thoroughly shaken for 5 minutes after each addition. The resultant mixture was left to settle overnight. The separated layers, containing the digested fatty acids and the extraction solvents, were decanted into 250 ml beakers respectively. The mixture was then placed in the fume cupboard for 30 minutes to vent off the solvent content. 3 mL of diethyl ether and 3 mL of chloroform were added to the remainder oil (fatty acids) sample, which was then transferred into a 15 mL test tube. The sample was dried with nitrogen at 40 ºC. In the final stage, 2 mL H_2SO_4 and 1 ml toluene were added to the oil (fatty acid-extracted oil) sample at 100 ºC for 45 minutes. The resultant mixture (containing the fatty acids in ester form) was cooled to room temperature, after which 5 mL of deionized water was added to it followed by 1 mL of hexane, followed by settling to isolate the unreacted sulfuric acid and methanol. The top layer containing the methylated fatty acids was then dried with anhydrous Na_2SO_2. The remaining top layer, being the digested and methylated fatty acid sample, was transferred into a vial and sent for GC analysis for (fatty acid) characterisation (further described in section 3.2.1.1).

3.2.1.1 Fatty acid characterisation

The prepared oil feedstock from section 3.2.1, was compositionally characterized (for product identification and quantification) in a pre-calibrated GC system (model HP88 GC of 7890B)

(Agilent, USA) coupled with a flame ionization detector (GC-FID) and equipped with a polar capillary column. The column detects C_1-C_{12} as well as C_{12}–C_{23} hydrocarbons. The set injection volume of 1 µL of the oil sample was injected into the GC by a hydrogen carrier gas, flowing at the rate of 40 mL/min at injection temperature of 240 ºC. The initial oven temperature was set at 100 ºC for 5 minutes; and then raised to 250 ºC at the rate of 3 ºC/min for an additional period of 15 minutes. The various fatty acid constituents in the oil, as pre-calibrated by FAME standards, were detected at various retention times with respective weight proportions. The weight % (wt. %) of each FFA constituent was calculated using the respective peak area on the chromatograph as given by equation 3.1.

$$\boldsymbol{Weight\ \%\ FFA} = \frac{\boldsymbol{Area\ of\ FFA\ peak\ on\ the\ chromatograph}}{\boldsymbol{Sum\ of\ chromatogram\ peak\ areas - peak\ area\ of\ internal\ standard}} \times 100 \qquad (3.1)$$

The above procedure was also applied for the characterisation of FAME produced over the synthesised catalysts (Section 3.5.4). Further, the molecular weight (mw) of the characterized maggot oil, using the average molecular weight of the above obtained fatty acids (amw_{acid}) and that of glycerol present in the oil ($mw_{glycerol}$), was determined using equation 3.2 as per da Cunha et al. (2009). The above calculation was confirmed via the online Triglyceride Molecular weight Calculator (Biodiesel Education Program, 2017).

$$\text{Molecular weight (g/mol)} = 3(amw_{acid}) + mw_{glycerol} - 3(mw_{water}) \qquad (3.2)$$

Where amw_{acid} is the average molecular weight of fatty acids detected in the oil (g/mol)

$Mw_{glycerol}$ is the molecular weight of glycerol in the oil (g/mol) and

Mw_{water} is the molecular weight of water (g/mol) and

3.2.2 Determination of acid value

Acid value was determined according to ISO 1242:1999 through the titrimetric method of potassium hydroxide (KOH) solution into the oil (MagOil). 2 g of the oil was transferred into a 250 mL Erlenmeyer flask, and to this 10 mL of isopropanol and three drops of phenolphthalein indicator were added and mixed thoroughly (prior to titration). 5 mL of 0.1 N (N) potassium hydroxide solution (KOH) was charged into the burette and titrated into the oil containing mixture (while swirling) until the end point was attained (indicated by pink

persistent color for at most 30 seconds). The volume of the KOH solution consumed/titrated (V) was recorded and used to determine the acid value by equation 3.3. The above experiment was repeated three times and the average acid value of the oil was recorded.

$$\text{Acid value (mg KOH/g)} = \frac{V \times N \times 56.1}{M} \quad (3.3)$$

Where V is the volume of KOH solution consumed or titrated (mL)
N is the concentration of KOH solution (N)
M is the Mass (wt.) of oil taken (g)

3.2.3 Determination of saponification value

Saponification value (SV) was determined according to the ISO/ASTM standard by titration of the oil in the excess alcoholic medium/solution of potassium hydroxide. 1 g of oil was mixed with 25 mL of 0.5 M potassium hydroxide solution (in ethanol) and the mixture was heated to reflux for 90 minutes, and then cooled to room temperature. Droplets of phenolphthalein indicator were added to the mixture, followed by titration with a required volume of 0.5 M hydrochloric acid solution (V_{Hcl}) until the end point. The same protocol was followed (titration with hydrochloric acid) over the blank (V_B) mixture in a separate flask without the oil present. The experimental procedure was carried out in triplicate for oil sample so as to obtain the average SV using equation 3.4.

$$\text{SV (mg KOH/g oil)} = \frac{(V_B - V_{HCl}) \times N \times 56.1}{g\ of\ oil\ sample} \quad (3.4)$$

Where V_B volume of HCl solution required by the blank
V_{HCl} is the volume of HCl solution consumed or titrated (mL)
N, the concentration of HCl solution (N)

3.2.4 Density measurement

The oil density was measured according to the ASTM standard D1298 using an Anton Paar portable density meter DMA 35 (Anton Paar, Austria). Maggot oil as a fat solid state at room temperature was first preheated to 27 ºC so as to convert it to liquid form suitable for measurement Approximately 1 mL of the oil sample was injected into the instrument. The

measurement was immediately initiated; the reading was allowed to stabilize for a few seconds and then recorded. Interchangeably, density was measured via a more traditional method by using a 10 mL laboratory density bottle. Known volume of the oil (10 mL) was weighed and its mass was recorded with the weighing balance. The density was then calculated as a ratio of the mass to volume as given by equation 3.5.

$$\rho = \frac{mass}{volume} \tag{3.5}$$

3.2.5 Viscosity measurement

Viscosity of the feedstock oil, was determined using an Anton Paar Rheometer (model RheolabQc) (Anton Paar, Austria), operating on a rotational principle of a spindle. 20 mL of the oil sample was used for the measurement at a temperature set from 40 to 60 ºC. The instrument was coupled with RheoCompass software for data recording at various time and temperature intervals within the set range. The measurement was duplicated for maggot oil in its crude and purified form. Viscosity measurement was interchangeably determined at 40 °C using a Discovery HR-1 hybrid (DHR) rheometer (TA instruments, United States).

3.3 Catalyst preparation and modification

HS-zeolite product of interest was synthesised from fly ash via a direct hydrothermal method as well as a fusion-assisted method. Zeolite-X, being the other form of zeolite, was synthesised only via the fusion-assisted method. The direct synthesis method involved the dissolution of fly ash (at mild conditions) in an alkaline solution of sodium hydroxide followed by hydrothermal reaction. Whereas fusion-assisted method involved the fusion of NaOH with fly ash at high calcination temperature (550°C) prior to the hydrothermal reaction. The process flow diagram depicting the synthesis of HS via both methods is presented in Figure 3.2. Synthesis of zeolite-X via fusion-assisted method is depicted in Figure 3.3.

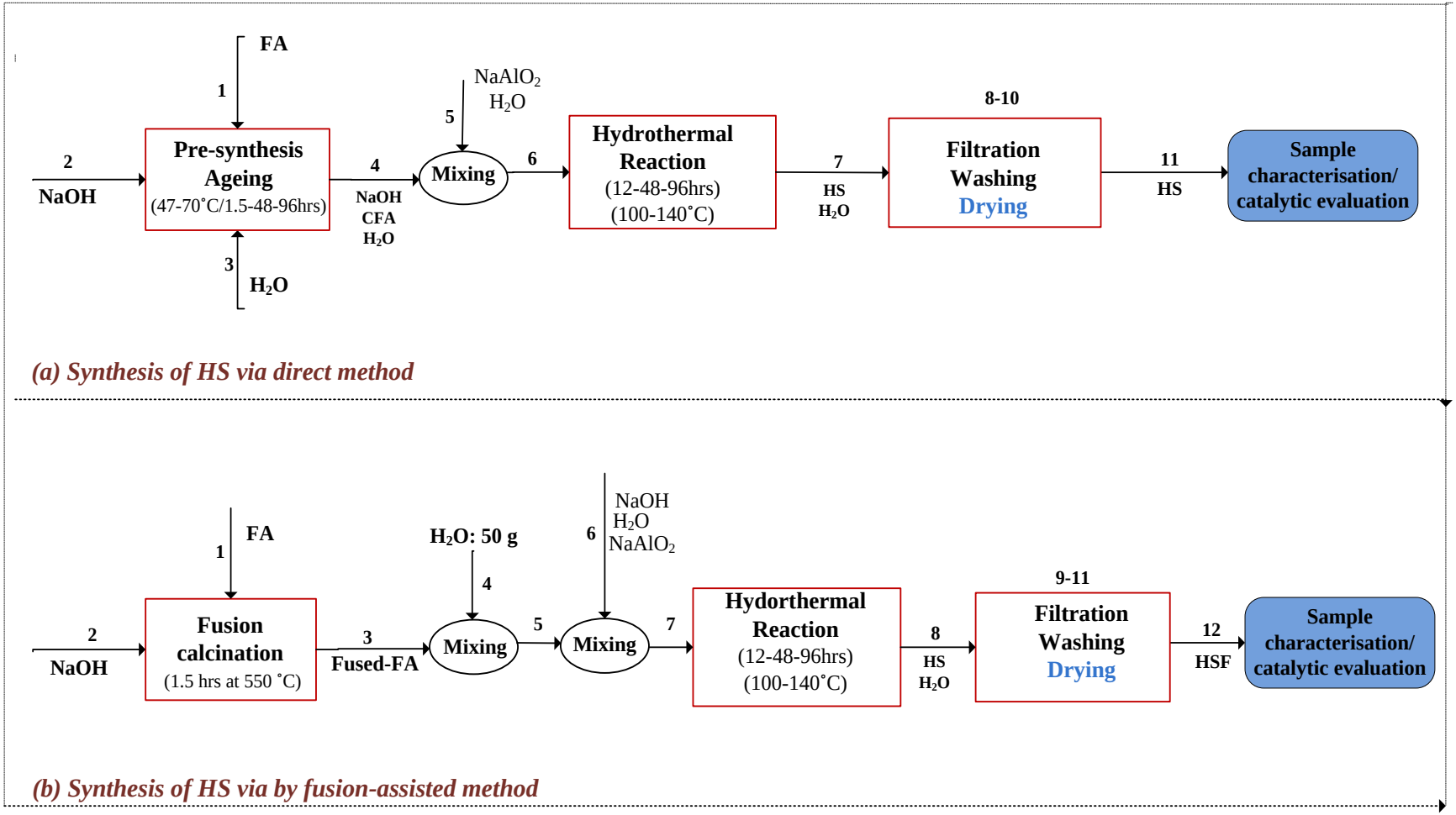

Figure 3. 2. Process flow depicting the synthesis of HS zeolite from CFA via **(a)** direct hydrothermal method, **(b)** fusion-assisted method

(Annotation 1-12 represent order of stream number of per chemical engineering standard of process flow diagram)

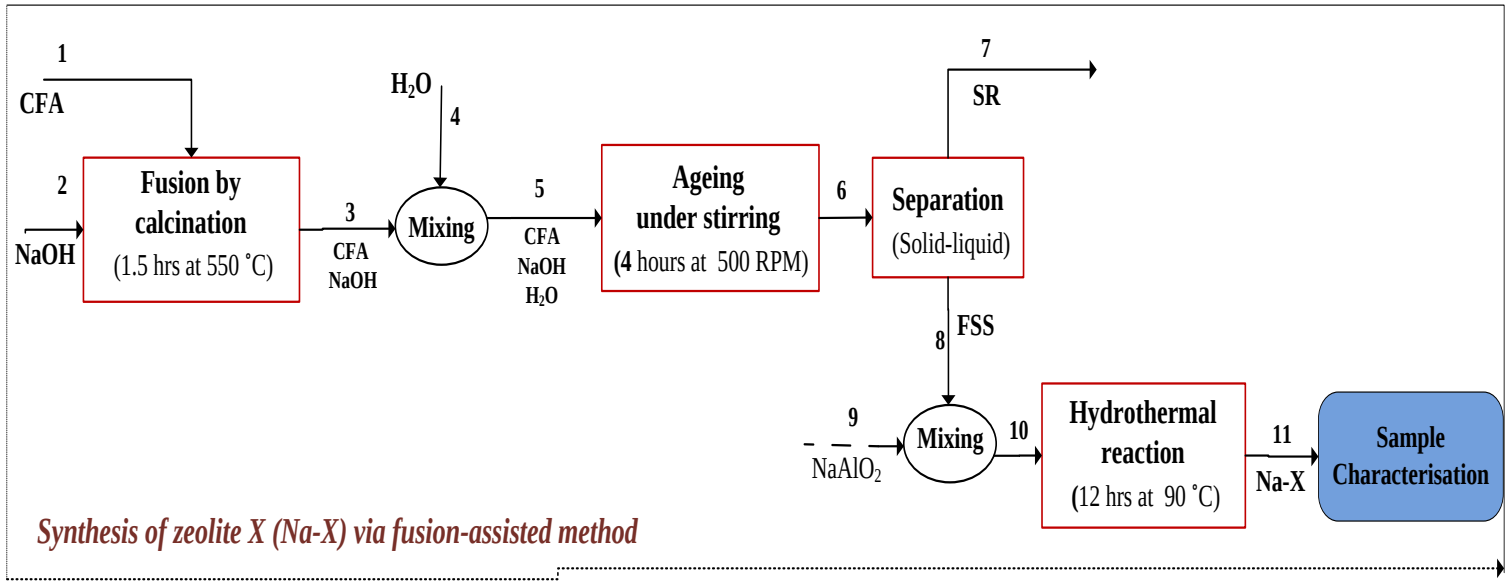

Figure 3. 3. Process flow depicting the synthesis of zeolite Na-X from coal fly ash via fusion-assisted hydrothermal method

3.3.1 Procedure for the preparation of hydroxy sodalite via direct hydrothermal method

Coal fly ash (CFA) was mixed with 5M solution of NaOH in a 250 mL polystyrene bottle, to achieve a feedstock of NaOH/CFA ratio a 1:1. CFA was initially dissolved in deionised water to form a slurry of 5:1 water/CFA mass ratio. The formed slurry was then subjected to ageing in an oil bath whilst stirring on a magnetic hotplate (47 °C, 800 rpm, and 48 hours). Subsequent to the ageing process, the resultant suspension was transferred into a 100 mL Teflon lined, stainless-steel autoclave, which was placed in an oven for hydrothermal crystallisation at 140 °C for 48 h. The resultant product was then cooled to room temperature, filtered through a vacuum filtration unit and thoroughly washed with deionised water until a filtrate with a pH of about 10 was obtained. The solid product was dried in an oven at 70 °C for 12 hours. The dried sample was weighed, stored for later catalytic application and a certain amount was characterised. The rest was stored for modification in the later stage of the experiment (section 3.3.4 and 3.3.5). This first sample was coded as sample HS-A48h (Table 3.2).

The above procedure was repeated by varying water/CFA ratio from the baseline ratio of 5:1 to 9:1, followed by the ratio of 12.5:1. This yielded samples with code names of HS-A48h,HS-A48h(7.5H_2O) and HS-A48h(12.5H_2O) respectively (Table 3.2). Following the same procedure at optimised water/CFA condition, the investigation of HS zeolite synthesis was carried out by varying the presynthesis ageing time from the initial 48-hour baseline to various prescribed ageing time (48 h, 96 h, 1.5 h). This was followed by varying the presynthesis ageing temperature (47, 70^{o}C) at fixed conditions as reported in Table 3.2. Consequently, samples coded with names HS-A96h, HS-A1.5h (or HS-47°C) and HS-70°C for the respective varying presynthesis ageing times and temperatures, were obtained. Further investigation was carried out by varying NaOH/CFA ratio from the initial 1:1 baseline to various prescribed ratio (1:1, 1.2:1, 1.3:1 and 1.4:1) at optimised condition of the previous investigated parameters and at fixed conditions. The yielded samples with corresponding code names obtained by varying the pre-synthesis conditions are reported in Table 3.2.

Further investigation of direct hydrothermal synthesis of HS zeolite, based on the optimised chemical and physical pre-synthesis ageing parameters above, was conducted by varying the hydrothermal synthesis time from the initial baseline to various prescribed condition (48, to 12, 24, 72 and 144 h) at 140 °C. The resultant samples in order of increasing synthesis time, were coded with names HS-12, HS-24, HS-48, HS-72 and HS-144 (Table 3.2). With further varying

synthesis temperature from 140 to 100 °C at 144 hours, as part of the investigation and following the exact same synthesis procedure, sample with a code name HS-144(100°C) was yielded (Table 3.2). The process flow diagram (PFD) depicting the above protocol procedure for the synthesis of HS zeolite from CFA at the various investigated conditions, is reported in Figure 3.1. Table 3.2 presents all the samples synthesised via the direct hydrothermal method, the various parameters investigated as per stage of experiment, and the corresponding code names of the produced samples.

Table 3.2. Code names of direct hydrothermal produced samples & corresponding synthesis conditions

Parameter investigated [(a)]	Sample code	Pre-synthesis parameter (physical & chemical)				Hydrothermal parameter	
		Water/CFA	**Ageing time (t)**	**Ageing temp. (°C)**	**NaOH/CFA**	Synthesis time	Synthesis temp
Water/CFA ratio	**HS-A48h**	**5:1**	48h	47°C	1:1	Synthesis time: 48h	Synthesis temp.: 140°C
	HS-A48h(9.5H_2O)	**9.5:1**	48h	47°C	1:1		
	HS-A48h(12.5H_2O)	**12.5**	48h	47°C	1:1		
Ageing time	HS-A48h	5:1	**48h**	47°C	1:1		
	HS-A96h	5:1	**96h**	47°C	1:1		
	HS-A1.5h	5:1	**1.5**	47°C	1:1		
Ageing temperature	HS-A1.5h / HS-A47°C	5:1	1.5	**47°C**	1:1		
	HS-A70°C	5:1	1.5	**70°C**	1:1		
NaOH/CFA ratio	HS-A70°C	5:1	1.5	70°C	**1:1**		
	HS-A70+1.2NaOH*	5:1	1.5	70°C	**1.2:1**		
	HS-A70+1.3NaOH	5:1	1.5	70°C	**1.3:1**		
	HS-A70+1.4NaOH	5:1	1.5	70°C	**1.4:1**		
Hydrothermal Synthesis time	HS-12	5:1	1.5	70°C	1:1	**12 h**	140 °C
	HS-24	5:1	1.5	70°C	1:1	**24h**	140 °C
	HS-48*	5:1	1.5	70°C	1:1	**48h**	140 °C
	HS-72	5:1	1.5	70°C	1:1	**72h**	140 °C
	HS-144	5:1	1.5	70°C	1:1	**144h**	140 °C
Synthesis temp.	HS-144(100°C)	5:1	1.5	70°C	1:1	144h	**100°C**

Ageing at fixed stirring conditions of 800 rpm for all direct method presynthesis stages in this work; & amount of $NaAlO_2$ = 20mL of 0.6M

***HS-A70+1.2NaOH** = HS-48; $NaAlO_2$: 20mL of 0.6M

Table 3.3. Code names of fusion hydrothermal, modified and Zeolite X produced samples & corresponding synthesis conditions

Parameter investigated [(a)]	Sample code	Pre-synthesis parameter (physical & chemical)				Hydrothermal parameter	
		Fusion temp. & time	**Ageing process**	**Water/CFA**	**NaOH/CFA**	Synthesis time	Synthesis temp
Synthesis time	HSF-12	550 °C, 1.5h	-	5:1	1.2:1	**12h**	100°C
	HSF-24	550 °C, 1.5h	-	5:1	1.2:1	**24h**	100°C
	HSF-48	550 °C, 1.5h	-	5:1	1.2:1	**48h**	100°C
	HSF-72	550 °C, 1.5h	-	5:1	1.2:1	**72h**	100°C
	HSF-144	550 °C, 1.5h	-	5:1	1.2:1	**144h**	100°C
NaOH/CFA	Na-X (1.1)	550 °C, 1.5h	25°C, 4h (550 rpm)	5:1	**1:1**	12h	90 °C
	Na-X (1.2)	550 °C, 1.5h	25°C, 4h (550 rpm)	5:1	**1.2:1**	12h	90 °C
		Modification parameters (conditions)					
K^+ Ion exchange	K/HS-144 (100°C) **K/HSF-144**	Ion exchange conditions: 70°C, 24 h, Post calcination: 550°C, 2h				-	-
Bifunctional modification	**Bi/ HS-144(100°C)**	Ion exchange conditions: 80°C, 24 h Calcination: 550°C, 6hrs Hydration: 6h, 60°C				-	-
	Varied parameter conditions of NaOH/CFA ratio (1:1, 1:2) and synthesis time (12h, 24144h)						

Amount of $NaAlO_2$ for all runs = 20mL of 0.6M ; *Optimised condition from previous stage of experiment and kept fixed in all the next stages

3.3.2 Procedure for the preparation of hydroxy sodalite via fusion-assisted hydrothermal method

The procedure for synthesis via the fusion-assisted hydrothermal method was adopted from Musyoka (2009). Similar to the direct method earlier described, 12 g of dry NaOH was mixed with 10 g of coal fly ash feedstock in powder form to achieve a 1.2:1 mass ratio of NaOH to CFA. The obtained mixture was crushed in a mortar and pestle crucible, then calcined in a muffle furnace (550 °C, 1.5 h). 10 g of the fused-fly ash was mixed with deionised water at ratio of 5:1 fused-fly-to-water, labelled as solution 1. On the other hand, solution 2 was formed by dissolving 1.2 g of dry NaOH into a 20 mL of water (~20g), and to this 0.6 g of $NaAlO_2$ was added and mixed to achieve a concentration of 0.6 M $NaAlO_2$ in the solution. Solutions 1 and 2 were then both transferred into the 100 mL Teflon-lined autoclave, mixed for 10 minutes prior to hydrothermal synthesis reaction at 100 °C for various synthesis time periods (same as investigated earlier for direct method. i.e. 12, 24, 48, 72 and 144 hours). Following the above reaction, the same downstream steps as was previously described for the direct method (Section 3.3.1), were applied. Similarly, the obtained dried products were stored for later application as catalysts, an amount from each was sent for characterisation, and the remaining kept for sample modification in section 3.3.4 and section 3.3.5. The produced samples corresponding to the various synthesis time and in order of the increasing condition at 100 °C are listed in Table 3.3. with code names HSF-12, HSF-24, HSF-48, HSF-72 and HSF-144. The process flow diagram depicting the synthesis of the above samples via the fusion-assisted method is incorporated with that of the direct synthesis method in Figure 3.2.

3.3.3 Determination of the yield and process material balance

For either synthesis route applied for the preparation of HS zeolite, the yield for the direct and fusion-assisted hydrothermal products obtained exclusively at optimised conditions (including for those of modified samples in section 3.3.5) was determined as per Bukhari et al. (2014) using equation 3.6

$$Yield\ (\%) = \frac{mass\ of\ zeolite\ product\ obtained}{mass\ of\ precusor\ CFA+NaOH} \text{ x } 100 \qquad (3.6)$$

To substantiate for the product yields obtained by either hydrothermal synthesis route for HS zeolite at optimum conditions, a material balance was conducted across each synthesis stage unit illustrated in Figure 3.1. This was achieved by weighing the mass of the input, intermediate and final materials throughout the synthesis process.

3.3.4 Procedure for the preparation of zeolite X (Na-X)

Zeolite X (Na-X) was synthesised via the fusion-assisted method. The procedure used to synthesise this product, was adopted from work done by Brassell (2017) and Musyoka et al. (2014). Coal fly ash was mixed with NaOH pellets in a mortar and pestle crucible at a NaOH/CFA mass ratio of 1:1. The mixture was crushed, thoroughly mixed, then calcined in a muffle furnace (550 °C, 1.5 hours). The fused fly ash was cooled to room temperature. This was followed by the addition of deionised water to achieve water/CFA mass ratio of 5:1. The resultant fused fly ash suspension was then aged (4 hours, 500 rpm and room temperature). The aged suspension was filtered to separate the supernatant from the solid residue (SR). The latter was dried in an oven overnight at 70 °C and stored. The supernatant filtrate (SF) on the other hand, was subject to adjustment of Si/Al ratio required for zeolite-X (Na-X) form of zeolite. For this, a certain amount of $NaAlO_2$ was added to the filtrate at a mass ratio of 1:10 of $NaAlO_2$. The mixture was then allowed to stir for 10 minutes, followed by transfer into the Teflon-lined autoclave reactor for hydrothermal reaction (crystallisation) for 12 hours at 90 °C. Following the reaction, the resultant product was cooled to room temperature, filtered, washed and dried at 70 °C for 12 hours. The dried solid product was weighed, and coded with the name Na-X (1.1NaOH) (Table 3.3). A certain amount of the produced product was sent for characterisation,

and the other portion stored for use as catalyst in the transesterification of maggot oil. The synthesis of zeolite Na-X was repeated by varying the mass ratio of NaOH/CFA in the synthesis mixture from 1:1 to 1.2:1, and following the above procedure at fixed conditions to produce a sample with the code name Na-X(1.2NaOH) (Table 3.3). Like HS zeolite (section 3.3.1-3.3.2), the yield of Na-X zeolite obtained from either case, was also determined using equation 3.6 (section 3.3.3). The process diagram depicting the above-described synthesis procedure for zeolite Na-X, is presented in Figure 3.2 (section 3.3).

3.3.5 Catalyst modification by ion exchange and bifunctional method

Sample HS-144(100°C) and HSF-144 highlighted or among those produced in section 3.3.1-3.3.2, were selected for ion exchange and bifunctional modification. The selection of these samples was based on their best-exhibited properties and catalytic performance in the transesterification of maggot oil (Chapter 5 and Chapter 6, section 6.1). The K^+ ion-exchange modification of the selected sample in a KOH solution was performed according to the procedure described by Babajide et al. (2012) and Shabani (2017). The above modification was conducted with a view to further improve the sample's performance in the transesterification of maggot oil. A 1g of the selected synthesised HS, was mixed into a 180 mL 1 M prepared solution of KOH at a mass ratio of 1:10 (HS/soln). The resultant mixture was then ion-exchanged under stirring (800 rpm) over a hotplate for 24 hours at 70 °C. Following this operation, the resultant slurry was filtered, washed (with deionised water) and dried at 120 °C for 24 hours. The dry solid sample was then calcined in a muffle furnace at 550 °C for 1.5 hours. The final solid product was weighed to account for the yield (equation 3.6, section 3.3.3), a certain amount stored for evaluation in biodiesel production, and the remaining amount was sent for characterisation as detailed in section 3.5. The produced modified zeolite samples listed in Table 3.3 (section 3.3.1), were coded as K/HS-144(100°C) and K/HSF-144.

3.3.5 Bifunctional modification

Bifunctional modification of the produced HS zeolite was conducted by adopting the procedure described by Volli (2015). Sample HS-144(100°C) was selected for the modification, owing to its best HS zeolite characteristic among the direct method samples and better performance in biodiesel production. The process flow diagram depicting the bifunctional modification of the HS zeolite sample and including all the reagents required thereof, is presented in Figure 3.4

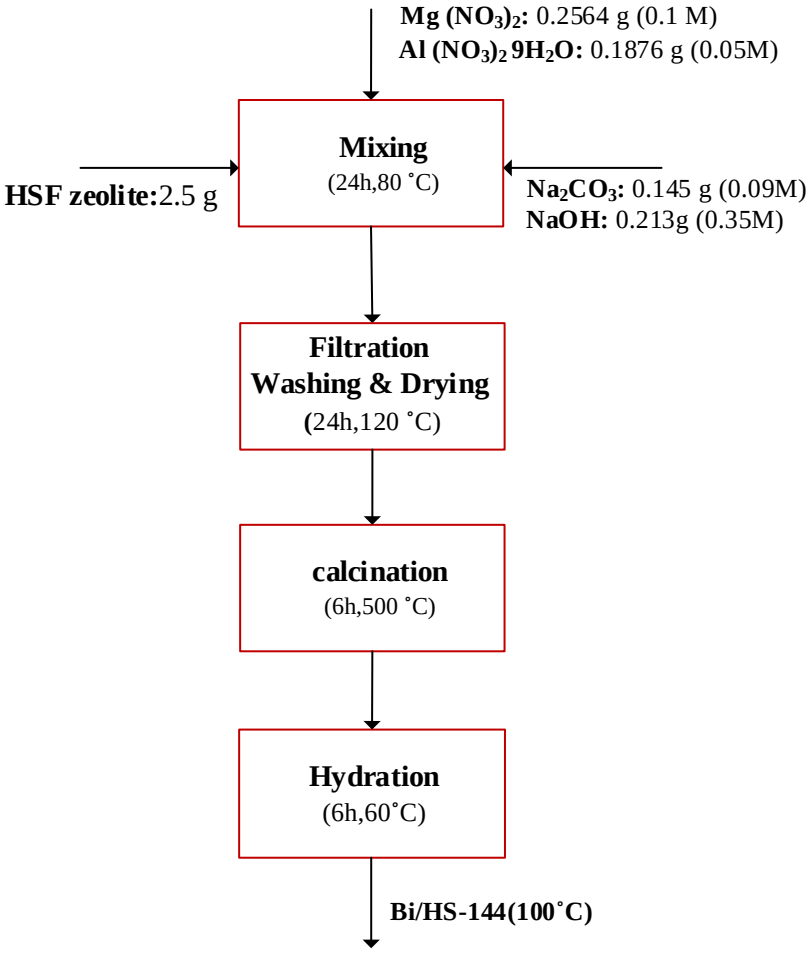

Figure 3. 4. Process flow depicting bifunctional modification of HS zeolite [HSF: fusion-assisted derived hydroxy sodalite, precursor sample to the modification and the bifunctional-modified hydroxy sodalite, Bi/HS]

The produced bifunctional modified sample was coded as Bi/HS(100°C) and also listed in Table 3.3. Like previously, the yield of the obtained sample was determined using equation 3.6 (section 3.3.3), a portion of the sample was sent for prescribed characterisation in section 3.5, and the remaining amount was stored for biodiesel catalytic evaluation.

3.4 Coal fly ash and catalyst sample characterisation

All the synthesised samples (Section 3.3.1-3.3.4) were characterised using X-Ray diffraction (XRD), Fourier transform infrared (FTIR), Scanning electron microscopy (SEM) coupled with energy-dispersive spectroscopy (EDS), and Brunauer–Emmett–Teller (BET) coupled with the

Barret-Joyner-Halenda (BJH) measurement. The as-received coal fly ash was also characterised using all the above techniques, except the BET measurement.

XRD is the qualitative analysis of the mineral and amorphous phases in crystalline samples. The analysis was conducted to determine the mineralogical phases (purity or composition/concentration), crystallinity and estimate crystal size of the produced catalyst samples, using a Bruker AXS, equipped with LynxEye detector and operating with Cu-Kα radiation (ńKα1 = 1.5406 Å) at 40 kV and 40 mA. The raw XRD data of the characterised samples were afterwards interpreted with the aid of the Origin analysis software (version 8.5). The identification of the HS phase of interest was conducted using the standard and simulated XRD material data of sodalite, obtained from the database of the International Zeolite Association (IZA) (Treacy and Higgins, 2007). The same applied with other phases that were identified/detected in various synthesised samples such as zeolite Na-X (X), zeolite Na-P (P), Zeolite Na-A and unconverted crystalline phases of mullite (M), quarts (Q) and magnetite (Mag) in coal fly ash (CFA). Phase crystallinity of each synthesised sample, with reference to HS zeolite, was determined as a relative crystallinity as prescribed by Ameh et al. (2017), Du Plessis (2014) and Stepto and Szostak (1998). That is, as the ratio of the sum of the peak areas of HS crystalline phase (of interest) in the pattern of a synthesised sample over the sum of peak areas of HS phase in the pattern of the reference sample (equation 3.7). The reference sample was selected based on the highest sum of areas of HS peaks identified, of which the crystallinity with regard to HS phase was assigned as 100 %. In addition to HS phase crystallinity, mineralogical purity of synthesised samples with respect to HS phase present therein, was determined as prescribed by Brassell (2017) and Volli (2015). That is, as the ratio of the sum of the areas of assigned peaks of HS over the sum of the areas of all assigned peaks of phases (all crystalline + all amorphous phases) present in the samples (equation 3.8). The area of the peaks for the existing phases in the XRD patterns in both cases (phase crystallinity and purity), was estimated using the Gaussian multiple peak fit functions (Origin software). The algebraic expression of phase crystallinity in percentage (%), and that of HS mineralogical phase purity, are given by equation 3.7 and equation 3.8 respectively

$$\%\ \text{relative crystallinity} = \frac{\text{Sum of areas of the crystalline phase of interest (CPI)}}{\text{Sum of the area of CPI in the reference sample}} \times 100 \qquad (3.7)$$

$$\% \text{ phase purity} = \frac{\text{Sum of areas of the crystalline phase of interest (CPI)}}{\text{sum of areas of all crystalline and amorphous phases}} \times 100 \quad (3.8)$$

The average crystal size of the synthesised samples was determined using the Scherrer equation presented by equation 3.9.

$$B(2\theta) = \frac{K\lambda}{LCos\theta} \quad (3.9)$$

Where L is the average crystallite size of interest in the sample in nm,
B is the average peak Width or Full Width at Half maximum (FWHM),
θ is the diffraction angle in degree (converted to Radians)

The SEM-EDS is a qualitative analysis used to gain insight of the transformations which have taken place in terms of the crystal morphology and elemental composition of reactant and product, during hydrothermal treatment. The (SEM-EDS) analysis was used to determine the elemental composition, crystal morphology and to estimate the porosity of synthesised samples (in conjuction with BET or BJH measurements). The analysis was performed using a high magnification ZeiSS Gemini Auriga instrument, equipped with a CDU-lad detector operating at 25 kV. Powder of each sample was mounted on a stub coated with carbon conductive tape. Over this, the SEM-EDS (data) mapping spectra were generated at three different regions of each sample. The resultant data were used to determine the crystal morphology and elemental composition of each synthesised sample. The data of the EDS elemental composition were obtained as the average detected at each spectrum region and normalised without accounting for carbon content derived from coating.

The Fourier transform infrared (FT-IR) analysis is one that provides information or monitors the corresponding changes in the molecular structure of a sample. The analysis was used to determine the structural configuration of the synthesised samples and was performed using a Perkin Elmer 100 FT-IR instrument (coupled with a computer programme). Approximately 60 mg of fly ash and produced samples in each case was placed in the sample holder of the instrument, whereby the instrument generated the sample configuration data in the set range of between 450 and 2000 cm^{-1}. The analysis was also performed on the oil sample, and compared to the IR-spectra of sunflower and palm oil for further characterisation purpose.

BET is an important physical-surface analysis of a crystalline sample that uses the gravimetric nitrogen Brunauer–Emmett–Teller (N_2-BET). In this study, the Brunauer–Emmett–Teller

(BET) was used to determine the total surface area of selected zeolite samples by Nitrogen (N_2) adsorption and desorption. External surface area, micropore area and micropore volume were determined using the t-plot method/analysis. The Barret-Joyner-Halenda (BJH) was used to determine the total pore volumes (by single point) and average pore width (or diameter) by adsorption and desorption technique. An amount of 0.317 g of the selected samples in each case, was outgassed at 110 °C on the Flow Prep 060 using helium gas. A 3Flex micromeritics instrument (3Flex version 5.00, serial # 990) was used with nitrogen as the analysis gas, to measure the adsorption-desorption isotherms at 77.6 K for 5 hours

3.5 Biodiesel production and characterisation

The application of synthesised samples as catalysts in the transesterification of maggot oil, was conducted in a batch-biodiesel production unit illustrated in Figure 3.5. This consisted of a 250 mL, three-neck, round bottom flask equipped with a reflux condenser, over a laboratory hotplate (Figure 3.5).

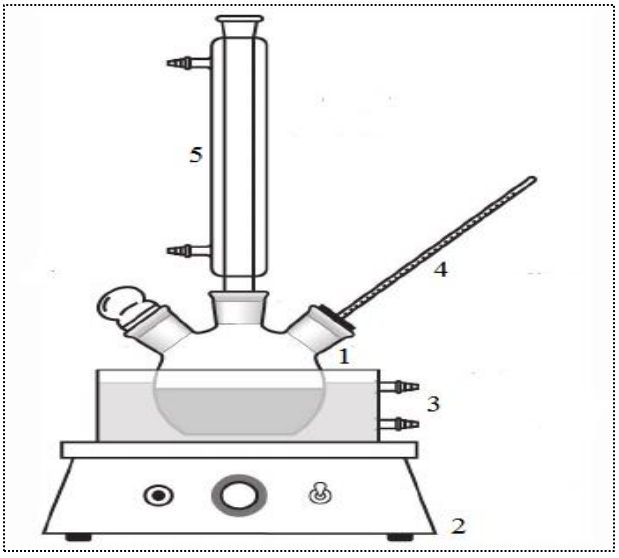

Figure 3. 5. Illustration of the batch-biodiesel production unit used for the transesterification of maggot oil. Equipment (1) Round-bottom flask; (2) Magnetic Stirrer; (3) recirculating water bath; (4) Thermometer and (5) reflux condenser.

3.5.1 Procedure for biodiesel production over synthesised catalyst samples

20 g of feedstock oil was weighed and preheated in the round-bottom flask to 60 °C (selected reference temperature) prior to reaction. 0.5 g of a selected catalyst sample (corresponding to 1.5 % weight of the catalyst to the oil) was weighed and mixed with methanol of an amount equivalent to 6:1 meOH/oil molar ratio (~12 g). The above mixture was then added to the preheated oil in the flask, mixed prior to transesterification (trans.) at 60 °C for a period of 1.5 hours. The reaction was conducted over a magnetic hotplate stirrer as illustrated in Figure 3.5, with the mixture stirring at 400 rpm. The above initial transesterification conditions were adopted from literature and set as baseline in this study (Leung et al., 2010, Alamu et al., 2008, Verma and Sharma, 2016, Ramezani et al., 2010, Ma and Hanna, 1999). The resultant product mixture was cooled to room temperature; the product was centrifuged for 10 minutes to separate the various phases present and the catalyst thereof. The spent catalyst was recovered by taping it out from the bottom of centrifuge tube, dried and stored. The phase containing glycerol, unreacted methanol, water and traces of unrecovered catalyst was tapped off from the biodiesel phase via a separating flask. The phase containing biodiesel was then washed several times with preheated deionised water of 60 °C, until the wash water became clear. The washed biodiesel was transferred into a 75 mL beaker, in which this was dried by heat and addition of sodium sulphate (Na_2SO_4) dehydrant. The biodiesel product was then cooled to 40 °C, immediately weighed and stored in a 50 mL test-tube prior to characterisation. The yield of biodiesel as depicted in equation 3.9 was determined as the ratio of the mass of the biodiesel obtained over the initial mass of the feedstock fed.

$$BD\ yield\ (\%) = \frac{Mass\ of\ biodiesel\ obtained,\ g}{Mass\ of\ oil\ feedstock,\ g} \times 100 \tag{3.9}$$

The process flow diagram depicting the above-described procedure for biodiesel production is presented in Figure 3.6.

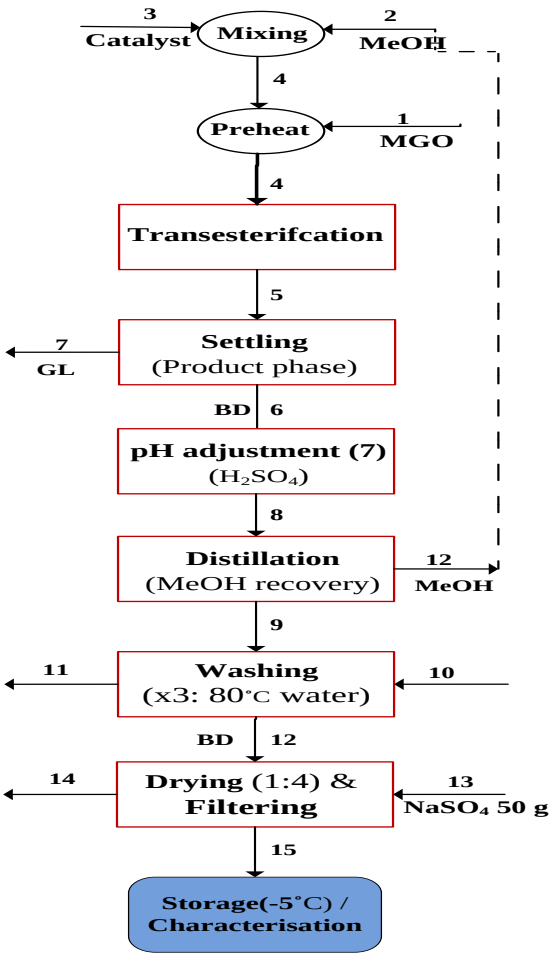

Figure 3.6. Process flow depicting the biodiesel production procedure from maggot oil over synthesised catalyst sample (BD, biodiesel; GL glycerol).

The above procedure was repeated at various conditions of temperature (50, 65 °C), MeOH-to-oil ratio (10:1, 15:1), stirring speed (600, 100 rpm), catalyst weight (3, 5 %) and reaction time (1, 2 hours) using a fixed-selected catalyst sample (HSF-144). The experimental set-up for optimisation screening tests for the various parameters is presented in Table 3.4.

Table 3.4. Single parameter optimisation for biodiesel production from maggot oil

Parameters	condition 1	condition 2	condition 3	Fixed condition
Temperature (°C)	50	**60**	65	[a]
MeOH/oil (molar ratio)	**6:1**	10:1	15:1	*
Stirring speed (rpm)	**400**	600	1000	**
Catalyst weight (wt. %)	0.5	**1.5**	3	***
Reaction time (hour)	1	**1.5**	2	****

[a] Parameter **baseline condition**(s) = 6:1 MeOH/oil, 400 rpm, 1.5 % catalyst wt., 1.5h reaction time
* baseline conditions & optimised temperature
** baseline conditions, optimised temperature & MeOH/oil ratio
** baseline conditions, optimised temperature, MeOH/oil ratio and stirring speed
*** All optimised conditions

Upon establishing the optimum condition for individual parameter with regards to biodiesel yield, catalytic evaluation using selected produced HS samples was conducted (at the established fixed conditions) by applying the same procedure illustrated in Figure 3.5.

For baseline/preliminary studies to assess the feasibility of maggot oil as feedstock, biodiesel production from maggot oil was conducted similarly using conventional homogenous catalyst (KOH and NaOH). On the other hand, using the same protocols at fixed optimised conditions, biodiesel was produced from refined sunflower oilusing produced HS zeolite sample that exhibited the optimum yield of biodiesel from maggot oil (i.e. HSF-144). The same biodiesel production protocols were applied for process optimisation using the response surface methodology (RSM) (section 3.5.2).

3.5.2 Optimisation of biodiesel production via response surface methodology

Multi-variance optimisation of transesterification of maggot oil, with respect to biodiesel yield, and statistical analysis were performed following the response surface methodology (RSM) and design of experiments (DoE), using DesignExpert® Software Version 11 (Stat-Ease, Inc., Minneapolis, USA). Three independent variables were undertaken for the design and their selection was based on their influence on the yield of biodiesel in section 3.5.1. Based on performance, sample HSF-144 was the selected catalyst adopted for the optimisation procedure. A full-factorial central composite design (CCD) was used to study the variable effects of MeOH/oil ratio, stirring rate and reaction time. This design was selected due its

effectiveness as compared to other RSM's designs (Bezerra et al., 2008). The established CCD design of experiment at their various simulated levels is presented in Table 3.5.

Table 3. 5. Actual and coded values for the CCD's experimental design factors

Run	Actual values of variables			Coded values of variables		
	Factor 1 A:MeOH:Oil (n/n)	Factor 2 B:Stirring rate (rpm)	Factor 3 C:Time (hour)	A	B	C
1	6	800	1.5	-1	1	-1
2	10.5	600	1	0	0	-1.667
3	15	800	1.5	1	1	-1
4	15	800	3	1	1	1
5	10.5	600	2.25	0	0	0
6	18	600	2.25	1.667	0	0
7	15	400	1.5	1	-1	-1
8	10.5	600	2.25	0	0	0
9	15	400	3	1	-1	1
10	10.5	600	2.25	0	0	0
11	3	600	2.25	-1.667	0	0
12	6	800	3	-1	1	1
13	10.5	935	2.25	0	1.675	0
14	6	400	3	-1	-1	1
15	10.5	600	2.25	0	0	0
16	10.5	600	2.25	0	0	0
17	6	400	1.5	-1	-1	-1
18	10.5	265	2.25	0	-1.675	0
19	10.5	600	3.5	0	0	1.667
20	10.5	600	2.25	0	0	0

$-\propto$: Lower Axial -1: lower value/point 0: Medium/central point 1: high point $\propto$: Upper Axial point

Analysis of Variance (ANOVA) was used to evaluate the statistical analysis of experimental data and model obtained by the design. The significance of data obtained by the generated model and model coefficients was evaluated by F-Tests and P-Test (95 % confidence level) respectively. The accuracy of the model was measured using the R^2 correlation coefficient. The DesignExpert® Software was further used to draw response surface plots required to determine the optimised conditions.

3.5.3 Kinetic studies for the transesterification of maggot oil

Kinetics of transesterification of maggot oil in this study was conducted using the Pseudo first-order technique (section 2.7.3, chapter 2). The study was conducted based on change in the yield of biodiesel with increase in reaction time, using the catalyst sample (HSF-14) with best performance (section 6.1) and at optimised conditions (of parameters) established in section 3.5.1: catalyst weight (1.5 %), MeOH/oil ratio (15:1), stirring rate (600 rpm), reaction temperature (60^{o}C). The varying reaction time conditions employed for the study were 1.5 h, 2 h, 3 h, and 8 h. The procedure employed to obtain the respective biodiesel yields was the same as described in Figure 3.6 (section 3.5.1).

Based on yield of biodiesel obtained with varying reaction time, the rate of reaction (r_{TG}) using the Pseudo first-order technique was determined as the variation in triglyceride (TG) concentration over the course of the reaction (equation 3.10)

$$r_{TG} = \frac{d[TG]}{dt} = -k^{'}[TG]_{t} \qquad (3.10)$$

where [TG] is related to conversion and yield of biodiesel

3.5.4 Biodiesel product characterisation

The physicochemical properties of maggot oil-derived biodiesel obtained over all evaluated catalyst samples, including those of biodiesel samples obtained over conventional homogeneous catalysts, were determined according to the EN14214 and ASTMD 6751 standard methods.

Acid value (AV) and saponification value (SV) of the product was determined by titrimetric methods described in sections 3.2.2 and 3.2.3 respectively.

Iodine value (IV) was determined according to the Wij's method as reported by Japir et al. (2017). This was also used to characterise the feedstock maggot oil. In this method, 0.2/0.4 g of the oil was mixed with 20/25 mL Wij's solution of glacial acetic acid and iodine monochloride (ICl). Then, 10/15 mL of equi-volume of cyclohexane and chloroform mixture was added to the existing mixture. The resulting mixture was kept in the dark for 30 minutes

and agitated after every 10 minutes. This was followed by the addition of 15/20 mL of potassium iodide (KI) and 100 mL of deionised water to the mixture, prior to titration against 0.1 M sodium thiosulphate ($Na_2S_2O_3$) until the observed yellow colour appeared. 1 mL of prepared starch solution (1%) was then added to the mixture and titration was continued until the blue (starch-iodine colour) disappeared. The iodine value (IV) was calculated using equation 3.11.

$$\text{IV } (I_2/\ 100 \text{ g oil}) = \frac{(V_B - V_S) \times N\ of\ titrant \times 0.01269}{g\ of\ oil\ sample} \times \frac{g\ I_2}{100\ g\ sample} \qquad (3.11)$$

Where V_B volume of titrant solution required by the blank

V_S is the volume of $Na_2S_2O_3$ solution titrated or titrant (mL)

N, the concentration of HCl solution (N)

0.01269 is gram equivalent of 1 mL of $Na_2S_2O_3$ solution

Density and viscosity values of the biodiesel product samples were determined using the density meter (DMA) and rheometer (DHR) respectively, following the procedures described in sections 3.2.4 and 3.2.5 respectively.

Viscosity of synthesised samples at 40°C, was determined using Anton Paar Rheometer (model RheolabQc) according to the procedure described in section 3.2.5. The viscosity measurement was interchangeably determined at 40 °C using a Discovery HR-1 hybrid (DHR) rheometer.

The refractive index of the synthesised samples was determined using a digital Refractometer (#PA203 Misco model). The analysis was also conducted on the maggot oil feedstock

The fatty acid methyl ester (FAME) profile (also known as ester content) of the produced biodiesel samples was characterised via the pre-calibrated GC-FID (HP88GC) following the same operational protocols employed for determination of fatty acid in the oil feedstock in section 3.2.1.1. The FAME was determined as the sum of the fatty acid constituents present in the produced biodiesel samples (equation 3.12). This exclude the internal standard ($C_{11,}$ dodecane) used for FAME determination of either the feedstock oil or produced biodiesel samples.

FAME or ester (%) = $Sum\ of\ wt\ \%\ fatty\ acid\ esters$ in produced BD - $wt\ \%\ of\ C_{11}$ (3.12)

Further, the cetane number ($\emptyset_i$) of the produced bodiesel samples was estimated using the derived empirical correlation as per Ramírez-Verduzco et al. (2012) (equation 3.13)

$$\emptyset_i = -7.8 + 0.302.M_i - 20\ .N \tag{3.13}$$

Where $\emptyset_i$ is the cetane number of biodiesel FAME (ester content)
M_i is the molecular weight of ith FAME (ester component in biodiesel sample)
and N is the number of double bonds in a given FAME (ester component)

3.6 Methodology and corresponding result sections

This section presents a short summary, accounting for the subsequent chapters in which the results obtained from various methodology sections, are presented and discussed. The various methods and the corresponding result sections for the synthesis, characterisation and evaluation of zeolites samples, are presented in Table 3.6.

Table 3. 6. Methodology and corresponding result section

Methodology & section	Result chapter/section	Results Appendix
Section 3.2 (3.2.1-3.2.5)	Chapter 4	Appendix 2
Section 3.3 (3.3.1-3.3.3) & section 3.4	Chapter 5 & chapter 5 (summary)	Appendix 1
Section 3.3 (3.3.4-3.3.5) & section 3.4	Chapter 5 (summary)	
Section 3.5 (section 3.5.1 – baseline[(a)])	-	Appendix 2
(section 3.5.1 [(b)])	Chapter 6 (section 6.1)	
(section 3.5.1 – far end)	Chapter 4	
Section 3.5 (section 3.5.2)	Chapter 6 (section 6.2)	Appendix 2
Section 3.5 (section 3.5.3)	Chapter 6 (section 6.3)	
Section 3.5 (section 3.5.4)	Chapter 4, chapter 6 (section 6.1-6.2)	

[(a)] Initial baseline transesterification conditions, for which optimised conditions by single parameter approach, are not reported in the result & discussion chapter (-); but summarised in Appendix 2
[(b)] upon optimised individual transesterification parameters, with result & discussion chapter given for selected HS catalysts

Table 3.6 shows that the characterisation of maggot oil feedstock, for which the given protocols are described by section 3.2 (section 3.2.1 – 3.2.5), are reported for results and discussion section of chapter 4. Chapter 4 also includes the attested results of maggot oil conversion to biodiesel using the preliminary conventional homogenous catalysts. For this, the protocols taken are described at far end of section 3.5.1.

Following the synthesis in section 3.3 (section 3.3.1- section 3.3.5), the results of the subsequent characterisations (section 3.4) of all the samples produced in this work, are presented and thoroughly discussed in chapter 5 (section 5.1-section 5.3).

Further, the catalyst evaluation using selected samples for biodiesel production as described in section 3.5.1, are presented for results and discussion in section 6.1 of chapter 6. The outcome of the optimisation of biodiesel production using the research surface methodology study (RSM) in section 3.5.2, is reported in section 6.2 of chapter 6. Furthermore, the kinetic study of the biodiesel production process given the approach by section 3.5.3, have the results presented and discussed in later section 6.3 of chapter 6. The results of biodiesel characterisation, is tied to the various methodology sections that involve catalytic evaluation (section 3.5.1, section 6.1-section 6.2).

Chapter Four

Waste-derived maggot oil's potential as feedstock for biodiesel production

This chapter discusses maggot oil's physicochemical properties with the view to substantiate its emergence and use as a feedstock for biodiesel production. The oil feedstock potential is further evaluated via transesterification to biodiesel using conventional homogeneous catalysts. The chapter consist of four sections (section 4.1-4.4), which each respectively discusses the results of the following obtained physicochemical properties of maggot oil: fatty acid characterisation of maggot oil and related properties; acid and saponification value; iodine value coupled with density, kinematic viscosity and refractive index; and the potential of maggot oil as feedstock via conventional homogenous-catalysed transesterification. The first section on the compositional, structural, and related characteristics of maggot oil, are discussed as follows.

4. Result and discussion

4.1. Fatty acid composition, fatty acid profile and properties of maggot oil

Maggot oil was compositionally characterised through a pre-calibrated GC-FID and each of its constituent fatty acid from the resultant chromatograph, was quantitatively calculated as a ratio of the respective peak area over the sum of all peak areas. The thorough procedure for the determination of the above is described in chapter 3 (section 3.2.1.1). The corresponding results are reported in Table 4.1.

Table 4.1. Average fatty acid content of maggot oil (experimental vs. literature)

Fatty acid (wt. %)	Structure	This work		Literature	
		Maggot oil[(a)]	Maggot oil[(b)]	(Wang et al., 2017)	(Ushakova et al., 2016)

Lauric	C12:0	41.5	37.14	18.89	38.43
Myristic	C14:0	7.44	7.1	9.91	12.33
Palmitic	C16:0	20.91	23.84	20.96	15.71
Palmitoleic	C16:1	3.28	3.16	-	-
Stearic	C18:0	3.21	2.52	6.5	2.95
Oleic	C18:1	14.57	17.81	22.54	8.81
Linoleic	C18:2	7.93	8.44	12.67	0.23
Linolenic	C18:3	-	-	-	-
Arachidic	C20:0	1.54	-	-	-
Mw[(c)]	(g/mol)	825.32	803.86	-	-

[(a)] maggot oil (crude form) [(b)] maggot oil (purified form)
[(c)] Average molecular weight of maggot oil

The maggot oil feedstock was characterised as containing the following variety of free fatty acids (FFAs) as shown in Table 4.1. 37.14-41.5 % lauric acid (C12:0), 7.1-7.44 % myristic acid (C14:0), 20.91-23.84 % palmitic acid (C16:0), 3.16-3.28 % palmitoleic acid (C16:0), 2.52-3.21 % stearic acid (C18:0), 14.57-17.81% oleic acid (C18:1), 7.93-8.44 % linoleic acid (C18:2), and 1.54 % arachidic acid (C20:0) (in trace amounts). Although each component might be detected at different proportions, the above contents are comparable to the composition profile of typical vegetable oils, such as of those earlier provided in Table 2.1 (section 2.2.2). Gonfa Keneni et al. (2017) and Lam et al. (2010) attest that the waste-derived maggot oil is a triglyceride containing representative oil.

The above composition of maggot oil also appears to be similar, both in profile and in fatty acid proportions, as reported of the same oil (commonly published as "lipids of Black solider fly") in the few existing publications (Wang et al., 2017, Ushakova et al., 2016, Surendra et al., 2016). According to the author's knowledge, apparently less than five open literature studies (inclusive of the cited), have reported on the maggot oil characteristics with respect to fatty acid composition.

From the experimental measurement of the oil using both a crude and purified sample provided, the oil by weight proportion appeared to have constituted majorly of lauric acid (37.14-41.5 %), followed by palmitic (20.91– 23.84 %), oleic (14.57-17.81 %) and linoleic acid (7.93-8.44 %). The slight differences in respective proportions of the oil content in comparison to literature's proportions, is mainly attributed to the fact that the different oil samples derived from different waste organic sources (Leong et al., 2016).

Furthermore, from the fatty acid composition provided in Table 4.1, the result displaying the degree of fatty acid saturation of the oil by summing up the constituent fatty acids' weight percentage profile based on saturation, monounsaturation and poly unsaturation of bond between carbons , is presented in Figure 4.1.

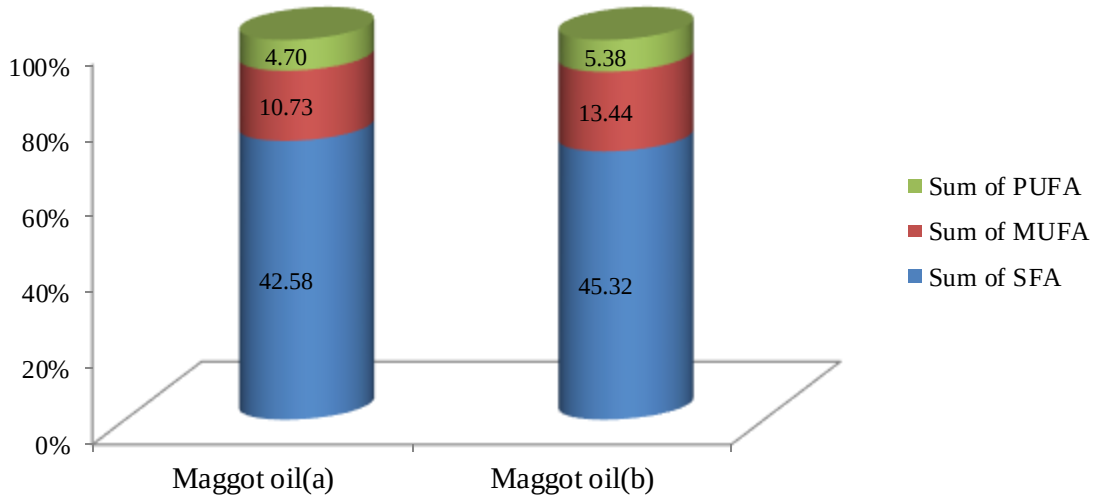

Figure 4.1. Fatty acid profile of waste-derived maggot oil: (a) crude maggot oil, (b) purified maggot oil

According to Figure 4.1, both samples of maggot oil by degree of saturation, constituted majorly of Saturated Fatty Acids (SFA) at a range of 42.58-45.32 %, with Mono Unsaturated Fatty Acids (MUFA) between 10.73-14.44 % and a minor concentration of Poly Unsaturated Fatty Acid (PUFA) of 4.70-5.38 %. The relatively moderate proportion of SFA and low proportion PUFA is likely to improve the poor cold flow or low temperature characteristics of biodiesel that could result from high SFA concentration. Likely, this proportion also would improve the poor oxidative stability of biodiesel usually associated with high concentration of PUFA in oil (Surendra et al., 2016). Consequently, maggot oil (in this work) is ascertained as a potential feedstock for high-quality biodiesel production (Surendra et al., 2016) due to the low proportions of SFA and PUFA.

Furthermore, the molecular weight of maggot oil, using the average molecular weight of the obtained fatty acids reported in Table 4.1, was determined using equation 3.2 and an online calculator as described in chapter 3 (section 3.2.1) (Biodiesel Education Program, 2017, da Cunha et al., 2009). The molecular weight of the respective maggot oil samples (magOil$^{(a)}$ and magOil$^{(b)}$), also reported in Table 4.1, was obtained as 825.32 and 803.86 g/mol. The obtained

molecular weight values closely correspond to the range of molecular weight values reported of typical biodiesel feedstocks, such as that of beef tallow of 858.5 g/mol with a molecular of(da Cunha et al., 2009).

Moreover, structural configuration of maggot oil was also determined using a Perkin Elmer FT-IR instrument as described in Chapter three (section 3.4). Sunflower and palm oil were also characterised for the above for comparison purpose. The resultant FT-IR spectra of the respective oils are depicted in Figure 4.2.

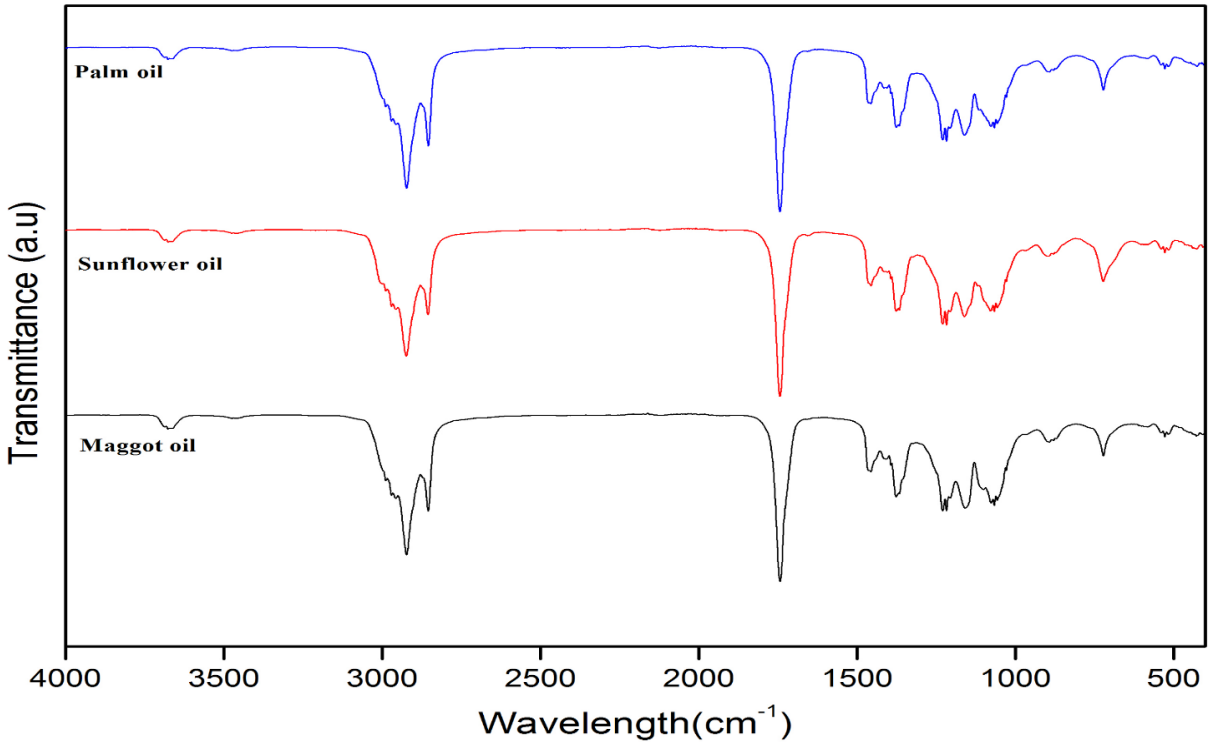

Figure 4. 2. Comparison of FT-IR spectra of waste-derived maggot oil and conventional biodiesel oil feedstocks

The oils as measured from FT-IR data depicted in Figure 4.2, exhibited similar structures and functional groups as those of conventional biodiesel-feedstock vegetable oils (Gonfa Keneni et al., 2017, Salvi and Panwar, 2012). A least of 6 to 7 noticeable distinctive FT-IR bands were observed in maggot oil that are commonly found in sunflower and palm oil. The major band detected at between 2800 and 300 cm^{-3} can be attributed to symmetric and asymmetric vibration of aliphatic $–CH_2$ group. The other major symmetric band detected between 1700 and 1800 cm^{-1} (~1750 cm^{-1}), is most likely representative of triglyceride and free fatty acids (FFA) content in the oil (Leong et al., 2016).

4.2 Acid and saponification value

This section discusses the results of acid value (AV) and saponification value (SV) properties of maggot oil. AV and SV were determined titrimetrically by use of potassium hydroxide solution as described via respective procedure in chapter 3 (section 3.2.2 and section 3.2.3). The AV, like previous properties, was also determined for both samples of maggot oil (crude and purified form). The results of the AV and SV of maggot oil, as determined, are reported in Table 4.2.

Table 4. 2. Acid and saponification value of maggot oil

Sample	**Acid value** ($mg\ KOH \cdot g^{-1}\ oil$)		**Saponification value** ($mg\ KOH \cdot g^{-1}\ oil$)
	Non-esterified	Esterified	
MagOil[(a)]	10.1[(c)]	-	-
MagOil[(b)]	7.2 [(d)]	1.4[(e)]	176.43

(a) maggot oil (crude) **(b)** maggot oil (purified) **(c)** 10.1 g KOH/g oil ≈ 5.08 wt.% FFA
(d) 7.2 g KOH/g oil ≈ 3.38 wt.% **(e)** 1.4 g KOH/g oil ≈ 0.7 wt.% FFA

The acid value (AV) of the maggot oil samples (crude and purified), from the described tritrimetric measurement, was 10.10 and 7.20 mg KOH/g oil respectively (Table 4.2). The above values expressed in percentage as oleic acid, were determined as 5.08 wt. % and 3.38 wt. % Free Fatty Acid (FFA). These obtained values categorise the oil as a high FFA feedstock for biodiesel production (Lam et al., 2010, Gonfa Keneni et al., 2017). Consequently, this profile could possibly hamper the quality of both the process reaction and biodiesel obtained thereof (Lam et al., 2010). In alleviation, an additional treatment step, namely esterification prior to the actual transesterification reaction, may be required (Zhang et al., 2010).

By selecting the relatively low-FFA maggot oil sample (magOil[(a)]) (3.38 % FFA), esterification was successfully conducted in a sulphuric acid catalytic medium with view to assess the viability of FFA reduction. This consequently, resulted in FFA levels as low as 0.7 % (~1.4 mg KOH/g oil) (Table 4.2), thus adhering to the required standard of below 2 mg KOH/g oil (< 2 mg KOH/g oil) or < 1wt. % FFA (Zhang et al., 2010, Lam et al., 2010, Jahirul et al., 2014).

Nonetheless, biodiesel production in this work was conducted without the additional step due to incurring possible additional cost. This work, instead, focused on the development of heterogeneous catalysts with the view to counteract the need for such possible additional

processing steps. This would integrate esterification and transesterification into one-step and alleviate the need for washing steps as required due to high FFA feedstocks.

The oil as also characterised titrimetrically for SV in chapter 3 (section 3.2.3), resulted to high saponification value (SV) of 176.43 mg KOH/g oil (Table 4.2). Such high saponification value corresponds to the high acid value (7.2 mg KOH/g) and high molecular weight (803.86 g/mol) as previously reported in Table 4.2 and Table 4.1 respectively, and the value is attributed to short-chain fatty acids present in the oil. Consequently, the above indicates that the oil possesses viscous flow characteristics such that even prior to measurement, the oil can be considered highly viscous. The SV obtained of the oil also corresponds to those of various oils and fats that have proven potential as feedstocks in biodiesel production (Karmakar et al., 2010, Baroutian et al., 2009). The next section discusses on further properties characterised, density, iodine value and refractive index of maggot oil.

4.3 Density and kinematics viscosity, iodine value and refractive index

This section discusses the results of density, kinematic viscosity and iodine value (IV) of maggot oil.

Density of maggot oil samples (magOil[(a)] and magOil[(b)]) was determined using a portable density meter at 27 °C and 40 °C, as procedurally described in Chapter 3 (section 3.2.4). The result of the obtained density values at the various temperature sets, is reported in Table 4.3.

Table 4. 3. Characteristic density and kinetic viscosity of maggot oil at various temperatures

	Density (g/cm^3)		**Kinematic viscosity** ($mm^2 \cdot s^{-1}$)					**IV**[(c)]	**nD**[(d)]
Temperature (°C)	27	40	20	25	30	35	40	-	-
MagOil[(a)]	-	0.883	102.51	100.15	91.46	82.43	57.27	-	-
MagOil[(b)]	0.913	0.875	78.36	75.97	68.03	60.35	43.16	44.27	1.465

(a) Maggot oil in crude form **(b)** Maggot oil (purified form) **(c)** IV: iodine value (I_2/100 g oil)

(d) nD: refractive Index

Maggot oil sample having relatively low acid value (i.e. magOil [(b)]) was characterised with a density of 0.913 g/cm^3 at 27 °C, which changed to a reduced density of 0.875 g/cm^3 at 40 °C. The former density value corresponds to the density of oils of a similar saturation as maggot oil at the given temperature, and this similarly corresponds to the densities of various conventional (biodiesel) oil feedstocks (e.g. soybean, palm oil, etc.) (Karmakar et al., 2010).

The latter density of 0.883 g/cm^3, appeared to be comparable to the density of biodiesel-derived from the same oil as exclusively reported by Li et al. (2011).

Nonetheless, both values (which decreases with an increase in temperature), are associated with effective dissociation (break up) and mixing of the oil molecules upon pre-heating, alcohol mixing and oil processing transformation (i.e. transesterification) to biodiesel (Jayasinghe and Hawboldt, 2012).

The maggot oil samples were further characterised for kinematic viscosity via a rheometer (at temperature intervals between 20-40 ^{o}C) according to the procedure described in chapter 3 (section 3.2.5). The result of the obtained kinematic viscosity values is reported in Table 4.3. According to the data provided in Table 4.3, the viscosities of the maggot oil samples (magOil$^{(a)}$ and magOil$^{(b)}$) at 40 ^{o}C were 57.27 and 43.16 mm^2/s respectively. Both values can be said to lie within the range of high viscosity for a biodiesel feedstock oil (Karmakar et al., 2010), and validate the assumption previously stated of direct correlation between high FFA and high viscosity. In other words, the above (high) viscosity values were mainly attributed to high percentage FFA as respectively reported for the two samples in terms of acid value as shown in Table 4.2.

The viscosity at 40 ^{o}C of the first sample (magOil$^{(a)}$ = 57.27 mm^2/s) can be categorised as being in a much higher or excessive range because it did not comply with the common range reported for typical biodiesel feedstocks (Karmakar et al., 2010, Jahirul et al., 2014). The second sample (magOil$^{(b)}$ = 43.16 mm^2/s) however, complied with this range, which is often reported between 35-45 mm^2/s (Baroutian et al., 2009). The above served among the reasons of selection of magOil$^{(b)}$ for further research and findings in this work.

The highly viscous oil would have low flow characteristic, poor atomisation, ineffective mixing of the oil, revealing that the oil cannot be directly used as a fuel in a diesel engine and that it will require pre-heating, high alcohol-to-oil ratio and high reaction temperature for effective conversion and yield of biodiesel from the oil (Jayasinghe and Hawboldt, 2012).

The obtained high viscosity of maggot oil, is also a characteristic of its high molecular weight of 803.86 g/mol as reported previously in Table 4.1 (da Cunha et al., 2009). In other words, a direct correlation was observed between FFA concentration, molecular weight and viscosity.

On the other hand, the high viscosity can be an indication of a low iodine value of the oil (da Cunha et al., 2009). To prove the above, iodine value (IV) of the maggot oil sample (magOil$^{(b)}$)

was determined according to Wij's method and corresponding procedure reported in Chapter 3 (section 3.5.4) and consequently a low iodine value of 44.27 g I_2/100 g oil was recorded. The value obtained also served as an indication of the potential reactivity of the oil in biodiesel production. Refractive index of the maggot oil sample was also measured using a refractometer as reported in chapter 3 (section 3.5.4). A high refractive Index value of 1.4649 was recorded for the oil sample, which corresponded to its high viscosity of 43.16 mm^2/s. The results of the test properties, are highlighted in Table 4.3. The next section, further, discusses the results of conversion potential of maggot oil to biodiesel over conventional homogeneous catalysts.

4.4 Characteristic potential of maggot oil via transesterification using homogenous catalysts

This section discusses the characteristic potential of maggot oil for biodiesel production via transesterification (trans.) using conventional homogeneous catalysts. The transesterification activities for the above investigation were carried as baseline studies for further assessment of the oil over heterogeneous catalysts synthesised in this work. The separate reactions using KOH and NaOH as catalysts in methanol medium, were carried out with a laboratory batch set-up, at established optimum conditions (60 ^oC; 15:1 MeOH/oil ratio; 600 rpm; 1.5 % catalyst weight and 1.5 hour) and according to the biodiesel production procedure described in chapter 3 (section 3.5.1).

The potential characteristics of waste maggot oil as further evaluated was conducted using the purified maggot oil sample (magOil$^{(b)}$) because of its relatively low acid value and viscosity as reported previously in sections 4.2 and 4.3 respectively. A low value for the above properties promotes the feedstock's suitability for the reaction, such as ease of mixing or pumping in case a flow system (Jayasinghe and Hawboldt, 2012). The result depicting the yields of biodiesel obtained over both KOH and NaOH catalysts, is presented in Figure 4.3.

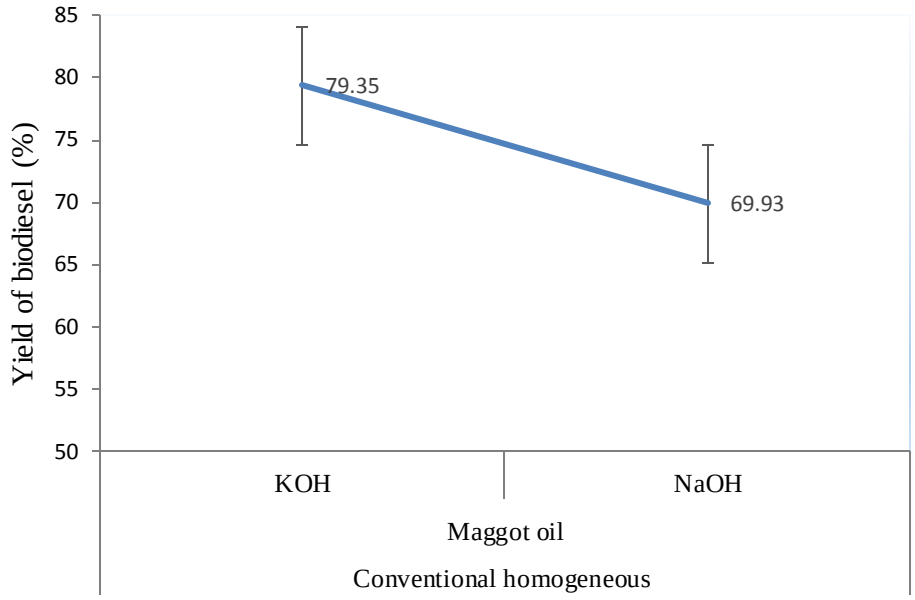

Figure 4. 3. The yield of biodiesel from maggot oil over NaOH and KOH homogeneous catalyst (Transesterification conditions: 60 °C; 15:1 MeOH/oil ratio; 600 rpm; 1.5 % catalyst wt. and 1.5 h) (maggot oil above refers to magOil[(b)])

Further, the physicochemical properties of the obtained biodiesel samples were determined by various respective methods and procedures as described chapter 3 (section 3.5.3). The obtained results are presented in Table 4.4.

Table 4.4. Physicochemical properties of maggot oil-biodiesel produced over conventional homogenous catalyst

Biodiesel properties	Characteristics of maggot oil versus FAME characteristic of biodiesel samples for respective homogeneous catalysts			B-Standard[a]
	Maggot oil[(b)]	KOH	NaOH	ENS[b] /ASTM[c]
Acid value (mg KOH/g)	7.2	0.35	0.28	0.5/0.8 Max
Saponification value (mg KOH/g)	176.43	146.64	124.33	-
Ester content[d] (% m/m)	-	94.67	98.3	96.5
Iodine value (g of I_2/100 g)	44.27	82.63	69.02	/130
Density at 40 °C (g/ml)	0.883	0.874	0.862	0.86-0.90
Kinematics viscosity at 40 °C (mm^2/s)	43.16	4.39	3.8	3.5-5.0 /1.9-6.0
Refractive index[e]	1.4649	1.4457	1.4456	/1.479
Cetane number	-	-	-	51/47

[a] Biodiesel Standard Specifications; [b] ENS14214 (European) and [c]ASTMD6751 (American for FAEE)
[d] Obtained from GC characterisation of respective biodiesel FAME samples
[e]Figures reported in four significant figures to enhance accuracy or minimize error of comparison
MagOil[(b)], selected due to better overall characteristic than magOil[(a)]

Biodiesel yield of 69.93 % and 79.35 % (Figure 4.3) was obtained by transesterification over NaOH and KOH respectively. Further, the quality of biodiesel obtained over the above catalysts complied with the specification standards with respect to all the quality criteria (physicochemical properties) presented in Table 4.4. The characteristic obtained consequently, attests to the potential of the feedstock maggot oil for biodiesel production using homogeneous catalysts to transesterify the feedstock magOil[(b)] (Table 4.4).

A lower acid value (AV) of 0.28 mg KOH/g oil of NaOH-catalysed biodiesel, as compared to the initial value 7.2 mg KOH/g oil, indicates an effective conversion and a fuel with no corrosive attributes and better stability for engine performance (Canesin et al., 2014). A saponification (SV) of 124.33 KOH/g oil (for NaOH-catalysed biodiesel), accounted for a biodiesel sample with a good potential for biodiesel production, one with lower medium-chain fatty acids and hence good flow characteristics than the KOH-catalysed biodiesel (da Cunha et al., 2009). The above-mentioned (low AV, flow characteristics and less saturation) corresponded to the low density obtained (0.862 g/mL) and are reflective of such low viscosity of 3.8 mm^2/s.

Moreover, the NaOH-catalysed biodiesel with the resulted IV of 69.02 I_2/100 g oil, is associated with a fuel which was less saturated, one with a good reactive, ignition potential and a moderate cold flow characteristic property (Canesin et al., 2014, da Cunha et al., 2009). Further, this IV value coupled to the low AV (0.28 mg KOH/g oil), attested to a biodiesel sample with a good oxidative and storage stability (Jayasinghe and Hawboldt, 2012).

Like NaOH, maggot oil-biodiesel obtained over KOH also exhibited compliance with all the above-discussed properties to the standard specification. With the exception of the iodine value (IV), biodiesel obtained over KOH catalyst (in overall) appeared to have relatively low quality compared to NaOH-catalysed biodiesel: a relatively high acid value (AV) (0.35 mg KOH/g oil) corresponding a given higher density (0.874 g/mL) and viscosity (4.39 mm^2/s). By the exception of higher IV of 82.63 I_2/100 g oil, biodiesel sample obtained over the KOH catalyst, was more reactive and with better ignition characteristics than the NaOH-catalysed.

In addition to the above properties, suitable biodiesel quality was achieved over both homogenous catalysts due to the high ester content exhibited by the respective biodiesel samples (da Cunha et al., 2009), with 98.3% ester content in biodiesel obtained over NaOH, and 94.67 % over KOH. It is to be noted that although KOH resulted in higher biodiesel yield

than NaOH (79.35> 69.93 %) (Figure 4.3), the higher yield did not correspond to a higher overall quality of biodiesel obtained. NaOH exceeded KOH in terms of the overall quality of biodiesel. Based on the results and discussed properties, as well as its application, maggot oil was validated or proven to have potential as a suitable feedstock for biodiesel production.

4.5 Summary of Chapter 4

In this chapter, the physico-chemical characteristics of maggot oil, was investigated to determine its suitability as a biodiesel feedstock. The oil, both compositionally and structurally, exhibited a high-profile fatty acid content; demonstrated a high fatty acid saturation profile, with lauric acid as the major constituent, presenting values ranging between 37.14 - 41.5 %. The high fatty acid profile corresponded (or directly correlated) to an obtained high acid value (AV) of 7 mg KOH/ g oil, a low iodine value (IV) of 44.27 g of I_2/100 g oil and high saponification value (SV) of 176.43 mg KOH/g oil. The high acid value of the maggot oil feedstock was modified by esterification to a reduced value of 1.4 mg KOH/g oil, showing adaptability with suitable heterogeneous catalysts. The maggot oil low iodine value reflects potential reactive property while the maggot oil SV could be associated with high-medium chain fatty acids. In addition, maggot oil demonstrated a common biodiesel feedstock viscosity of 43.16 mm^2/s, coupled with a low density of 0.883 g/cm^3, revealed good flow and atomisation characteristic of the feedstock for transesterification. Based on these attributes, maggot oil successfully validates its potential as a suitable feedstock for biodiesel production while also presenting conversion yields of up to 69.93 % and 79.35 % over NaOH and KOH homogeneous catalysts to produce high quality-compliant biodiesels.

Chapter Five

Hydrothermal synthesis of HS zeolite from coal fly ash

5. Introduction

Chapter 5 reports and discusses in detail the characteristic properties of feedstock coal fly ash and all the derived HS zeolite samples produced in this work. The chapter is divided into three major sections (5.1-5.3). Section 5.1 reports on the properties of HS zeolite samples synthesised via direct hydrothermal method, with the outlook of synthesis parameters consecutively investigated. Section 5.2 discusses in detail the results of the characteristic properties of HS zeolite synthesised via fusion-assisted method with varying synthesis time. Both section 5.1 and section 5.2 also briefly present and discuss the yield of the obtained zeolites and the corresponding process material balance for the best-case scenarios. Section 5.3, draws out a summary of the two synthesis methods with regard to characteristic properties and yield of HS zeolite and briefly compares the products obtained at optimal synthesis conditions of the two-synthesis methods.

The experimental procedures for the synthesis of HS zeolite via either the direct hydrothermal or the fusion-assisted method are reported in sections 3.3.1 and 3.3.2. Phase crystallinity and purity characteristic of obtained samples were determined via XRD analysis. The crystal morphology was deduced from micrograph images obtained via SEM analysis, and the crystal size from XRD data (patterns) using the Scherrer equation are presented. The elemental composition and structural configuration of synthesised catalysts were determined using EDS and FT-IR analysis. Further sample analysis was done using BET Nitrogen isotherms and t-plot analysis to determine the textual properties of selected synthesised catalysts. The experimental procedures employed for all the above-mentioned characterisation techniques are described in section 3.4 (chapter 3).

5.1 Synthesis of HS zeolite from coal fly ash via direct hydrothermal method

This section discusses in detail the characteristic properties of HS zeolite obtained via direct hydrothermal method on the basis of different synthesis mixtures with varying water/CFA ratio, varying ageing time and temperature, varying NaOH/CFA ratio and varying the hydrothermal crystallisation time and temperature. The detailed experimental procedure for the samples produced via the direct hydrothermal method, is reported in section 3.3.1 (chapter 3). The section also presents the mineralogical composition, morphology, elemental and structural composition of the Matla coal fly ash (CFA) as feedstock for the synthesis of HS zeolite in this work.

5.1.1. Characterisation of coal fly ash

Coal fly ash (CFA), the feedstock material for the synthesis of HS zeolite in this work, was obtained from Matla coal-fired power station (South Africa). The material was characterised along with the synthesised catalyst samples, using the XRD, SEM, EDS and FT-IR analysis as thoroughly described in section 3.4.

Figure 5.1 depicts the mineralogical composition of coal fly ash (CFA), which was determined using the XRD analysis as described in section 3.4. The respective mineralogical composition depicted by the various peaks, were identified using X'Pert HighScore Plus software.

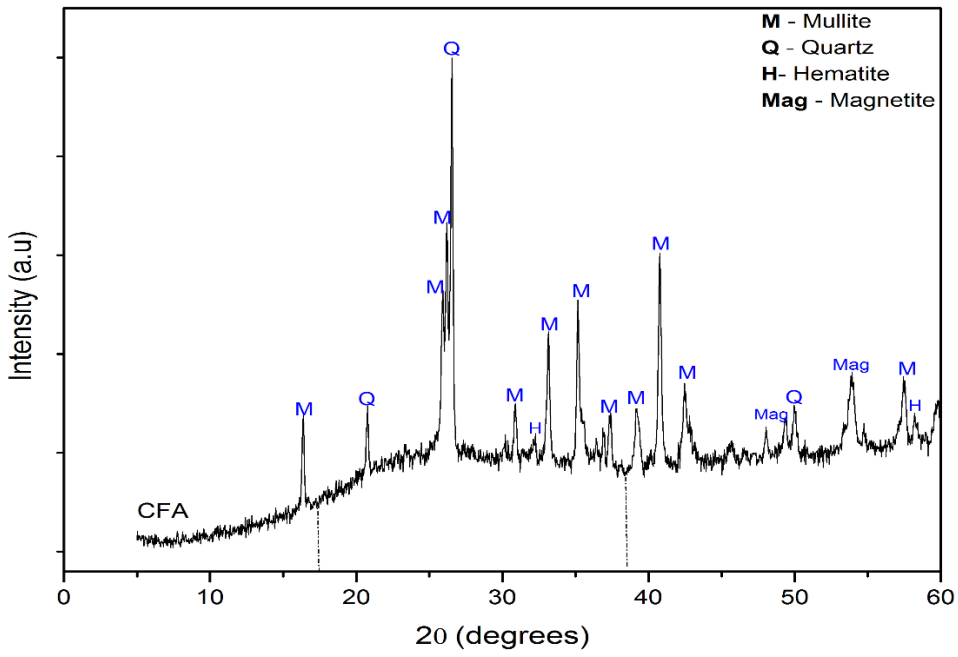

Figure 5. 1. XRD pattern of Matla coal fly ash (CFA)

The mineralogical composition of CFA in Figure 5.1 shows crystalline phases of quartz (Q) and mullite (M) in significant proportion, and showed traces of hematite (H) and magnetite (Mag) phases. The major peaks of quartz phases (SiO_2) were shown at around 21°, 36.7° and 50° 2θ, and those of mullite phases (3 $Al_2O_3.SiO_2$) at 16.5°, 26.4, 33, 35.1 and 41.3 2θ. The amorphous glassy phases were shown as the broad diffraction hump between around 17.5 and 38° 2θ (Musyoka et al., 2011, Luo et al., 2016). Notably, this substantiates that the amorphous aluminosilicate glass comprised the major proportion of the CFA. No measurement was taken to relatively quantify the above-mentioned mineralogical composition of CFA, but based on the inspection of the hump as by Ameh et al. (2017) and Musyoka (2012), peak areas and frequency of the assigned composition on the XRD pattern (Figure 5.1); the order of the mineral phases in terms of relative weight proportion, can be deduced as: Amorphous > Mullite > Quarts > Magnetite > Hematite. From XRD pattern conducted on CFA by Steenbruggen and Hollman (1998), the above order of the respective mineral phases was substantiated with 70 % amorphous phases, 15 % mullite, 8 % quartz and 4 % magnetite and hematite. Brassell (2017) similarly via XRD analysis of fly ash from same source (Arnot power station), quantitatively reported CFA with 54.55% amorphous, 26.48 % mullite, 16.23 % quartz and 2.74 % magnetite phase composition. According to Querol et al. (2002), the high proportion of amorphous glass is favourable for high yield of zeolite; whereas the low proportion of magnetite and hematite phases, owing to their unreactive nature, is favourable for the conversion of fly ash to zeolite.

The crystal morphology of the coal fly ash material determined using SEM analysis is described in section 3.4. The SEM micrograph in Figure 5.2, presents the morphology of the coal fly ash material

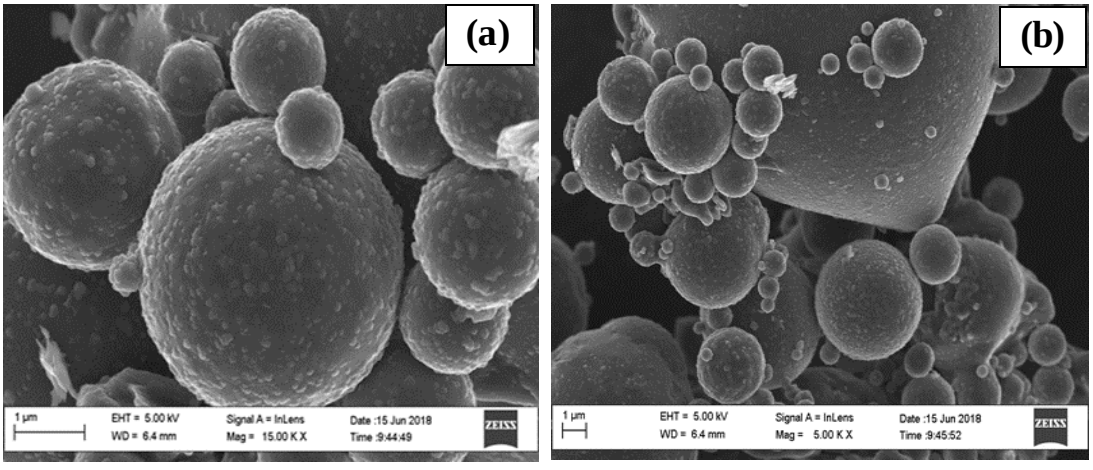

Figure 5. 2. SEM micrograph of the South African Matla coal fly ash, **(a)** image of 15000x and **(b)** of 5000x magnification.

The SEM micrograph of coal fly ash in Figure 5.2, shows that the material contains smooth spherical crystals, which is typical of fly ash morphology generally reported in literature (Murayama et al., 2002, Steenbruggen and Hollman, 1998). Brassell (2017) attributed the spherical shape of the fly ash crystals to their solidification when suspended and heated in flue gas, prior to being subject to cooling in the coal boiler (Brassell, 2017). The smooth surface observed to have covered the fly ash particles, are reflective of the amorphous glass content (Musyoka et al., 2011, Ameh et al., 2019) that was previously revealed via the XRD pattern in Figure 5.1.

The elemental composition of coal fly ash was determined using EDS analysis, according to the procedure described in section 3.4. Table 5.1 presents the elemental composition of Matla coal fly ash, with the triplicate of the analysis over five spectrum regions of the sample (n) and data normalised without accounting for carbon content from coating.

Table 5. 1. EDS analysis of the elemental composition of coal fly ash (n=5)

Sample	**Element** (atomic, w/w %)											
	O	**Al**	**Si**	**Na**	**Mg**	**K**	**Ca**	**Ti**	**Fe**	**P**	Total	**Si/Al**
CFA(spectrum 1)	70.62	10.41	15.23	-	0.68	0.19	1.57	0.34	0.95	-	100.0	1.46
CFA(spectrum 2)	57.5	13.9	18.8	-	2.5	-	4.4	0.3	2.6		100.0	1.35
CFA(spectrum 3)	61.8	11.0	11.0	-	1.9	-	12.4	-	0.9	1.10	100.0	1.00
CFA(spectrum 4)	67.20	12.30	18.85	-	-	0.32	0.66	0.23	0.44	-	100.0	1.53
CFA(spectrum 5)	72.32	9.98	13.16	-	1.24	0.18	1.64	0.37	1.10	-	100.0	1.32
Average	65.89	11.52	15.39	-	1.56	0.23	4.15	0.31	1.19	1.10	100.0	1.33

The EDS analysis in Table 5.1, presents the elemental composition of fly ash. The fly ash in question was observed to consist of silicon (Si) and aluminium (Al) in major proportion, each attached to oxygen elements as metal oxides (as illustrated in Table 2.2, section 2.3.1 and Figure 2.4 (a) and (b), section 2.4) resulted from the coal combustion process (Si–O–Al). The above two major metal oxide contents made up to 76.38 % of the fly ash on a mass basis. The fly ash also constituted of other metal oxides listed in the following order of relative weight proportion: calcium (Ca) (4.32 %), magnesium (Mg) (1.54 %), phosphorus (P) (1.25%), iron (Fe) (1.13 %) and potassium (K) (0.23 %) in trace amounts. The above elemental composition for the fly ash, is in agreement with the general composition of fly ash reported in literature (Murayama et al., 2002, Zielke-Olivier and Vermeulen, 2016, Musyoka et al., 2011). Since the

fly ash shows the combined average weight percentage (77.51%) of Si, Al and Fe to be greater than 70 % and equivalently contains less than 10 % CaO (based on the monovalent proportion of Ca), the material in accordance to ASTM method C168 (ASTMC618-92a) and Dwivedi and Jain (2014), is classified as class F fly ash. It may also be noted that Musyoka (2009) suggests that the low amount of Ca and Mg identified in the fly ash, will be advantageous for high zeolite crystallisation since low levels of divalent cations are likely to minimise interference of competing cations during synthesis.

It is further observed in Table 5.1 that the coal fly ash material exhibited an average Si/Al ratio of 1.32. This ratio, although it appears to be lower than that of fly ash reported in several findings (Murayama et al., 2002, Golbad et al., 2017, Musyoka, 2009), is however suitable for the synthesis of HS zeolite in particularly. Several researchers (Querol et al., 2002, Nanganoa et al., 2016, Musyoka et al., 2011) have identified HS as a low siliceous zeolite, with an average Si/Al ratio of 1.00. Accordingly, the obtained Si/Al ratio depicted by the coal fly ash in Table 5.1, shows that the direct use of the material may therefore not be suitable for the synthesis of HS. For this reason, therefore, this work was prompted to reduce the Si/Al ratio of HS by additional Al content in the framework structure of the zeolite. Sodium aluminate ($NaAlO_2$) was used as the additional source of Al in the experimental procedure described in section 3.3.1-3.3.4.

The FT-IR spectra of the fly ash (CFA) feedstock is presented in Figure 5.3. The spectra were obtained from FT-IR analysis, which was conducted on the material as described in section 3.4.

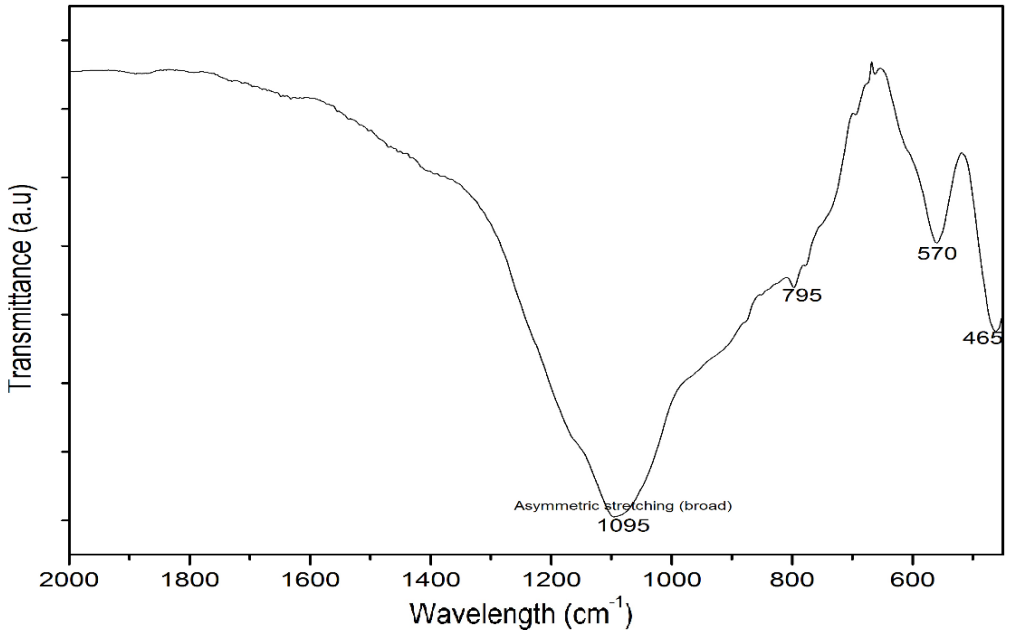

Figure 5. 3. FT-IR spectra of Matla coal fly ash

The FT-IR of fly ash in Figure 5.3, illustrates the structural configuration of the material. The major aluminosilicate characteristic bands shown in Matla fly ash were visible at 465 cm^{-1}, 570 cm^{-1}, 795 cm and 1095 cm^{-1}. The band at 465 cm^{-1} was associated with T–O bending vibrations (Babajide, 2011), the band at 570 cm^{-1} was associated with octahedral aluminium present in the mullite (SiO_2) phase of coal fly ash (Fernández-Jiménez and Palomo, 2005), and the narrow band at 795 cm^{-1} was associated with symmetric T-O (T = Al, Si) stretching vibration of quartz (3 $Al_2O_3.SiO_2$) in CFA (Ameh et al., 2019, Brassell, 2017). According to Nyale et al. (2014) and Fernández-Jiménez and Palomo (2005), the broad asymmetric band observed around 1095 cm^{-1}, is associated with T–O–Si (T = Al, Si) present in mullite, quartz and the glass phase of CFA.

The above presents the characteristic bands of Matla coal fly ash that are comparable to those of other fly ash materials used in cited literature sources. Babajide et al. (2012) reported an additional T-O (T = Al, Si) symmetric stretching vibration band of quartz in CFA at 704 cm^{-1}, a band associated with symmetrical vibration of the Al–O–Si groups at 700 cm^{-1}, and additional band attributed to the glassy phase at 950 cm^{-1}. The absence of the above characteristic bands in Matla CFA, could be due to different or lower proportion of Si–O groups therein as proven based on Si/Al ratio as compared to (for example) Arnot coal fly ash used by Babajide (2011). The following section reports on the results of the actual synthesis of HS zeolite from coal fly ash via direct hydrothermal method.

5.1.2. Effect of water/CFA ratio on the formation of HS zeolite

In the first stage of experiment, three synthesis mixtures with varying water/CFA of 5:1, 9:1 and 12.5:1, were used for the synthesis of HS zeolite at fixed conditions shown in Table 8.1 (Appendix 1) (ageing time, 48 hours; ageing temperature, 47 °C; NaOH/CFA ratio, 1:1; hydrothermal synthesis time and temperature, 48 hours, 140 °C) (Table 3.2, section 3.3.1). The resultant samples in order of increasing water/CFA ratio were assigned with code names HS-A48h, HS-A48h(7.5H_2O) and HS-A48h(12.5H_2O) (Table 3.2, chapter 3). The product samples were characterised using XRD, EDS and FT-IR analyses as described in section 3.4.

The (constituent peaks of the) XRD patterns of all samples produced in this work, were assigned in accordance to the standard simulated diffraction patterns of sodalite obtained from the International Zeolite Association's (IZA) database of zeolite structures. The same applied to any other peaks that identified non-HS phases present in many of the obtained samples. Figure 5.4 presents the simulated diffraction pattern of sodalite, against which the XRD patterns of all the obtained samples were assigned.

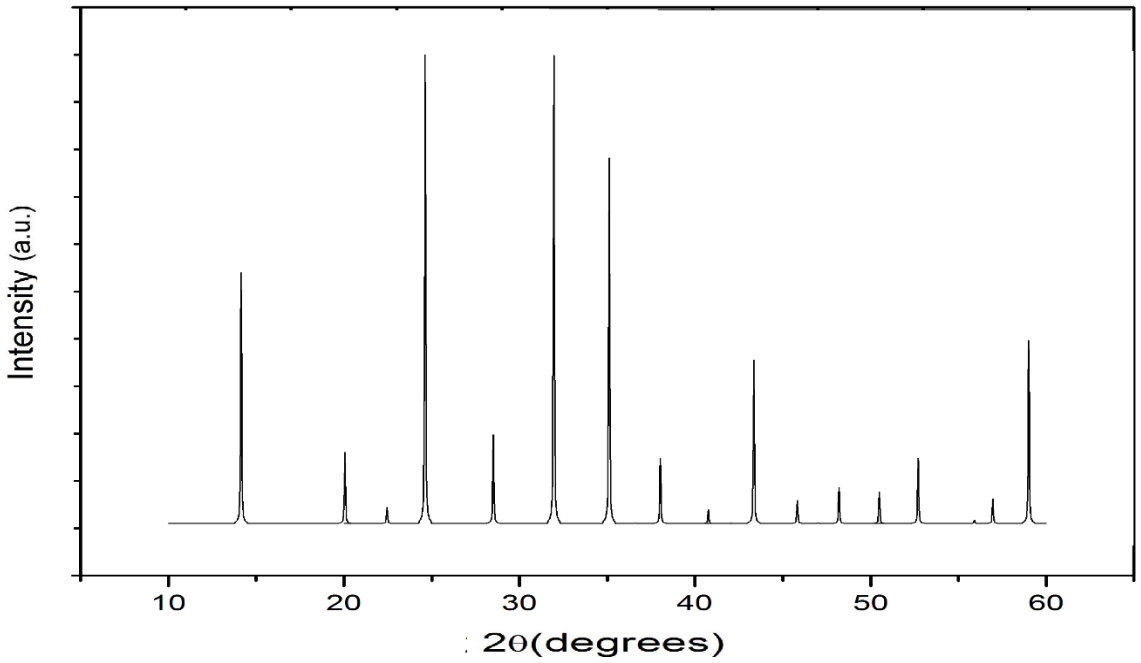

Figure 5. 4. Simulated diffraction (XRD) pattern of sodalite from IZA's database of zeolite structure (Treacy and Higgins, 2007).

Figure 5.5 presents the XRD patterns of the samples obtained with varying water/CFA ratio at initial fixed conditions shown in Table 8.1.1 (Appendix 1).

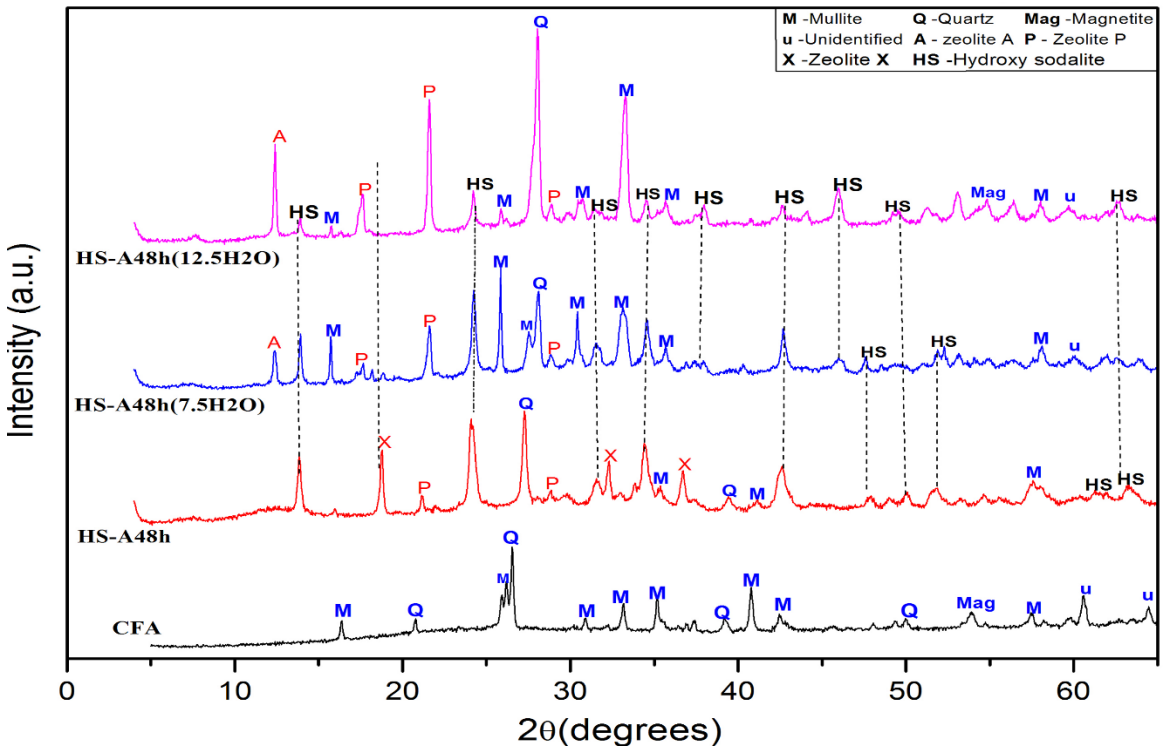

Figure 5. 5. XRD patterns of the samples obtained with varying water/CFA ratio (HS-48 sample for 5:1, HS-A48h(7.5H2O) for 9.5:1 and HS-A48h(12.5H2O) for 12.5:1 ratio) at initial fixed synthesis conditions.

From the diffraction patterns of the produced samples (e.g. Figure 5.5), crystallinity characteristic with regard to the mineralogical phase of HS zeolite, was determined using equation 3.7 as reported in section 3.4 (Chapter 3). Mineralogical phase purity was determined using equation 3.8 as follows.

$$\%\ \text{Crystallinity} = \frac{\text{Sum of areas of the crystalline phase of interest (CPI)}}{\text{Sum of the area of CPI in the reference sample}} \times 100 \qquad (3.7)$$

$$\%\ \text{phase purity} = \frac{\text{Sum of areas of the crystalline phase of interest (CPI)}}{\text{sum of areas of all crystalline and amorphous phases}} \times 100 \qquad (3.8)$$

Figure 5.6 shows the effect of varying water/CFA ratio on crystallinity and purity of the obtained HS zeolite samples

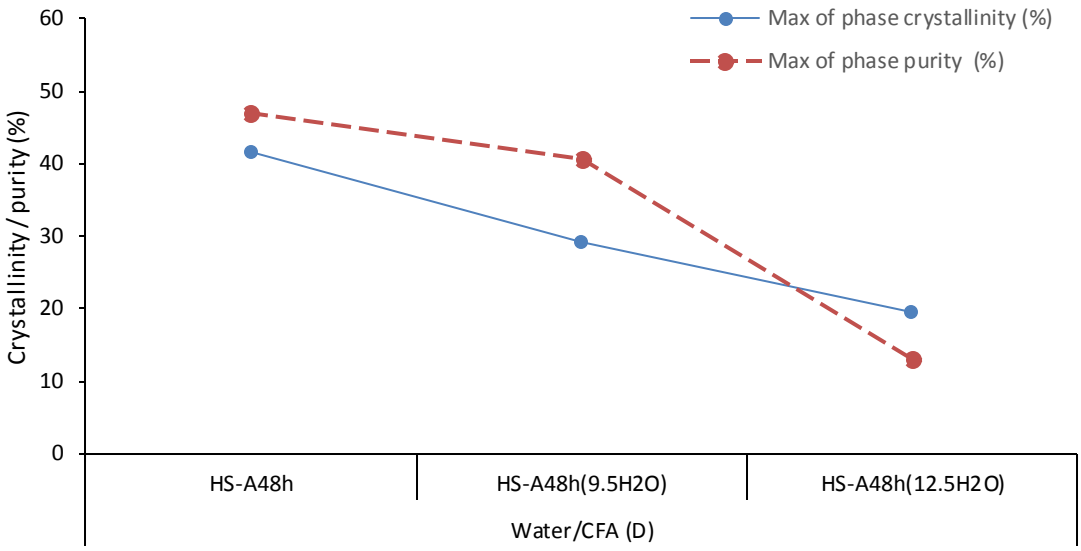

Figure 5.6. Phase crystallinity and purity of samples obtained with varying water/CFA ratio of 5:1, 9.5:1 and 12.5:1 (Ageing = 48h, 47°C, NaOH/CFA ratio = 1:1; hydrothermal condition = 48h, 140 °C).

It is observed that sample HS-A48h demonstrated a moderately pure phase HS zeolite, mixed with phases of zeolite X, P and unconverted quartz (Figure 5.5). With an increase in water/CFA ratio to 7.5:1, it was observed that the intensity of all the common and major HS zeolite peaks (2θ = 14.14°, 24.64, 35.1 and 43.36°) decreased. Sample HS-A48h(9.5H_2O) only showed two minor additional peaks of HS at 45.99 and 47.6° 2θ, and showed additional and considerable high intensity peaks of mullite phases (at 2θ = 15.75°, 25.84, 27.6, 30.4 and 33.15°), including a peak of zeolie P (P) with considerably increased intensity at 21.6° 2θ. Consequently, sample HS-A48h(9.5H_2O) showed a lower phase purity of HS zeolite than the previous sample (HS-A48h). The intensity of the major zeolite A (A), P, Q and M peaks observed at 12.5°, 21.6°, 28.08° and 33.15° 2θ respectively, significantly increased as water/CFA ratio further increased to 12.5:1. The intensity of all the HS zeolite phase in contrast, decreased considerably, such that sample HS-A48h(12.5H_2O) further showed lower phase purity of HS zeolite. Nonetheless, it is largely observed that quartz (as a major fly ash constituent) was not fully transformed under all the various conditions applied.

By the observation made based on the intensity of HS peaks, phase crystallinity was determined relative to the reference sample using the area of the peaks as indicated by equation 3.7 (section 3.4). Phase purity was determined as the concentration of HS peaks relative to sum of peaks of phases present in the sample as shown by equation 3.8. Based on the above, Figure 5.5 showed

that sample HS-A48h exhibited a phase crystallinity (indirect reflection of peak intensity or area) and purity of 41.5 % and 47 % respectively. Phase crystallinity was decreased to 29.2 % and phase purity to 40.56 % with an increase in water/CFA ratio of 7.5:1, whereas these further decreased to 19.6 % and 13 % respectively with further increase in water/CFA ratio of 12.5:1. The trend of increasing water/CFA ratio with decrease in both phase crystallinity and purity of HS (associated with poor conversion of amorphous content in fly ash), is in agreement with the finding reported by Ameh et al. (2020) on BEA zeolite. Ameh et al. (2020) found that nucleation and crystal growth is associated with reduced water content, of which the minimum water/CFA ratio of 5:1 in this work, proved to be the optimum in this regard. Further analysis of the samples obtained by varying water/CFA ratio, was conducted using the SEM analysis.

Figure 5.7 depicts the micrographs of obtained samples with varying water/CFA ratio. The corresponding average crystal sizes of the obtained samples, determined from XRD data using the Scherrer equation (equation 3.9), are reported in Table 8.1.1 (Appendix 1).

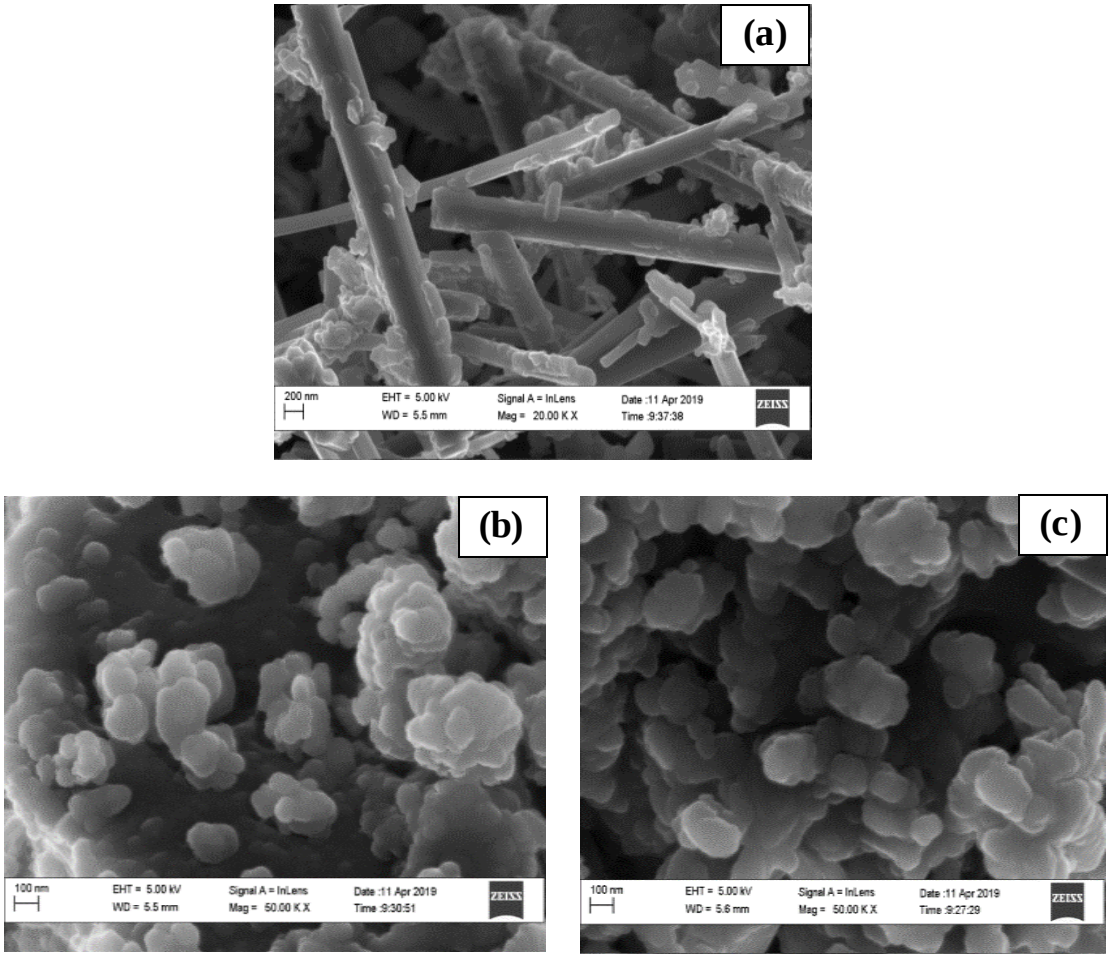

Figure 5. 7. SEM micrographs of samples obtained with varying water/CFA ratios of **(a)** 5:1; **(b)** 9.5:1 and **(d)** 12.5:1 at Ageing = 48h, 47 °C.

SEM micrographs in Figure 5.7 depict the crystal morphology of samples obtained from varying water/CFA ratio. The baseline sample HS-A48h (a) was observed with nanocrystals (20.16 nm) with flake-like particles in major and comparable proportion. As the water/CFA ratio was increased, the above particles were transformed to form agglomerated of crystals (Figure 5.6b), consequently resulting in increased crystal size of 29.46 nm. This could have indicated that the disappearance of the flake-like particles in sample HS-A48h(7.5H_2O), mainly corresponded to phase of zeolite (X) previously shown in sample HS-48h via XRD pattern (Figure 5.5). Slight disintegration of the agglomerated morphology was observed with further increase in water/CFA ratio (12.5:1), which corresponded to the decreased crystal size of 27.95 nm shown by sample HS-A48(12.5H_2O) (Table 8.1.1, Appendix 1). The eventual transformation of particles gradually occurred with an increase in water/CFA ratio, which is a reflection of slower nucleation of particles mainly caused by dilution of the synthesis mixture (Ameh et al., 2020). From the above, it was therefore found that the morphology depicting the combination of nanosized and flakes-like particles was associated with optimal water/CFA ratio (5:1) at corresponding fixed conditions (Table 8.1.1, Appendix 1). The optimal condition thus far, was based on high phase crystallinity and purity characteristic revealed previously. Thus increasing water content did not prevent phase impurity. Further analysis of the samples was carried out using the FT-IR analysis.

The FT-IR analysis was conducted as described in section 3.4. Origin (version 8.5) was used to translate the generated raw data to graphical form and the spectra of produced samples were restricted for the characteristic bands between the region of 450 and 2000 cm^{-1}. The resultant vibrational bands in the FT-IR spectra of the samples with varying water/CFA ratio, including those of all the produced samples reported in Table 3.2 (section 3.3.1), were assigned in accordance to the general fingerprint vibrational modes of zeolites indicated in Table 5.2.

Table 5. 2. General infra-red vibrational modes of zeolites (Puppe and Weitkamp, 1999, Fernández-Jiménez and Palomo, 2005)

Type of vibrational mode	Frequency range	Location of vibration in relation to framework
OH^- deform (bending)	1600-1700	Internal tetrahedral
Assymetric stretch (Si–O–Si)(T–O)	950-1250	
Symmetrical stretch (O–T–O group)	650-720	
T–O bending	420-500	
Assymmetric stretch	1050-1150	External linkage
Symmetric stretch	750-850	
DR4units	720-730	
DR6 units	630-640	
Double rings	500-650	
Pore opening	420-300	

The FT-IR spectra of the samples synthesised with varying water/CFA ratio, with assigned characteristic bands, are reported in Figure 8.4.1(c) (Appendix 1).

The FT-IR spectra presented in Figure 8.4.1(c) in the appendix, present the structural configuration of various synthesised samples, starting with the samples obtained with varying water/CFA ratio (as per order of experimental stage reported in Table 3.2, section 3.3.1). The characteristic bands in the spectra of the samples involved are respectively listed as follows and were assigned in accordance to vibrational modes of zeolite (Table 5.2). The spectrum of sample HS-48h (baseline) exhibited three minor characteristic bands at 450 cm^{-1}, 627 cm^{-1} and 1630 cm^{-1}, and one relatively broad band at 980 cm^{-1}. According to the generally assigned vibrations of zeolites (Table 5.2), the above bands were attributed to pore opening in the internal tetrahedral ring, external linkage of double rings, OH^- bending vibration and T–O–T (T = Si or Al) assymmetric stretching as respectively (Fernández-Jiménez and Palomo, 2005, Puppe and Weitkamp, 1999). The band at 627 cm^{-1} disappeared and the broader band at 980 cm^{-1} gradually narrowed as water/CFA ratio was varied to both increased ratios (Figure 8.4.1(c)) during observation. This could have been due to hindered nucleation and lower zeolite characteristics induced thereof, as discussed earlier.

In comparison to several other assigned vibrations reported in literature however (Fernández-Jiménez and Palomo, 2005), the FT-IR spectra of all the varying samples (Figure 8.4.1(c), Appendix 1) commonly depicted only a single relative broad band at 980 cm^{-1}. Based on this, the respective samples are not corresponding to the configuration structure of HS zeolite. This finding correlates to their low phase crystallinity and purity of the sample reported earlier (Figure 5.6). HS-A48h sample, based on the relatively high number of zeolite vibrational mode observed and comparably broad T-O peak at 980 cm^{-1}, presented yet the optimal water/CFA ratio (5:1) in terms of structural configuration (Figure 8.4.1(c)).

Further analysis of the samples was conducted using the EDS analysis as described in section 3.4. Table 5.3 presents the monovalent elemental composition of the samples obtained with varying water/CFA ratio.

Table 5. 3. Elemental composition of samples obtained with varying water/CFA ratio

Sample	**Element** (atomic, w/w %)												
	O	**Al**	**Si**	**Na**	**Mg**	**K**	**Ca**	**Ti**	**Fe**	**P**	Total	**Si/Al**	**Na/Al**
HS-A48h	44.48	13.46	19.94	14.71	0.76	-	3.35	0.94	2.36	-	100.0	1.48	1.09
HS-A48h(12.5H_2O)	43.54	15.50	21.53	11.89	0.69	-	3.28	0.85	2.71	-	99.5	1.39	0.77
HS-A48h(7.5H2O)	43.79	14.31	20.63	13.41	0.91	0.18	3.54	0.97	2.27	-	100.0	1.44	0.94

The EDS data in Table 5.3 shows that sample HS-48h consisted dominantly of Si (19.94 %), Al (13.46 %) and O (65.15%) to which the above elements and other alkali metals present are attached to form their oxides form (Si–O–Al). A significant proportion of sodium (Na) (14.71 % by weight) was also observed in HS-48h. There was a gradual increase in both Si and Al proportion with variation in water/CFA ratio. This trend was reversed with Na. Consequently, nearly a comparable Si/Al ratio was observed (1.48>1.44>1.39) with the consecutive increase in water/CFA ratio, whereas Na/Al ratio decreased (1.09>0.94>0.77) due to the decreasing proportion of Na. This implies that Na content deriving from NaOH became diluted or under-saturated with an increase in water content. According to Rayalu et al. (2000), the insufficient concentration of Na restricts stabilisation of zeolite framework. This is presented in terms of decreasing Na/Al ratio in this work (Table 5.3) and corresponds to the impure framework structure as per FT-IR spectra (Figure 8.4.1(c)), induced with an increase in water/CFA ratio.

The identification of the Si, Al (T-atoms) or Si–O–Al units as major components, followed by Na (sodium) elements (Table 5.3), proves that the respective samples evaluated for water/CFA ratio, reflected the characteristic of a typical zeolite in terms of elemental composition in their structure. This is in agreement to literature work reported concerning zeolite materials (Querol et al., 2002, Weitkamp, 2000). HS-A48h sample exhibited the highest proportion of the characteristic major elements, given with Si/Al ratio of 1.48 and Na/Al ratio of 1.09 (Table 5.3). The above validate that HS-A48h sample was associated with relatively more stable zeolite configuration structure (Rios et al., 2009, Volli, 2015) and yet, presents the optimal water/CFA ratio for HS zeolite in terms of elemental composition.

5.1.3. Effect of presynthesis ageing time on the formation of HS zeolite

This subsection reports on the effect of presynthesis ageing time in the formation of HS zeolite. The investigation was carried in the second stage of the experiment (at optimised water/CFA ratio, Table 3.2) following the same procedure described in section 3.3.1. Three ageing conditions of 48, 96 and 1.5 hours were used for the investigation, of which sample HS-A48h previously presenting the optimal water/CFA ratio at 48-hour ageing time proposed by Musyoka et al. (2011), was used as the baseline (Table 3.2, section 3.3.1). The ageing conditions in order of decreasing ageing time were assigned with code names HS-A96h, HS-48h and HS-1.5h. The samples with the varying ageing time conditions were produced in the second stage of catalysis synthesis according to the procedure reported in section 3.3.1. The resultant products were characterised using XRD, EDS and FT-IR analyses as described in section 3.4.

XRD patterns of the obtained samples with varying ageing time are presented in Figure 8.2.1(c) (Appendix 1). The effect of varying water/CFA ratio on crystallinity and purity of the obtained HS zeolite samples is shown in Figure 5.8.

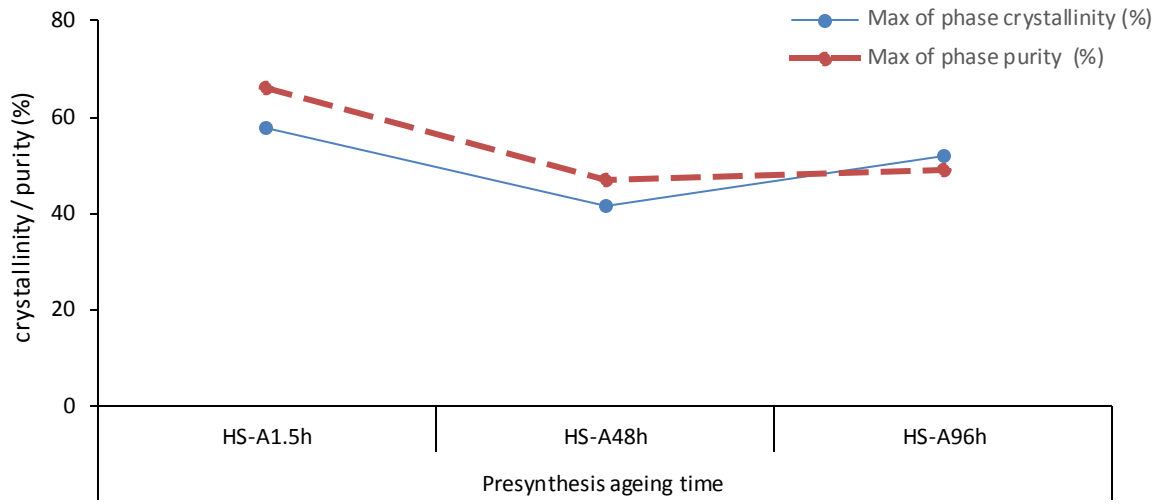

Figure 5. 8. XRD patterns of samples obtained with varying ageing time at 47°C ageing temperature

Sample HS-48h previously, showed a moderately phase purity of HS at 47 % purity, and by virtue of assigned HS XRD peaks of high intensity, showed a phase crystallinity of 41.5 % (Figure 5.6, section 5.1.2). According to Figure 8.2.1(c-d) (Appendix 1), mixed phase HS zeolite (coexisting with zeolite X, P and quartz and mullite precursors) that retained from varying water/CFA ratio, still remained after varying the ageing time at fixed conditions prescribed in Table 3.2 (section 3.3.1). The proportion of the constituent co-existing phases however differed, yielding purer phase HS in the course of varying ageing time at optimised water/CFA ratio (Figure 8.2.5, Appendix 1).

With relative increase in ageing time from the 48-hour baseline to 96 hours, crystallinity of the produced HS zeolite (HS-A96h) increased to 51.8 %, and the obtained HS sample showed a negligibly decreased purity of 47 % (Figure 5.8). The major peaks of HS at 14.14°, 24.64° and 35.1° 2θ appeared broader as the ageing time varied to 96 hours (Figure 8.2.1(d), Appendix 1). Nonetheless, the intensity of the above peaks, including those of HS observed at 32.4° and 43.01° 2θ, increased as ageing time was decreased to 1.5 hour. It was also observed simultaneously that the intensity of the major quartz (Q) and zeolite X (X) peaks at 27.4° and 18.8° 2θ, significantly decreased as the ageing time decreased to 1.5 hour.

The above increase in phase crystallinity of 57.6 % and phase purity of 66 % (shown by sample HS-1.5h) was determined via the XRD pattern using equation 3.7 and 3.8 (section 3.4). Querol et al. (2002) suggests that the observed increase in the above characteristics can be attributed to relatively high dissolution of Si and Al from the amorphous and crystalline phases (M, Q)

of fly ash at the ageing period of 1.5 hour. The reduced 1.5-hour ageing condition differs to the optimised condition of 48 hours proposed by Musyoka et al. (2011) and presents a more cost-effective ageing condition for HS zeolite from this work. Hence, the ageing time condition of 1.5 hour, in lieu of the baseline ageing condition of 48-hour as proposed initially in this work, was chosen as the optimal ageing time to improve crystallinity and purity of HS zeolite.

Figure 5.9 presents the SEM micrographs of the obtained samples with varying ageing time. The corresponding average crystal sizes are reported in Table 8.1.1 (Appendix 1).

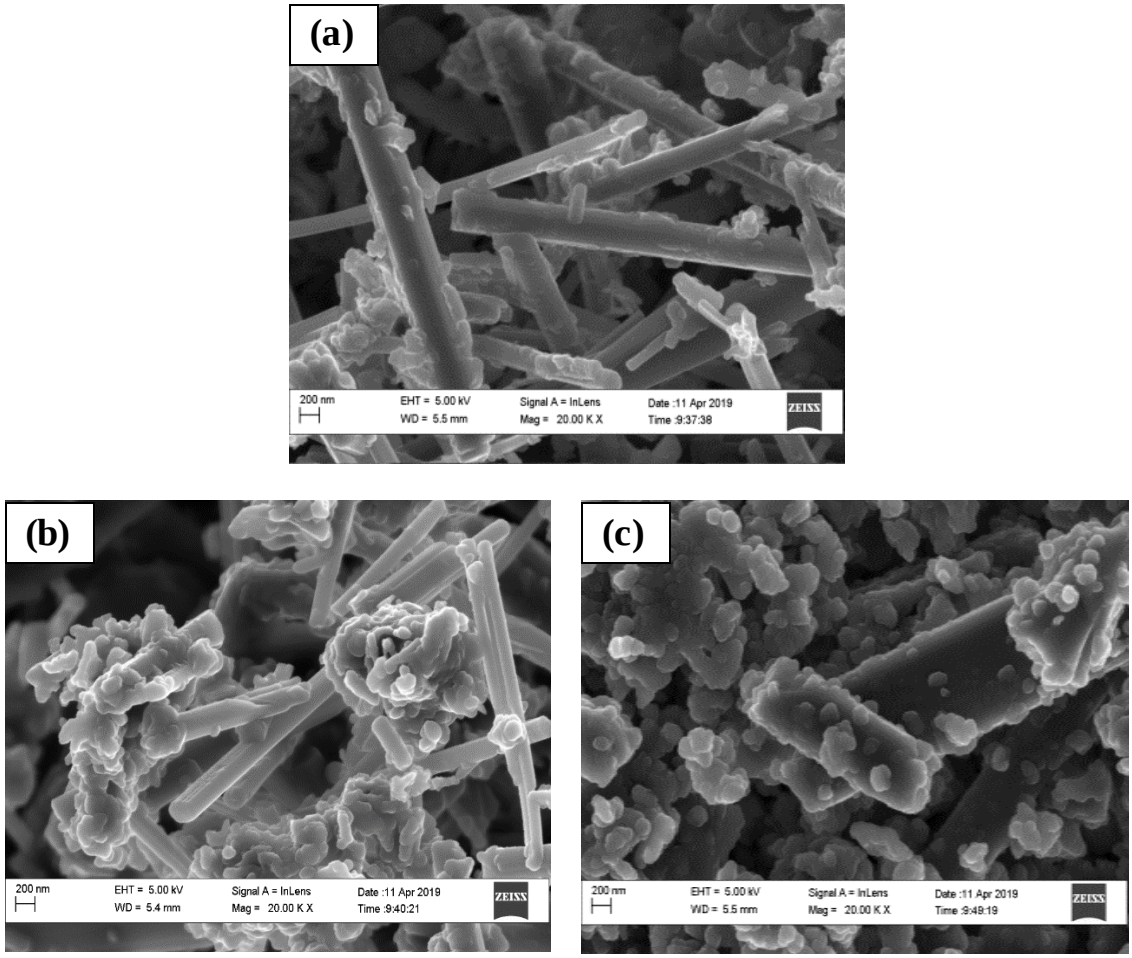

Figure 5.9. SEM micrographs of samples obtained with varying ageing time (1.5, 48 and 96 h) at 47 °C ageing temperature, **(a)** HS-A48h, **(b)** HS-A96h and **(c)** HS-A1.5h (previously coded as HS-A47 °C).

The SEM micrographs in Figure 5.9 presents the crystal morphology of the samples obtained with varying ageing time. Sample HS-A48h (baseline) as previously stated, showed mixed morphology of nanocrystals and flake-like particles (Figure 5.9a). As the ageing time was varied to 96 hours, the above particles were transformed into a slightly more integrated and

more crystalline semi agglomerated-shape crystals (HS-A96h sample). A much more crystalline HS sample, majorly containing rectangular-shaped crystals, resulted from decreased ageing time to 1.5 hour (sample HS-A1.5h). On the basis of the metastable behaviour of zeolites, it is suggested by Belviso et al. (2010) that the particles retained in sample HS-96h and in minor proportion in HS-A1.5h, are associated with quartz (Q), zeolite P and X coexisting with the phase of HS in these samples (Figure 8.2.1(d), Appendix 1). The identified HS particles (crystals) in sample HS-48h were characterised with average crystal size of 16.87 nm (HS-48h). This by virtue of slightly more integrated and thicker crystals observed in HS-A96h sample, with a size of 20.16 nm with an increase in ageing time to 96 hours. Larger HS crystals with an average size of 27.71 nm, evolved resulted with a decrease to 1.5-hour ageing time (Table 8.1.1, Appendix 1). In agreement with Buhl et al. (2011), the above demonstrates that variation in synthesis protocols affect crystal size, the increase in average crystal size as observed, is in direct correlation with the increase in crystallinity observed of the respective samples (Table 8.1.1). Hence, ageing at 1.5 hour (sample HS-1.5h), based on a more evolved and defined crystalline morphology and which corresponds to relatively high crystallinity and purity shown by HS-1.5h, is validated as the optimal ageing time. Further analysis to validate the above, was conducted using the FT-IR as described in section 3.4.

The FT-IR spectra of the samples obtained with varying ageing time, is presented in Figure 8.4.1 (b&d)(Appendix 1). The FT-IR spectra (Figure 8.4.1(d), Appendix 1), depicting the structural configuration of the product samples with varying ageing time, revealed that sample HS-48h as previously reported, showed characteristic bands at 450 cm^{-1}, 565 cm^{-1}, 627 cm^{-1}, 637 cm^{-1}, the most relatively broad band at 980 cm^{-1} and, a minor band at 1630 cm^{-1}. The intensity of all the presented bands assigned previously (Fernández-Jiménez and Palomo, 2005) drastically decreased as the ageing time was increased to 96 hours (HS-96h); whereas this conversely increased as the ageing time was reduced to 1.5-hour. The relatively improved structural configuration shown by sample HS-A1.5h, is suggested by Rayalu et al. (2000) and Volli (2015) to have been due to comparably higher concentration of Na (sodium) content present in the sample. The above is substantiated based on higher Na/Al ratio (Na/Al = 0.95) shown by the sample (Table 5.4), suggesting in this case that the improved configuration of HS-A1.5h sample directly correlates with its higher crystallinity in relation to both HS-A48h and HS-A-96h sample (obtained after 48 hour and 96-hour ageing time).

Table 5.4 presents the EDS data of the produced samples from varying ageing time conditions.

Table 5. 4. EDS data of samples obtained with varying ageing time at 47°C ageing temperature

Sample	**Element** (atomic, w/w %)											
	O	**Al**	**Si**	**Na**	**Mg**	**K**	**Ca**	**Ti**	**Fe**	Total	**Si/Al**	**Na/Al**
HS-A48h	46.48	13.46	19.94	9.69	0.76	-	3.35	0.94	2.36	100.0	1.48	0.72
HS-A96h	46.64	13.73	19.48	11.95	0.57	0.22	2.85	0.79	1.23	100.0	1.42	0.87
HS-1.5h/HS-A47°C	44.38	14.04	20.38	13.34	0.79	-	3.86	1.17	2.04	100.0	1.45	0.95

Table 5.4 shows that sample HS-A1.5h, followed by HS-A96h and HS-A48h respectively, contained the most Na (sodium) on mass basis (13.34 wt. %). Based on the above, Li and Yu (2014) and Buhl et al. (2011) suggests that the additional band shown by HS-A1.5h at 1450 cm^{-1}, is associated with sodium (Na) carbonate (CO_3) in the sample derived from sodium hydroxide.

Further, Rayalu et al. (2000) support that sample HS-A1.5h with a higher Na/Al ratio exhibited a higher Na content as compared to HS-A48h and HS-A96h. This corresponds to the following order of improved zeolite structural configuration (framework stability) of the respective samples: HS-A1.5h > HS-A96h> HS-A48h. The presented order strongly validates the order of structural configuration as previously discussed and reported from the actual FT-IR spectra of the samples in Figure 8.4.1 (b&d) (Appendix 1).

Hence, ageing at reduced condition of 1.5 hour under fixed conditions, was found sufficient as the optimal ageing time with respect to phase crystallinity, purity, crystal morphology and structural configuration. Further investigation on varying ageing temperature was therefore carried out based on the optimised ageing time obtained, owing to its relatively low energy requirement and cost-effectiveness with regard to HS zeolite synthesis via the direct hydrothermal method.

5.1.4. Effect of presynthesis ageing temperature on the formation of HS zeolite

After optimising the ageing time condition discussed previously, this subsection discusses the effect of ageing temperature on the formation of HS zeolite. The investigation was carried in the third stage of the experiment (Table 3.2, section 3.3.1) following the protocol described in section 3.3.1. Two ageing temperature conditions were selected for the investigation, 47 and 70 °C. Sample HS-A1.5h presenting the optimal ageing time was the baseline sample regarding ageing temperature of 47 °C. The additional sample with the varying presynthesis ageing

temperature of 70 °C produced in the third stage of synthesis following the procedure reported in section 3.3.1. Both product samples, in order of increasing ageing temperature coded as HS-47°C (instead of HS-A1.5h) and HS-70°C (Table 3.2). For comparison purposes, the additional sample (HS-70°C) was also characterised using XRD, EDS and FT-IR analyses as described in section 3.4.

XRD patterns and the corresponding phase crystallinity and purity characteristics of the obtained samples with varying ageing time are presented in Figure 5.10.

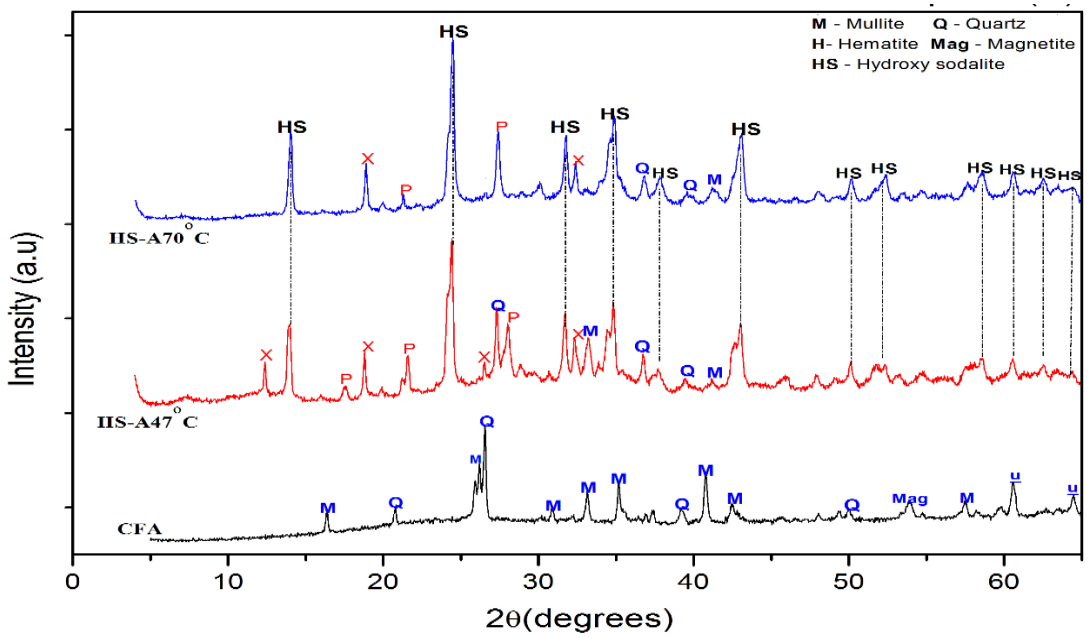

(a)

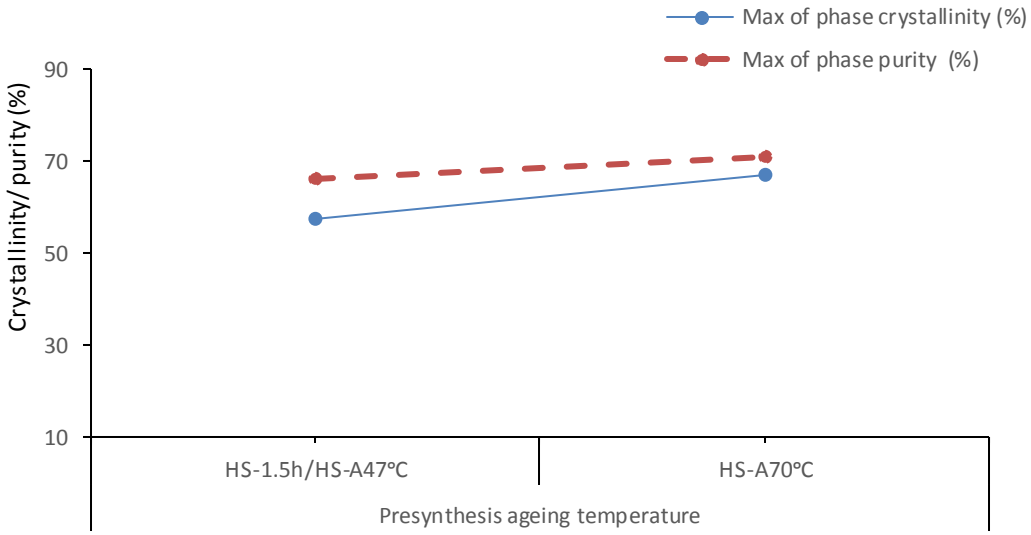

(b)

Figure 5.10. (a) XRD patterns of samples obtained with varying presynthesis ageing temperatures, **(b)** effect of varying ageing temperature on crystallinity and purity of HS zeolite at 1.5-hour ageing time.

The XRD data shown in Figure 5.10, presents the mineralogical composition (a), crystallinity and purity (b) of samples produced with varying ageing temperatures. Sample HS-47°C, previously coded as HS-1.5h (Figure 5.8), consisted of mixed phases including major peaks of HS identified at 13.92°, 24.24° and 34.77° 2θ, and several peaks of quartz and other zeolite forms (Zeolite P, X,) presented in Figure 8.2.1(d).

As it can be observed in Figure 5.10(a), the intensity of most major peaks of HS (14.02°, 24.43° and 34.89° 2θ) increased as presynthesis ageing temperature was increased to 70 °C. This corresponded to the observed increase from 57.6 to 67 % phase crystallinity with an increase in the ageing temperature. Phase purity on the other hand, was also slightly increased from 66 to 71 % as the ageing temperature increased. The above was majorly attributed to disappearance of the following peaks: zeolite X (X) peaks at 12.31°, zeolite P at 17.52 ° and mullite (M) at 33.15° 2θ. Additionally, it was observed that intensity of various noticeable peaks in sample HS-47°C, such as zeolite P at 21.5° and quartz (Q) content at 27.37° 2θ, considerably decreased owing to increased phase purity with an increase in presynthesis ageing temperature.

The resultant increase in crystallinity could be attributed to sufficient supersaturated conditions at the increased ageing temperature to form HS-70°C sample (Rayalu et al., 2000, Murayama et al., 2002). This is proven by relatively highest Na (sodium) content shown by HS-70 °C sample (Table 5.5). The above demonstrates that Na^+ ions promote HS zeolite, Si and Al dissolution from CFA improved at 70 °C, thus enhancing the synthesis of HS zeolite (Rios et al., 2009). Ageing at 70 °C differs from the ageing condition of 47 °C proposed by Musyoka et al. (2011) for HS synthesis with respect to crystallinity and purity of HS zeolite. In support of XRD findings discussed above, further analysis regarding varying ageing temperature, was conducted using the EDS analysis (see section 3.4).

Table 5.5 presents the elemental composition as per EDS of the samples evaluated for varying ageing temperature.

Table 5. 5. EDS data of obtained samples with varying ageing temperature at 1.5-hour ageing time

Sample	**Element** (atomic, w/w %)											
	O	**Al**	**Si**	**Na**	**Mg**	**K**	**Ca**	**Ti**	**Fe**	Total	**Si/Al**	**Na/Al**
HS-1.5h/HS-A47°C	44.38	14.04	20.38	13.34	0.79	-	3.86	1.17	2.04	100.0	**1.45**	**0.95**
HS-A70°C	51.12	13.61	13.52	20.18	0.31	0.06	0.75	0.19	0.26	100.0	**0.99**	**1.60**

The elemental composition as per EDS for samples obtained with varying synthesis temperature (Table 5.5), revealed a considerable change in Si and Al ratio as ageing temperature was increased from 47 to 70 °C. Consequently, the above resulted to decrease in Si/Al ratio from 1.45 to 0.99 as observed. Several researchers have suggested that the Si/Al ratio shown by sample HS-70°C, closely agreed to that of HS zeolite reported in their published work (Nanganoa et al., 2016, Querol et al., 2002). It can also be observed that there was a considerable increase in Na/Al ratio (0.95→ to 1.60). The above resultant Na/Al ratio implies more than sufficient concentration of Na content present in the sample, which as suggested by Volli (2015), is associated with relatively improved framework stability (structural configuration) of sample HS-70°C. Hence, the FT-IR analysis was conducted to validate the above claim.

The FT-IR spectra of the two samples evaluated for varying ageing temperature, in after samples obtained with varying ageing time, are presented in Figure 5.11.

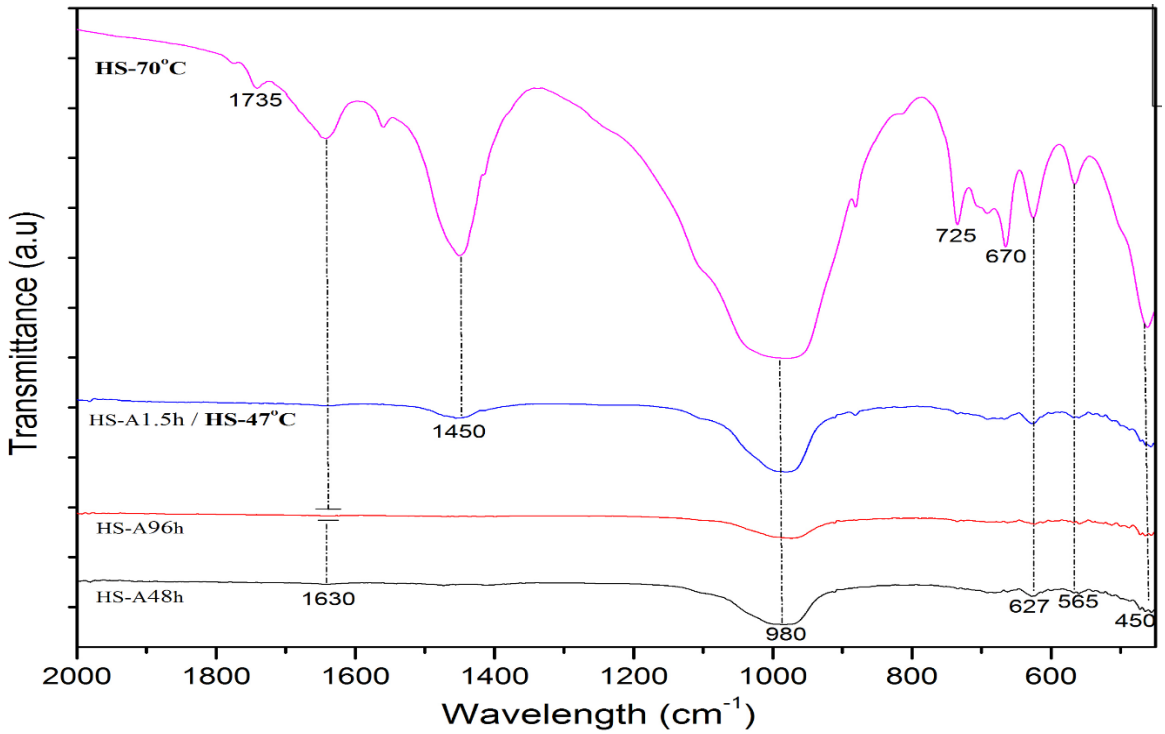

Figure 5.11. FT-IR spectra of samples obtained with varying ageing temperature at 1.5-hour optimised ageing time.

The FT-IR spectra in Figure 5.11, depicts the structural configuration of the evaluated samples. The result previously revealed that samples HS-47°C (earlier coded as sample HS-A1.5h) demonstrated a poor configuration structure of zeolite, with regard to exclusively low intensity bands at 450 cm^{-1} (pore opening) and 980 cm^{-1} (T–O–T units), and a double ring characteristic band at 627 cm^{-1} (Figure 8.4.1(d), Appendix 1 or Figure 5.11) (Puppe and Weitkamp, 1999). It was however observed that the peak of the T–O–T band became broader, and multiple additional bands appeared as the ageing temperature was increased to 70 °C. These include additional double ring vibration observed at 570 cm^{-1}, two symmetric Si–O–Si stretching modes at 670 and 730 cm^{-1}, sodium carbonate (CO_3) impurities at 1450 cm^{-1} and OH^{-1} deforming mode at 1637 cm^{-1} respectively (Fernández-Jiménez and Palomo, 2005, Buhl et al., 2011). The carbonate (CO_3) impurities as also earlier demonstrated by sample HS-96h (Figure 5.11), could arise due to excess concentration of sodium (Na) deriving from sodium hydroxide in the synthesis mixture, shown in terms of high Na/Al ratio of 1.6 in HS-70°C (Table 5.5).

Hence, the framework configuration validates the evidence of better structure caused by the increase in ageing temperature. Thus far, the obtained structural configuration shown by sample HS-70°C (associated with an increase in presynthesis ageing temperature), emerged as

the most improved structure of HS zeolite in this work. HS-70 °C sample was further analysed for SEM in view to evaluate the effect of varying ageing temperature on crystal morphology.

SEM micrographs of the samples evaluated for varying ageing temperature are reported in Figure 5.12. The corresponding average crystal size are reported in Table 8.1.1 (Appendix 1)

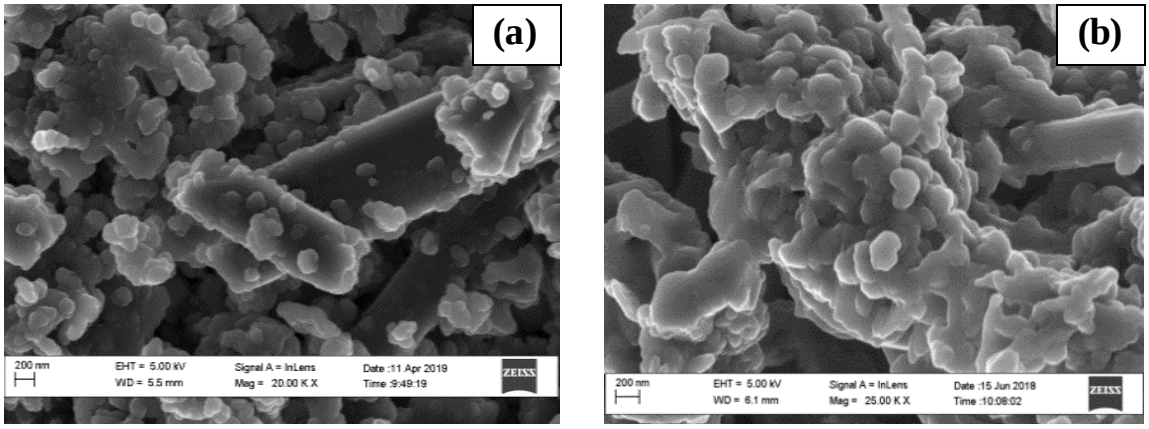

Figure 5. 12. SEM micrographs of samples obtained with varying presynthesis ageing temperatures (47, 70 °C) at 1.5h optimised ageing time, **(a)** HS-47°C (previously coded as HS-A1.5h) and **(b)** HS-70°C.

The rectangular-shaped crystals shown in sample HS-A47°C (as previously shown when coded as HS-A1.5h), were transformed into a much-improved crystalline structure with aggregated pentagonal crystals (HS-70°C), as the ageing time was increased.

As observed, the particles in the resultant sample were closely agglomerated with increase in ageing temperature. Consequently, this corresponded to increase in particle/crystal size (27.71→ 29.08 nm) with the increase in ageing temperature (Table 8.1.1, Appendix 1). As far the author's knowledge is concerned, there is no open literature that describes the crystal morphology of HS as the one for the improved crystalline structure shown by sample HS-70°C (rectangular-shaped) (or either of the samples discussed so far). Nonetheless, based on the finding reported by Buhl et al. (2011) of a unique crystal morphology, it is deduced that HS product is likely to appear with a varieties of crystal morphologies. The crystalline structure is dependent on the synthesis conditions and quality of the product. Owing to improved overall characteristics of HS zeolite because of increase in ageing temperature, further analyses of the evaluated samples were conducted using the BET, t-plot and BJH analysis as described in section 3.4.

The BET, t-plot, BJH data and N_2 adsorption isotherms of samples obtained with varying ageing temperature, are reported in Table 8.6.1 and Figure 8.6.1(b)-(c) respectively (Appendix 1). The pore size distribution curves of the respective samples are presented in Figure 8.6.2(a)-(b) (Appendix 1). The BET, t-plot and BJH (adsorption-desorption) data in Table 8.6.1, presents the textual properties (surface area, pore volume and pore diameter) of samples obtained with varying ageing temperature. Table 8.6.1 (Appendix 1) reveal that HS-47°C sample demonstrated a considerable total exposed BET surface area of 23.12 m^2/g and pore volume characteristic of 0.101 cm^{-3}/g, which considerably decreased to values of 7.57 m^2/g and 0.029 cm^{-3} (as the ageing temperature varied from 47 °C to 70 °C). attributes the decrease in both characteristics to framework and pore blockages caused by an oversaturation of sodium (Na+) in the structural framework of the resultant HS-70°C sample. The above was reflected in terms of increased Na/Al ratio (Na/Al = 1.60) as earlier depicted with increase in ageing temperature (Table 5.5). It is observed that both the total surface area and pore volume characteristic shown by HS-47°C, and the consequent decrease shown by HS-70°C sample, differs to about two to six times less than the literature reported given values for good quality HS zeolite (Nanganoa et al., 2016, Golbad et al., 2017).

Further characterisation using BHJ analysis, Table 8.6.1 (Appendix 1) revealed that HS-47°C sample exhibited an average pore size (diameter) distribution of between 19.2 - 21.9 nm. This was observed to have increased to the range of 21.6 - 22.9 nm, as the ageing temperature was increased (HS-70°C). Notably, the pore size distributions in Figure 8.6.2 (Appendix1) reveal that both samples majorly constituted of 4 nm pore widths, which far exceed the general literature's reported pore diameter value of HS (0.22-0.28 nm) (Querol et al., 2002, Musyoka et al., 2011). The obtained pore size suggests that both samples evaluated for varying ageing temperature, are characteristics of mesoporous HS zeolite (Weitkamp, 2000). This implies that both samples are anticipated to have enhanced molecular diffusion and could therefore serve as suitable catalysts in biodiesel production (Viswanadham et al., 2012). From the finding discussed, ageing at 70 °C, was deemed the optimum presynthesis ageing temperature condition to promote the overall characteristic of HS zeolite (improved crystallinity of 67 % and purity of 71 %). The increased ageing temperature most noticeably promoted the structural configuration of HS zeolite and further was associated with a larger pore size distribution compared to ageing at 47 °C. Although the 70 °C ageing condition was not favourable with regard to total surface area and pore volume characteristics of HS zeolite, the condition was

established as a basis for further investigation and prompted further investigation concerning enhancing the above characteristics. The next section investigates the effect of NaOH concentration in the synthesis mixture, on the characteristic properties of HS zeolite.

5.1.5. Effect of NaOH concentration on the formation of HS zeolite

This subsection discusses the effect of NaOH concentration in the synthesis mixture on the overall formation of HS catalyst. The parameter was investigated in the fourth stage of the experiment as described in section 3.3.1, followed by investigation and establishment of optimal ageing time and ageing temperature in the second and third stage respectively. In view to enhance overall characteristic properties, HS was synthesised using four different NaOH concentrations from baseline NaOH/CFA ratio of 1:1, then varying to 1.2:1, 1.3:1 and 1.4:1. Each of the mixtures was subjected to the optimised ageing conditions of 1.5 hours and 70 °C, followed by hydrothermal synthesis at 140 °C for 48 hours, and the resultant samples in order of increasing NaOH/CFA ratio were assigned with code names HS-A70°C, HS-A70+1.2NaOH, HS-A70+1.3NaOH, HS-A70+1.4NaOH, respectively (Table 3.2, section 3.3.1). The products were characterised using XRD, EDS, FT-IR and BET analyses as described in section 3.4 (chapter 3).

Figure 5.13 presents the XRD patterns of the produced HS samples with varying NaOH concentration in the synthetic mixture. The peak intensities and areas of the XRD patterns were used to estimate the crystallinity and purity of HS zeolite in the obtained samples using equation 3.7 and equation 3.8 respectively (see section 5.1.2). Figure 5.13 shows the effect on crystallinity and mineralogical purity of the synthesised samples.

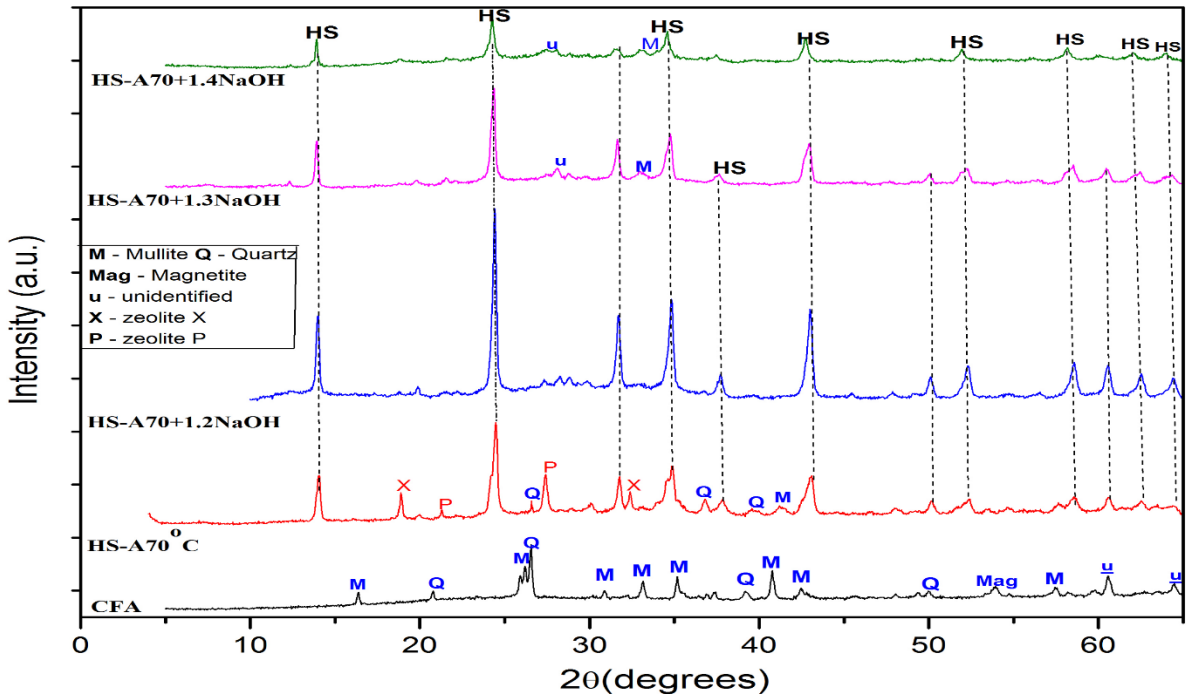

[a]

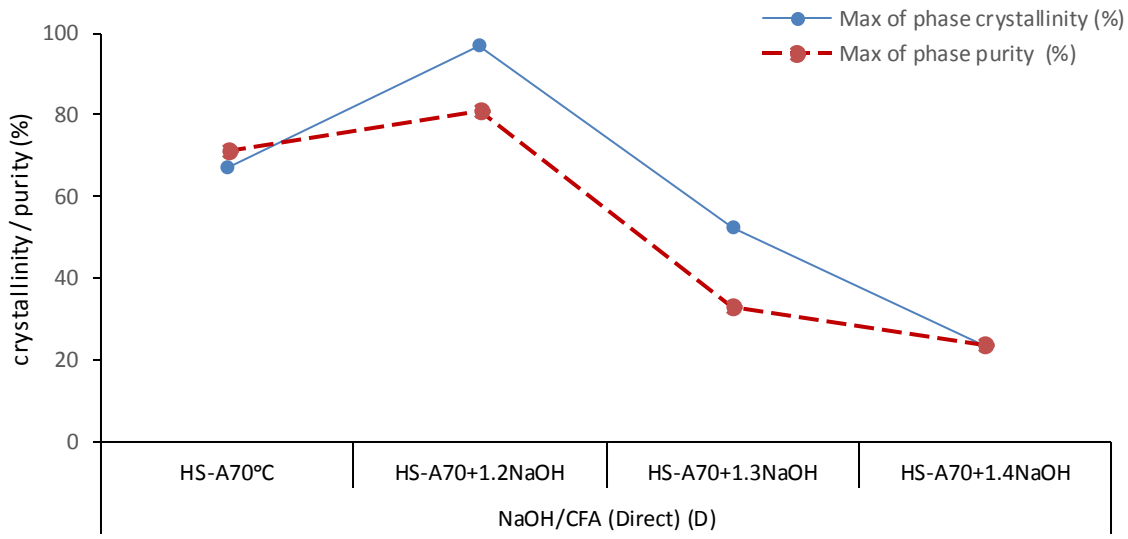

[b]

Figure 5.13. (a) XRD patterns of HS samples obtained with varying NaOH/CFA ratio (1:1, 1.2:1, 1.3:1 and 1.4:1) and **(b)** Effect of NaOH/CFA on phase crystallinity and purity of HS zeolite.

It is observed in Figure 5.13(b) that upon variation of the NaOH/CFA ratio from a baseline ratio of 1:1 to the ratio of 1.2:1, there was a considerable increase in crystallinity of HS zeolite sample from 67 to 97 % and phase purity from 71 to 81 % respectively. Figure 5.13 (a) shows that nearly all quartz (Q) and mullite (M) phases initially present in coal fly ash, disappeared

upon the increase in NaOH/CFA ratio; confirming improved conversion of coal fly ash to HS zeolite.

With a further increase of NaOH concentration in the synthesis mixture (NaOH/CFA of 1:1.3 and 1:1:4), there was a reversal in both phase crystallinity and purity characteristic in 52.3 % and 23.5 % phase crystallinity from the respective concentration, and 23.71 % and 23.64 % phase purity thereof (Figure 5.13b). The resultant decrease in the characteristic properties can be attributed to oversaturation of Na^+ and OH^+ ion associated with possible pore or structural blockages, which in turn might have obstructed the dissolution gradient of aluminosilicate in fly ash and the required crystallisation procedure for HS synthesis (Murayama et al., 2002, Volli and Purkait, 2015). The overall result revealed that there was an inverse correlation between NaOH concentration and both the phase crystallinity and purity characteristics after the optimum at 1.2:1. Thus, NaOH concentration of 1.2:1 was recorded as the optimum chemical condition for synthesis of HS zeolite from fly ash. The above concentration encompasses the optimum NaOH concentrations employed for zeolite synthesis in existing literature (Brassell, 2017, Henmi, 1987, Volli and Purkait, 2015).

The NaOH/CFA ratio of 1.2:1, appeared to be the optimum NaOH concentration with regard to phase crystallinity and purity of synthesised HS zeolite. To validate the results, SEM analysis and crystal size were determined via XRD data as described in section 3.4.

Figure 5.14 and Table 5.6 respectively, present the SEM micrographs and crystal size of synthesised samples as a function of NaOH concentration in the synthetic mixture (Sample HS-A70^{o}C, HS-A70+1.2NaOH, HS-A70+1.3NaOH and HS-A70+1.4NaOH).

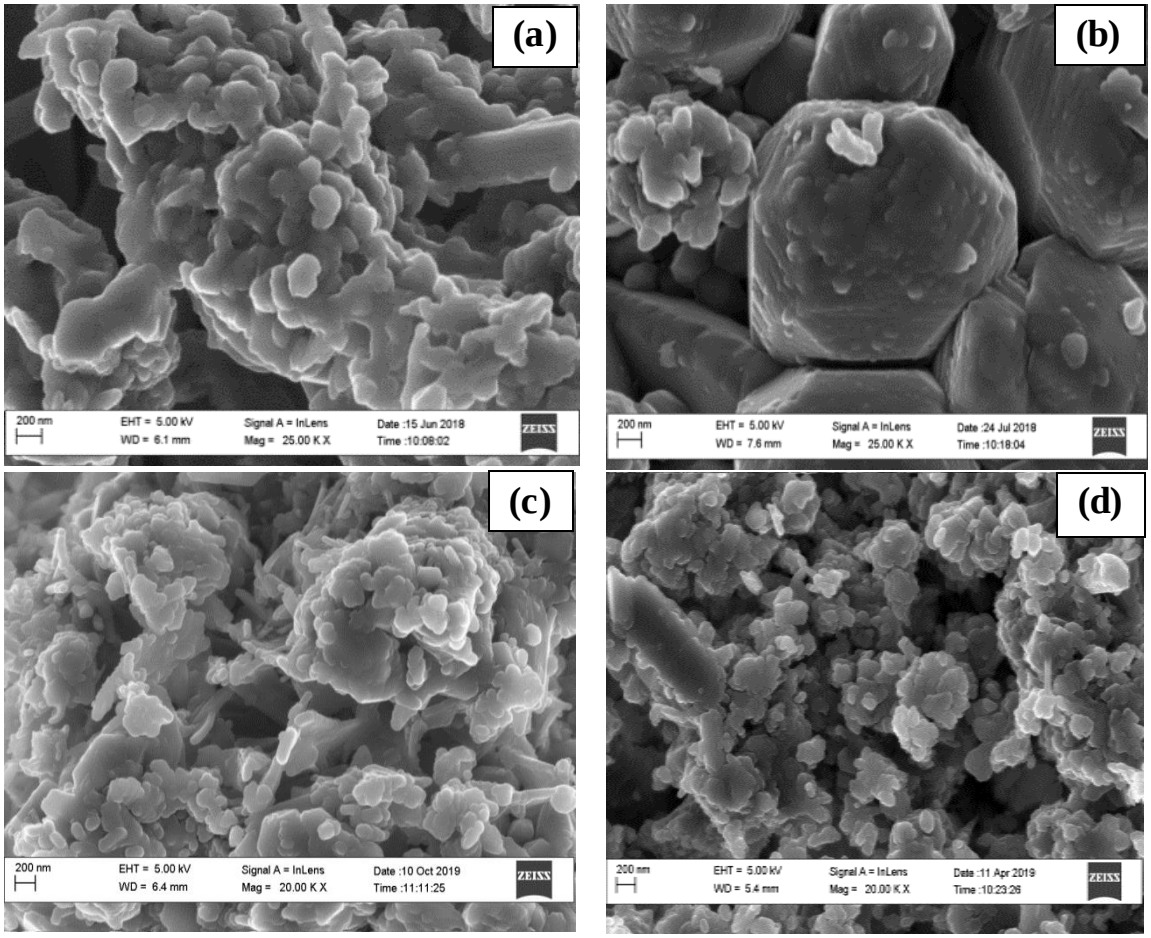

Figure 5.14. SEM micrographs of samples obtained with varying NaOH/CFA ratio (1:1, 1.2:1, 1.3:1 and 1.4:1) in the synthetic mixture at optimised ageing conditions (1.5 h,70 °C) and fixed hydrothermal conditions (48h, 140 °C), **(a)** HS-A70°C; (**b)** HS-A70+1.2NaOH; (**c)** HS-A70+1.3NaOH and **(d)** HS-A70+1.4NaOH

Table 5. 6. Crystal size of samples obtained with varying NaOH/CFA ratio in precursor mixture

Sample	NaOH/CFA ratio	Crystal size[(a)] (nm)
HS-A70°C	1:1	29.08
HS-A70+1.2NaOH	1:1.2	32.38
HS-A70+1.3NaOH	1:1.3	27.94
HS-70+1.4NaOH	1:1.4	24.62

[(a)]Average crystal size determined using scherrer equation (section 3.4)

The SEM micrographs in Figure 5.14 depict the crystal morphology of synthesised samples obtained with varying NaOH concentration in the synthesis mixture. Like previous

characteristics discussed, varying NaOH/CFA ratio in the synthesis mixture affected crystal morphology of the produced HS zeolite samples. Initially, the baseline sample (1:1) HS-A70°C dominantly consisted of aggregated crystals (Figure 5.14a) characterised with an average crystal size of 29.08 nm. By an increase in NaOH/CFA ratio to 1.2:1, the above crystals were evolved into more uniform, defined and large hexagonal-cubic crystals shown in Figure 5.13b. The above corresponded to the observed increased crystal size of 32.38 nm shown by HS-70+1.2NaOH (Table 5.6). With a further increase in NaOH/CFA of 1.3:1 denoted by HS-70+1.3NaOH sample, a relatively less crystalline morphology showing similar crystal habit to HS-70°C crystals, resulted. The latter morphology was retained and rod-like crystals appeared upon further increase in NaOH/CFA ratio of 1.4:1, shown by HS-70+1.4NaOH sample. The former and latter samples (HS-A70+1.3NaOH & HS-70+1.4NaOH), exhibited relatively decreased crystal sizes of 27.94 nm and 24.62 nm. It can be deduced that the crystal habit of the evaluated samples, was directly linked to their crystallinity and purity (Buhl et al., 2011) (Figure 5.13b). An inverse correlation between NaOH/CFA ratio and crystalline morphology feature of the evaluated samples derived from different NaOH concentration mixtures is deduced thus, NaOH/CFA ratio of 1.2:1 is retained as the optimum ratio based on well-defined and high crystalline morphology feature and relatively larger crystal size obtained herein. The optimal crystals of hexagonal-cubic morphology exhibited by HS-70+1.2NaOH sample differ from the thread ball-like morphology typically reported concerning HS zeolite in existing publications (Nabavi et al., 2014, Makgaba and Daramola, 2015). The deviation could have been due to different synthesis conditions, feedstock sources and phase crystallinity and purity characteristic between the existing literature and this work. This work therefore proves that HS zeolite can be characterised with diverse crystalline morphology depending on the synthesis conditions employed and/or crystallinity/purity obtained.

The hexagonal-cubic morpoghology feature was associated with NaOH concentration of 1.2 NaOH/CFA ratio, was considered the optimum crystalline morphology for HS zeolite. Further validation of the synthesised samples (as HS zeolites) using varying NaOH concentration in the synthetic mixture, was carried out using EDS analysis as described in section 3.4.

The elemental composition of the HS zeolites synthesised from the different NaOH ratios in the synthesis mixture, is presented in Table 5.7.

Table 5.7. Elemental composition of HS samples obtained with varying NaOH/CFA in synthesis mixture at optimised ageing conditions.

Sample	**Element** (atomic, w/w %)												
	O	**Al**	**Si**	**Na**	**Mg**	**K**	**Ca**	**Ti**	**Fe**	**P**	Total	**Si/Al**	**Na/Al**
CFA	65.15	11.23	14.86	-	1.54	0.23	4.32	0.30	1.13	1.25	100.0	1.32	-
HS-A70°C	67.51	8.61	8.52	13.79	0.31	0.06	0.75	0.19	0.26	-	100.0	0.99	1.60
HS-A70+1.2NaOH	45.09	14.32	19.5	14.62	0.65	-	3.57	0.93	1.33	-	100.0	1.36	1.02
HS-A70+1.3NaOH*	-	-	-	-	-	-	-	-	-	-	-	-	-
HS-A70+1.4NaOH	45.11	12.25	18.13	14.02	0.96	-	3.71	1.07	3.57	-	99	1.48	1.14

*No analysis conducted for the sample

In addition to the proportional amount of elements contained in each sample, elemental composition was evaluated in terms of Si/Al and Na/Al ratio. These served to predict the surface acidity.

According to Table 5.7, it was found that all samples evaluated consisted of similar elemental composition. This majorly/mainly reflects the oxides of silicon and aluminium in their structural framework (Si-O-Al) (Table 5.7). The samples also exhibited a considerable amount of Na (sodium) in their structural framework.

As previously, the effect of NaOH concentration on the elemental composition was investigated with reference to the baseline sample assigned the code name HS-70°C. This sample was derived from a synthesis mixture containing NaOH and fly ash in the mass ratio of 1:1 (NaOH/CFA = 1.1) (Table 3.2, section 3.3.1). The sample shows major composition of Si, Al and Na; equivalent to Si/Al mass of 0.99 and Na/Al of 1.6. Upon an increase in NaOH ratio to the optimal mass ratio of 1.2:1 NaOH/FA, a drastic increase was observed in the proportion of Si (8.52→19.5 wt. %) and Al components (8.61 →14.32 wt. %). There was also a minor increase in Na content shown in sample HS-70+1.2NaOH due to the additional NaOH in the synthetic mixture (Na = 13.79 →14.62). Consequently, the above were associated with an increase in Si/Al framework ratio (from 0.99 to 1.36); whereas on the other hand the significant increase in Al (aluminium) content, exceeding the Na in the zeolite product, was associated with the observed decreased in Na/Al ratio (1.60→1.02). No EDS data is provided for the addition of NaOH to form the HS-70+1.3NaOH sample (NaOH/CFA = 1.3:1), however, the HS-70+1.4NaOH sample shows that the proportional amount of each of the above-mentioned element was slightly reversed upon further increase to NaOH/CFA mass ratio of 1.4:1.

These findings reveal an overall direct correlation between NaOH concentrations in the synthesis mixture as well a high Si and Al content in the HS products. NaOH/CFA ratio of 1.2:1, was deemed the optimum concentration, as proven via HS-70+1.2NaOH sample. This suggests that the synthesis mixture with NaOH/CFA ratio of 1.2:1, was associated with optimal extraction and dissolution of aluminosilicate glass and dissolution of the quartz and mullite matrix in CFA as compared to other ratios employed (Querol et al., 2002). In connection to the mentioned aluminosilicate extraction, HS-70+1.2NaOH sample was earlier reported to have a Si/Al ratio of 1.36. This ratio differs from the literature values commonly reported for HS zeolite (Si/Al ≈ 0.84-1.00) (Musyoka et al., 2011, Querol et al., 2002), and suggests that HS-70°C sample has presented Si/Al ratio which more closely approximates to literature Si/Al ratio of HS zeolite (Si/Al = 0.99). However, higher HS phase crystallinity, phase purity and better-defined crystalline morphology demonstrated by sample HS-70+1.2NaOH (Figure 5.3b, Figure 5.4(b)), in this work is rather suggested for the obtained Si/Al ratio of 1.36. Addition of NaOH, overall, also corresponded to an increased concentration of Na content in the respective products. The overall increase in Al content and Si/Al framework ratio, depicted an overall inverse correlation between NaOH concentration and Na/Al ratio.

Several published work (Viswanadham et al., 2012, Lam et al., 2010) revealed that Si/Al and Na/Al ratio, as reflective of the main elements associated with the framework structure of zeolites, are directly linked to total surface area and pore volume characteristic of zeolite products. Sample HS-70+1.2NaOH, identified with high Si/Al ratio in conjunction with a relatively decreased Na/Al ratio of 1.02, predicts that the corresponding NaOH/CFA ratio may be associated with comparably higher total surface areas and pore volume characteristics (Viswanadham et al., 2012).

From the findings discussed, it can be concluded that high alumina silica (Si and Al) content corresponding to Si/Al ratio of 1.36, and high Na content equivalent to Na/Al ratio of 1.02 shown by HS-70+1.2NaOH, was found to describe high quality HS zeolite. This, hence, attests that the corresponding NaOH/CFA of 1.2:1 is the optimum ratio for the synthesis of HS zeolite from coal fly ash in this work. Further analysis for samples evaluated for varying NaOH/CFA ratio, was conducted using FT-IR.

The FT-IR spectra of HS zeolite from synthesis mixture with different NaOH/CFA ratios are presented in Figure 5.15. The graphical spectra were obtained from the raw spectrum data using

origin software (v.8.5) and is restricted for band characteristic between the region of 450 and 2000 cm^{-1}.

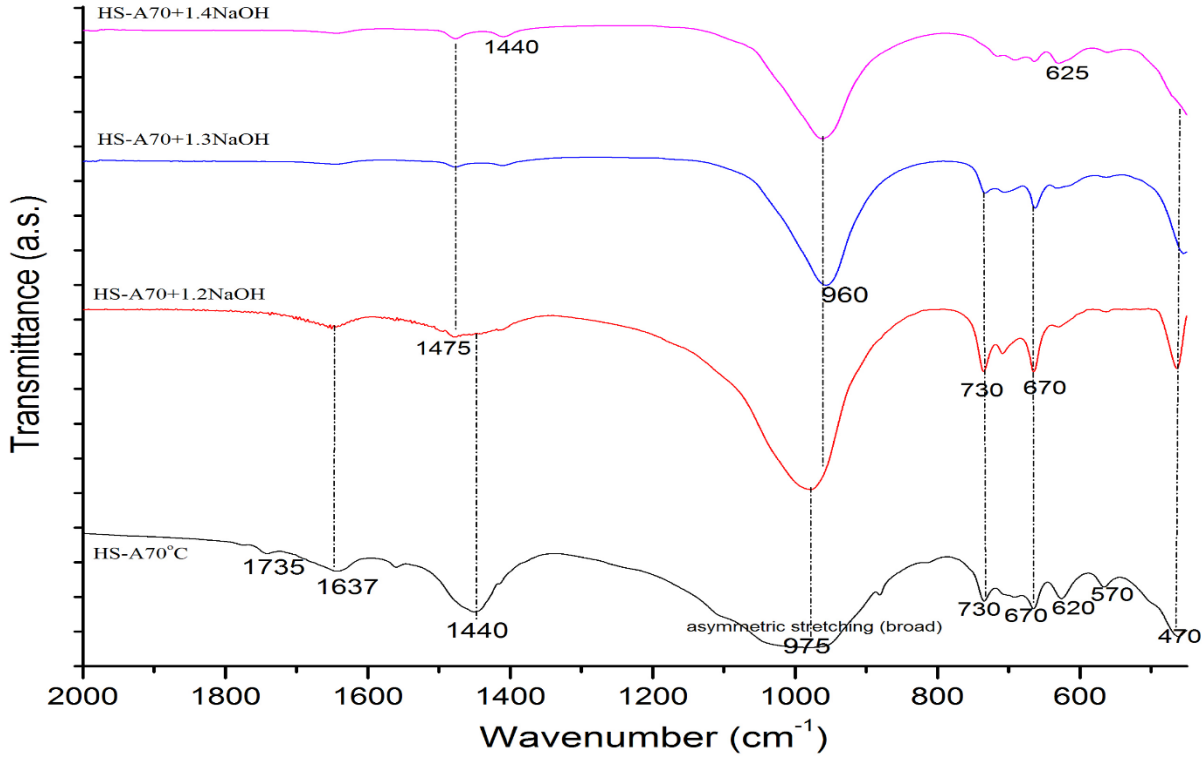

Figure 5.15. FT-IR spectra of direct hydrothermal HS samples obtained with varying NaOH/CFA ratios (1:1, 1.2:1, 1.3:1 and 1.4:1) in the synthesis mixture (optimised ageing condition, 1.5h,70 °C and hydrothermal conditions, 48h, 140 °C).

The FT-IR spectra in Figure 5.15 depicts the structural configuration of samples obtained with varying NaOH/CFA in the synthesis mixture. The spectrum of CFA feedstock as earlier reported initially presented a broad characteristic band exactly at 1095 cm^{-1} (Figure 5.3, section 5.1.2). This band as observed in Figure 5.15, disappeared after synthesis steps and shifted towards lower frequency to form a comparably broader asymmetric stretching band of T–O–T (T = Si or Al) at 975 cm^{-1}. The latter was observed in all samples obtained with varying NaOH concentration, and serve as the least evidence to suggest for successful conversion of CFA to HS zeolite from the various synthesis mixtures.

Sample HS-70°C, initially deriving from the mixture of NaOH/CFA ratio of 1:1 (ageing = 70, 1.5h), presented the condition that emanated the structural configuration of HS zeolite (Section 5.1.4) in this work (Figure 8.4.1(b), Appendix 1). The FT-IR spectrum of HS-70°C sample (prior increase in NaOH/FA ratio) depicted multiple characteristic bands. The bands detected

between the region of 450 and 1060 cm^{-1}, Shirani Lapari et al. (2015) and Musyoka et al. (2011) suggest that HS-70°C sample already represented the structural configuration of a typical HS zeolite. Upon increase in NaOH/CFA from the baseline ratio of 1:1 to of 1.2:1, the asymmetric T–O–T band at 975 cm^{-1}, became narrower as indicated by HSA70+1.2NaOH (Figure 5.15). The narrower band conveys a weaker band, retained at same higher frequency as in previous sample (950 cm^{-1}) (Figure 5.15). Beside the above band, bands at 730 and 670 cm^{-1} in the spectrum of sample HS-70°C, became slightly broader (were evolved) in sample HS-A70+1.2NaOH at 725 cm^{-1} and 650 cm^{-1} respectively. These weak consecutive bands attributed to Si–O–Si bonds were stronger bonds in sample HS-70+1.2NaOH as compared to sample HS-70°C (Musyoka et al., 2011). Further, sample HSA70+1.2NaOH as similar as sample HS-70°C, depicted a more noticeable band at 470 cm^{-1} (between 400 and 490 cm^{-1}). This band was attributed to internal tetrahedron bending vibration of T–O (T= Si or Al) contained in both samples (Musyoka et al., 2011, Brassell, 2017).

It was further observed that the relative increase in NaOH concentration to form sample HS-70+1.2NaOH, resulted in weakening of the observed symmetric band at 1440 cm^{-1} (Figure 15). This band, which prior was attributed to T–O–Al (T= Si or Al) (majorly Al-O units) framework units and compensated for the balance between Si–O and Al–O units in sample HS-A70°C, turned out to be associated rather with Si–O units in sample HS-70+1.2NaOH. The evolved Si-O units corresponds to relatively increased Si/Al ratio exhibited by HSA70+1.2NaOH sample (Table 5.7). Further, the band detected at 1637 cm^{-1} in HS-70°C sample, was attributed to the frequency of OH^- bending deforming (Malonda Shabani et al., 2019, Brassell, 2017). In common to HS-70+1.2NaOH, the above band and the region beyond (i.e. >1637 cm^{-1}), were attributed to OH^- bending deforming. The latter represents water molecules adsorbed and attached within the internal framework unit of HS sodalite (Li and Yu, 2014).

All the characteristic bands observed in the spectrum of sample HS-70+1.2NaOH, were retained and similarly observed upon further increase in NaOH/CFA ratio to form HS-70+1.3NaOH and HS-70+1.4NaOH sample. Narrower bands were however observed upon the gradual increase in NaOH concentration, beyond the NaOH/FA ratio of 1.2:1. The major band detected at 975 cm^{-1} became gradually narrowed in sample HS-70+1.3NaOH, followed by sample HS-1.4NaOH (Figure 5.15). The same applied to bands at 725 cm^{-1} and 670 cm^{-1}.

The narrowing of the bands corresponded to a gradual increase in NaOH concentration. This could be attributed to the degree of saturation of Na content (presented in terms of Na/Al ratio)

(Volli and Purkait, 2015). With an increase in NaOH concentration as reported earlier, there was a decrease in Na/Al ratio (Table 5.7). Hence, the broadness of the major band detected at 975 cm^{-1} for sample HS-70°C, is associated with supersaturation of Na content (high Na/Al ratio = 1.6). This might have impaired the nucleation and growth of HS crystals. The best ratio was most demonstrated by sample HS-70+1.2NaOH, in exhibition of a Na/Al ratio of 1.02 (Table 5.7).

From the finding reported, it is noted that Na (sodium) as charge balance cation associated with Al in the framework units of a zeolite product (i.e. equivalent to Na/Al ratio) is in correlation with structural configuration of the respective HS sample. The structural configuration in turn, based on samples obtained with varying NaOH/CFA in the synthesis mixture, directly correlates to phase crystallinity, purity and morphological crystalline feature of HS zeolite (as previously reported). The spectrum of HS-70+1.2NaOH, by virtue of all the above-mentioned, depicted vibration modes or structural configuration that highly corresponds to HS zeolite.

5.1.6. Effect of direct hydrothermal synthesis time and temperature on the formation of HS zeolite

This subsection focuses on the effect of the direct method synthesis time and temperature condition on the formation of HS zeolite. The experimental protocols for the investigation of the above factors as the fourth and fifth stage (Table 3.2) are described in section 3.3.1 (chapter 3). In reference to 48-hour baseline synthesis time (at 140 °C), four more synthesis conditions of 12, 24, 72 and 144 hours were used to synthesise HS catalyst samples via direct method hydrothermal synthesis at 140 °C (section 3.3.1). The resultant samples in order of increasing synthesis time were assigned with code names HS-12, HS-24, HS-48, HS-72 and HS-144 (Table 3.2, chapter 3). Further synthesis was also conducted at the extended synthesis time (144 hour) but lower synthesis temperature (100°C), yielding the sample assigned with code name HS-144(100°C). The products like previously, were characterised using XRD, EDS, FT-IR and BET analyses as described in section 3.4 (chapter 3). From the resultant XRD patterns, the relative phase crystallinity and purity of obtained samples were determined using the peak intensities and areas by applying equation 3.7 and equation 3.8. The XRD patterns of the obtained samples and effect of the synthesis time and temperature on the corresponding crystallinity and purity of HS, are depicted in Figure 5.16.

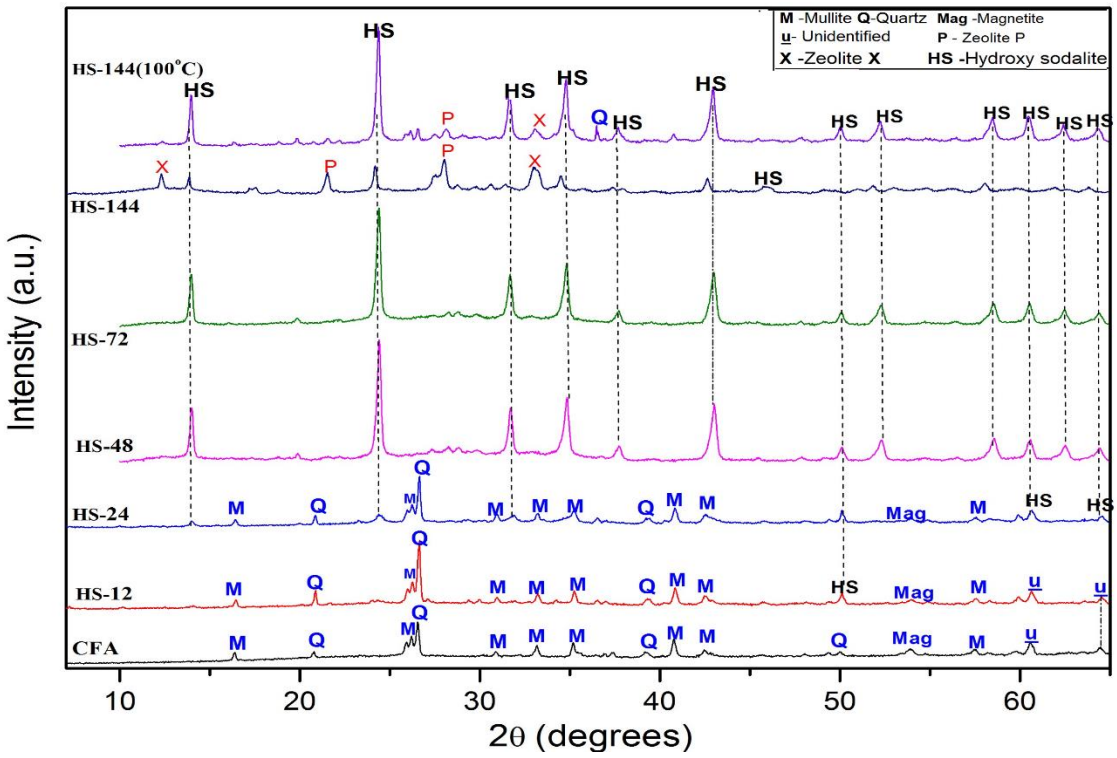

(a)

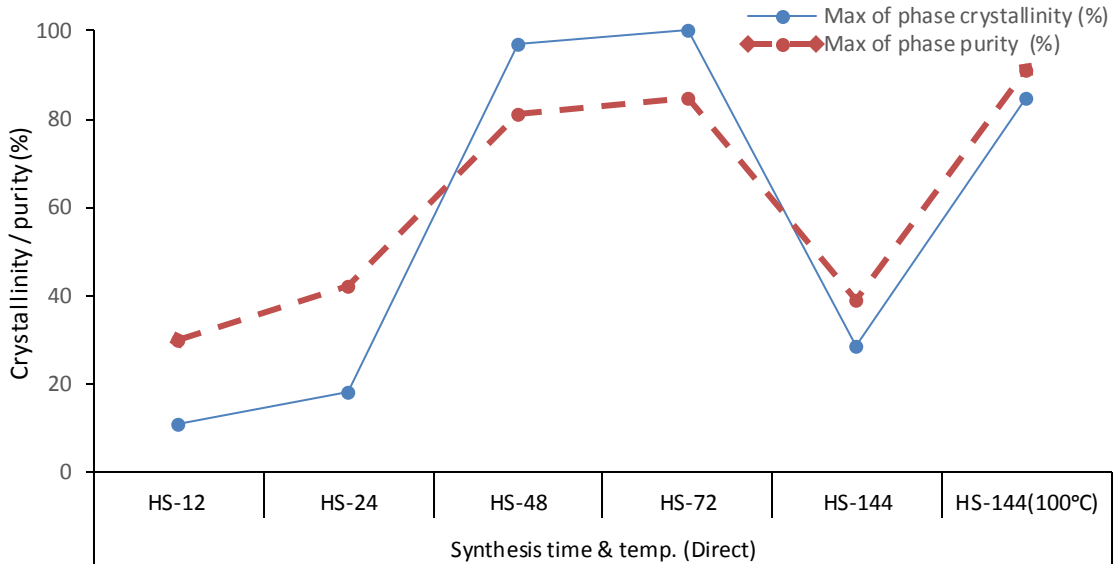

(b)

Figure 5.16. (a) XRD patterns, **(b)** crystallinity and purity of HS zeolite samples obtained with varying direct hydrothermal synthesis time (12, 24, 48, 72 and 144 h) at 140 °C compared to varying temperature (140 h, 100 °C) at 144 hours.

Synthesis time is a crucial determinant factor towards the quality of zeolites (Zhang et al., 2013, Nabavi et al., 2014). This parameter, following on from investigation of NaOH concentration in the synthesis mixture (NaOH/CFA ratio), proved more effective on the overall HS

characteristic properties. Further, lowering synthesis temperature to 100 °C at extended reaction time of 144 hours, also improved the overall characteristic properties of HS zeolite.

Reference synthesis period of 48 hours (HS-48 sample), the analogous condition to the previously obtained optimal NaOH concentration (HS-70+1.2NaOH sample) (section 5.1.5), showed considerable crystallinity of 97 % coupled with HS product purity of 81 %. Upon varying/exploring synthesis at shorter period of 12 hours and 24 hours at initial fixed temperature of 140 °C, the resultant product sample HS-12 and HS-24 demonstrated very poor HS characteristic with regard to phase crystallinity of 11 % and 18 %, and phase purity of 30 and 42 % respectively (Figure 5.16(b)).

The 72-hour synthesis period for sample HS-72, reversed to maximum relative crystallinity of 100 % and a high purity of 85 %. Upon further variation to 144-hour synthesis at a fixed temperature of 140 °C, a reduced phase crystallinity of 28.5 % and 39 % low phase purity, similar to sample HS-24, resulted (Figure 5.16(b)), showing there was an optimum synthesis time to achieve phase crystallinity and purity characteristic of synthesised HS zeolites until 72 hours. If the time is extended, the temperature needs to be reduced (HS-144(100°C)).

The results revealed that at short synthesis time conditions of 12 and 24 hours, a major proportion of quartz (Q), mullite (M) as well as the diffraction hump characterising the amorphous material in fly ash (between 18-38^{o} 2θ), were considerably retained in the respective samples (Figure 5.16(a)). These suggest a low conversion of fly ash to HS zeolite and directly correspond to low purity shown by the respective samples (Ameh et al., 2017, Steenbruggen and Hollman, 1998). There was a complete disappearance of quartz and mullite phase as synthesis time increased from 48 hours and further to 72 hours, of which this can be associated with an improved conversion of the coal fly ash components strictly to HS zeolite (Figure 5.16(a)). The above also corresponds to the shown high purity HS zeolite (no crystalline Q, M, zeolite X and P detected) and comparably reduced humps of precursor amorphous phases at the respective conditions (Figure 5.16(a)). With further increased synthesis time of 144 hours (140 °C), Zeolite P and X emerged and there was also no quartz (or mullite) present in the resultant sample (HS-144) (Figure 5.16(a)). This is also associated with high conversion of coal fly ash more selectively to the emerged phases, by so corresponding to low sample phase purity with respect to HS zeolite (Figure 5.16(b)). The low crystallinity (28.5 %) shown by sample HS-144 is confirmed by low peak intensities (Figure 5.16(a)).

There is apparently no existing literature that directly backs up the trend obtained in this study at the various synthesis periods as stated in this thesis. The result however agrees with Belviso et al. (2009) concerning the increase in (direct method) hydrothermal synthesis time (until the prescribed 72-synthesis time) in line to metastable and denser phase HS zeolite which is based on the Ostwald's ripening theory (Baldan, 2002).

The results reported shows the synthesis of HS for a 48-hour period at 140 °C as the shortest synthesis time condition and the most cost-effective for overall high characteristic properties of HS zeolite. The obtained conditions also differ from the actual hydrothermal reaction conditions (time and temperature) employed in various studies for the synthesis of HS zeolite from CFA (Golbad et al., 2017, Luo et al., 2016, Henmi, 1987). The same applies to the prolonged synthesis time of 72 hours at 140 °C (HS-72 sample). Hence, direct hydrothermal after 48 and 72-hour synthesis time at 140 °C and at optimised pre-synthesis conditions obtained previously (section 5.1.2-5.1.5), are presented as the novel synthesis time (at 140 °C higher temperature) for high crystalline and pure phase HS zeolite. The latter 72-hour condition however, is optimum in this regard. Further investigation on characteristic properties of HS zeolite via the direct method, was explored by varying synthesis temperature at fixed synthesis time of 144 hours (Table 3.2, chapter 3).

Varying ageing temperature from 140 to 100 °C was conducted at 144-hour synthesis time, owing to low phase crystallinity and purity characteristic exhibited by sample HS-144 (Figure 5.4b). For comparison, the XRD pattern, crystallinity and purity of the sample obtained with varying synthesis temperature, are also presented in Figure 5.16(a) and Figure 5.16(b) respectively. In reference to baseline temperature of 140 °C, varying the temperature to 100 °C was adopted from Henmi's work (1987) in view to improve the poor crystallinity, purity and overall characteristics of HS shown by sample HS-144. The above approach also compensated for energy intensity associated with the higher temperature (140 °C) at long synthesis time condition. Further, synthesis at 100 °C for 144-hours synthesis time, was also explored in order to enable comparison between direct hydrothermal and fusion method. This owes to the fact that the above condition as revealed in section 5.2, was associated with optimal characteristic properties of HS obtained via fusion-assisted method. The sample obtained with varying direct hydrothermal synthesis temperature, HS-144(100°C), was also characterised (Table 3.2, chapter 3). The XRD pattern of the sample obtained with varying synthesis temperature, as

well as crystallinity and purity, are also presented in Figure 5.16(a) and Figure 5.16(b) respectively

Figure 5.16(b) shows that the relative decrease in synthesis temperature as anticipated, led to enhanced crystallinity of 85 % and purity of 91 % of the HS zeolite. HS-144(100°C) sample, which thus far, demonstrated the purest phase (highest purity) HS zeolite coupled with high crystallinity obtained via the direct hydrothermal method. The increased phase purity exhibited by sample HS-144(100°C) corresponded to decreased proportion of zeolite X and P and the most comparably low content of amorphous phases shown via XRD pattern (Figure 5.16(a)). The enhanced characteristic shown by HS-144(100°C), could be due to high extraction of Si and Al from fly ash associated with supersaturated sodium (Na) content in the sample's framework unit (Table 8.5.1, Appendix 1) (Molina and Poole, 2004, Volli, 2015). Direct method synthesis of HS at 100 °C was therefore identified as the optimum temperature condition, which validated Henmi (1987). On the other hand, reduction in synthesis temperature to favour a high crystalline and pure HS zeolite, appeared to have altered the Ostwald's ripening theory (Belviso et al., 2009, Brassell, 2017). The findings in this work, establishes 100 °C as the optimum temperature for HS synthesis from CFA (based on long synthesis time), suggesting that the Ostwald's theory could work at 100 °C.

The HS zeolite synthesis from CFA for 72-hours at a fixed temperature of 140 °C was the optimum synthesis time to obtain a high crystallinity and purity value. Direct method synthesis at 100 °C proved as the optimum temperature with regard to phase crystallinity and purity characteristic of HS zeolite from coal fly ash. Based on the above, the study recommends further synthesis investigation at 100 °C for the various synthesis time employed. The validation of crystallinity and purity of the varying samples as discussed, were carried out by conducting SEM analysis and determining crystal size from XRD data (section 3.4).

Figure 5.17 presents the SEM micrograph data and Table 5.8 the average crystal size of samples synthesised via direct hydrothermal method as a function of synthesis time (HS-12, HS-24, HS-28, HS-48, HS-72, HS-144) and temperature (HS-144(100 °C)).

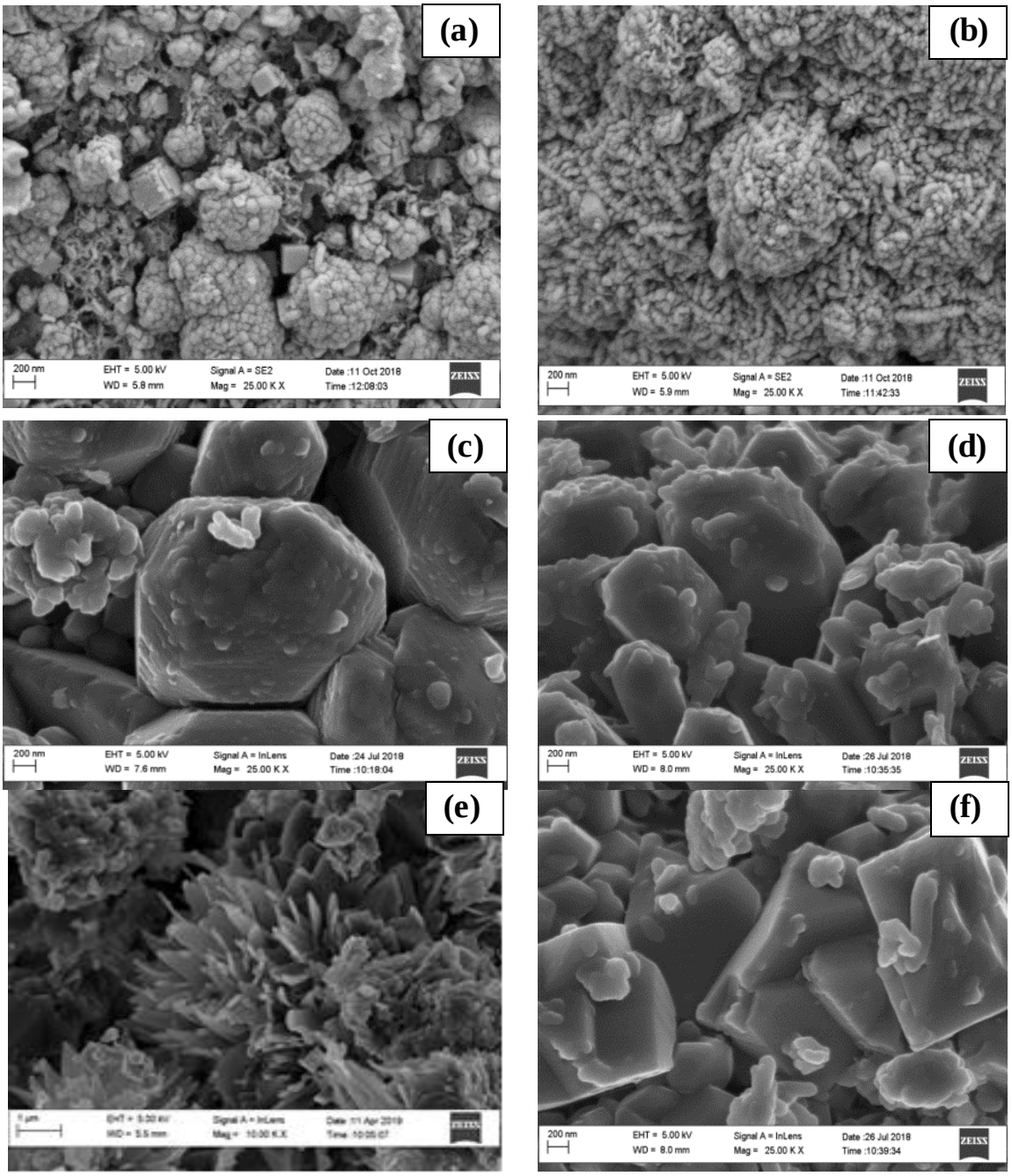

Figure 5.17. SEM micrographs of samples obtained with varying direct hydrothermal synthesis time (12, 24, 48, 72 and 144 h) at 140 °C and varying synthesis temperature (140, 100 °C) at 144 hours: **(a)** HS-12, (b) HS-24, **(c)** HS-48**; (d)** HS-72, **(e)** HS-144, and **(f)** HS-144(100°C).

Table 5. 8. Crystal size of samples synthesised with varying direct hydrothermal synthesis time at 140 °C and for 144 hours at 100°C

Sample[(a)]	Synthesis time (hour)	Crystal size[(a)] (nm)
HS-12	12	23.58
HS-24	24	24.13
HS-48	48	32.38
HS-72	72	31.90
HS-144	144	26.50
HS-144(100°C)	144	38.09

[(a)] Average crystal size determined using Scherrer equation (section 3.4)

Like NaOH concentration evaluated previously, variation in synthesis time or temperature, led to significant changes in crystal morphology and size of the obtained samples (Figure 5.17). According to Figure 5.17(a), it is shown that HS-12 sample obtained after shortest synthesis time, exhibited segregated partially-spheroidal crystals in large proportion and cuboidal-shaped crystals in minor proportion. The irregular and large crystals in HS-12 with most retaining shape as fly ash (Figure 5.2, section 5.1.1), could be due to amorphous characteristic coexisting or agglomerated with minor sodalite phase exhibited by the sample (Ameh et al., 2017, Buhl et al., 2011). This therefore attests to low conversion of CFA (poor nucleation and growth of HS zeolite) after 12-hour synthesis time, corresponding to poor crystallinity and purity in the HS-12 sample (Figure 5.16(b)) and low range average nanocrystal size of 23.58 nm (Table 5.8).

At increased synthesis time of 24 hours (140 °C fixed temperature); the evolved crystals transformed into a typical HS thread ball-like morphology (Figure 5.17b) as typically reported in existing publications (Nabavi et al., 2014, Makgaba and Daramola, 2015). However, in this work, the morphology in question has been found to be associated with poor crystallinity of the HS zeolite (Figure 5.16b). It is assumed that the observed thread-like crystals, are comingled with quartz (Q) and mullite (M) precursors retained or coexisting in major proportion within the HS-24 sample based on XRD (Figure 5.16a). Nonetheless, synthesis after 24 hours resulted in higher crystallinity and a considerable average crystal size of 24.13 nm. This suggests improved conversion of previously coexisting amorphous material to yielding a sample towards the actual HS zeolite crystal size (Nabavi et al., 2014). The improved

conversion is further supported by XRD (Figure 5.16), where this directly correlates to increased crystallinity and phase purity shown by HS-24 sample (Buhl et al., 2011).

Further, after 48 hours (HS-48 sample) the crystals with the most uniform hexagonal-cubic habit formed (Figure 5.17c). The crystals further transformed into elongated hexagonal-cubic shape after 72 hour-synthesis time, at which time the crystals included an intra-crystalline pores (Figure 5.17d). Sample HS-48 presented an improved conversion of coal fly ash and was associated with a crystal size of 32.38 nm. Sample HS-72, being the reference sample for relative crystallinity (section 3.4), exhibited an average crystal size of 31.90 nm (Table 5.8). In contrast to thread-ball (or flower-like) and smaller crystals typically reported of HS zeolite in publications (Nabavi et al., 2014, Makgaba and Daramola, 2015, Shirani Lapari et al., 2015), this work instead presents hexagonal cubic shaped-crystals of larger size as the morphology associated with high quality HS zeolite exhibited by the HS-48 and HS-72 samples (Figure 5.16(b)).

In comparison to other HS samples, HS-144 sample presenting the longest applied synthesis time at 140 °C, showed, a stack of flower-like crystals (Figure 5.17f). The partial-platelet crystal habit observed may be associated with the phase of zeolite X and P coexisting in the sample as shown via XRD (Figure 5.16(a)). The partial spherical aggregates therein, is comparable to the morphology shown by HS-24 sample (Figure 5.17b). By virtue of this, HS-144 sample depicted a similar crystallinity and purity characteristic as HS-24 sample (Figure 5.16(b)), and consequently a comparably small crystal size (26.50 nm) as HS-24 sample (24.13 nm).

Like earlier reported with varying NaOH concentration, crystalline morphology of the discussed samples obtained with varying hydrothermal synthesis time, was directly linked to crystallinity and purity of the samples. In other words, with varying synthesis time from 12 hours until 72-hour (at 140 °C fixed temperature), there was a direct correlation between crystalline morphology and phase purity of HS zeolite. Likewise and in partial agreement with Nabavi et al. (2014), a direct correlation (like previously) has also been validated between average crystal size and crystallinity of HS zeolite. From this work therefore, the well-defined hexagonal cubic-shaped crystal of average crystal size of 31.90 nm, has been associated with high quality HS zeolite (based on crystallinity and purity) achieved at the optimum synthesis time of 72 hours at 140 °C.

With further investigation on synthesis temperature to validate the previous results (crystallinity and purity), the SEM images of HS-144(100°C) exhibited platelet-shaped crystals (Figure 5.17g). The crystal size was relatively higher at 38.09 nm (Table 5.8). This indicates that varying synthesis temperature at a fixed synthesis time of 144 hours (like varying synthesis time from 12 to 72 hours), directly affected the crystalline morphology of HS zeolite. Hence, the platelet structure coupled with the relatively larger crystal size shown by HS-144(100°C) sample, and high phase purity of HS zeolite was also achieved at a temperature of 100 °C for 144 hours.

This morphology is different from the one typically reported of HS zeolite in literature (Nabavi et al., 2014, Makgaba and Daramola, 2015). Hence, a lower synthesis temperature of 100 °C for 144-hour, produced HS zeolite with crystals of average size of 38 nm via direct hydrothermal method offering a more cost efficient and energy route. Further validation of the HS zeolite samples obtained with varying synthesis time and varying temperature was carried out using the EDS analysis as described in section 3.4. Table 5.9 presents the elemental composition (as per EDS) of HS zeolites prepared from the different synthesis time (and temperature) via direct hydrothermal method.

Table 5. 9. Elemental composition of samples obtained with varying direct hydrothermal synthesis time at 140 °C and varying synthesis temperature (140, 100 °C) at 144 hours

Sample	**Element** (atomic, w/w %)											
	O	**Al**	**Si**	**Na**	**Mg**	**K**	**Ca**	**Ti**	**Fe**	Total	**Si/Al**	**Na/Al**
HS-12	58.63	17.08	17.49	3.04	0.58	0.37	1.30	0.90	0.62	100.0	1.02	0.18
HS-24	59.35	16.50	13.33	4.89	0.99	0.38	2.69	0.78	1.09	81.4	0.81	0.30
HS-48	45.09	14.32	19.5	14.62	0.65	-	3.57	0.93	1.33	100.0	1.36	1.02
HS-72	44.77	13.97	19.07	15.24	0.96	-	3.78	0.79	1.43	100.0	1.37	1.09
HS-144	43.96	13.91	19.96	12.4	0.84	0.83	4.01	2.64	1.44	100.0	1.43	0.89
HS-144(100°C)	43.47	13.76	17.42	20.67	-	-	2.16	1.23	1.29	100.0	1.27	1.50

Like the samples derived from varying NaOH concentration (section 5.1.5), variation in synthesis time and temperature had an effect on elemental composition and corresponding framework composition of respective samples (Table 5.9). Table 5.9 shows that sample HS-48, analogous to HS-70+1.2NaOH sample and associated with the baseline synthesis time of 48 hours at 140 °C, exhibited high proportion of silicon (Si), aluminium (Al) and Na. The

above composition, as earlier reported, corresponded to high Si/Al ratio of 1.36 and Na/Al ratio of 1.02 (Table 5.7, section 5.1.5). Based on the above composition, HS-48 sample may have a considerable total surface area and weaker acidic active sites (Ferreira Madeira et al., 2012, Lam et al., 2010).

With decrease in synthesis time to 24 or 12 hours, was associated with an increase in Al content in HS-12 and HS-24 sample (Table 5.9). The above corresponded to the observed decrease in Si/Al ratio of 0.81 and 1.02 respectively, and corresponding Na/Al ratio of 0.30 and 0.18 exhibited by HS-24 and HS-12. According to Rayalu et al. (2000), such low Na/Al ratio suggests too few charge balancing Na cations to stabilise the structure of HS-24 and HS-12 sample. This, consequently, attests to poor crystallinity, purity, poor morphological and structural configuration exhibited by either HS-24 or HS-12 sample (Figure 8.2.5, Appendix 1). The sample HS-48, resulted in a nearly similar proportion of both Si and Al content, as well as Na (sodium) content compared to the HS-72 sample. Both samples demonstrated a comparable Si/Al ratio and Na/Al ratio. Consequently, the above suggests that HS-72 sample exhibited the same overall characteristic properties as HS-48 with regard to HS zeolite as previously validated in terms of crystallinity and phase purity (Figure 8.2.5, Appendix 1), crystalline morphology (Figure 8.3.2(c-d), Appendix 1) and configuration (Figure 8.4.2(a), Appendix 1). Further, with varying synthesis time to 144 hours, there was less Na incorporated as charge balancing cation due to the decrease in Na content. Thus, the HS-144 sample demonstrated a comparably higher Si/Al ratio of 1.43 and rather low Na/Al ratio of 0.89 as indicated in Table 5.9. Rios et al. (2009), validates the poor overall properties of HS-zeolite demonstrated by the HS-144 sample (Table 8.1.2, Appendix 1). From the obtained finding discussed above, it can therefore be observed that both Si/Al and Na/Al ratio in the product correlated with varying the direct hydrothermal synthesis time.

Based on the Na content available to charge balance the framework of the produced zeolite, HS-72 sample with Na/Al of 1.09, showed that 72-hour hydrothermal synthesis time (at 140 °C) best achieved the desired properties of HS zeolite in this work. HS-48 sample, characterised with a Si/Al ratio of 1.36, differs from the variously literature reported Si/Al ratios that describes HS zeolite (Musyoka et al., 2011, Querol et al., 2002). Hence, HS-72 sample (sample obtained after 72 hours), followed by HS-48 sample obtained at 48 hours at 140 °C (unlike 12, 24 and 144 hours), have been validated by their elemental composition via EDS analysis for high quality HS zeolite.

Further changes in elemental composition, were observed for sample HS-144 at a fixed synthesis time of 144 hours. This was compared with HS-144(100°C) sample (Table 5.9).

It was previously found that HS-144(100°C) demonstrated high crystallinity, purity and well-defined crystal morphology feature of HS zeolite (Table 8.1.2, Appendix 1). The sample in question, as obtained at 100 °C at 144 hours, showed a relatively decrease in Si (17.42 %) and a most considerable increase in Na (sodium) content (20.67 %). HS-144(100°C) sample, consequently, shows agreement with Molina and Poole (2004) concerning decrease in Si/Al ratio at lower temperature, and conversely resulted to high Na/Al ratio of 1.50. The lower temperature applied affected both Si/Al and Na/Al ratios. The Na/Al ratio, increased with the decreased synthesis temperature. In both cases however, the Na/Al ratio was a strong dictating factor of good crystallinity and phase purity of HS zeolite.

Further, on the basis of comparably low Si/Al (Si/Al = 1.27), HS-144(100°C) sample among the direct hydrothermal sample proven for high quality HS-zeolite, is likely to have strong acidic active sites (Ferreira Madeira et al., 2012, Lam et al., 2010, Endalew et al., 2011). The high Na/Al ratio on the other hand (Na/Al ratio = 1.50), suggests an excess of Na (Na^+ ions) as charge balancing cations of the framework structure of the zeolite (Volli, 2015, Rios et al., 2009). The above (high Na/Al ratio) was similarly demonstrated by HS-70°C sample previously in section 5.1.4 (Table 5.5) (Figure 8.4.1b-d, Appendix 1). Further, HS-144(100°C) sample, owing to high Na/Al ratio, is suggested to have pore and structural blockages (Volli and Purkait, 2015, Babajide et al., 2012). Consequently, HS-144(100°C) sample, unlike the acidic characteristic and anticipated structural configuration , is predicted to have a relatively small total surface area and pore volume feature as compared to as high quality direct hydrothermal HS-72 sample (Babajide et al., 2012). Nonetheless, in addition to Si/Al ratio of 1.36 demonstrated by HS-72, HS-144(100°C) sample presents a Si/Al ratio of 1.27, which is approximating to the literature reported ratio for HS zeolite (1.27 > 1.00) (Musyoka et al., 2011, Querol et al., 2002, Nanganoa et al., 2016).

From the findings obtained, it was therefore found that reducing the synthesis temperature to 100 °C for 144 hours, proved to be a condition that may result in high quality HS zeolite compared to hydrothermal temperature of 140 °C at same or shorter synthesis times. Direct hydrothermal crystallisation at 100 °C, further as characterised with a low Si/Al ratio and high Na/Al ratio of 1.5, could be associated with stronger acidic sites and XRD showed high phase purity and crystallinity. Further investigation to validate the characteristics of this series of HS

zeolites as a function of direct hydrothermal synthesis time and temperature, was conducted by FT-IR analysis as described in section 3.4 (chapter 3).

Figure 5.18 presents the FT-IR spectra of samples obtained with varying synthesis time and temperature.

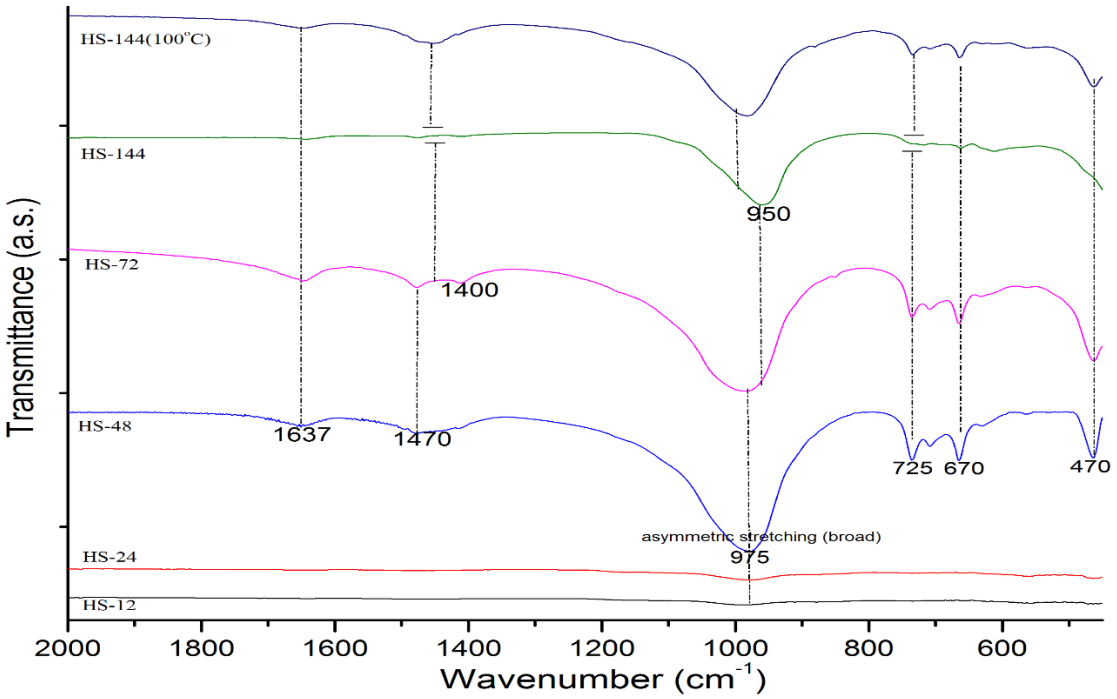

Figure 5.18. FT-IR spectra of samples obtained with varying direct hydrothermal synthesis time (12, 24, 48, 72, 144 h) at 140 °C and varying synthesis temperature (140, 100 °C) at 144 hours.

The FT-IR spectra in Figure 5.18 depicts the structural configuration of samples obtained with varying synthesis time and temperature, with characteristic bands restricted between the region of 450 and 2000 cm^{-1}. The broad T–O–Si (T = Al, Si) asymmetric band in CFA at 1095 cm^{-1}, shifted to lower position (higher frequency) at 975 cm^{-1} with varying synthesis time and temperature. Very poorly resolved bands were observed with low synthesis times of 12 hours and 24 hours (HS-12 and HS-24 sample), confirming poor conversion of coal fly ash to HS zeolite, and validates the poor overall HS quality revealed previously at short synthesis conditions (Figure 5.16 - 5.17, Table 5.9).

Samples obtained from 48 hours and above (HS-48, HS-72, HS-144(100°C)), showed spectra evolved with multiple and well-structured vibrational modes of zeolite. The major bands observed were the broad symmetric transmittance band at 975 cm^{-1}; weak bands at 725 cm^{-1}

and 670 cm^{-1} (between 450 and 750 cm^{-1}); and the band at peak 470 cm^{-1}. The above bands were attributed to T–O–T (T = Si, Al) or Si–O–Al units, two symmetric Si–O–Si stretching modes, and internal tetrahydron bending vibration mode of T–O (T= Si or Al) respectively (Musyoka et al., 2011, Brassell, 2017, Buhl et al., 2011).

As the synthesis time increased from 48 to 72 hours, there was almost no variation in either of the bands/peaks found in sample HS-48; except a minute split and formation of an additional weak band at 1400 cm^{-1}. This band was associated with additional Si–O units, which reflected the minute difference in Si/Al ratio shown by sample HS-72 (Table 5.9). It is observed that similarity in the structural configuration of HS-48 sample and HS-72 sample, corresponds to their similarity in terms of all the previously reported characteristics (i.e. phase crystallinity/purity, crystal morphology, and elemental composition).

It was observed that the intensity of assigned symmetric stretching band at 975 cm^{-1} reduced, and the band shifted to higher frequency (lower position) of 950 cm^{-1} as the synthesis time increased to 144 hours (Figure 5.18), but all the previously observed bands disappeared as the synthesis time increased. This indicates a poor configuration structure of HS zeolite exhibited by HS-144 sample, and in turn corresponds to poor crystallinity and purity (Figure 5.16b). The poor configuration structure of HS zeolite exhibited by HS-144 sample also affirms the under-saturation of Na (low Na/Al ratio of 0.89) as shown earlier via EDS data in Table 5.9, and the correspondingly predicted poor configuration (framework) structure exhibited by HS-144 sample (Rios et al., 2009, Volli, 2015).

As the synthesis temperature was reduced to 100 °C to form HS-144(100°C) sample, the single stretching band at 950 cm^{-1} in HS-144 sample re-shifted to lower frequency (high position) at 975 cm^{-1}, and all the assigned structural bands as present in HS-72 sample, were present in HS-144(100°C). According to Balkus and Ly (1991) and Rios et al. (2009), the above can be explained by decreased concentration of Si or decreased Si/Al ratio in HS-144(100°C) in relation to HS-144 (Table 5.9), and considerably increased Na/Al ratio (Na content) in promoting the crystallinity of HS-144(100°C) as compared to HS-144. The HS-144(100 °C) sample exhibited nearly all structural bands as HS-72, with the Si–O units weak bands (at 1400 and 1470 cm^{-1}) in HS-72 integrating into the broader band of 1440 cm^{-1} in HS-144(100°C). All the structural bands shown by HS-144(100°C) were however constricted and their intensity was low as compared to HS-72 sample. From the above finding, a direct correlation was drawn between FT-IR structural configuration and crystallinity of the respective samples. Hence, with

crystallinity and purity proven in direct correlation with synthesis time (as previously reported), increase in synthesis time until 72 hours has also been found to be in direct correlation with the structural configuration of HS zeolite (based on respective samples). Synthesis temperature, based on the two conditions evaluated (140→ 100 °C) at 144-hours, also proved to improve properties.

All samples synthesised via the direct hydrothermal method by varying synthesis time at 140 °C, were successfully validated as HS zeolite via FT-IR analysis. In addition to highest crystallinity (100 %) coupled with considerable purity HS of 86 %, the sample obtained after 72 hours (HS-72) best described HS zeolite in terms of structural configuration. This was followed by HS-48 sample. Varying synthesis temperature to 100 °C at 144-hour synthesis time, proved to be the optimal temperature with regard to structural configuration of HS zeolite. Further analyses of the samples obtained via direct method with varying synthesis time and temperature, were conducted using the BET, t-plot and BJH analysis to determine the textural properties as described in section 3.4.

In addition to the previously discussed as a result of varying presynthesis ageing temperature (Section 5.1.4), Table 8.6.1 (Appendix 1) presents the textual properties of samples obtained with varying direct hydrothermal synthesis time and temperature, and merges the results due by variation in NaOH/CFA ratio from 1:1 to 1:1.2. The above analyses were strictly conducted on HS-72 and HS-144(100°C); owing to their best overall characteristics of HS zeolite among the direct method samples obtained with varying hydrothermal conditions. Estimations are made for the textual property results of the remaining intermediate samples evaluated for either varying NaOH/CFA ratio (i.e. from 1:1 to 1.2:1) or direct hydrothermal synthesis time (HS-48; HS-144).

According to Table 8.6.1, HS-70°C sample obtained from NaOH/CFA of 1:1 and as previously reported (section 5.1.5), resulted in a minimal BET total surface area and total pore volume of 7.57 m^2/g and 0.029 cm^3/g respectively. With increase in NaOH/CFA ratio from 1:1 to 1.2:1, followed by increase in synthesis time to 72 hours at 140°C, the characterised and resultant HS-72 sample showed an increase in BET total surface area and total pore volume of 17.60 m^2/g and 0.089 cm^3/g. Without measurement taken for the intermediate sample HS-48 obtained precisely due to increase in NaOH/CFA ratio, it can be assumed that sample HS-48 possessed much similar BET surface and pore volume value as HS-72 sample. This is due to equal

balancing (or concentration) of Na^+ ion in the framework units of the two samples (i.e. Na/Al ratio), and an equally framework Si/Al ratio (Table 8.5.1, Appendix 1) (Volli and Purkait, 2015, Viswanadham et al., 2012, Lam et al., 2010). Further as synthesis time increase to 144 hours at 140°C, it is similarly assumed that HS-144 sample mainly by virtue of lower balancing of Na^+ in its framework unit, is likely associated with a higher surface area (> 17.60 m^2/g) than the previous samples (HS-72). A considerable total surface area of 13.17 m^2/g (total pore volume of 0.081 cm^3/g) and which are assumed to be lower than those of HS-144 (evidently lower than HS-72), resulted as the synthesis time was longer (144 h) while hydrothermal temperature reduced to 100°C. The resultant sample HS-144(100°C) evidently, and in validation of the above-mentioned literature sources, considerably showed an excess of Na+ ion in its framework units – associated with pore and surface area blockages (Volli and Purkait, 2015, Babajide et al., 2012). Hence from the finding discussed, it is therefore evident that HS-72 sample (equally to HS-48) presents the best NaOH/CFA ratio and hydrothermal synthesis time condition at 140 °C with regards to textual properties of HS zeolite obtained via direct method.

Figure 8.6.1 and Figure 8.6.2 (c-d) respectively presents the N_2 isotherms and pore size distribution data of the samples in question. The N_2 isotherms of HS-72 in Figure 8.6.1(b) shows a characteristic type III isotherm according to 1985 IUPAC classification (Sotomayor et al., 2018). The isotherms depicts a micropore filling at lower relative pressure (P/P_o) below 0.425 and a capillary condensation in mesopores at P/P_o above 0.425. The curve depicts a type H_3 hysteresis loop, suggesting that beside the major proportion/coverage of mesopores, there is a minor coverage of macropores (macroporous sites) in the sample that are incompletely filled with pore condensate (Thommes et al., 2015). Evidently, the mesopores contributed largely to total pore volume and total surface area of the sample (Table 8.6.1, Appendix 1). The pore size distribution curve of HS-72 in Figure 8.6.2 (c) shows the direct method sample to have most frequent pore size of 3.75 nm and average pore size of 21.22-23.98 nm. This suggests a mesoporous sample as confirmed earlier via the isotherm data (Weitkamp, 2000, Sotomayor et al., 2018). Further investigation was conducted to determine the yield of HS zeolite obtained via the direct hydrothermal method. A process material balance was also conducted in substantial of the above investigation.

The yield of the optimum direct method HS zeolite obtained at 72-hour synthesis time at 140 °C (HS-72), was determined as reported in section 3.3.2 (equation 3.6) (Bukhari et al., 2014).

$$Yield\ of\ zeolite\ product,\% = \frac{mass\ of\ zeolite\ product\ obtained}{mass\ of\ precusor\ CFA+NaOH} \times 100 \qquad (3.6)$$

Figure 8.7.1 (Appendix 1) presents the yield of the zeolite product as obtained via direct hydrothermal method. A process material balance was performed across the entire synthesis route to substantiate the yield of the zeolite (HS-72) (section 3.3.2). The material balance resulting thereof is presented in Figure 8.7.2 (a) (Appendix 1).

Figure 8.7.1 demonstrates that the production synthesis of HS zeolite via direct hydrothermal method at optimum conditions resulted in a maximum yield of 22.55% for HS-72 sample and 26.47 % for HS-144(100°C). The material balance in Figure 8.7.2 (a) shows an equivalent product mass of 4.96 g (HS-72), from the initially 10 g and 12 g of CFA and NaOH feed respectively. Such a low yield might have resulted due to much fragmented slurry initially formed from the ageing step, which carried up after hydrothermal synthesis step (stream 7). Consequently (due to dense and sticky characteristic of the slurry), there was a wastage of the material during a longer filtration process and the required intense washing step (stream 9 and 10) prior to drying. There was 62.62 g of solution recovered and discarded (wasted) from filtration, out of the 70 g (50 +20g) initially fed. It is assumed that the discarded solution carried along a significant amount of dissolved NaOH reagents, in such that only about 10.1 g of the material was recovered after both the filtration and washing step. It was also observed that a significant amount of the material along with the dissolved reagent(s) was washed off through a water input amount of 600 g. Notably, far more than 600 g of output water solution was recovered, attesting to the contained material therein. The obtained product yield agrees with Bukhari et al. (2014), whom also reported on low yields (below the range of 40 % yield) of zeolite products from fly ash via direct hydrothermal synthesis method.

From the study conducted, the direct hydrothermal method has demonstrated to be associated with the following benefits:

- Requires no high temperature and neither intensive presynthesis conditions to obtain high quality zeolite product (cost-effective approach)
- Worth for energy saving.

The following section discusses the characteristic properties of HS zeolite obtained via fusion-assisted hydrothermal method with varying synthesis times.

5.2 Synthesis of HS from coal fly ash via fusion-assisted hydrothermal method

Fusion-assisted hydrothermal synthesis for zeolites, is a well-known and reported method (Bukhari et al., 2014, Deng et al., 2016). This method however, based on existing literature, has been reported particularly for the synthesis of zeolite A and zeolite X (Volli and Purkait, 2015, Babajide et al., 2012, Zhao et al., 2006, Bukhari et al., 2014). To the best of author's knowledge, only a single study has been published with regard to the synthesis of HS zeolite via fusion method (Nanganoa et al., 2016). Nanganoa et al. (2016) selected the method mainly due to the rigid nature of the clay feedstock used, which is different to the coal fly ash feedstock employed in this work.

The fusion-assisted method as a way to break down the recalcitrant quartz and mullite in fly ash, was adopted in this study as a presynthesis step with the view to further optimise the overall characteristic properties of HS zeolite, following the synthesis investigation via direct method. The fusion method is also investigated with attempt to minimise energy intensity associated with longer synthesis time for high quality HS zeolite obtained via direct method. Hence, presenting a novelty with regard to synthesis of HS zeolite from coal fly ash via fusion-assisted hydrothermal method.

This section discusses in detail the formation of HS with varying synthesis times via fusion-assisted hydrothermal method with respect to phase crystallinity, purity, crystal morphology, elemental composition, structural configuration and textual properties. The detailed experimental procedure for the derived samples via the fusion method, is described in section 3.3.2 (chapter 3). The fusion step, preceding the hydrothermal reaction, involved calcination of CFA-NaOH mixture (1.2:1) at 550 °C for 1.5 hours. The investigation of hydrothermal synthesis time using this method, was carried out at the optimised 100 °C temperature from previous section (5.1). The selection of 100 °C was also supported in view to compensate or minimise energy intensity associated with zeolite synthesis via the fusion-assisted method (Musyoka et al., 2014).

5.2.1 Effect of fusion-assisted synthesis time on the formation of HS zeolite

This subsection reports on the characteristic properties of HS zeolite obtained with varying synthesis time after the fusion-assisted protocol. The detailed procedure for the synthesis of HS using the hydrothermal fusion method, is reported in section 3.3.2. After the fusion step, five hydrothermal synthesis time conditions (12, 24, 48, 72, 144 hours) were selected to convert the fused fly ash into zeolite. The resultant HS zeolite samples in order of increasing synthesis time via the fusion method, were assigned with code names HSF-12, HSF-24, HSF-48, HSF-72 and HSF-144 (Table 3.3, chapter 3). Each product sample was characterised using XRD, EDS, FT-IR and BET analyses as described in section 3.4 (chapter 3).

The XRD patterns of the samples obtained with varying synthesis time via fusion method, including the pattern of the fused fly ash intermediate prior hydrothermal reaction, are reported in Figure 5.19.

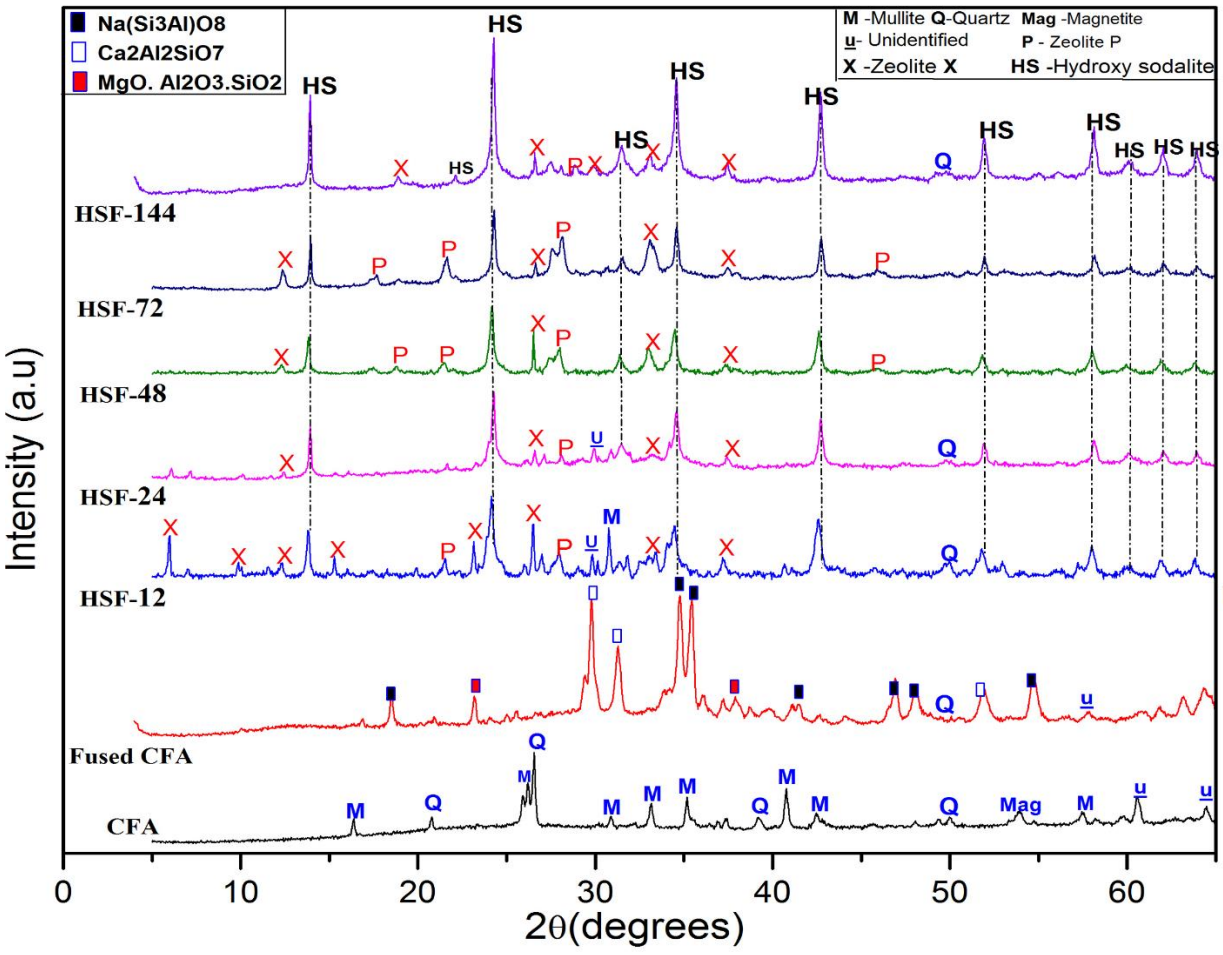

Figure 5.19. XRD patterns of samples obtained with varying fusion-assisted hydrothermal crystallisation time (12, 24, 48, 72 and 144h) at 100 °C.

Figure 5.19 shows that after the alkali fusion of CFA, the crystalline phases of quartz (q), mullite (M) and magnetite (Q) in CFA were transformed into the silicate and aluminate mineral phases of sodium ($NaSi_3Al)O_8$ and lightly of calcium ($Ca_2Al_2SiO_7$) and magnesium (Mg) ($MgO.Al_2O.SiO_2$). The XRD of the fused fly ash (FFA) demonstrates that the intermediate material contained new formed phases and almost no quartz or mullite remained, and the material also shows high amorphous species (Ameh et al., 2017, Bukhari et al., 2014). This also proves that the fusion step does not make zeolite and that the actual hydrothermal conditions are needed subsequently to attain a zeolite product. It is observed that after the initial short-hydrothermal synthesis time of 12 hours (following the fusion step), the XRD pattern of zeolite X is prominent but already major peaks of HS (14^o, 24^o, 35^o and 43^o 2θ) are present. Sample HSF-12 was observed to have mixed phases containing majorly zeolite X (6^o, 10^o, 12^o, 23^o, 26.5^o, 33.5^o 2θ), and minor proportion of zeolite P (22.5^o, 28^o 2), and traces of mullite (31.5^o 2θ) and quartz (50.5^o 2θ). There was almost no change in the intensity of peaks of HS, whereas nearly all the peaks of zeolite X and that of mullite (M) listed above, disappeared as the synthesis time was extended from 12 to 24 hours. Additional peaks of zeolite P (17.5^o 2θ) and X (12.5^o 2θ) were observed and other reappeared (P = 22.5^o, 28^o & X = 26.5, 33.5^o 2θ) as the synthesis time was further increased to 48 hours. The same mixed crystalline phases were maintained, with the intensity of the non-HS peaks rather increased as the synthesis time was again increased to 72 hours. With further increase to 144-hour synthesis time, the intensity at all the assigned peaks of HS were significantly increased and nearly all the peaks of other phases (zeolite P, X) either disappeared or their intensity were considerably decreased as the synthesis time was extended to 144 hours. Hence, it is noted that shorter synthesis times and lower temperatures are more desirable if more open framework (or less condensed zeolite) zeolite phases are desired. This agrees with Brassell (2017) and Musyoka (2012). It is also observed that the diffraction hump initially present in both fly ash and fused fly ash (FFA) between 17.5 and 38^o 2θ, progressively lowered in the resultant hydrothermal products, suggesting progressive conversion or transformation of amorphous phases in fly ash to zeolites as the reaction time increased until 144 hours (Ameh et al., 2017, Musyoka, 2012).

Figure 5.20 illustrates the trend of relative crystallinity and purity of the fusion samples obtained with varying synthesis time. The above characteristics were determined from the XRD patterns provided (Figure 5.19) using equation 3.7 and 3.8 respectively as described in section 3.4.

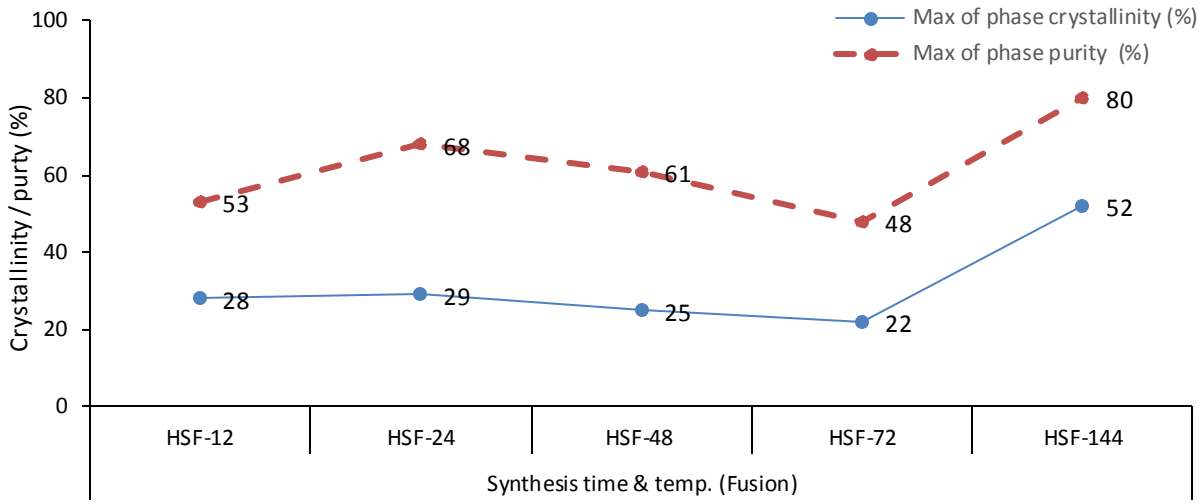

Figure 5. 20. Relative crystallinity and purity of HS zeolites obtained with varying fusion hydrothermal crystallisation time (12, 24, 48, 72 and 144h) at 100 °C (HS-72 reference sample assigned as 100 % crystalline)

As observed in Figure 5.20, there was almost no variation and rather an overall minor decrease in phase crystallinity (28-22 %) as the synthesis time increased from 12 to 72 hours. This, however, considerably increased to 52 % as the synthesis time was varied to 144 hours. The low crystallinity range obtained between 12 and 72 hours, is more due to changes in availability of primary building units (Si, Al) after fusion (Molina and Poole, 2014), which might have required higher temperature condition (beyond 100 °C) or longer synthesis times to counteract (Ojha et al., 2004). Hence, until 72 hours, the observed trend of synthesis time and phase crystallinity differs from the direct correlation trend reported by Nabavi et al. (2014). This only became evident as the synthesis time was increased from 72 to 144 hours; due to metastable phase behaviour of zeolite, crystal growth with denser or more stable phase HS forming only with an increase in hydrothermal synthesis time (Ojha et al., 2004, Baldan, 2002).

It is suggested by Querol et al. (2002) that achieving the above moderate crystallinity over such longer hydrothermal synthesis period (144 hour), could be an indication of lower amorphous glass content in either CFA or fused fly ash prior hydrothermal synthesis. The fusion hydrothermal method thus resulting in a lower crystalline zeolite than the direct method at the same or optimum hydrothermal conditions (Figure 8.8.1 or Figure 8.2.5, Appendix 1), agrees with both Deng et al. (2016) and Bukhari et al. (2014).

Phase purity of HS zeolite was enhanced as the synthesis time was increased, with an increase of 68 % from 12 to 24 hours, and further to 80 % as the synthesis time was extended to 144

hours. The above, as suggested by (Ojha et al. (2004)), can be attributed to the transformation of zeolite P and X, which as earlier reported via XRD pattern, disappeared to form more dense and a purer phase HS zeolite.

The findings revealed that the highest purity HS zeolite synthesised via fusion method, with phase crystallinity of 52 % and purity of 80 %, was obtained at a longer synthesis time of 144 hours. To validate the above with regard to characteristics of HS zeolite, further analysis was conducted using SEM, and the Scherrer equation to determine the average crystal size of the obtained samples.

Figure 5.21 and Table 5.10 respectively present the SEM micrographs and crystal size of the obtained samples with varying synthesis time. It may be noted however that no SEM data was provided for the sample synthesised for 48 hours (HSF-48) due to its low crystallinity (Figure 5.20).

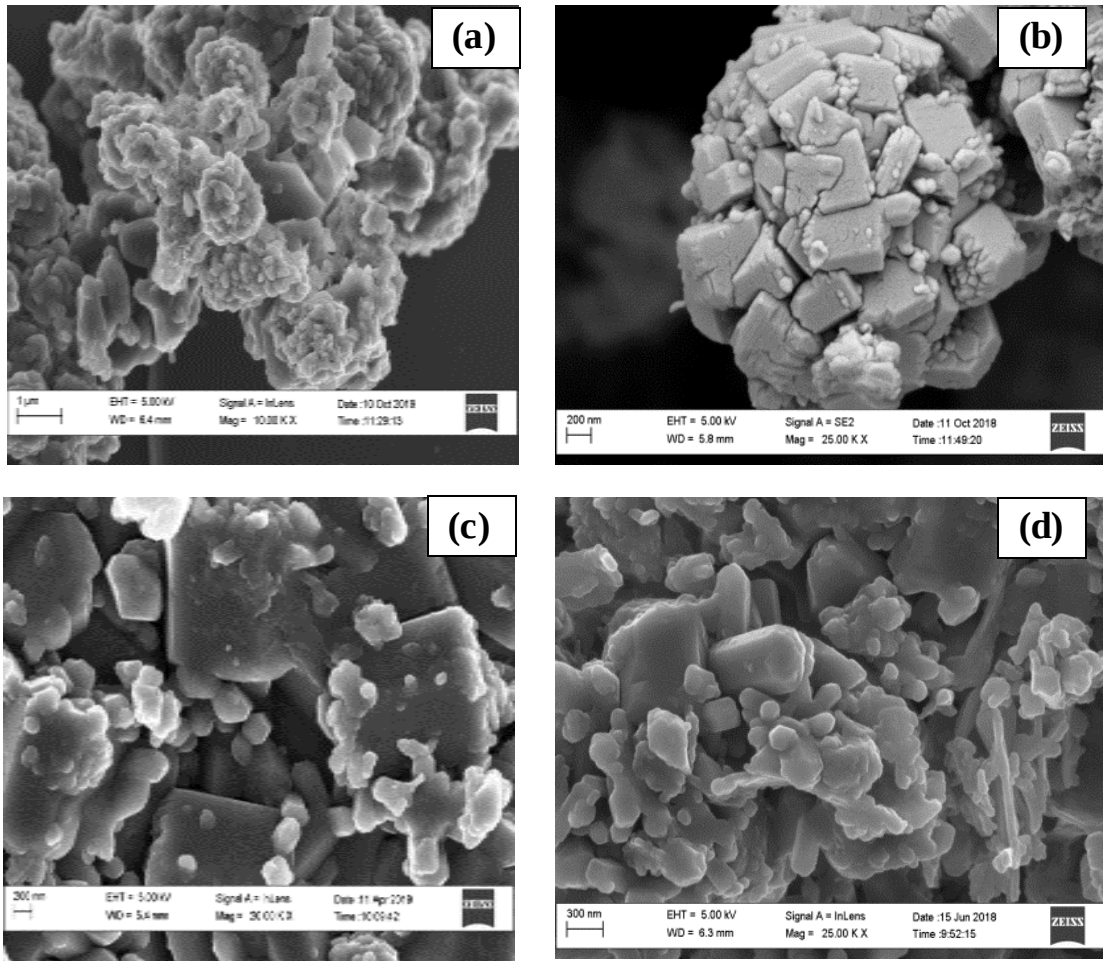

Figure 5.21. SEM micrographs of samples obtained by fusion-assisted hydrothermal method with varying synthesis time (12,24,48, 72, 144 h) at 100 °C, **(a)** HSF-12; **(b)** HSF-24, **(c)** HSF-72 and **(d)** HSF-144

Table 5.10. Average crystal size of samples obtained by fusion-assisted method with varying synthesis time at 100 °C

Sample	Synthesis time (hour)	Crystal size[(a)] (nm)
HSF-12	24	32.92
HFS-24	24	36.30
HSF-48	48	31.72
HSF-72	72	35.31
HSF-144	144	37.39

[(a)] Average crystal size determined using Scherrer equation (section 3.4)

The SEM micrographs in Figure 5.21 presents the crystal morphology of the samples obtained with varying synthesis time. Various morphologies were observed with the varying synthesis time conditions.

From the short 12-hour synthesis time condition, sample HSF-12 exhibited agglomerated spherical crystals mixed with a minor proportion of platelet-shaped crystals. As the synthesis time increased to 24 hours, the above crystals were transformed into cuboidal-like crystals, which formed an aggregate. As the morphology became slightly more aggregated, this resulted in an increase in average crystal size (32.92→36.30 nm) with variation to 24-hour synthesis time. Further, aggregated platelet-like crystals were observed as the synthesis time was increased to 72 hours, and were further transformed into hexagonal crystals as the synthesis time was further increased to 144-hour. As it can be observed, the fusion hydrothermal samples commonly demonstrated a more integrated crystal morphology in such that they are assumed to be associated with small intercrystalline porosity.

As the morphology transformed into a planar structure after 72-hour synthesis time, the average crystal size of fusion-assisted HS slightly decreased (36.30→35.31 nm), then increased to larger size (37.39 nm) as the synthesis time increased to 144 hours. The above reveals that until 72 hours, there was a partial correlation between crystal size and synthesis time and that crystal size was more in correlation with synthesis time between 72 and 144 hours, and likely with corresponding crystallinity and phase purity of the obtained HS. The finding is in agreement with Nabavi et al. (2014) and Buhl et al. (2011).

It may be noted that none of the resulted morphology corresponds to the typical crystal habits that describe HS zeolite in literature (Makgaba and Daramola, 2015, Nanganoa et al., 2016).

This work therefore presents a route to prepare hexagonal-shaped crystals with larger average size of 37.39 nm, as the morphology that describes a moderate quality HS zeolite obtained at optimal condition of 144 hours via the fusion-assisted hydrothermal method. Additional characterisation to validate the characteristic properties of the obtained samples with varying synthesis time via fusion-assisted method, was conducted using the FT-IR analysis as described in section 3.4.

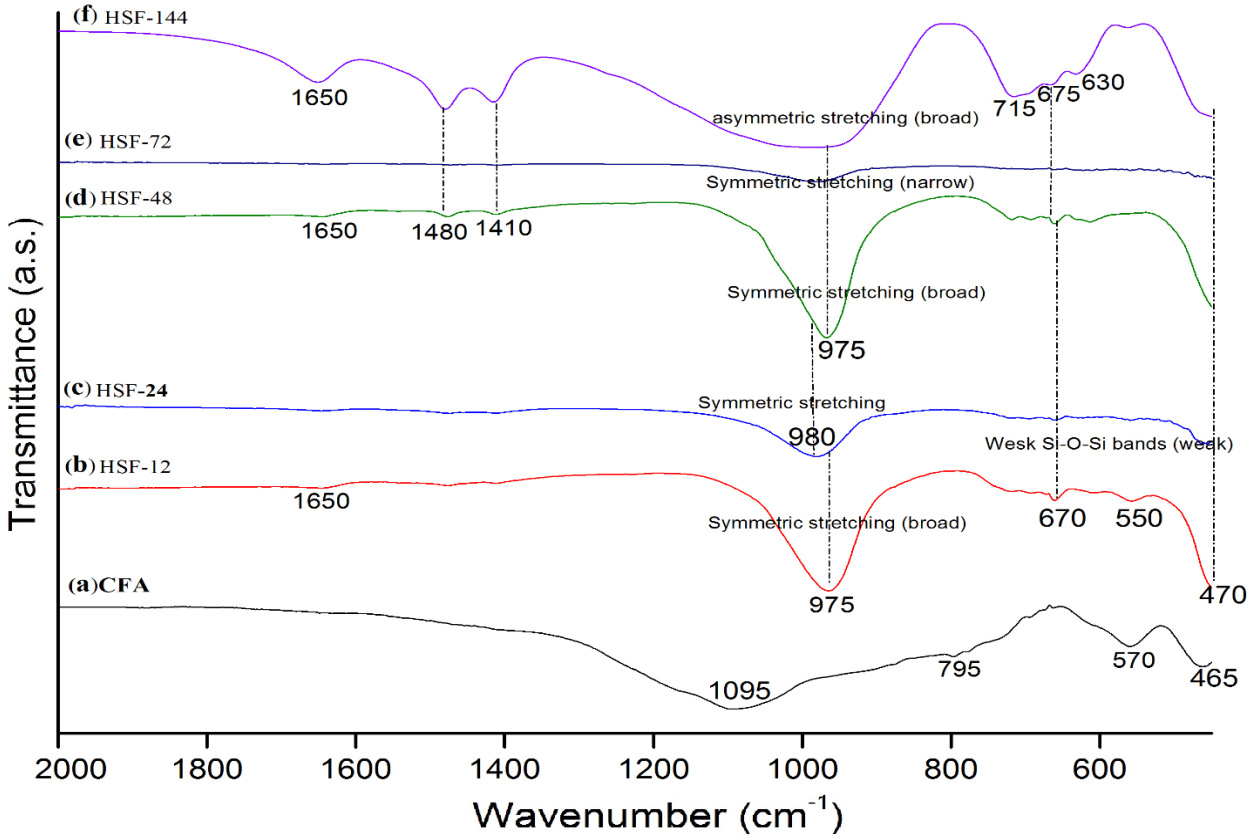

Figure 5.22. FT-IR spectra of samples synthesised by fusion-assisted method with varying synthesis time (12, 24, 48, 72 and 144 h) at 100 °C

The FT-IR spectra in Figure 5.22 illustrates the structural configuration of samples obtained via fusion-assisted method at different synthesis time. The characteristic bands of each spectra and vibrational modes to which the respective bands are attributed in correspondence to literature, is reported in Table 5.11.

Table 5. 11. FT-IR vibrational modes for samples obtained by fusion-assisted method with varying synthesis time at 100 °C

Frequency of vibrational bands (cm^{-1})							
12hrs	24 hrs	48 hrs	72 hrs	144 hrs	Literature range	Assignment	Reference
470	-	470	-	470	420-500	T–O bending[(a)]	Fernández-Jiménez and Palomo (2005); Buhl et al. (2011).
550	-	-	-	-	500-650	Double ring[(b)]	
650	-	670	-	675	650-720	Symmetrical stretching	
-	-	-	-	715		(O–T–O group)[(a)]	
975	980	975	975	975	950-1250	Assymetric stretching	
						(Si–O–Si group)**[(a)]**	
-	1410	1400	-	1410	1410-1450	Carbonate (CO_3) of Na,	
-	-	1480	-	1480		Ca and K	
1650	-	1650	-	1650	1600-1700	OH^- deform (bending)**[(a)(c)]**	

(a) Bands located at internal tetrahedral
(b) Bands located at external linkage
(c) OH^- deform (bending) or water adsorbed

It can be observed in Figure 5.22 that the bands exhibited in the spectra between 12 and 72-hour hydrothermal produced samples, poorly or moderately corresponded to zeolite bands assigned in literature (Fernández-Jiménez and Palomo, 2005). In the samples made using 144 hours however, the exhibited bands correlate best with the literature values (Table 5.2_section 5.1.2, Table 5.11).

As for the moderately zeolite corresponding bands shown after 12 hours (HSF-12), the intensity of T–O band at 470 cm^{-1} and that of the asymmetric T–O–T band at 975 cm^{-1}, significantly decreased while simultaneously the latter band shifted to 980 cm^{-1} in the sample after 24 hours (HSF-24). Concurrently, the double ring band at 550 cm^{-1} and the symmetric band at 650 cm^{-1}, disappeared in sample HSF-24 (Table 5.11). The above, as suggested by Querol et al. (2002), could be attributed to low Si and Al content observed in sample HSF-24 as compared to HSF-12 (see Table 5.12_upcoming). Since Si and Al are the elements that constitute the framework building blocks of zeolites (Querol et al., 2002), their restricted dissolution or significant reduction shown in sample HSF-24, counteracted the outcome of a more corresponding zeolite structural configuration as anticipated due to relatively high Na/Al ratio exhibited by the sample.

From the observed poorly corresponding zeolite configuration shown by HSF-24, the peak intensity of the major bands at 980 cm^{-1} and 470 cm^{-1} (exhibited earlier by HSF-12) increased, and the 980 cm^{-1} band shifted back to 975 cm^{-1} as the synthesis time was increased to 48 hours (HSF-48). The sample after 72 hours (HSF-72), showed the poorest structure with the lowest intensity of both zeolite vibrational mode at 470 and 950 cm^{-1}. The above as suggested by Rayalu et al. (2000), was strongly attributed to insufficient concentration of Na content to compensate charges in its framework units, which is equivalent to relatively lowest Na/Al ratio shown by the sample (see Table 5.12). The vibrational modes and the peak intensity were observed to increase the most as the synthesis time was further extended to 144 hours (HSF-144). Sample HSF-144 showed a much broader T-O-T asymmetric bands (975 cm^{-1}), and two symmetric T–O–T stretching modes (675 cm^{-1} and 715 cm^{-1}) and two sodium carbonate (CO_3) impurity-associated bands (1410 cm^{-1} and 1480 cm^{-1}). According to Buhl et al. (2011), the relatively broader band at 975 cm^{-1} shown by HSF-144 sample corresponds to the moderate crystallinity of the sample (Figure 5.19), while the carbonate (CO_3) bands derive from aqueous solution of sodium hydroxide and are stated to be often present in a hydrothermal grown HS (cage filling). The formation of the two T–O–T symmetric bands (675 and 715 cm^{-1}) in the internal framework of HSF-144 (Table 5.2_section 5.1.2 or Table 5.11), affirm the most progressive/significant transformation of amorphous phase in fly ash (or fused FA) to HS zeolite (or HS crystals) (Ameh et al., 2017), as also confirmed through XRD results (Figure 5.19). Buhl et al. (2011) describes the two symmetric bands (as between 660-740 or 650-720 cm^{-1}) as the fingerprint vibrations of sodalite ("sodalite fingerprint" vibrations). It may be noted that the most stable structure exhibited by sample HSF-144, correlates with its crystallinity shown in Figure 5.20. Furthermore, the obtained configuration best describing HS zeolite, can be attributed to the relatively high Na/Al ratio shown by the sample (HSF-144) being equivalent to highest sodium (Na) concentration in its relative framework units (Volli, 2015) (Table 5.12_upcoming).

The elemental composition as substantiated by EDS in support of the structural analysis of the samples obtained with varying synthesis time, is presented in Table 5.12. This was determined via EDS analysis according to the corresponding procedure reported in section 3.4.

Table 5.12. EDS data of samples obtained by fusion hydrothermal method with varying synthesis time at 100 °C.

Sample	**Element** (atomic, w/w %)												
	O	**Al**	**Si**	**Na**	**Mg**	**K**	**Ca**	**Ti**	**Fe**	**P**	Total	**Si/Al**	**Na/Al**
CFA	65.15	11.23	14.86	-	1.54	0.23	4.32	0.30	1.13	1.25	100.0	**1.32**	-
HSF-12	51.3	14.11	17.86	12.46	0.49	-	2.2	0.53	1.05	-	100	1.27	0.88
HSF-24	61.28	10.90	13.11	12.31	-	-	1.35	0.26	0.79	-	100	**1.20**	**1.13**
HS-48*	-	-	-	-	-	-	-	-	-	-	-	-	-
HSF-72	43.46	19.5	19.75	11.96	-	0.19	2.97	0.61	1.57	-	100.0	1.01	0.61
HSF-144	65.35	12.42	14.65	11.55	0.39	-	1.18	0.29	0.57	-	100.0	**1.18**	**0.93**

*No analysis conducted for the sample due its lower crystallinity and limited selection for characterisation

The EDS data illustrating the elemental composition in Table 5.12 shows that both components (Si, Al) were increased as synthesis time was increased to 72 hours, The lowest Si/Al ratio of 1.01 was observed with increase to 72-hour synthesis time (HFS-72), followed by the ratio of 1.18 in the sample obtained after 144 hours (HSF-144). The above feature as suggested by Viswanadham et al. (2012) and Lam et al. (2010), implies that sample HSF-72 possibly possessed strongest acidic active sites, followed by sample HSF-144.

Further, Na/Al ratio (mainly due to increased proportion of Al) was lowest at a ratio of 0.61 in sample HSF-72 and a considerably higher Na/Al ratio of 0.93 was resulted in the sample obtained after 144 hours (HSF-144). The above by prediction based on Volli and Purkait (2015)'s finding, implies that sample HSF-72 could be in possession of the largest total surface area, followed by sample HSF-144. Nonetheless, the comparably high Na/Al ratio shown by sample HSF-144 (Table 5.12), coupled with a considerable proportion of Si and Al content therein, implies that this sample corresponds more to HS zeolite in terms of structural configuration as compared to the sample obtained after 72 hours (Rayalu et al., 2000). The above was supported by the obtained FT-IR spectra reported in Figure 5.22 (or data in Table 5.11). It may also be noted that the higher Na/Al ratio coupled with the high Si and Al content shown by the sample obtained after 144 hours (HSF-144), directly correlated to its higher phase crystallinity that exceeded that shown by sample HSF-72 (Figure 5.20). Hence, sample HSF-144 conformed to HS zeolite in terms of overall characteristics, but was characterised with a Si/Al ratio that is slightly higher than the literature reported range for HS (1.18 > 0.88-1.00) (Nanganoa et al., 2016, Querol et al., 2002). Since samples obtained after 12 to 72 hours showed similar trends of low crystallinity, additional analysis of BET, t-plot and BJH were

conducted for only sample HSF-144 (as described in section 3.4) owing to its best overall characteristic among the samples obtained via fusion-assisted method.

The textual properties exclusively for the as-made sample obtained (via fusion method) after 144 hours are reported in Table 5.13 (see also Table 8.6.1, Appendix 1). The pore size distribution curve is reported in Figure 8.6.2 (Appendix 1).

Table 5.13. Textual properties of sample obtained via fusion-assisted method after 144 hours at 100 °C

Synthesis method	Sample	Surface area (m^2/ g)		
		Total[(a)]	Meso.[(b)]	Micro.[(b)]
Fusion	HSF-144	44.98	42.94	2.74

(a) Obtained by BET equation / method at p/po 0.99; **(b)** Measured by t-plot method

Table 5.13 presents the BET total surface area, micropore and mesopore area of the sample obtained via fusion-assisted method after 144 hours at 100 °C. It is observed that sample HSF-144, depicts a relatively large BET total surface area of 44.98 m^2/g. So far in this work, the above result is the highest textual property of all the samples obtained via the fusion-assisted hydrothermal method. It is suggested by Volli and Purkait (2015) and Babajide et al. (2012) that the obtained high values of total surface area and mesopore area shown by the fusion sample HSF-144, can be associated with few pore and framework surface blockages, due to low content of charge balancing cations ($Na^{+,}$ Mg^{+}, K^{+}, Ca^{+}, Fe^{+}) associated with the framework structure of the sample (Table 5.12). It may also be suggested that the obtained product characteristics could be associated with the high temperature fusion step to which the product's synthesis mixture (precursor) was subjected prior to hydrothermal synthesis (Makgaba and Daramola, 2015). Further, it is observed that the obtained BET total surface area corresponds to those of HS reported by Golbad et al. (2017) and Nanganoa et al. (2016). It is also observed that the higher textural property of the sample is not in direct correlation with its degree of crystallinity (Figure 5.20), of which this agrees with the finding by Nanganoa et al. (2016) and Shirani Lapari et al. (2015). The average pore size distribution curve in Figure 8.6.2(e) reveals that sample HSF-144 shows a dominantly pore diameter of 4 nm. According to Weitkamp (2000), the mesopores in the fusion-assisted sample HSF-144 (2–50 nm), could be associated with high diffusive property and hence be of interest as a catalyst in biodiesel production (Viswanadham et al., 2012, Guo and Fang, 2011, Shirani Lapari et al., 2015).

Figure 5.23 reports on the N_2 adsorption isotherms curve of sample HSF-144.

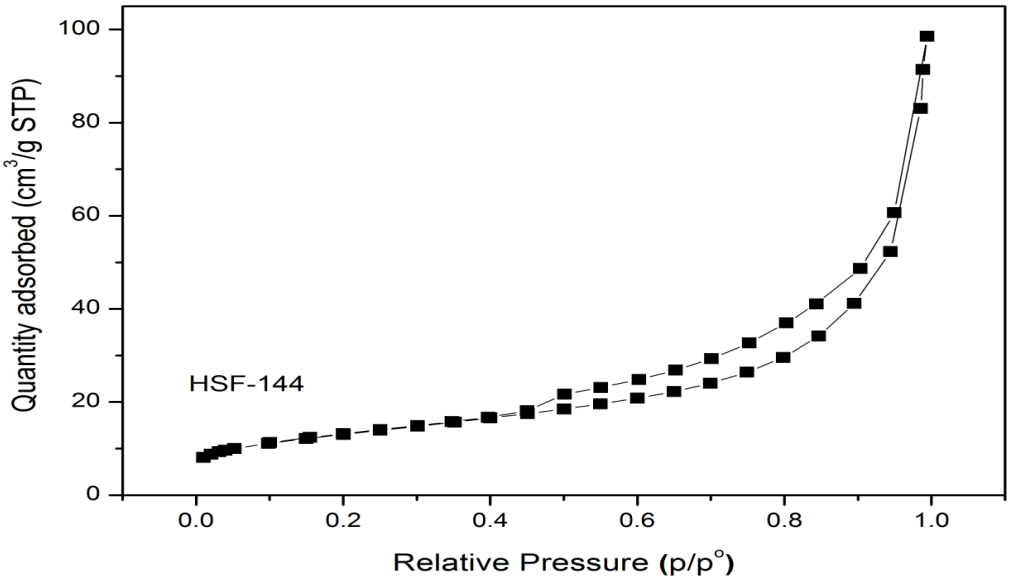

Figure 5.23. N_2 adsorption isotherms of samples obtained via fusion-assisted method after 144 hours at 100 °C

The N_2 adsorption isotherm curve of the sample obtained after 144 hours, is presented in Figure 5.23. The isotherm of the sample shows a typical isotherm, which according to 1985 IUPAC classification, represents characteristic type III isotherm of Langmuir adsorption (Thommes et al., 2015). The isotherm curve depicts a micropore filling in the region of P/P_o below 0.4 and the curve further, shows a small adsorption type H3 hysteresis loop in the range of $P/P_o > 0.45$, showing mesoporosity as previously suggested through Figure 8.6.2 (Appendix 1).

According to Sotomayor et al. (2018), the loop indicates mesopores that enhanced capillary condensation of the adsorbed nitrogen. Thommes et al. (2015) reports that the type H3 hysteresis loop, suggests a very low micropore area. The mesopores contributed majorly to the high BET surface area and total pore volume shown by sample HSF-144 (Table 5.13 or Table 8.6.1, Appendix 1). Owing to the characteristic isotherm mentioned earlier, Viswanadham et al. (2012) and Sotomayor et al. (2018) support that the obtained fusion-assisted HS sample has characteristics of mesoporosity.

Further, the yield of HS zeolite from coal fly ash was calculated only for the respective optimum sample (among the fusion products) obtained at extended synthesis time of 144 hours (HSF-144). Equation 3.6 to determine the yield was used as previously (section 3.3.2, section 5.16).

Figure 8.7.1 (Appendix 1), in addition to the yields of the optimum zeolites obtained via direct hydrothermal method (section 5.1.6), presents the yield of the as-made fusion-assisted zeolite product. As observed in Figure 8.7.1, the product yield for the fusion-assisted sample HSF-144, was 56.3 %. This value exceeded by twice the yield for both the optimum direct hydrothermal products (HS-72 and HS-144(100°C) (Figure 8.8.2, Appendix 1), and thus agrees with both Bukhari et al. (2014) and Mezni et al. (2011) concerning higher yield of zeolite products obtained by fusion-assisted method compared to direct hydrothermal method.

To substantiate for the product yield obtained for the fusion hydrothermal sample HSF-144, a process material balance just like previously conducted for the direct hydrothermal synthesis, (section 5.1.6) and as described in section 3.3.3, was conducted across each stage unit of the synthesis: from the initial to the final stage of production. Figure 5.24 presents the material balance performed to obtain the fusion-assisted hydrothermal HS zeolite.

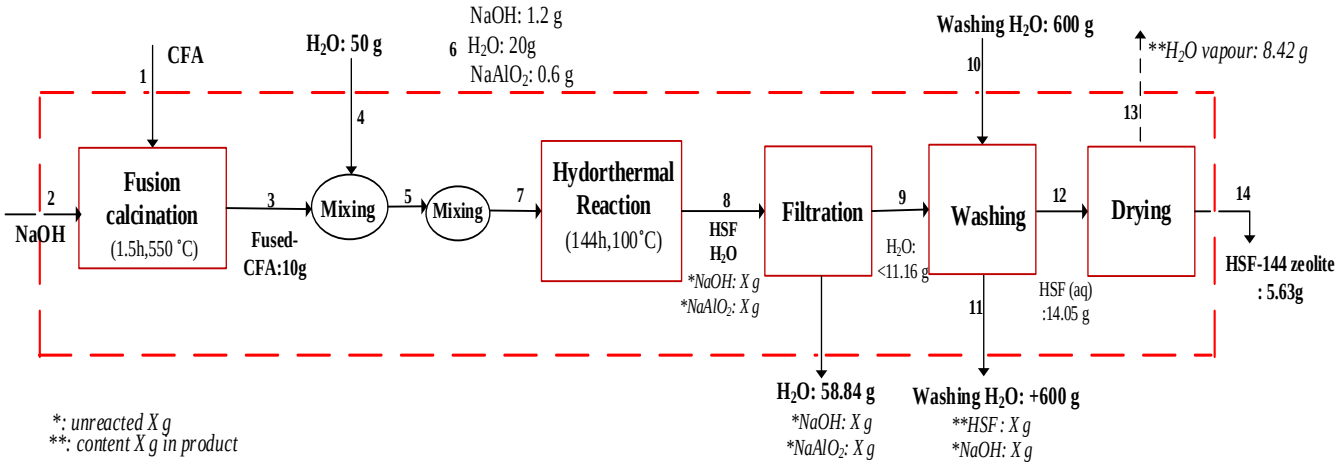

Figure 5. 24. Material balance for the fusion hydrothermal synthesis of HS zeolite at 100 °C for 144 hours (i.e. optimal conditions)

According to Figure 5.24, 5.63 g is shown as the mass of the HS zeolite equivalent to the obtained product yield of 56.3 %. There was only 4.37 g of the material wasted in the process, from 10 g of the fused fly ash initially fed into the reaction (the basis). Like previously, it is assumed that a significant amount of NaOH fused/embedded into the fly ash (after fusion) was wasted in the discarded filtrate solution after filtration. Quiet a huge amount of the filtrate (54.84 g) recovered and discarded, from the initially 70 g (50+20) of feed solution fed (stream 4 & 6). It is also assumed that most of the material was wasted through the washing step, proven

by the fact that far over 600 g of wastewater resulted from the initially 600 g fed for washing. It could however be recommended to conduct an elemental analysis of the discarded solutions to affirm the loss incurred from the process. Bukhari et al. (2014) found the highest product yield of 53.75 % from the various synthesis trials of zeolite via fusion assisted method. The yield obtained in this work therefore, slightly exceeded the above but corresponds within the same range to the literature value.

From the finding discussed in this section, it can be concluded that sample HSF-144 among the fusion-derived, displayed the best HS zeolite properties in terms of crystallinity and purity, structural configuration, and the sample (followed by HSF-72) was coupled with considerable total surface area and mesoporosity, and estimated possible strong acidic characteristic sites. Moreover, the synthesis of the sample throughout the process resulted in a maximum product yield of 56.3 %. Based on the above characteristics, it is suggested that the fusion product sample (HSF-144) will be relevant in catalysis of biodiesel production.

5.3 Summary of results and discussion for chapter 5

This section gives a summary of the results of zeolite samples (HS and zeolite X) synthesised by direct hydrothermal and fusion-assisted method, and briefly narrows down to comparison between HS zeolites obtained at optimum conditions of either method (over the best case scenarios). The section also gives a brief discussion of the resultant properties of HS zeolites modified by ion-exchange and bifunctional method (section 3.3.5). The procedures employed for either the synthesis or modification of all the mentioned samples, are described through the entire section 3.3 (chapter 3). The summary of the results and corresponding properties is presented in Table 8.1.1-Table 8.1.2 (Appendix 1).

HS zeolite was successfully synthesised by direct and fusion-assisted hydrothermal methods investigated in this work. The initial stage of the investigation shows that as the water/CFA ratio was increased, the overall characteristic of HS decreased. The baseline water/CFA mass ratio of 5:1 in this case (HS-48h sample), was retained as the optimum water content that resulted in a mixed phase HS zeolite product of 41.5 % crystallinity and 49 % phase purity (Figure 8.2.5, Appendix 1). With further investigation on ageing time, the overall characteristic of HS considerably improved as ageing time was reduced from 48-hour baseline to 1.5 hour,

yielding a (moderately high) crystalline HS zeolite with 57.6 % crystallinity and 66 % purity (Figure 8.2.5). As ageing temperature varied from 47 to 70 °C, a supersaturated concentration of sodium (Na) balancing cation in the framework of the synthesised product enabled the best structural configuration of HS zeolite (Figure 8.4.1(b)). The structural configuration further improved by varying NaOH/CFA from 1:1 to 1.2:1, and this variation simultaneously resulted in a drastically improved crystallinity of 97 % and phase purity of 81 % (Figure 8.2.5). The overall characteristic of HS zeolite further improved as synthesis times varied at 140 °C from 48-hour baseline to 72-hour at the optimised NaOH/CFA ratio of 1.2:1 (Figure 8.2.5). The latter presented an optimal synthesis time at 140 °C with an HS zeolite of 100 % crystallinity and improved purity level of 85 % (HS-72). The phase purity of HS increased to 91 %, produced a crystallinity of 85 % under synthesis temperatures from 140 °C to 100°C at 144 hours (HS-144(100°C), Figure 8.2.5). 100 °C proved to be optimum direct hydrothermal temperature condition, and on this basis the temperature was adopted for further investigation of HS synthesis via fusion-assisted method. Hence, the direct hydrothermal method, gave the optimum pre-synthesis conditions of 5:1 water/CFA ratio, ageing for 1.5h (reduced time) and at 70°C (increased temperature), 1.2:1 NaOH/CFA (increased ratio), and resulted in two optimum hydrothermal conditions (72h, 140 °C; 144h, 100 °C) with regard to overall characteristic properties of HS zeolite. The fusion-assisted method demonstrated exclusively one optimum hydrothermal condition at prolonged synthesis time (144h, 100 °C), showing a mixed phase HS sample with moderate crystallinity and high phase purity of 52 % and 80 % respectively. In line with high phase purity, it was estimated by means of XRD humps and peak roughness that both the hydrothermal methods (at optimal conditions) demonstrated a nearly equal proportion of unconverted amorphous phases in the obtained products (Figure 8.8.1, Appendix 1) and are hence suggested for a high and comparable conversion of fly ash from hydrothermal process.

In correspondence to high crystallinity and purity characteristic, a more crystalline morphology feature and a better structural configuration characteristic of HS zeolite was shown by the (optimum) direct hydrothermal products (Figure 8.4.2(c)). Both synthesis methods at optimum conditions, presented novel crystal morphologies (cubic-platelet and hexagonal cubic-shape) in description of HS zeolite, with the fusion-assisted product exhibiting a more integrated crystal morphology than the direct hydrothermal product.

Further, the fusion-assisted product sample showed higher characteristic textual properties with regard to total surface area (44.98 m^2/g, three-time larger) and possible acidic sites strength

than the direct hydrothermal products (Table 8.6.1, Appendix 1). While both synthesis methods resulted in a novel and highest pore size distribution of 3.75-4 nm, the fusion-assisted HS zeolite showed higher mesoporosity (4 >3.75nm) based on isotherm, average pore size and pore size distribution data (Figure 8.6.2 & Figure 8.6.1, Appendix 1).

Moreover, the fusion-assisted hydrothermal method resulted in HS zeolite of a considerable yield of 56.3 %, which was twice the yield of the products obtained via direct method at optimal conditions (Figure 8.8.2, Appendix 1). The direct hydrothermal method therefore presented itself as a more versatile approach with regard to obtaining high overall quality (crystalline and purer phase) HS zeolite and was associated with being more energy efficient due to the much less energy intense ageing conditions, coupled with the option of relatively lower hydrothermal optimum conditions. The fusion-assisted hydrothermal method resulted in an HS product of moderate quality (crystallinity). Hence, the direct hydrothermal method is deemed more feasible for upscale production of HS zeolite compared to fusion-assisted method. Accordingly, HSF-144 sample (in addition to the direct method HS zeolite HS-72 and HS-144(100°C) sample) was selected for catalytic application in the transesterification of maggot oil for biodiesel production in chapter 6. This very sample was used for biodiesel yield screening tests to establish the optimum single-parameter transesterification conditions (section 3.5.1, Table 3.4). The direct method HS-70°C and HS-70+1.2NaOH (also coded as HS-48) were also selected for catalytic application (at optimised single-parameter conditions) due to most intermediate improvement in overall characteristic of HS zeolite prior to varying hydrothermal synthesis time and temperature (Table 8.1.1, Appendix 1).

HS zeolite modified by ion exchange and bifunctional method were prepared using one of the optimum direct hydrothermal (HS-144(100°C) and the optimum fusion-assisted (HSF-144) HS zeolites as precursors (sections 3.3.5). The selection of the optimum HS samples was because of their high catalytic activity in the transesterification of maggot oil (chapter 6). By modification of both the direct hydrothermal (K/HS-144(100°C)) and fusion HS zeolite with ion exchange (K/HSF-144), the resultant overall characteristic as well as yields of the product were suppressed. After ion exchange, a drastic reduction in crystallinity of the direct hydrothermal product was observed (85 →25%), and the same similarly applied to the fusion product (52→34 %) (Figure 8.2.5, Appendix 1). The textual properties (with regard to total surface area and pore volume) were also suppressed because of ion exchange modification (Table 8.6.1, Appendix 1). The poor overall characteristics after ion exchange, could be attributed to an over exchange/saturation of K^+ ion and resultantly pore and framework

blockages induced in the structure of the respective modified samples. Consequently, and unintended, the ion exchange modification adversely affected the acidic characteristics of the zeolite product, resulting in poor cation exchange capacity (CEC) of the precursor HS products used for the modification. Like ion exchange demonstrating a poor product yield below 10 % (Figure 8.7.1), it was discovered that bifunctional modification of the direct hydrothermal HS zeolite, also resulted in poor product with regard to crystallinity (85→34 %), overall characteristic and low yield of the product (29.8 %) (Figure 8.2.5, Figure 8.7.1, Appendix 1). Owing to poor overall characteristic and poor yields demonstrated by products obtained via the ion exchange and bifunctional methods, no discussion was reported in the content of the thesis (chapter 5) with regard to both modification of HS zeolite.

In addition to HS zeolite, Na-X was also successfully produced in this work as described in section 3.3.4. It was found that a considerable high crystalline and pure phase Na-X zeolite obtained via fusion-assisted hydrothermal method, also resulted with varying NaOH/CFA ratio from 1:1 to 1.2:1 at 90 °C and 12-hour hydrothermal conditions (Figure 8.1.4(c), Appendix 1). The high quality Na-X zeolite however, demonstrated an extremely poor product yield of between 1.06 % and 0.16 % (Figure 8.7.1). This was majorly due the use of supernatant filtrate (SF) as a precursor, other than the use of the entire mixture (with the solid residue, SR) obtained after calcination as in the synthesis of HS zeolite via the fusion-assisted method (section 3.3.2). The poor Na-X zeolite yield being considered uneconomically feasible for upscale production, prompted discontinuity of further investigation on the synthesis of Na-X zeolite via the prescribed method in this work. Consequently, there is no discussion reported on the synthesis of the zeolite in question in the content of the thesis.

Chapter Six

Catalytic application of the synthesised coal fly ash-derived HS zeolite in the transesterification of maggot oil for biodiesel production

This chapter reports the application of the produced HS zeolite catalysts in biodiesel production using waste-derived maggot oil as feedstock. The chapter is divided into three major sections (6.1-6.3). The first section (section 6.1) discusses the results of catalytic performance (in terms of yield and quality of biodiesel products) of the direct method and fusion-derived HS zeolite samples (characterisation reported in chapter 5) in the transesterification of maggot oil. Using the optimum catalyst from the above evaluation, the section further evaluates the catalytic performance of HS zeolite in the transesterification of sunflower oil, vis-à-vis its performance-using maggot oil as feedstock. Further, section 6.2 discusses the biodiesel process optimisation from maggot oil using response surface methodology (RSM) technique. Section 6.3 reports on the kinetics of biodiesel production process (transesterification) from maggot oil.

Product characterisation (yield and quality)

The experimental procedures and conditions for biodiesel production using the various synthesised HS zeolites as catalysts, is reported in section 3.5.1. The procedure for process optimisation (via RSM) and kinetic studies are reported in section 3.5.2 and section 3.5.3 respectively. The yield of obtained biodiesel samples throughout was determined using equation 3.10 as follows.

$$BD\ yield\ (\%) = \frac{Mass\ of\ biodiesel\ obtained,\ g}{Mass\ of\ oil\ feedstock,\ g} \times 100 \qquad (3.10)$$

The FAME content in the produced biodiesel samples was determined using the pre-calibrated GC-FID. This was obtained as a sum of constituent fatty acid esters (C_{12}-C_{20}) in weight % (equation 3.13, section 3.5.4), represented as peaks or peak areas (excluding the peak area of internal standard, C_{11}) on the chromatographs of the respective analyzed biodiesel samples (BD) (Figure 8.10.1 & Figure 8.10.2, Appendix 2). FAME content is also referred to as "ester content" property of biodiesel, for which equation 3.12 was given earlier (section 3.5.4).

FAME or ester (%) = $Sum\ of\ wt\ \%\ fatty\ acid\ esters$ in produced BD - $wt\ \%\ of\ C_{11}$ (3.12)

where C_{11} represents the internal standard (dodecane) used for FAME determination of either the feedstock oil or produced biodiesel samples via GC analysis.

Other physicochemical properties (acid value, saponification value, Iodine value, density, viscosity, refractive index, FAME/ ester content) of the produced biodiesel samples were determined according to the (EN14214 and ASTMD 6751) standard methods described in section 3.5.4.

6.1. Catalytic application of the synthesised HS zeolite samples in the transesterification of maggot oil for biodiesel production

The direct method HS zeolite samples with optimal characteristics employed herein are samples HS-72 and HS-144(100°C). HS-70°C and HS-70+1.2NaOH samples are also evaluated herein based on the fact that these samples, among those obtained with varying NaOH/CFA ratio, were associated with the most intermediate improvement in overall characteristic of HS zeolite in the course of investigation (prior to varying synthesis time and temperature to obtain HS-72 and HS-144(100°C)). The fusion HS zeolite sample used is HSF-144. Catalytic evaluation test using each of the selected samples was separately carried out according to the biodiesel production procedure described in section 3.5.1. The evaluation tests was conducted at the following prescribed (single parameter approach-based) optimised conditions: catalyst weight (wt.) of 1.5 % of the oil (w/w), methanol-to-oil molar ratio (MeOH/oil) of 15:1, stirring rate of 600 rpm, reaction temperature of 60 °C and reaction time of 1.5 hours. The results of biodiesel yield optimisation by single parameter approach (Table 3.4, procedure described in section 3.5.1) in acquiring the above prescribed optimised conditions using sample HSF-144, are reported in Figure 8.10.3 (Appendix 2).

6.1. Results and discussion

6.1.1. Catalytic performance of HS zeolite as a function of varying NaOH/CFA ratio in catalyst synthesis mixture

Variation in NaOH/CFA ratio in catalyst synthesis from 1:1 to 1.2:1, proved to be a significant factor in the catalytic performance of the synthesised sample. The yield of maggot oil-derived biodiesel and FAME content therein as a function of varying the NaOH/CFA ratio in the catalyst synthesis mixture, is presented in Figure 6.1.

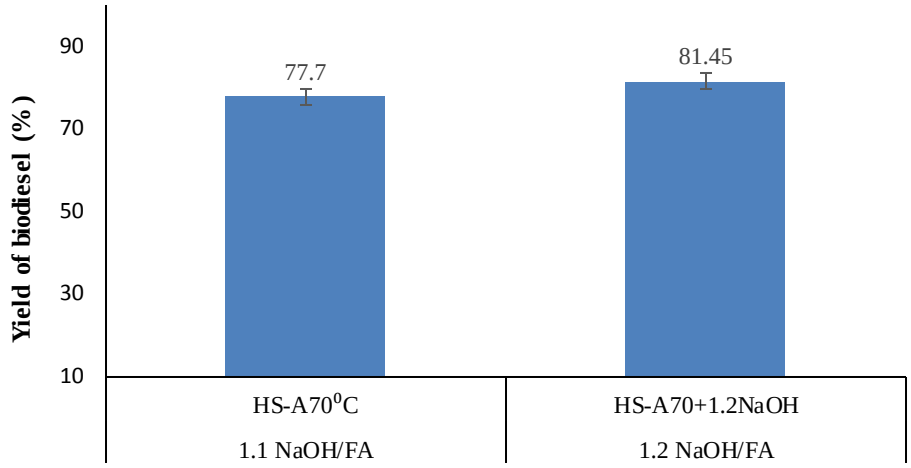

Figure 6. 1. Yield of maggot oil-derived biodiesel as a function of NaOH/CFA ratio in catalyst synthesis (Trans. conditions: 60 °C; 15:1 MeOH/oil ratio; 600 rpm; 1.5 % catalyst wt. and 1.5 h) (NaOH/FA= NaOH/CFA)

According to Figure 6.1, sample HS-70°C (NaOH/CFA ratio of 1:1) being the initial sample evaluated, led to a considerable biodiesel yield of 77.70 %. A congruent increase in biodiesel yield (81.45 %) was observed as NaOH/CFA in the catalyst synthesis mixture was increased from the initial ratio of 1:1 to 1.2:1 (with the use of HS-zeolite sample). The above increase can be attributed to the observed higher surface area, offered by HS-A70+1.2NaOH catalyst sample as compared to HS-70°C sample (Makgaba and Daramola, 2015, Volli and Purkait, 2015) (Table 8.6.1 & Table 8.5.1, Appendix 1). Viswanadham et al. (2012) suggests that the activity is associated with increased porosity, because of enhanced diffusion property and reduced contact time of the reacting molecules with the catalyst sample favouring the increased biodiesel yield obtained. Further catalytic evaluation of the selected samples with varying NaOH/CFA ratio, was carried out in terms of physicochemical properties of the biodiesel produced. Table 6.1 presents the physicochemical properties of biodiesel obtained using the two selected catalysts obtained by varying NaOH/CFA ratio.

Table 6.1. Physicochemical properties of maggot oil-derived biodiesel as a function of NaOH/CFA ratio in catalyst synthesis mixture

Biodiesel properties	FAME characteristics obtained as a function of NaOH/FA ratio for respective synthesized catalysts		B-Standard[a]
	HS-A70°C	HS-A70+1.2NaOH (also coded as HS-48)	ENS[b] /ASTM[c]
Acid value (mg KOH/g)	0.53	0.53	0.5/0.8 Max
Saponification value (mg KOH/g)	145.53	145.37	-
Ester content[d] (% m/m)	50.66	35.83	96.5
Iodine value (g of I_2/100 g)	49.38	59.02	/130
Density at 40 °C (g/ml)	0.914	0.893	0.86-0.90
Kinematics viscosity at 40 °C (mm^2/s)	5.82	5.73	3.5-5.0 /1.9-6.0
Refractive index[e]	1.4449	1.4444	/1.479
Cetane number	56.71	36.63	51/47

[a] Biodiesel Standard Specifications; [b] ENS14214 (European) and [c]ASTMD6751 (American for FAEE)
[d] Obtained from GC characterisation of respective biodiesel FAME samples

It is revealed in Table 6.1 that the use of HS-A70°C sample as catalyst at fixed conditions, led to a biodiesel sample with a quality that moderately complies with the ASTM and ENS specifiation standards (Dias et al., 2009, Jayasinghe and Hawboldt, 2012). This refers to ester (FAME) content (50.66 %), a density slightly exceeding the limit (0.914 g/mL), a high viscosity value in order of the limit standard (5.82 mm^2/s), and a closely compliant cetane number (56.71). Upon variation of the above catalyst sample for HS-70+1.2NaOH (i.e. increase in NaOH/CFA ratio in catalyst feed mixture), density was decreased to the compliant value (0.893 g/mL), viscosity was slightly decreased (5.73 mm^2/s) and iodine value (IV) was improved from 49.38 to 59.02 I_2/100 g. Like the increased yield (Table 6.1), Dehkhoda (2010) suggested that the above improved quality (properties) of biodiesel can be attributed to the more exposed catalyst total surface area (Table 8.5.1, Appendix 1) and corresponding high acid density thereof.

In contrast, a decreased FAME (ester) content of 35.83 % (50.66 →35.83 %) was observed with increasing NaOH/CFA ratio, indicating decreased conversion of maggot oil over the catalyst sample (HS-70+1.2NaOH). According to Volli and Purkait (2015), the above is suggested to have been associated with relatively weaker acidic site strength induced by varying NaOH/CFA ratio from 1:1 to 1.2:1 (i.e. demonstrated by HS-70+1.2NaOH as

comparated to HS-70°C). This is based on increasing Si/Al ratio shown in Table 8.5.1 (Appendix 1) as per Ferreira Madeira et al. (2012). The decrease in the FAME content can also be suggested to have been due to increased porosity shown by HS-70+1.2NaOH (Figure 8.3.1(h)/section 8.3, Table 8.6.1, Appendix 1), as this is associated with shorter contact period between the reacting mixture and the catalyst (Dehkhoda, 2010). According to Volli and Purkait (2015), this is further suggested for the lower conversion by HS-70+1.2NaOH sample.

From the findings discussed, it is deduced that HS-70+1.2NaOH catalyst sample, resulted in better overall quality of biodiesel with the exception of ester content. The enhanced iodine value (IV) (49.38→59.02 I_2/100g oil) attested to a derived-biodiesel sample that is less saturated in relation to the oil feedstock with better cold flow and a relatively high storage and reactive characteristics (Surendra et al., 2016, da Cunha et al., 2009, Canesin et al., 2014). According to Jayasinghe and Hawboldt (2012), the improved kinematic vsicosity (5.82 → 5.73 mm^2/s), and a density in order of the limit standard (0.907 g/mL), is an indication of derived-biodiesel with good ignition characteristics. The above also revealed a fuel with a good atomisation and flow characteristic as obtained over HS-70+1.2NaOH (Canesin et al., 2014). Additional mixing efficiency in the course of the reaction, could have improved the cetane number to being closer to the standard value (36.63→51/47). Further, the derived-biodiesel exhibited a high saponification value (SV) of 145.37 mg KOH/g oil (lower than the oil feedstock). Further evaluation of biodiesel production was carried using the selected optimum direct method zeolite samples obtained because of varying hydrothermal catalyst synthesis time and temperature.

6.1.2. Biodiesel production over HS zeolite catalyst obtained with varying direct hydrothermal synthesis time and temperature

Figure 6.2 presents the yields of biodiesel and FAME (ester) obtained using the optimum direct hydrothermal HS zeolite catalysts (These refer to HS-72 and HS-144(100°C)) and the solely selected fusion HSF-144 sample as stated in chapter 5.

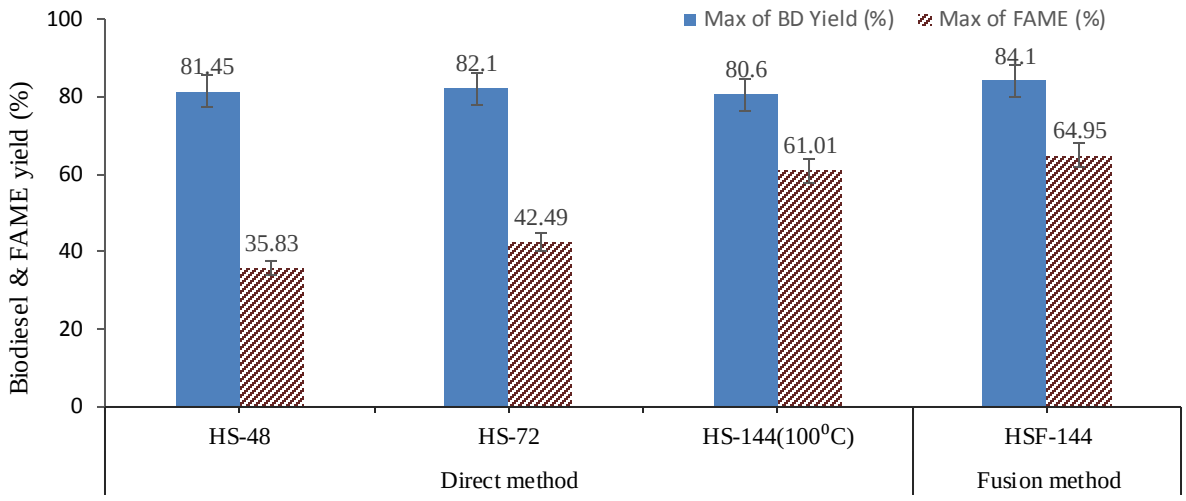

Figure 6. 2. Yield of maggot oil-derived biodiesel using the optimum direct hydrothermal and fusion-assisted HS zeolite catalysts (note that HS-48 = HS-70+1.2NaOH) (Trans. conditions: 60 ^{o}C; 15:1 MeOH/oil ratio; 600 rpm; 1.5 % catalyst wt. and 1.5 h)

As can be observed in Figure 6.2, biodiesel yield of 81.45 % was obtained using the catalyst sample HS-48. This sample is analogous to HS-A70+1.2NaOH sample reported previously and represents the baseline synthesis time of 48 hours (HS-A70+1.2NaOH or HS-48 sample). It was however observed that with an increase in catalyst synthesis time by use of the optimum HS-72 sample, there was a small increase in biodiesel yield to 82.10 % and recovery in FAME (ester) content of 42.42 %. The increase in the yield can be explained by larger intercrystalline porosity demonstrated by HS-72 (Figure 8.3.2(d)), whereas the enhanced FAME yield is rather attributed to the enhanced intracrystalline porous structure shown by HS-72 in comparison to HS-48 sample (Figure 8.3.2(c-d)) (Dehkhoda, 2010). Consequently, HS-72 sample offered an improved reactant mixture-catalyst contact (Fayyazi et al., 2018), suggesting a possibility of higher conversion of maggot oil to biodiesel (Leung et al., 2010).

Further, Figure 6.2 shows that with a reduction in catalyst synthesis temperature from 140 to 100°C at 144-hour reaction time (100 °C, 144h), the optimal HS-144(100°C) zeolite reduced the biodiesel yield slightly to 80.60 % and increased the FAME (ester) content to 61.01 %. The observed decrease in the yield can be attributed to comparably decreased surface area demonstrated by the sample (as compared to HS-72) as a result of the decrease in synthesis temperature (Table 8.6.1/section 8.6, Appendix 1) (Volli and Purkait, 2015, Makgaba and Daramola, 2015). The considerable increase in FAME content on the other hand (60.17 %) ,

was attributed to stronger acidic sites of HS-144(100°C) shown in chapter 5 (based on its Si/Al ratio) (Table 8.5.1/section 8.5, appendix 1) (Ferreira Madeira et al., 2012), coupled with a lower intercrystalline porosity observed thereof (Figure 8.3.2f /Section 8.3 & Table 8.6.1, Appendix 1) (Viswanadham et al., 2012). The latter improved reactant-catalyst contact when using HS-144(100°C) compared to all direct method catalysts (both HS-72 and HS-48, as well as HS-70°C) and indicates a progressively improved conversion of maggot oil to FAME, which correlated with increasing catalyst hydrothermal synthesis time and reducing hydrothermal temperature. Higher FAME content obtained using HS-144(100°C) compared to HS-70°C (60.17 > 50.66 %), can be explained by the improved contact coupled with higher surface area of HS-144(100°C) compared to HS-70°C (Volli and Purkait, 2015) (Table 8.6.1/Section 8.6, Appendix 1).

As well as FAME (ester) content, Table 6.2 reports on other physicochemical properties of biodiesel samples obtained using the optimum selected direct method HS zeolite catalysts (HS-48, HS-72, HS-100°C). The biodiesel properties obtained from the fusion HS zeolite (HSF-144) are also presented therein.

Table 6.2. Physicochemical properties of maggot oil-derived biodiesel over direct and fusion method synthesised HS zeolite catalyst

Biodiesel properties	FAME characteristics for respective direct method versus fusion synthesized HS heterogeneous catalysts				B-Standard[a]
	HS-48	HS-72	HS-144 (100°C)	HSF-144	ENS[b] /ASTM[c]
Acid value (mg KOH/g)	0.53	0.49	0.47	0.53	0.5/0.8 Max
Saponification value (mg KOH/g)	145.37	145.40	145.40	147.87	-
Ester content[d] (% m/m)	35.83	42.49	61.01	64.95	96.5
Iodine value (g of I_2/100 g)	59.02	56.86	60.17	65.01	/120-130
Density at 40 °C (g/ml)	0. 907	0.881	0.897	0.877	0.86-0.90
Kinematics viscosity at 40 °C (mm^2/s)	5.73	5.70	5.73	5.16	3.5-5.0 /1.9-6.0
Refractive index[e]	1.4454	1.4450	1.4461	1.4455	/1.479
Cetane number	36.63	36.64	36.60	36.63	51/47

[a] Biodiesel Standard Specifications; [b] ENS14214 (European) and [c]ASTMD6751 (American for FAEE)
[d] Obtained from GC characterisation of respective biodiesel FAME samples

Table 6.2 reveals that both of the catalyst samples obtained with varying hydrothermal synthesis time and temperature (HS-72 and HS-144(100°C)), demonstrated improved overall

biodiesel quality. Increase in FAME (ester) content from 35.83 to 61.01 % as earlier reported, was observed, as the catalyst synthesis time increased from 48 h baseline to 144 h. Improved biodiesel densities to compliant values of 0.881 and 0.897 g/mL, were derived for HS-72 and HS-144(100°C) catalyst samples respectively. The above were coupled with compliant kinematic viscosity values (5.70 and 5.73 mm^2/s) and refractive index (n_D = 1.4450 and 1.4461). According to Jayasinghe and Hawboldt (2012), these indicate that the derived-biodiesel is within acceptable flow and mixing characteristic properties. Further, the considerably improved and lower biodiesel acid value (0.47 mg KOH/g) obtained over HS-144(100°C) sample, suggests a fuel with better engine performance (Ferreira et al., 2012). Further, sample HS-144(100°C) demonstrated an improved IV (60.17 I_2/100g oil), revealing that this catalyst sample is suited for producing a biodiesel with good oxidation and storage stability (Canesin et al., 2014). A moderately compliant cetane number of 36.30 was retained with variation in catalyst synthesis time and temperature, which suggests a biodiesel fuel with moderate ignition characteristics (Jayasinghe and Hawboldt, 2012).

As can be observed, all biodiesel samples obtained over the selected optimum catalysts demonstrated properties complying with the specification standard (ASTMD6751 and EN14214). These biodiesel samples obtained as a function of increasing hydrothermal synthesis time and varying synthesis temperature were more compliant with the standards compared to samples obtained with varying NaOH/CFA ratio in catalyst synthesis mixture. Catalyst sample HS-144(100°C) (as predicted in chapter 5) proved to be the catalyst with optimum performance, with respect to yield and quality of biodiesel from maggot oil. Therefore, further evaluation of biodiesel production, was evaluated using the solely selected fusion-derived catalyst HSF-144 sample.

6.1.3. Biodiesel production over HS catalyst samples synthesized via fusion-assisted method

Figure 6.2 (section 6.1.2) presents results obtained over catalysts made with varying synthesis conditions or by use of the optimum fusion-assisted catalyst sample HSF-144, showed a relatively increased biodiesel yield of 84.10 %, and resultant increased FAME content of 64.95 % (~65 %). The observed yield increase can be associated with the highest total surface area offered by this sample as compared to direct method catalyst samples (Table 8.6.1, Appendix

1) (Volli and Purkait, 2015, Makgaba and Daramola, 2015, Dehkhoda, 2010). The increased FAME (ester) content can be attributed to the stronger acidic sites (predicted previously based on framework Si/Al ratio, section 5.2.1) and both lower intercrystalline and intracrystalline porosity depicted by the sample (Table 8.6.1 & Figure 8.3.3/section 8.3, Appendix 1) as compared to direct hydrothermal products (Ferreira Madeira et al., 2012, Viswanadham et al., 2012). do Nascimento et al. (2011) suggests that both low porosity of HSF-144 and high distribution of Al^{+} (high Al content) in the sample's structure, corresponding to low Si/Al ratio (Table 8.5.1, Appendix 1), facilitates access of reactant-mixture to the catalyst acidic sites. Therein, the adsorptive medium promoted mixing between the oil and methanol, enhancing the rate of reaction and conversion of maggot oil with an increased ester content (FAME) obtained over this catalyst sample (Endalew et al., 2011).

The improved ester content of 64.95 % obtained using the sample, was the highest reported in comparison to all other or direct HS zeolite catalysts. Further, the biodiesel obtained using the fusion HS zeolite catalyst (HSF-144), demonstrated higher SV (147.87 mg KOH/g), enhanced iodine value (65.01 I_2 /100 g oil) and kinematic viscosity (5.16 mm^2/s) (Table 6.1). These in conjunction with the characterising improved density of the derived biodiesel (0.877 g/mL), indicate a fuel with better oxidation, flow and mixing characteristics (Canesin et al., 2014, Jayasinghe and Hawboldt, 2012) compared to those obtained using the direct method catalyst samples. In addition to the above, the fuel exhibited a moderately compliant cetane value (36.36) and a compliant acid value (AV) (0.53 mg KOH/g). The latter indicates the use of an acid catalyst (Endalew et al., 2011, Lam et al., 2010, Leung et al., 2010), which promoted both esterification and transesterification reactions simultaneously from high FFA maggot oil feedstock (Table 4.2, section 4.2).

The biodiesel samples obtained over HSF-144 sample complied better with specification standards in terms of nearly all properties. Hence, the fusion catalyst has better performance in the transesterification of maggot oil. Owing to propects in comparison to other or direct method catalysts samples, the catalyst HSF-144 catalyst was therefore tested on refined sunflower oil (section 3.5.1, chapter 3).

The yield and FAME content (ester) of the obtained sunflower oil-derived biodiesel and that from maggot oil at same conditions, is presented in Figure 6.3.

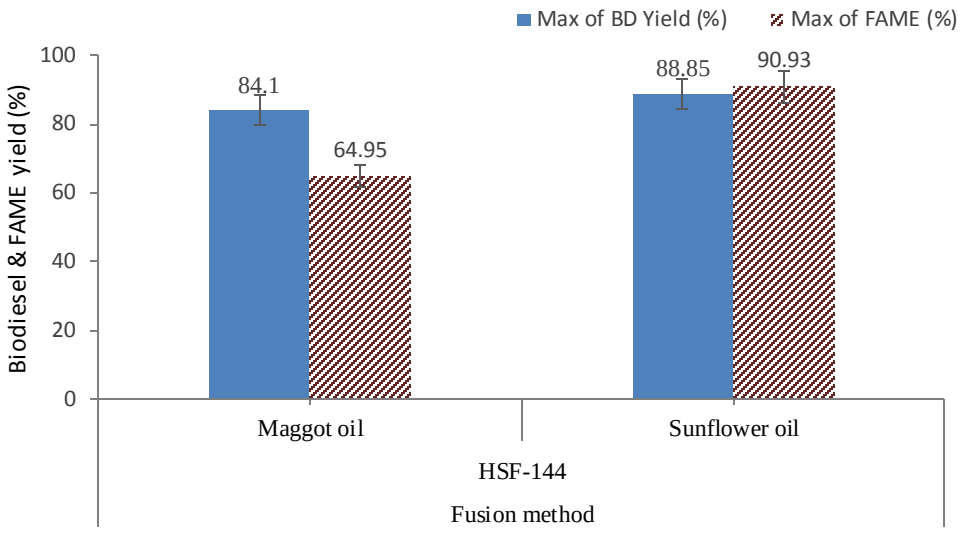

Figure 6.3. Comparison between the yield of biodiesel and FAME from maggot oil and sunflower oil using fusion HS zeolite as catalyst at fixed conditions (Trans. conditions: 60 °C; 15:1 MeOH/oil ratio; 600 rpm; 1.5 % catalyst wt. and 1.5 h).

Figure 6.3 reveals that the HS zeolite catalyst performed better in the transestetrification of sunflower oil, compared to its performance using maggot oil at the same conditions. A higher biodiesel yield of 88.85 % was obtained using sunflower oil (SF-biodiesel), and this contained a much higher ester (FAME) content of 90.93 %. Ramos et al. (2008) reports on high yield of biodiesel from sunflower oil using modified zeolite Na-X.

In addition to ester content, the comparision between biodiesel production from maggot oil and sunfower oil using the fusion HS zeolite (HSF-144), was evaluated in terms of other physicochemical chemical properties presented in Table 6.3.

Table 6.3. Comparison between biodiesel production from maggot oil and conventional sunflower oil (SF) using HS zeolite catalyst

Biodiesel properties	**Sunflower oil**	**Maggot oil-biodiesel** HSF-144	**SF-biodiesel** HSF-144	ENS[b] /ASTM[c]
Acid value (mg KOH/g)	0.76 (0.38 % FFA)	0.53	0.53	0.5/0.8 Max
Saponification value (mg KOH/g)	-	147.87	161.66	-
Ester content[d] (% m/m)	-	64.95	90.93	96.5
Iodine value (g of I_2/100 g)	-	65.17	68.56	/130
Density at 40 °C (g/ml)	0.92 [e]	0.877	0.864	0.86-0.90
Kinematics viscosity at 40 °C (mm^2/s)	32.6 [e]	5.16	4.19	3.5-5.0 /1.9-6.0
Refractive index	1.4744	1.4455	1.4555	/1.479
Cetane number	-	36.63	45.3	51/47

[a] Biodiesel Standard Specifications; [b] ENS14214 (European) and [c] ASTMD6751 (American for FAEE)
[d] Obtained from GC characterisation of respective biodiesel FAME samples – Also referred to as FAME content or yield
[e] Density and kinematic viscocisity value obtained from published source (Leung et al., 2010)

According to Table 6.3, the SF-biodiesel demonstrated a better iodine value (IV) of 68.65 I_2 /100 g oil, a lower and compliant kinematic viscosity and density of 4.19 mm^2/s and 0.864 g/mL respectively, an enhanced and closely compliant cetane number of 45.3, and an improved saponification value (SV) (161.66 mg KOH/g oil). The better SF-biodiesel yield and quality demonstrated above using HS zeolite, can be attributed to the higher unsaturated fatty acid content (MUFA+PUFA) in precusor sunflower oil (Figure 8.9.1(b) /section 8.9, Appendix 2), as well as the characterised much lower FFA content therein (0.38 % FFA) (acid value, 0.76 mg KOH/g oil) (Table 8.8.1/ Section 8.8, Appendix 2). The above is in contrast to maggot oil feedstock, which contained higher saturated fatty acid (SFA) and FFA of 3.38 % (Figure 8.9.1(a) & Table 8.6.1, Appendix 2).

From the results obtained, it can be concluded that the better activity of waste coal fly ash-based HS zeolite in the transesterification of sunflower oil, additionally attested to its potential as a novel heterogenous catalyst in biodiesel production. The catalyst has proven to perform better in converting sunflower to biodiesel compared to other zeolite types such as Na-X zeolite at either modified or non-modified form (Babajide et al., 2012, Ramos et al., 2008) (Table 2.6, section 2.7.1), as well as compared to the most typical non-zeolite CaO heteregeneous catalyst employed even at more extreme transesterification conditions (Di Serio et al., 2008).

6.2. Optimisation of biodiesel production process by response surface methodology studies (RSM)

This section discusses the optimisation of biodiesel production from maggot oil via response surface methodology (RSM). Catalyst sample HSF-144 was selected for the optimisation due to its excellent performance in comparison to other samples in terms of biodiesel yield and quality (section 6.1).

Three independent variables were undertaken for the optimisation using Design Expert® software version 11 (Table 3.5, section 5.5.2). The choice of variables was based on the biodiesel yield outcomes from screening tests (Figure 8.10.3, Appendix 2) and literature. Screening tests on biodiesel yield defined the conditions of the process variables in question. The biodiesel yield screening tests were conducted via single-parameter optimization approach (Table 3.4, section 3.5.1). The variables in question include methanol-to-oil molar ratio (MeOH/oil ratio), stirring rate and reaction time. The Central Composite RSM's Design (CCD) was chosen for the study in order to accommodate all three selected variables. The design was also selected because it requires the minimum number of experiments (as compared to other designs (e.g. Full three-level factorial method) and is proven to be as efficient as those with a large number of experiments – Cost effective RSM design (Bezerra et al., 2008). The statistical analysis of experimental data and model obtained by the design was evaluated by ANOVA (Analysis of Variance). The significance of data obtained by the generated model and model coefficients was evaluated by F-Tests and P-Test (95 % confidence level) respectively. The accuracy of the model was measured using the R^2 correlation coefficient.

6.2. Result and discussion

Optimisation of biodiesel production through the three selected operating variables and using HS catalyst (sample HSF-144), resulted in the following response in biodiesel yield (Table 6.4).

Table 6.4. Central composite Design (CCD) of experiments and actual/predicted response

Run	Factor 1 A:MeOH:Oil (n/n)	Factor 2 B:Stirring rate (rpm)	Factor 3 C:Time (hour)	Response Yield (%)	Predicted yield (%)
1	6	800	1.5	80.15	80.41
2	10.5	600	1	77.28	78.23
3	15	800	1.5	75.55	74.31
4	15	800	3	83.75	84.29
5	10.5	600	2.25	82.63	83.02
6	18	600	2.25	78.55	79.17
7	15	400	1.5	79.70	79.72
8	10.5	600	2.25	83.65	83.02
9	15	400	3	84.80	84.10
10	10.5	600	2.25	83.05	83.02
11	3	600	2.25	78.80	78.83
12	6	800	3	78.60	78.13
13	10.5	935	2.25	81.60	81.93
14	6	400	3	76.80	77.59
15	10.5	600	2.25	82.49	83.02
16	10.5	600	2.25	83.75	83.02
17	6	400	1.5	86.45	85.47
18	10.5	265	2.25	85.70	86.01
19	10.5	600	3.5	80.30	79.99
20	10.5	600	2.25	82.69	83.02

Factor coded with a letter. E.g., Factor 1, coded with A

Predicted vs. Actual response plot (See Figure 6.4(b), section 6.2.1 or Figure 8.11.1(c), Appendix 2)

Table 6.4 reveals that there is a good relationship between the actual response and predicted values of biodiesel yields, showing no more than 1 % difference between the actual and predicted values, which is best explained by a linear correlation. More clarity on the above is given via Figure 6.4 in section 6.2.1.

6.2.1 Statistical analysis for the optimisation of biodiesel production from maggot oil

From the optimisation conducted using the three factors (via CCD-RSM), the resultant model for the relationship between the experimental and predicted responses, best fitted a quadratic regression (equation 6.1).

$$\text{Yield } (Y) = 3.02+0.1020A-1.22B+0.5262C-0.0875AB+3.06AC+1.40BC-1.45A^2+0.3376B^2-1.41C^2 \quad (6.1)$$

The statistical analysis of the model generated by analysis of variance (ANOVA) is presented in Table 6.5.

Table 6.5. Analysis of Variance (ANOVA) for quadratic model of the optimisation of biodiesel production from maggot oil (response: yield)

Source	**Sum of Squares**	**Df[(a)]**	**Mean square**	**F-value**	**p-value**	
Model	172.12	9	19.12	26.33	< 0.0001	significant
A-MeOH:Oil	0.1412	1	0.1412	0.1944	**0.6687**	
B-Agitation rate	20.17	1	20.17	27.77	0.0004	
C-Time	3.75	1	3.75	5.17	0.0463	
AB	0.0613	1	0.0613	0.0843	**0.7774**	
AC	75.03	1	75.03	**103.31**	< 0.0001	
BC	15.68	1	15.68	21.59	0.0009	
A^2	29.44	1	29.44	40.53	< 0.0001	
B^2	1.62	1	1.62	2.24	**0.1656**	
C^2	27.78	1	27.78	38.24	0.0001	
Residual	7.26	10	0.7263			
Lack of Fit	5.79	5	1.16	3.94	0.0792	not significant
Pure Error	1.47	5	0.2939			
Cor Total[(b)]	179.38	19				

[(a)] Degree of freedom [(b)] Amount of variation around the mean of the observations

The statistical analysis generated by RSM (ANOVA), reveals that the model F-value of 26.33 indicates that the model was significant at 95 % confidence level (Table 6.5). The "model F-value" this significance has only 0.01 % chance to occur due to noise. The significance of the model was further justified by p-value < 0.05. The model terms B, C, AC, BC, A^2, and C^2 characterised with p-values < 0.05, were also significant. The model - term A, AB and B^2 with values greater than 0.1, were not significant (Behera et al., 2018, Tshizanga et al., 2017).

With the exception of MeOH/oil ratio (term A), ANOVA shows that linear effects of the independent process variables are significant on the yield of biodiesel. Agitation rate (B) was identified as the most significant, followed by reaction time (C). This is owing to corresponding lower p-value (far less than 0.05) (Table 6.5) and order of higher F-value. The above suggests that biodiesel yield from maggot oil could be efficient at different MeOH/oil ratios, provided a

ratio that is associated with excess amount of methanol is in favour of the forward reaction (Leung et al., 2010). Further, the interaction between MeOH/oil ratio and reaction time (AC) was the most significant towards the yield of biodiesel production in this work ($p < 0.001$, F-value =103.31), of which this could have been due to excess methanol and effective mixing into the oil after the reaction time counteractive to the backward reaction (Leung et al., 2010, Sun et al., 2015). The former attribution attests to the model's significance of the quadratic effect of MeOH/oil ratio (A^2).

Further, Table 6.5 shows that the model exhibited a lack of Fit F-value of 3.94, revealing a 7.92 % chance that such large value could have occurred due to noise. The above also indicates that there was a 7.92 % probability by which the model prediction missed the experimental data or observation. Hence, the obtained lack of fit is considered not to be significant since the corresponding p-value is greater than 0.05. This serves as a good indication that the model fits the experimental data well and agrees with Wang et al. (2014) concerning acquisition of such a model. The generated model fit statistic is presented in Table 6.6.

Table 6. 6. Model fit statistics for the production of biodiesel from maggot oil

Mean	Std deviation	C.V. %	R^2	Adjusted R^2	Predicted R^2	Adeq Precision
81.31	0.8522	1.05	0.9595	0.9231	0.7501	19.4087

Table 6.6 shows that the model demonstrated a high coefficient of determination ($R^2 = 0.9595$). This value shows that the developed model could explain more than 95 % (95.95 %) of the variability, or there is 95.95 % extent of estimation of the experiment data from the developed model (Zhang, 2010, Behera et al., 2018). This also implies that 95.95 % of biodiesel yields from maggot oil was attributed to the selected process operating variables (MeOH/oil ratio, agitation rate, reaction time). An adjusted (adj. $R^2 = 0.9231$) was in close agreement with the predicted correlation coefficient (pred $R^2 = 0.7501$) for the maggot oil-biodiesel production ($Adj.R^2 - Pred.R^2 < 0.2$, i.e. within the permissible limit). This reveals that the experimental data fitted the predicted values well (Uzoh et al., 2014). The model is associated with a marginal standard deviation of 0.8522. Moreover, the model demonstrated a coefficient of variance (CV) of 1.05 % and a design precision ratio of 19.4087. The ratio being greater than 4 ($19.4087 > 4$) is desirable and indicates an adequate signal-to-noise ratio (Uzoh et al., 2014). This proves that the model can be used to navigate the design space, is highly precise and reliable (Mewa-Ngongang et al., 2017).

The normal plots of residuals, and the plot of actual and predicted response values, are presented in Figure 6.4 (see Appendix 2, Figure 8.11.1/section 8.10 for additional plots of predicted and residual response values, and runs vs. residuals).

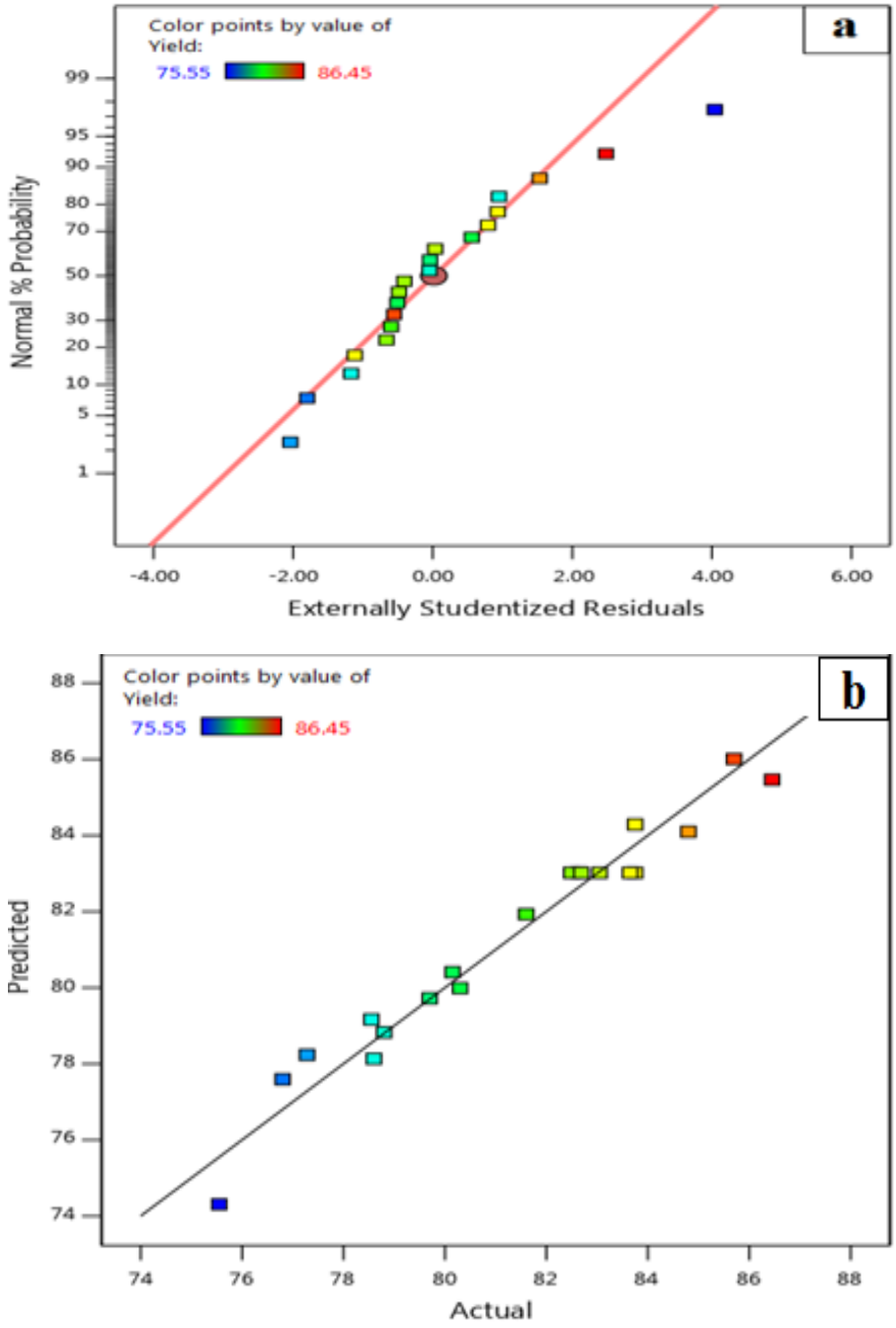

Figure 6. 4. Analysis of RSM-derived quadratic model, **(a)** Normal probability plots of residuals, and **(b)** predicted vs. actual response values

Normal plots of residuals in Figure 6.4(a) reveals that the points were closely distributed to the straight line of the plot and that the residuals followed the normal distribution. This shows that there was good relationship between the experimental and the predicted values of biodiesel yield. The model was adequate in predicting the yield based upon the experimental values (Table 6.4; Figure 6.4(b)).

6.2.2 Response surface plots for biodiesel process optimisation from maggot oil

In addition to Analysis of Variance (ANOVA), the response surface methodology (RSM), based on the developed model (equation 6.1), was further used to generate three-dimensional response surface plots (Figure 6.5 – Figure 6.7). The response surface plots demonstrate the interactions between the variables and reveal the optimum condition of each factor in the transesterification of maggot oil (with regard to biodiesel yield).

The combined effect of MeOH/oil molar ratio (A) and agitation rate (B) at constant reaction time of 1.5 hours and 60 °C, is presented in Figure 6.5.

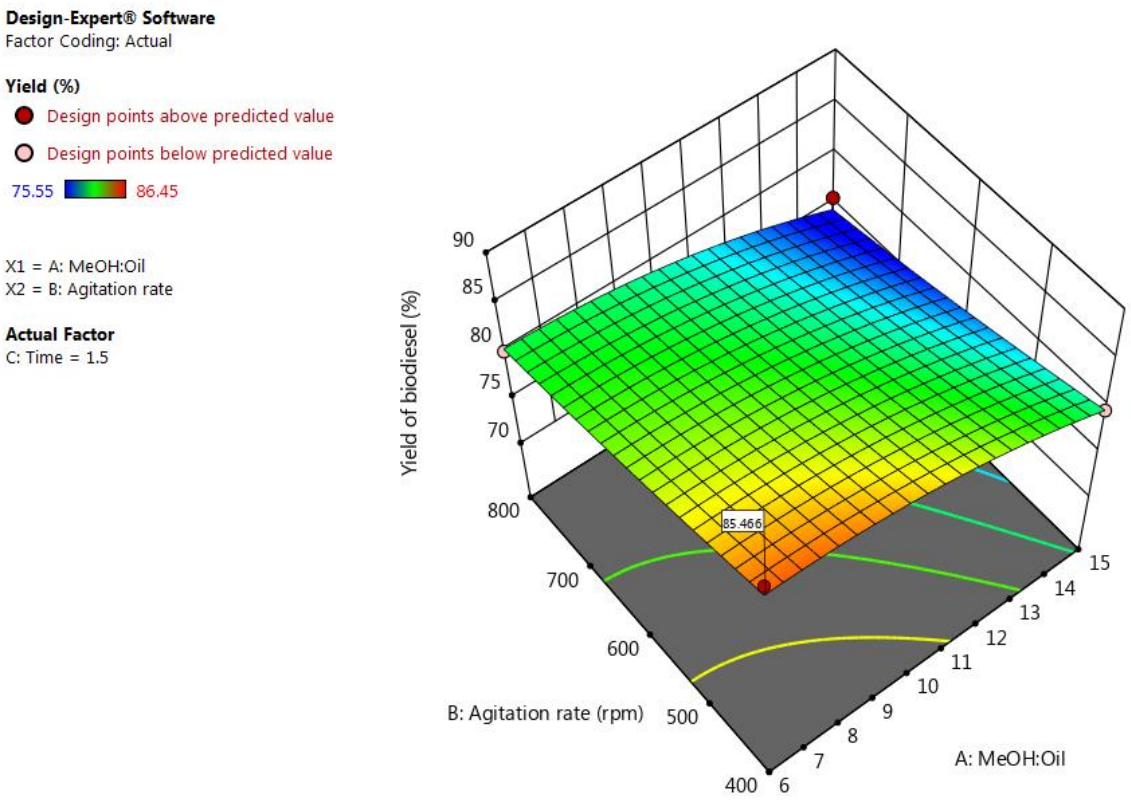

Figure 6.5. Response surface plots for the interaction/effect of MeOH-to-oil molar ratio (A) and agitation rate (B) on the yield of maggot oil-derived biodiesel.

Figure 6.5 reveals that the yield of biodiesel at low MeOH/oil ratio (between 6:1 and 9:1), was observed to increase as the agitation rate was decreased. With an increase in agitation rate, varying MeOH/oil ratio (B) resulted in poor yield of biodiesel. Ramezani et al. (2010) also suggests that high mixing intensity decreases the yield of biodiesel, of which this can be attributed to interruptions of interface between the oil and methanol leading to possibility of backward reaction (Mashkour and Mohammed, 2017). Hence according to Figure 6.5, the optimum conditions for the two factors involved, was revealed at the lower agitation rate of 400 rpm and MeOH/oil ratio of 6.1.

Further, the combined effects of MeOH/oil ratio (A) and reaction time (AC) at fixed and optimised agitation of 400 rpm were then investigated, and the response surface plot presented in Figure 6.6.

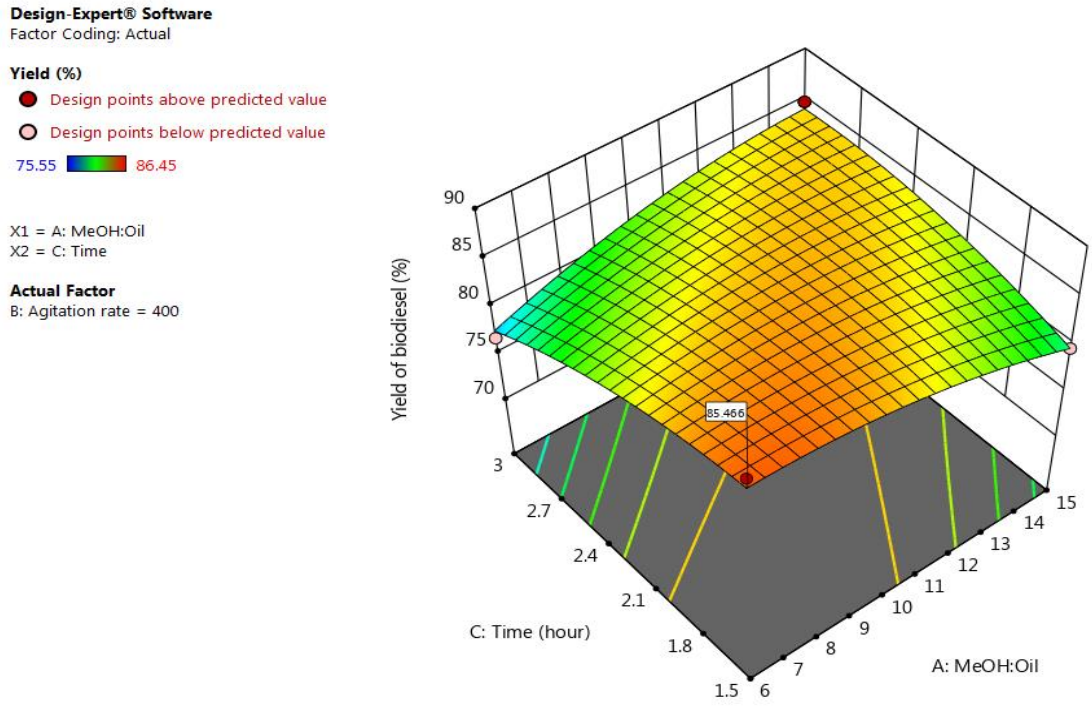

Figure 6. 6. Response surface plots for the interaction/effect of MeOH-to-oil molar ratio (A) and reaction time (C) on the yield of biodiesel (reaction temperature = 60 °C; catalyst wt. = 1.5 %)

The yield of biodiesel increased due to the interaction of MeOH/oil ratio and reaction time (AC) at constant agitation rate (400 rpm) (Figure 6.6). The yield of biodiesel was favoured as both parameters were decreased, reaching their optimum condition for maximum yield, at MeOH/ratio of 6:1 and reaction time of 1.5 hours. The MeOH/oil ratio of 6:1, exceeding the stoichiometric amount (Figure 2.8, Chapter 2) and corresponding to an excess amount,

successfully promoted contact between the reaction mixture and consistently shifted the reaction in the forward direction (Sun et al., 2015, Leung et al., 2010). Leung et al. (2010) suggests that the reaction time of 1.5 hours as identified above, is generally associated with maximum yield of biodiesel.

The interaction between agitation rate and reaction time (BC) was also investigated. The response surface plot for this interaction is presented in Figure 6.7.

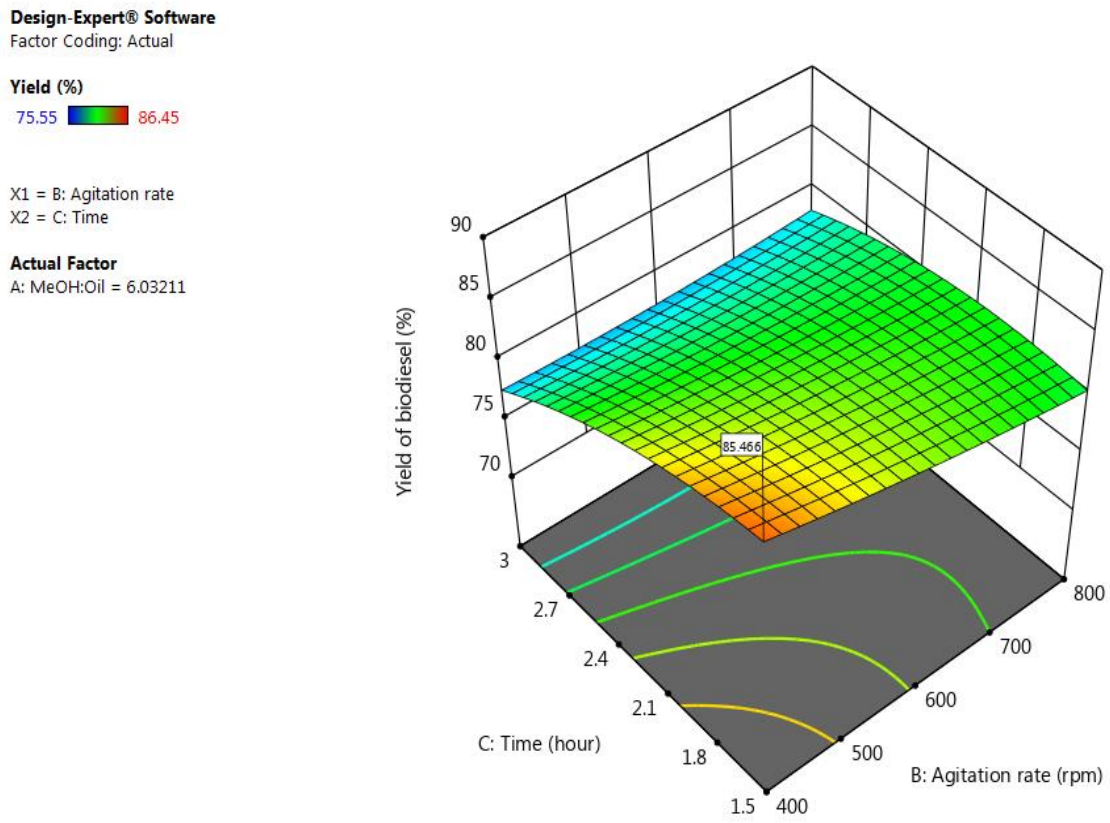

Figure 6.7. Response surface plots for the interaction/effect of agitation (B) and reaction time (C) on the yield of biodiesel from maggot oil (reaction temperature = 60 °C; catalyst wt. = 1.5 %).

The response surface plot in Figure 6.7 reveals that there was a significant effect on the yield of biodiesel upon a decrease in agitation rate (B) and reaction time (C) at constant MeOH/oil ratio of 6.032:1. It is observed that agitation rate (B) was more influential in its interaction with reaction time (C) (Table 6.5). This suggests that decreased mixing condition was effective in promoting excellent interface between methanol and oil's layers (Mashkour and Mohammed, 2017). The optimum condition for the above interaction for maximum biodiesel yield (~85.47 %) was revealed as 400 rpm (agitation rate, B) and 1.5-hour reaction time (C).

The optimum conditions of transesterification of maggot oil were found to be at MeOH/oil ratio (A) of 6:1, agitation rate (B) of 400 rpm and reaction time (C) of 1.5 hours in this study. The obtained conditions complied with the model highest desirability of 0.910, for a maximum yield of 85.47 %. As was observed, the optimum conditions are far less intense and more cost-effective than the optimised process conditions of biodiesel production in other reported studies (Zhang et al., 2010, Tshizanga et al., 2017). Therefore, optimisation of biodiesel production from maggot oil, using HS zeolite as catalyst, resulted in an improved approach with regard to biodiesel yield in comparison to several studies where heterogeneous catalysts have been used for optimisation (Kurniasih and Pardi, 2019, Usman and Garba, 2017). The obtained maggot oil-derived biodiesel prepared using the optimised condition was further characterised for physicochemical properties (section 3.5.4).

(i) Quality of biodiesel obtained at the optimised conditions

The physicochemical properties of the biodiesel sample derived from the optimised yield are presented in Table 6.7.

Table 6. 7. Comparison between physicochemical properties of biodiesel samples obtained over direct method catalyst and fusion-derived catalyst

Biodiesel properties	FAME characteristics over HS catalyst (sample HSF-144)		ENS[b] /ASTM[c]
	One-factor optimized condition [(e)]	RSM optimized conditions [(f)]	
Acid value (mg KOH/g)	0.53	0.53	0.5/0.8 Max
Saponification value (mg KOH/g)	147.87	143.30	-
Ester content[(d)] (% m/m)	64.95	84.76	96.5
Iodine value (g of I_2/100 g)	65.01	69.79	/130
Density at 40 °C (g/ml)	0.877	0.869	0.86-0.90
Kinematics viscosity at 40 °C (mm^2/s)	5.16	5.23	3.5-5.0 /1.9-6.0
Refractive index[e]	1.4455	1.4443	/1.479
Cetane number	36.63	35.5	51/47
Yield of biodiesel	84.10	85.47	-

[(a)] Biodiesel Standard Specifications; [(b)] ENS14214 (European) and [(c)] ASTMD6751 (American for FAEE)
[(d)] Obtained from GC characterisation of respective biodiesel FAME samples
[(e)] MeOH/oil ratio (15:1); agitatin rate (600 rpm); rection time (1.5 hour)
[(f)] MeOH/oil ratio (6:1); agitatin rate (400 rpm); reaction time (1.5 hour)

Table 6.7 reveals that the overall quality of biodiesel (for the fixed catalyst sample HSF-144) improved with the RSM optimisation. The above was proven in terms of lower SV obtained (145→143.20 mg KOH/g), increased iodine value (IV) (50.17→54.95 g I_2/100 g oil), decreased density (0.877→0.869 g/mL), and the most considerable increased FAME yield (64.95 → 84.76 %).

The above obtained properties indicate that the biodiesel derived at optimised conditions by RSM possessed enhanced potential (a good cold flow, reactive and good storage characteristics) for diesel engine application (Surendra et al., 2016, da Cunha et al., 2009). Canesin et al. (2014) suggests that the decreased density and a compliant viscosity (5.23 mm^2/s) of biodiesel obtained at optimised conditions, can be associated with good flow, atomisation and mixing characteristic.

The increased FAME content (84.76 %) is mostly compliant with specific standards and most crucially, suggests high quality biodiesel obtained (Kurniasih and Pardi, 2019). The above results obtained at optimised conditions, attests to the fact that excess methanol/oil ratio beyond 6:1, coupled with agitation rate above 400 rpm and reaction time longer than 1.5 hours, were less favourable towards the potential activity of HS zeolite catalyst (i.e. HSF-144).

From the findings discussed, the RSM-CCD could be successfully applied for the optimisation of biodiesel production from maggot oil. The developed model proved significant (F-value of 26.33), with the experimental response values fitting closely with the predicted values. The optimum condition for the multiple variance biodiesel optimisation, with the most significant model term of linear agitation rate (A), a biodiesel yield and methyl ester content of 85.47 % and 84.76 % respectively, resulted at MeOH/oil ratio of 6:1, agitation rate of 400 rpm and transesterification reaction time (C) of 1.5 hours.

6.3. Kinetics of transesterification of maggot oil over synthesised HS-zeolite

This section explores the kinetic study of biodiesel production from maggot oil using the pseudo first-order kinetic mechanism technique. The selected catalyst sample (HSF-14) with maximum performance was employed in this study. The kinetic evaluation was conducted

based on the change in the yield of biodiesel with increase in reaction time as described in section 3.5.3 (chapter 3). This section reports on a developed kinetic model and the characteristic kinetic parameters (reaction rate constant (k) and rate of reaction).

6.3. Result and Discussion

The pseudo first-order kinetics technique employed herein was adopted from a few previous studies on biodiesel production (Ramezani et al., 2010, Oladipo and Betiku, 2020, Lukić et al., 2013). This is based on the assumption that the use of an excess amount of methanol (over the feedstock) results in its marginal consumption during the reaction. Consequently, the backward reaction will be prevented, and the forward reaction promoted (Sun et al., 2015).

Variation in triglyceride concentration over the course of the reaction was the parameter chosen for the evaluation of kinetics in this study. From the transesterification reaction presented in equation 6.2, the relative reaction rate expression of each specie (reaction feedstock and products) involved is presented in equation 6.3.

$$TG + 3\ ML \rightarrow 3\ FAME + \text{GL} \tag{6.2}$$

$$\frac{-r_{TG}}{1} = \frac{-r_{ML}}{3} = \frac{+r_{FAME}}{3} = \frac{+r_{GL}}{1} \tag{6.3}$$

From equation 6.3, the rate of reaction expressed in terms of rate of change (or decomposition) of TG over time to yield FAME, is presented by equation 6.4:

$$r_{TG} = \frac{+r_{FAME}}{3} = \frac{d[TG]}{dt} = -k'[TG]_t \tag{6.4}$$

where $k' = k[MeOH]_0$

$$\frac{1}{[TG]_o} d[TG] = -k' dt \tag{6.5}$$

Integrating equation 6.5 gives equation 6.6:

$$-\int_{[TG]_0}^{[TG]_t} \frac{1}{[TG]_o}\, d[TG] = k' \int_{t=0}^{t} dt$$

$$-\ln\left(\frac{[TG]}{[TG]_o}\right) = k't \tag{6.6}$$

Since no data is provided for change in concentration of TG with time, triglyceride concentration ([TG]) in terms of conversion is given by equation 6.7:

$$[TG] = [TG]_o - [TG]_o X_{TG} \tag{6.7}$$

Simplifying Equation 6.7 into equation 6.8:

$$[TG] = [TG]_o(1 - X_{TG}) \tag{6.8}$$

Substituting equation 6.8 into 6.6 gives change in concentration with time in terms of conversion (equation 6.9):

$$-\ln(1 - X_{TG}) = k't \tag{6.9}$$

The conversion term in equation 6.9 can be presented in terms of biodiesel yield. According to equation 6.2, for every 3 mole of biodiesel produced (X_{BD}), one mole of TG is converted (equation 6.10) (Ramezani et al., 2010).

$$\frac{X_{TG}}{X_{BD}} = \frac{1}{3} \tag{6.10}$$

Substituting equation 6.10 into 6.9, presents the conversion term (X_{TG}) in terms of biodiesel yield (X_{BD}), leading to the kinetic model equation of biodiesel yield in terms of time (equation 6.11):

$$-\ln\left(1 - \frac{1}{3} X_{BD}\right) = k't \tag{6.11}$$

Equation 6.11 further simplified gives equation 6.12:

$$\ln(3 - X_{BD}) = -k't + \ln 3 \tag{6.12}$$

where $k' = k[MeOH]_o$

The kinetics of biodiesel production in this study was evaluated in terms of the change in the yield of biodiesel with reaction time. The above was achieved over the course of eight hours (480 minutes) time on stream with four reaction time sampling intervals (section 3.5.3), for which the results are presented in Figure 6.8.

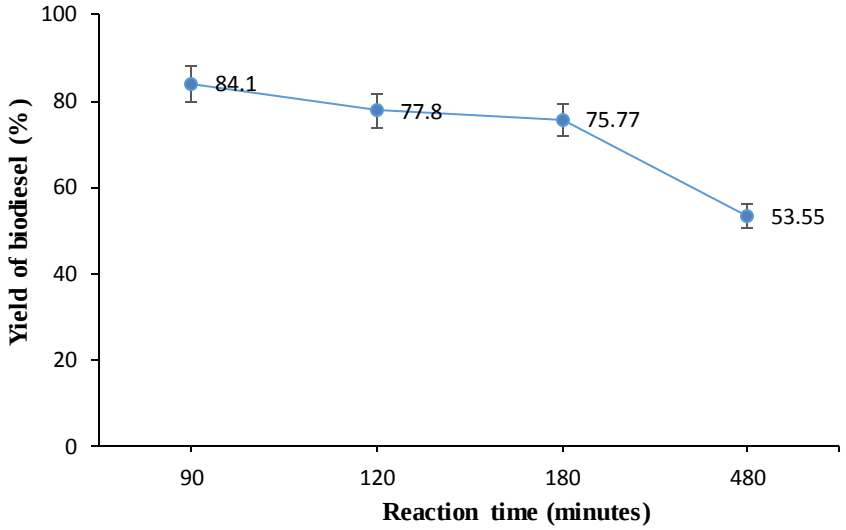

Figure 6.8. The actual yield of maggot oil-biodiesel as a function of reaction time (catalyst & wt. = HSF-144, 1.5 %; MeOH/oil ratio = 15:1; reaction temperature = 60 °C; and stirring rate = 600 rpm).

By substituting the results provided of biodiesel yields with varying reaction time (Figure 6.8) into equation 6.12, the plot of the kinetic model equation was developed as presented in Figure 6.9.

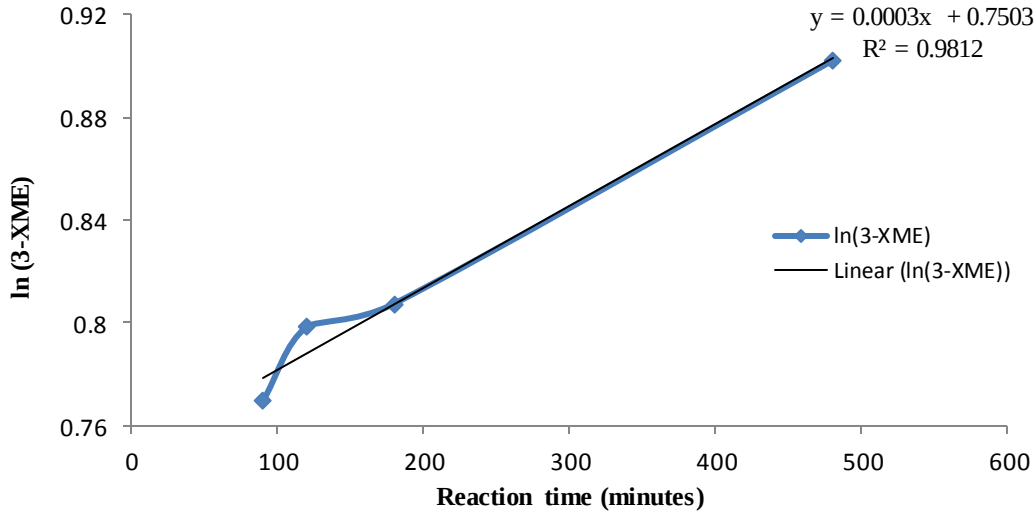

Figure 6.9. Plot of kinetic model illustrating predicted yield of biodiesel (X_{BD}) as a function of reaction time

Figure 6.8 shows that there was a gradual decrease in the yield of biodiesel as the reaction time was increased from 1.5 hour (90 minutes) until 8 hours (480 minutes). The observed decreased can be attributed to catalyst deactivation upon long and excessive exposure in the reaction medium, beyond 1.5 hour (Leung et al., 2010).

Nonetheless, the kinetic model in Figure 6.9, as developed using the obtained biodiesel yields data (Figure 6.8) and equation 6.12, revealed that there was an acceptable correlation coefficient (R^2 = 0.9812) in predicting the yield of biodiesel at any given time during the course of transesterification reaction. The model shows that the k'value, presented as gradient in the displayed equation (Figure 6.9), equalled 0.003. The latter was then used to determine the kinetic parameters using equation 6.4.

The computed kinetic parameters (rate constant, and further the rate of reaction) associated with variation in the yield of biodiesel with reaction time, are presented in Table 6.8.

Table 6.8. Reaction constant and rate of reaction for HS-catalysed transesterification of maggot oil at one factor–based optimised conditions

Reaction time		Yield	k' = k [MeOH]$_o$	[a] [MeOH]$_o$	Rate constant,	[TG]$_o$ (mol) [b]	**[TG]$_t$ [c]**	**Rate of reaction,**
hour	min	(X_{BD}), %			k (min^{-1})			r_{TG} (mol/cm^3.min) [d]
0	0	0	0	0.261	0	0.0249	[TG]$_o$ (1-1/3XME)= 0.0249	0
0.25	15	87.28[e]	0.0003	0.261	0.00115	0.0249	[TG]$_o$ (1-1/3XME)= 0.01764	**5.29×10^{-6}**
0.75	45	85.36[e]	0.0003	0.261	0.00115	0.0249	[TG]$_o$ (1-1/3XME)= 0.01780	5.34×10^{-6}
1.5	90	84.10	0.0003	0.261	0.00115	0.0249	[TG]$_o$(1-1/3XME)= 0.01791	**5.37×10^{-6}**
2	120	77.80	0.0003	0.261	0.00115	0.0249	[TG]$_o$(1-1/3XME)= 0.01843	5.53×10^{-6}
3	180	75.77	0.0003	0.261	0.00115	0.0249	[TG]$_o$(1-1/3XME)= 0.01860	5.58×10^{-6}
8	480	53.55	0.0003	0.261	0.00115	0.0249	[TG]$_o$(1-1/3XME)= 0.02044	**6.13×10^{-6}**

[a] [MeOH]$_o$ = $\frac{Mass\ of\ MeOH\ fed}{Mr}$ = 12/46 = 0.261. Note that methanol concentration ([MeOH]$_o$) due to excess amount used in comparison to TG

[b] [TG]$_o$ = mass of oil feedstock / molar mass of feedstock; [b] Assume a constant volume tank, hence reported in mol other than mol/m^3

[c] [TG]$_t$ = [TG]$_o$[1-(1/3)X_{TG}] = [TG]$_o$(1-1/3XME) ; **[d]** Rate of reaction, r_{TG} = k[ML]$_0$ × [TG]$_t$; r_{TG} or -$r_{(TG)}$

[e] Estimated biodiesel yields below 1.5-hour reaction time (see detailed plot in Figure 8.12.1, Appendix 2).

From the known initial and constant molar concentration of methanol ($[MeOH]_o$) determined (Table 6.8), the reaction rate constant (k) using $k' = k[MeOH]_o$ (equation 6.12) was 1.15×10^{-3} min^{-1}. The obtained rate constant suggests a moderate consumption of maggot oil TG throughout the course of the reaction over HS zeolite catalyst (Nasir et al., 2014). This rate constant value was observed to be 4 times less (1.15×10^{-3} << 4.19×10^{-3} min^{-1}) than the rate constant reported for homogeneous-catalysed transesterification of castor oil (Ramezani et al., 2010). The value was three times less than that obtained on heterogeneous-catalysed transesterification of rubber seed oil (1.15×10^{-3} << 4.19×10^{-3} min^{-1}) and waste cooking oil (1.15×10^{-3} << 3.3×10^{-3} min^{-1}) (Oladipo and Betiku, 2020, Lukić et al., 2013). The difference in the obtained k value in comparison to the above literature was mainly due to the difference in catalyst phase and reaction conditions employed in the various studies (Table 6.11). It is noteworthy to mention that a higher reaction temperature of 65 °C was employed by Ramezani et al. (2010) and by Oladipo and Betiku (2020). According to Darnoko and Cheryan (2000) and Noureddini and Zhu (1997b), the rate of reaction is temperature dependent, such that the difference in this factor alone is of significant impact on the reaction constant. Table 6.9 presents a survey of rate constants obtained for the transesterification of various feedstock oils in comparison to the rate constant obtained for the transesterification of maggot oil in this study.

Table 6.9. Kinetic and process parameters for transesterification of maggot oil and various feedstock oils over different catalysts

Feedstock	**Catalyst**	**Catalyst amount** (%)	**MeOH/oil ratio (n/n)**	**Reaction temperature** (^{o}C)	**Reaction Time** (hour)	**Reaction order**	**Rate constant,** k ($\times 10^{-3}$ min^{-1})	**Reference**
Maggot oil	HS zeolite	1.5	15:1	60	1.5-8	First-order[(a)]	1.15	This study
Castor oil	CH_3OK	0.5	8:1	65	2	First-order[(a)]	4.91	Ramezani et al. (2010)
Rubber seed oil	CKPH	3.5	6:1	65	1.25	First-order[(b)]	3.4	Oladipo and Betiku (2020)
Soybean	NaOH	0.2	6:1	50	1.5	Second-order	0.0784[(c)]	Noureddini and Zhu (1997b)
WCO	CaO.ZnO	2	10:1	60	-	First-order[(a)]	3.3	Lukić et al. (2013)
Oleic acid	ZMS-5	12.5	20:1[(d)]	78	10	Zero-first order[(e)]	0.0901	Sun et al. (2015)

CH_3Ok - Potassium methanolate (homogenous catalyst); CKPH – calcined kola nut pod husk (heterogeneous catalyst)
ZSM-5 (50) — High siliceous Zeolite catalyst (heterogeneous).
[(a)] Investigated using Pseudo first-order mechanism, whereby methanol (MeOH) is used at excess amount and is maintained at constant concentration throughout the reaction. Hence, only the oil is assumed to have much effect on rate of reaction.
[(b)] Investigated in inclusion of shunt mechanism, whereby only the overall transesterification reaction is considered as shown in equ ation 6.2 (without considering the intermediate reaction paths).
[(c)] For the overall transesterification reaction without considering the forwards and reverse intermediate reactions
[(d)] Ethanol, instead of methanol, was used. [(e)] Zero order with respect to ethanol in gas phase, first order w.r.t. oleic acid

By further use of the model equation generated in Figure 6.9, the estimated biodiesel yields (X_{BD}) at a given reaction time below 1.5 hour were determined and also presented in Table 6.10 (see plot in Figure 8.12.1, Appendix 2).

The estimated results in Figure 8.12.1 (Appendix 2, section 8.12), showed that high biodiesel yields at either 1.5-hour reaction time, could have also been achieved at reaction time that is twice or three time shorter than 1.5 hour. This could have been mainly due to the actual equilibrium nature of transesterification and a possible faster rate of diffusion induced among the three phases involved in the reaction mixture (Leung et al., 2010).

Further, the rate of reaction corresponding to various reaction time intervals (both below and above 1.5 hour) was reported and found to be between 5.37×10^{-6} and 6.23×10^{-6} mol/cm^3.min (Table 6.9). At 1.5-hour reaction run, the actual rate of reaction was 5.37×10^{-6} mol/cm^3.min. There was a gradual increase in the rate of reaction with an increase in reaction time, until 8 hours (6.12×10^{-6} mol/cm^3.min). This revealed a direct correlation between reaction time and rate of reaction, unlike biodiesel yield. The increase in rate of reaction with reaction time, was attributed to an increase in triglyceride concentration $[TG]_t$ as observed throughout after 15-minutes reaction time (see plot in Figure 8.12.2, Appendix 2/section 8.12). Purwanto et al. (2020) also reported a similar increase in reaction rate with an increase in triglyceride concentration using soybean oil as feedstock. Hence, from the above findings, it is suggested that TG concentration is the rate-determining factor. The catalyst was subject to deactivation as the reaction time increased after 1.5 hour, prompting an equilibrium shift in the backward direction in favour of increased TG concentration (Leung et al., 2010). Hence, owing to increased TG concentration, the reversible nature of transesterification (upon which the kinetic model was developed) was not successfully prevented after 1.5-hour reaction time.

From the results obtained, it can be concluded that the pseudo first-order kinetic was a suitable mechanism in predicting the yield of maggot oil-derived biodiesel with reaction time. The mechanism, however, fits best at an early stage of the reaction (i.e. after 15 minutes) owing to adhered assumption of irreversibility, other than the contrast revealed after 1.5 hours. A moderately high reaction rate constant (k) of 1.15×10^{-3} min^{-1} for HS zeolite-catalysed transesterification was obtained from the actual and estimated biodiesel yield response values. An estimated beginning rate of reaction (r_{TG}) of 5.39×10^{-6} mol/cm^3.min was obtained after 15-

minute reaction time, but owing to equilibrium backwards shift and increased TG concentration, progressively increased to 6.22 $\times 10^{-6}$ mol/cm^3.min with an increase in reaction time beyond 1.5 hour.

6.4 Overall summary of Chapter 6

Biodiesel from waste-derived maggot oil was successfully produced using HS zeolite catalysts (synthesised via both direct and fusion-assisted hydrothermal methods from waste coal fly ash). In this work, the yield of biodiesel alone, as reported in many publications, does not ascertain the actual biodiesel quality as compared to the FAME content characteristic of the biodiesel. The fusion HS zeolite catalyst (HSF) gave a comparably higher biodiesel, FAME yield (84.10 % yield, 64.95 % FAME) and better overall quality biodiesel compared to the direct method catalysts (HS) *(*80.20 - 82.1 *%)*. This was attributed to the high textual properties (total surface area), better acidity and possible porosity exhibited by the fusion HS zeolite compared to all the direct method catalysts. Consequently, the properties of the biodiesel produced using the fusion HSF-144 catalysts, complied the most with the biodiesel standard specifications. Further, the fusion HS zeolite demonstrated an enhanced activity in the transesterification of sunflower oil (89.70% biodiesel yield, 90.93 % FAME), exceeding that obtained over maggot oil (84.10 % biodiesel yield, 64.95 % FAME). The newly proven catalytic activity on maggot oil, attests to the excellent use of HS zeolite as a novel heterogeneous catalyst in biodiesel production.

During catalyst synthesis, variation in catalyst hydrothermal synthesis time and temperature gave a better approach than varying NaOH/CFA ratio with regard to preparing a catalyst suitable for biodiesel production from maggot oil. In most instances, the crystallinity of HS zeolite partially correlated to its catalytic performance, whereas phase purity was observed to have had a direct correlation with catalytic performance. However, from the findings, the most determinant factors for excellent performance in biodiesel production was acidic strength, porosity, surface area, purity and crystallinity whereas oil feedstock quality also had an impact on biodiesel quality. Figure 8.10.5 (section 8.10, Appendix 2) shows a fairly linear correlation between catalyst surface area and yield of biodiesel obtained. This linearity was interrupted for FAME yield obtained with regard to solely HS-72 sample among the catalysts used; of which

the deviation can be explained by poor acidity exhibited by HS-72 (section 6.1.1 & 6.1.2), acidity being a more determinant and synergetic factor towards FAME yield from maggot oil.

The optimisation of biodiesel production from maggot oil was successfully achieved using the RSM-central composite design of experiments. A quadratic model fitted the response and the model proved to be statistically significant at 95 % confidence level, with an F-value of 26.33. Moreover, the proposed model indicated a good fit between the experimental response of biodiesel yield and the predicted yields. This was proven by a negligible standard deviation of 0.8522 between the responses, a permissible limit (<0.2) between the adjusted ($R_{adj.}^2$ = 0.9231) and the predicted correlation coefficient (R_{pred}^2 = 0.7501), and close distribution of residual points around the normal distribution plot. Additionally, the model depicted a coefficient of determination (R^2) of 0.9595, proving that the model could explain more than 95 % of the reproducibility. The model was associated with significant terms of B, C, AC, BC, A^2, and C^2, with the linear effect of agitation rate (B) as the most significant with respect to response of biodiesel yield. In compliance to the model, the optimum biodiesel yield of 85.47 % was obtained from transesterification of maggot oil at methanol-to-oil ratio (A) of 6:1, agitation rate (B) of 400 rpm and reaction time of 1.5 hour. The above maggot oil-biodiesel yield (associated with RSM optimum conditions) proved as highest obtained in this work, and the derived-biodiesel in addition, complied the most with the quality specification standard of biodiesel. The above was proven in terms of all biodiesel properties and more specifically, the most progressive ester content of 84.76 % (revealed at the optimum condition).

A linear kinetic model equation for the prediction of biodiesel yield, with a high correlation coefficient of 0.9812 was obtained. The model is associated with a considerable reaction rate constant of 1.15×10^{-3} min^{-1}, and gradual increase in the rate of reaction (between 5.37×10^{-6} and 6.13×10^{-6} $mol/cm^3.min$) with an increase in reaction time. Further, it was revealed through the model that high biodiesel yields (84.10 %) that were obtained after 1.5-hour reaction time or beyond, could have been achieved within a shorter reaction time (15 minutes), or between 0.25 hour and 1 hour. Further, the trend of rate of consumption of triglyceride (TG) with time, demonstrated that the triglyceride (TG) concentration, was the rate-determining factor. The actual backward shift in equilibrium associated with the transesterification reaction, became apparent after 1.5-hour reaction time. Hence, it is only after 1.5 hours that the assumption of the irreversible nature of the reaction made for the pseudo-first order mechanism, was

contradicted. This held true for reaction time below 1.5 hour, which is the basis of the kinetic model. Hence, the use of another kinetic technique, which caters for the reversible nature of the reaction at longer reaction time, is recommended for further studies.

Chapter Seven
Conclusion and recommendations

Chapter 7 reports the conclusion and recommendations of the research study; gives an overview on the objectives of the study; answers the research questions posed in chapter 1 (section 1.5) and endorses the hypotheses made for the research (section 1.6). This chapter further points out the novelty of this study, aimed at filling research gaps and setting further development in biodiesel production using associated heterogeneous catalysts.

Hydroxysodalite (HS) was synthesised from fly ash for use as novel heterogeneous catalysts in the transesterification of waste-derived maggot oil for biodiesel production. Waste-derived maggot oil was successfully characterised for physiochemical properties because it offered excellent potential as a feedstock for biodiesel production. The oil presented a high saturated fatty acid profile, of which lauric acid constituted the highest concentration (ranging between 37.14% and 41.5 %). The oil was further characterised with a corresponding acid value of 7.2 mg/KOH (3.38 wt. % FFA), an iodine value (IV) of 44.27 I_2 / 100 g and a common biodiesel feedstock-range viscosity of 43.16 mm^2/s. The reactive potential of the oil and adaptability with a suitable heterogeneous catalyst for biodiesel production validated the feedstock's preliminary potential which was further validated upon its successful conversion to FAME over conventional homogenous catalysts by yielding up to 69.93 % - 79.35 % biodiesel of compliant quality to (ASTM/EN) specification standards.

The heterogeneous zeolite catalysts applied in this study were successfully developed from coal fly ash via direct and fusion-assisted hydrothermal synthesis method. Both methods resulted in high quality HS catalysts, with the direct method revealing optimal synthesis conditions such as a pre-synthesis ageing of 1.5 hour and 70 °C, feedstock NaOH/CFA ratio of 1.2:1, moderate hydrothermal synthesis time of 72-hour at 140 °C (HS-72), as well as from conditions with an extended synthesis time of 144 hours with lowered hydrothermal temperature of 100 °C (HS-144(100 ^{o}C). On the one hand, this work established the novel pre-synthesis ageing conditions of 1.5 hour at 70 °C (at 800 rpm constant stirring rate), as the ideal route for liberating the Si and Al species from the quartz and mullite phases of fly ash, which formed the basis on which the above optimum conditions of the direct hydrothermal zeolite synthesis method were achieved. On the other hand, the high temperature fusion-assisted

method demonstrated an overall high quality HS exclusively at extended synthesis time of 144 hours at 100 °C.

The optimum direct hydrothermal sample HS-72 and HS-144(100°C) gave better results in terms of crystallinity (100 % and 85 % respectively) and phase purity (85 and 91 % respectively) with characteristics of (purer phase) HS zeolite, as opposed to the fusion hydrothermal sample HSF-144 that gave better textural properties of BET total surface area (44.98 m^2/g and 0.148 cm^3) and possible stronger acidic (site) strength. This study presented the correlation between an increase in hydrothermal synthesis time and denser phase HS zeolite from both hydrothermal synthesis routes. Highly crystalline HS zeolite prepared from either methods, were best characterised by a novel hexagonal-cubic crystal morphology, a dominant mesopore size of 4 nm. The Si/Al framework ratio between 1.37 and 1.18 was strongly dictated by the Na/Al ratio. Both the direct method optimum samples resulted in a product yield (22.55, 26.47 %) that was half the yield of HS obtained via the fusion-assisted method (56.3 %); the direct method however resulted in a less energy intensive route mainly due to the less energy intense ageing step compared to fusion. Hence the direct method was deemed more feasible and economic for upscaled production of zeolite than the fusion-assisted route.

Ion exchange using K^+ and bifunctional modification of as-made HS zeolite samples were carried out but both approaches resulted in poor overall characteristics and consequently poor acidity, as well as lower yield of the obtained products than anticipated, thus modification was not advisable.

Three selected samples prepared via the direct method, and the sole fusion-assisted HS zeolite sample, were successfully applied as catalysts in the transesterification of maggot oil (at fixed pre-optimised conditions) and resulted in high activity with regards to the yield and (ASTM/EN) overall quality compliance of the derived-biodiesel samples. The fusion-assisted HSF-144 sample demonstrated a slightly better biodiesel yield (84.10 %) and higher FAME content (64.95 %) than the direct method optimum sample HS-144(100°C) which gave biodiesel yield and FAME content of 80.6 % and 61.01% respectively. This was ascribed to high textual properties (total surface area), better acidity and porosity of the sample.

The novel green HS heterogeneous catalyst further, gave an overall competitive performance compared to the conventional homogenous catalysts (NaOH, KOH) in the transesterification

of maggot oil, and a better activity in the transesterification of sunflower oil (88.85 % biodiesel yield, 90.93 % FAME).

The findings in this research revealed an independent correlation between the biodiesel yield and FAME content quality of biodiesel, such that the FAME is more crucial than the yield in determining the overall performance of catalysts used and of the biodiesel quality.

The research methodology studies (RSM) for the optimisation of transesterification of maggot oil using the HS catalyst (HSF-144), resulted in optimal conditions of methanol-to-oil ratio *(*A) of 6:1, agitation rate (B) of 400 rpm and reaction time of 1.5 hour at fixed reaction temperature (60 °C) and catalyst weight (1.5 wt. %). This condition corresponded to a biodiesel yield of 85.47 % and most improved maggot oil-derived FAME of 84.76 %.

The kinetics of the transesterification of maggot oil was successful evaluated using the pseudo-first order mechanism. A linear kinetic model resulted for the prediction of biodiesel yield with reaction time; the kinetic model held true its assumption of reaction irreversibility for a reaction time below 1.5 hour, giving the highest reaction rate of 5.37×10^{-6} mol/cm^3.min, a considerable reaction rate constant of 1.15×10^{-3} min^{-1}, and by which the model estimated a high biodiesel yield from as short as 0.25-hour reaction time.

Summary

A biodiesel yield of over 80 % derived from industrial waste-derived maggot oil by-product, demonstrated an economic and sustainable approach to biodiesel production as ascertained in this study. The feedstock gave a high FFA content of up to 3.38 wt. % and this considerable value had no impact on catalytic activity due to the strong acidic property offered by the catalyst to achieve a single-step esterification-transesterification process. In this study, the yield of biodiesel was minimised when the catalysts had undergone ion exchange and bifunctional modification. There was a correlation between the properties of the product catalysts in relation to catalytic activity in the mag-oil biodiesel production, with the acidity and surface area of the catalysts being identified as major factors responsible for high catalytic activity. All the maggot oil derived biodiesel samples showed compliance with ASTM and EN standards (in terms of crucial biodiesel properties). The maggot oil proved to offer excellent potential to being converted to biodiesel via the transesterification process, with the fly ash based HS zeolite

giving an advantage of inherent acidic properties as well as a considerable surface area. A strictly longer hydrothermal synthesis time was required to obtain high quality HS zeolite via the fusion-assisted method; resulting in the direct hydrothermal method to be a more energy saving approach (at less intense overall synthesis conditions) to obtain as high quality zeolite catalysts. A considerable reaction kinetic of maggot oil conversion over the utilised catalyst was observed, resulting in a maggot oil transesterification reaction rate constant of 1.15×10^{-3} min^{-1} and a competitive reaction rate of 5.37×10^{-6} $mol/cm^3.min$. The produced zeolite catalysts from coal fly ash were found suitable, offering a high yield of biodiesel that was compliant with standards.

Novelty of the study

The novelty of this research study is highlighted below and also stated in Table 8.13.1 (Appendix 2). This research was able to uniquely utilise two major industrial wastes as feedstocks for biodiesel production. The large and continual availability of the organic waste-derived maggot oil from black soldier fly (BSF) in South Africa, as well as the extreme availability of coal fly ash solid waste product from South African Coal power stations, ascertain a possibility of upscaled and sustainable production of biodiesel.

This work has attested to the potential conversion of maggot oil to biodiesel using conventional homogenous catalysts (NaOH and KOH) separately in a single-step transesterification resulting in 98.30 % and 94.67 % FAME yields respectively. This is unlike the feasibility tests for the oil conversion conducted using sulphuric acid by Leong et al. (2016), reporting a FAME yield of 48.46 %.

This research further demonstrated the viability of the synthesis and thorough optimisation of a hydroxy sodalite zeolite from fly ash feedstock for use as catalysts in the biodiesel production process. The adoption of the direct hydrothermal as well as the fusion-assisted methods to synthesise these catalysts and the comparison between the two methods with regard to HS zeolite was explored for the first time in this study. The study's catalyst synthesis optimisation established a novel pre-synthesis ageing time and temperature condition (1.5h, 70 °C) for HS zeolite synthesis via the direct method. The same applied with the actual direct hydrothermal synthesis time and temperature conditions of 72 h, 140 °C; 144h, 100 °C. The ageing time was drastically lowered (48 → 1.5 h) and the hydrothermal temperature reduced (140 → 100 °C)

compared to the baseline adopted conditions for HS zeolite synthesis from coal fly ash (Musyoka et al., 2014). A novel fusion-assisted hydrothermal synthesis time and temperature (144h, 100 °C) was also established. Consequently, the corresponding HS zeolite samples were characterised with a new hexagonal-cubic crystal morphology type (from both methods), framework Si/Al ratio of 1.3-1.4 and 1.2 for the direct and fusion method samples respectively, and the dominant mesopore size 4-3.75 nm as well as the typical micropore size of 0.23 nm. This study was the first to reveal the Na/Al ratio compositional characteristic as a strong dictating factor for crystallinity of HS zeolite from either method. The finding reveals that the direct hydrothermal method is the best approach for HS zeolite with regard to overall quality & energy efficiency, economic feasibility and up-scalability of the biodiesel heterogeneous (HS) catalyst synthesis process.

This research work also identifies as the first to explore the modification of (HS) zeolite by ion exchange (using KOH) and bifunctional modification for use as catalysts in biodiesel production. Both modification approaches hindered the overall characteristic of the precursor zeolite samples, the approaches however, showed potential for better characteristics if further investigations were to be carried out on the modification conditions.

The study has also presented itself as the first to explore the use of HS zeolite from coal fly ash as a heterogeneous catalyst for biodiesel production (novel CFA-based heterogeneous catalyst). For the first time, a heterogeneous HS catalyst was employed to aid the conversion of maggot oil to biodiesel, and the particular HS zeolite catalyst was also suitably employed for the conversion of the sunflower oil conventional feedstock. The findings showed high catalytic performance of the HS zeolite resulting in high maggot oil biodiesel yields (80.60; 84.10 %) and of considerable FAME yields (61.01, 64.95 %) prior to transesterification optimisation (via RSM). The HS zeolite showed competitive performance in the conversion of sunflower oil, giving a competitive result (88.85 % biodiesel yield with 90.93 % FAME content) when compared to previously employed heterogeneous catalysts (Ramos et al., 2008, Babajide et al., 2012). Notably, this study is set to be the first to differentiate and report both on the yield of biodiesel (equation 3.10, section 3.5.1) and that of FAME (equation 3.13, section 3.5.4) separately. Often these two have been used interchangeably in many studies to represent the yield of biodiesel, without accounting the quantitative and qualitative aspects of the product as set by ‘biodiesel yield’ and ‘FAME yield’ respectively.

This research has also been the first to optimise the conversion of maggot oil to biodiesel both by single-factor and RSM approach using the HS zeolite catalyst. The RSM optimisation of the transesterification of maggot oil resulted in a biodiesel yield of 85.47 % and a much-improved FAME content of 84.76 %. This was achieved at optimised transesterification conditions that are considerably milder than prior studies (i.e. 6:1 methanol/oil ratio, 400-rpm agitation rate, 1.5 h reaction time, and 60 °C). Further, the research was the first to study the kinetic behaviour of the transesterification of the waste-derived maggot over the produced (HS) zeolite catalyst. The finding gave out a moderately high reaction rate constant of 1.15×10^{-3} min^{-1} and a gradually increasing rate of reaction with an increase in reaction time (between 5.29×10^{-6} and 6.13×10^{-6} $mol/cm^3.min$).

The involvement of both synthesis and application of HS zeolite for biodiesel production in a single study, the successful beneficiation of both low cost feedstocks (maggot oil and feedstock) to obtain high biodiesel yield and quality; offers a reduction in overall biodiesel production cost and addresses the major challenge faced in biodiesel production globally.

Research recommendations

For further studies, it is recommended to quantify the various mineralogical phases in both coal fly ash and the derived zeolites (amorphous, quartz, mullite, zeolite, etc) as a measure to numerically determine the conversion efficiency of the fly ash to HS zeolite or zeolite X of interest.

Further studies also recommend exploring the synthesis of HS zeolite using the (lower) pre-synthesis ageing condition of 47 °C instead of 70°C. The approach is anticipated to obtain HS zeolite with enhanced total surface area, since the porosity was higher at 47 °C compared to the varied ageing temperature of 70 °C (Table 8.6.1) at the fixed conditions applied in the study (Table 8.6.1).

Further, the study also recommends the employment of hydrothermal temperature condition of 100 °C for HS synthesis via the direct method at the varying synthesis time conditions, other than at the extended 144-hour alone. Varying the temperature from 140 °C to 100 °C at the extended hydrothermal synthesis time via the direct method, proved a better approach to enhance the crystallinity and phase purity of HS zeolite in the study. On this basis, it is

anticipated that the same could have applied for the various investigated synthesis time conditions (12, 24, 48, 72 h at 100°C) and the approach could have simultaneously enhanced the energy efficiency of the HS synthesis. It is also recommended to investigate the synthesis of HS zeolite via the fusion-assisted method at 140 °C and extended hydrothermal temperature, being the temperature condition employed for the direct method synthesis. Based on the study conducted by Belviso et al. (2010), the research predicts that the fusion hydrothermal synthesis at the increased temperature (100→140°C) would align to the metastable behavior of zeolites, which predicts denser phase HS zeolite with an increase in hydrothermal temperature. In other words, a further recommended study anticipates that a much higher crystalline HS zeolite would be obtained via the fusion-assisted method either at synthesis times or at the optimum extended 144 hours, if the temperature beyond 100 °C or particularly 140°C is employed for hydrothermal synthesis.

Another recommendation set in this study addresses the use of fly ash unseparated bulk slurry (Musyoka, 2012) instead of the separated supernatant filtrate for the synthesis of zeolite X. This would have been a better approach to obtain high yield of the product as opposed to the actual approach adopted in the study (section 3.3.4; Figure 8.7.1, Appendix 1) (section 3.3). This approach could have also set a basis for a possible optimization of the synthesis of zeolite X from fly ash and the novel application of the zeolite in the transesterification of maggot oil.

Further recommendation pertains to the use of a structuring direct agent or template as a route to considerably enhance the total surface area, pore size distribution and meso-porosity structure of other zeolite phases (derived from either direct or fusion-assisted method). The above was inspired by a study conducted by Shirani Lapari et al. (2015) and was also a set recommendation from a peer-review conference at which the finding of this thesis was presented. Moreover, other existing literature studies (Viswanadham et al., 2012, Endalew et al., 2011) and the finding in this work, have also attested that enhancing the above characteristics would be favourable with regard to catalytic application of a zeolite; as being the case in this work by removing the diffusion limitations associated with the use of HS zeolite (due to its small micropore aperture) as a catalyst in biodiesel production.

A study is recommended for ion exchange using reagent source of H^+ ion proton (e.g. NH_4Cl) instead of ion exchange by K^+ (derived from KOH in this study). H^+ as proton for ion exchange possess a small atomic radius , thus, would therefore not cause blockages of the pores on the structure, possibly would have not suppressed the crystal growth and neither would have

hampered the exposed surface area of HS zeolite compared to the exchange with K^+ ion. Ion exchange using H^+ ion proton, could have been a better approach anticipated to enhance surface acidity of HS zeolite for better catalytic activity in the transesterification of maggot oil.

Additional characterizations of the prepared zeolite samples are also recommended, such as carrying out the temperature-programed desorption (using either NH_3-TDP or the CO_2-TDP analysis) for the actual determination of the (acidity or) active acidic sites on catalyst surfaces, vis-à-vis its relationship to the mechanisms of the catalytic reaction in this study. The relative acidity of HS zeolite samples in this work was estimated based on Si/Al framework ratios. The TEM analysis is also recommended for the precise determination of particle size, or the use of image J to validate for the average particle size values of samples obtained using Scherrer equation in this work.

Further recommendation from this study suggests the optimization of biodiesel production by response surface methodology (RSM) by selecting the catalyst weight and transesterification temperature as the independent process variables - in lieu of the independent variable of reaction time selected (chapter 6, section 6.2). It could have also been interesting to undertake RSM optimization categorically on the basis of the type of catalyst to be used, of which among, the direct method sample HS-144(100^{o}C) in addition to the actual catalyst employed (HSF-144) in this work, could have been the more suitable catalyst candidate for the above. Alternatively, it is also recommended to have used the optimum direct method sample HS-144(100^{o}C) as the catalyst for the RSM optimisation study (of biodiesel production); owing to the low energy and cost effectiveness associated with this catalyst synthesised via the direct hydrothermal method compared to the fusion-assisted catalyst HSF-144.

Further optimization studies via RSM using HS zeolite as catalyst, is recommended in view to enhance the FAME (ester) content of the maggot oil-derived biodiesel above the obtained value (84.76 %) from this study (Figure 8.10.4, Appendix 2), and to attain the exact compliant standard set by the ENS/ASTM (Table 8.9.1, Appendix 2). For this reason, the FAME content could even be set as a response for the RSM optimization, instead of the yield of biodiesel as conducted in the study. Likely with the estimated cetane value property of the maggot oil-derived biodiesel samples.

Another study suggests the use of alternative kinetic technique, which would cater for the actual reversible nature of transesterification, other than being restricted by the assumption of pseudo

first-order that mainly suited shorter reaction time below 1.5 hour. This would be the case of second-order kinetic order kinetic technique as by Noureddini and Zhu (1997a) and Freedman et al. (1986). Thus, it would also be recommended to investigate the kinetic of the reaction by including different temperature conditions so as to determine the activation energy (E_A) of the transesterification of maggot oil over HS zeolite catalyst.

8. Appendix

Appendix 1

8.1 Summary of results of characteristic properties of produced HS zeolites [Table 8.1.1- Table 8.1.2]

Table 8.1. 1. Pre-synthesis physical and chemical conditions for HS synthesis and corresponding characteristic properties of produced samples

Stage of experiment[(a)]	Parameter investigated [(a)]	Physical condition / chemical ratio	Fixed parameter[(b)]	Sample name/code [(c)]	Crystallinity (%)	Purity (%)	Crystal size (nm)	EDS		FTIR vibration modes[(d)] (№ &±wavelength)
								Si/Al	Na/Al	
1	**Water/CFA ratio**	5:1	Ageing (t) = 48h	**HS-A48h**	**41.5**	**47**	20.16	1.48	1.09	**4** (+450,625,975 cm^{-1})
		9.5:1	Ageing (T) = 47°C	HS-A48h(9.5H_2O)	29.2	40.56	27.947	1.44	0.94	**3** (-570,620, 670,730, 173
		12.5	NaOH/CFA = 1:1	HS-A48h(12.5H_2O)	19.6	13	29.459	1.39	0.77	**3** (-570,620, 670,730, 173
2	**ageing time**	48hrs	Ageing (T) = 47°C	HS-A48h	41.5	47	16.87	1.48	0.77	**4** (-670,730, 1637, 1735)
		96hrs	NaOH/CFA = 1:1	HS-A96h	51.8	49	20.16	1.45	1.45	**4** (-670,730, 1637, 1735)
		1.5hr	*Water/CFA = 5:1	**HS-A1.5h**	**57.6**	**66**	27.707	1.45	0.99	**5** (-670,730, 1637, 1735)
3	**ageing temperature**	47°C*	NaOH/CFA = 1:1	HS-A1.5h / HS-A47°C	57.6	66	27.707	1.45	0.99	**5** (+450,565,627, 980,145
		70°C	*Ageing = 1.5h	**HS-A70°C**	**67**	**71**	29.08	0.99	**1.60**	**8**-9 (- none)*
4	**NaOH/CFA ratio**	1:1	*Ageing = 70 °C	HS-A70°C	67	71	29.08	0.99	1.60	8-9 (+ all)*
		1.2:1		***HS-A70+1.2NaOH**	**97**	**81**	32.38	1.36	**1.02**	**6** (- 570, 620, 1735 cm^{-1})
		1.3:1		HS-A70+1.3NaOH	52.3	32.71	27.94	-	-	5 (-570,620, 1637 cm^{-1})
		1.4:1		HS-A70+1.4NaOH	23.5	23.64	24.62	1.48	1.14	4 (-570,670,730, 1637 cm

(a) Stage1-4: Parameter investigated for direct hydrothermal method (activation and chemical conditions) **(b)** Synthesis time = 48 hours and synthesis temperature = 140°C,

*Optimised condition from previous stage of experiment and kept fixed in all the next stages

(c) ***HS-A70+1.2NaOH** = HS-48 in stage 5

(d) All included in reference to bands present in baseline HS-70°C, except (x cm^{-1}): *vibration modes for HS-70°C (IUPAC): 470,570, 620/625,670,730, 975/960, 1440/1475,1637, 1735 cm^{-1}

Table 8.1. 2 (*Table 8.1 Cont'd*). Characteristic properties of direct hydrothermal HS, fusion HS, ion exchanged and bifunctional modified HS zeolite

*Stage of exp.	*Parameter investigated	Synthesis condition / chemical ratio	Fixed parameter[(a)]	Sample name/code	Crystallinity (%)	Purity (%)	Crystal size (nm)	EDS		FTIR vibration modes[(d)]
								Si/Al	Na/Al	
5	**Synthesis time (Direct)**	12hrs	Synthesis temperature, 140 °C	HS-12	11	30	23.58	1.02	0.18	**1** (- All, except 975 cm^{-1})
		24hrs		HS-24	18	42	24.13	0.81	0.30	**1** (- All, except 975 cm^{-1})
		48hrs		HS-48*	97	81	32.38	1.36	1.02	**6** (- 570, 620, 1735 cm^{-1})
		72hrs		**HS-72**	**100***	**85**	31.90	**1.37**	**1.09**	**6** (- 570, 620, 1735 cm^{-1})
		144hrs		HS-144	28.5	39	26.50	1.43	0.89	**2** (-All, +670, 950cm^{-1})
6	**Synthesis temperature**	140°C	Synthesis time, 144h	HS-144	28.5	39	26.50	1.43	0.89	**2** (-All, +670, 950cm^{-1})
		100 °C		**HS-144(100°C)**	85	**91**	38.09	**1.27**	1.50	**5** (- 570, 620, 1735 cm^{-1})
7	**Synthesis time (Fusion)**	12hrs	Fusion condition = 550 °C, 1.5 h; Synthesis temp., 140 °C	HSF-12	28	53	32.92	1.27	0.88	**5** (-620, 730,1440,1735 cm^{-})
		24hrs		HSF-24	29	68	36.30	**1.20**	1.13	**2** (- all, + 470, 980 cm^{-1})
		48hrs		HSF-48*	25	61	31.72	-	-	**5** (-570,620, 730,1637,1735)
		72hrs		**HSF-72**	22	48	35.31	**1.01**	**0.61**	**1** (- all, +470, +980 cm^{-1})
		144hrs		HSF-144	**52**	**80**	37.39	**1.18**	**0.93**	**7** (-570, 620, 1735 cm^{-})
8	**K^+ Ion exchange**	70°C, 24 h, 550°C	70°C, 24 h, 550°C	K/ HS-144 (100°C)	25	-	19.71	1.20	0.54	-
				K/HSF-144	24	-	17.62	**1.35**	0.81	-
	Bifunctional modification	Exchange: 80°C, 24 h; Hydration: 6 h, 60°C	-	**Bi/ HS(144(100°C)**	34	-	**29.42**	**1.28**	0.71	-

*Stage 5-6: *Parameter investigated for direct hydrothermal method (synthesis time and temperature conditions) * HS-48 is **HS-A70+1.2NaOH** in stage 4

(a) Stage 5-6: Synthesis conducted at optimised conditions obtained between stage 1-4: Water/CFA = 5:1, Ageing time & temperature = 1.5 h,70°C and NaOH/CFA = 1.2:1

(b) Stage 7: Optimised conditions obtained from stage 1-6: Water/CFA = 5:1, NaOH/CFA = 1.2:1; Alkaline fusion temperature = 550°C; hydrothermal temperature = 100 °C

(d) All included in reference to bands present in baseline HS-70°C, except ($-x$ cm^{-1}): *vibration modes for HS-70°C (IUPAC): 470,570, 620/625,670,730, 975/960, 1400-40/75,1637, 1735 cm^{-1}

8.2 XRD data of synthesised samples at various conditions [Figure 8.2.1- Figure 8.2.4]

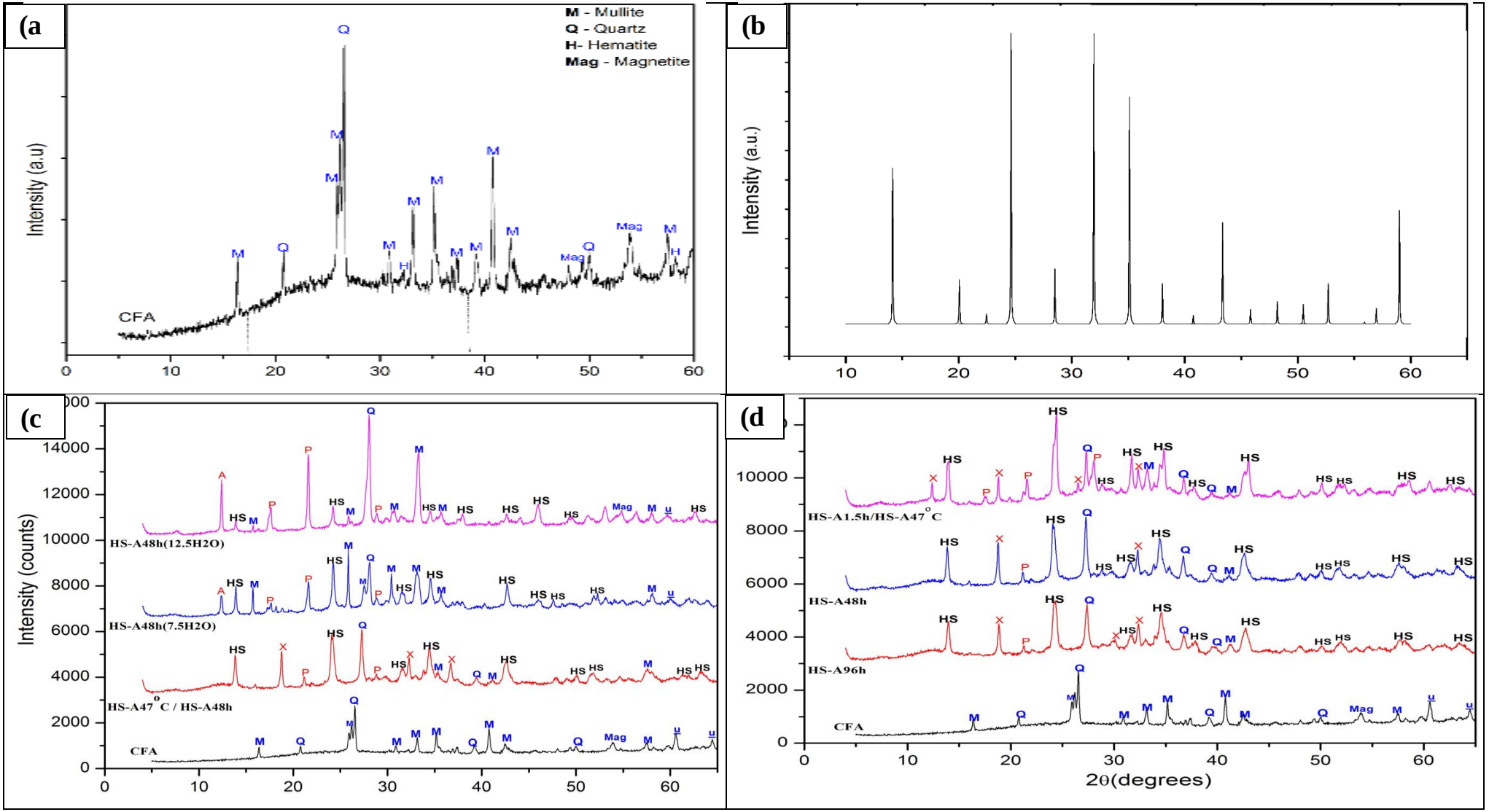

Figure 8.2. 1. XRD patterns of **(a)** Matla CFA, **(b)** simulated sodalite as per IZA, **(c)** illustrating formation of HS with varying water/CFA ratio, **(d)** with varying ageing time

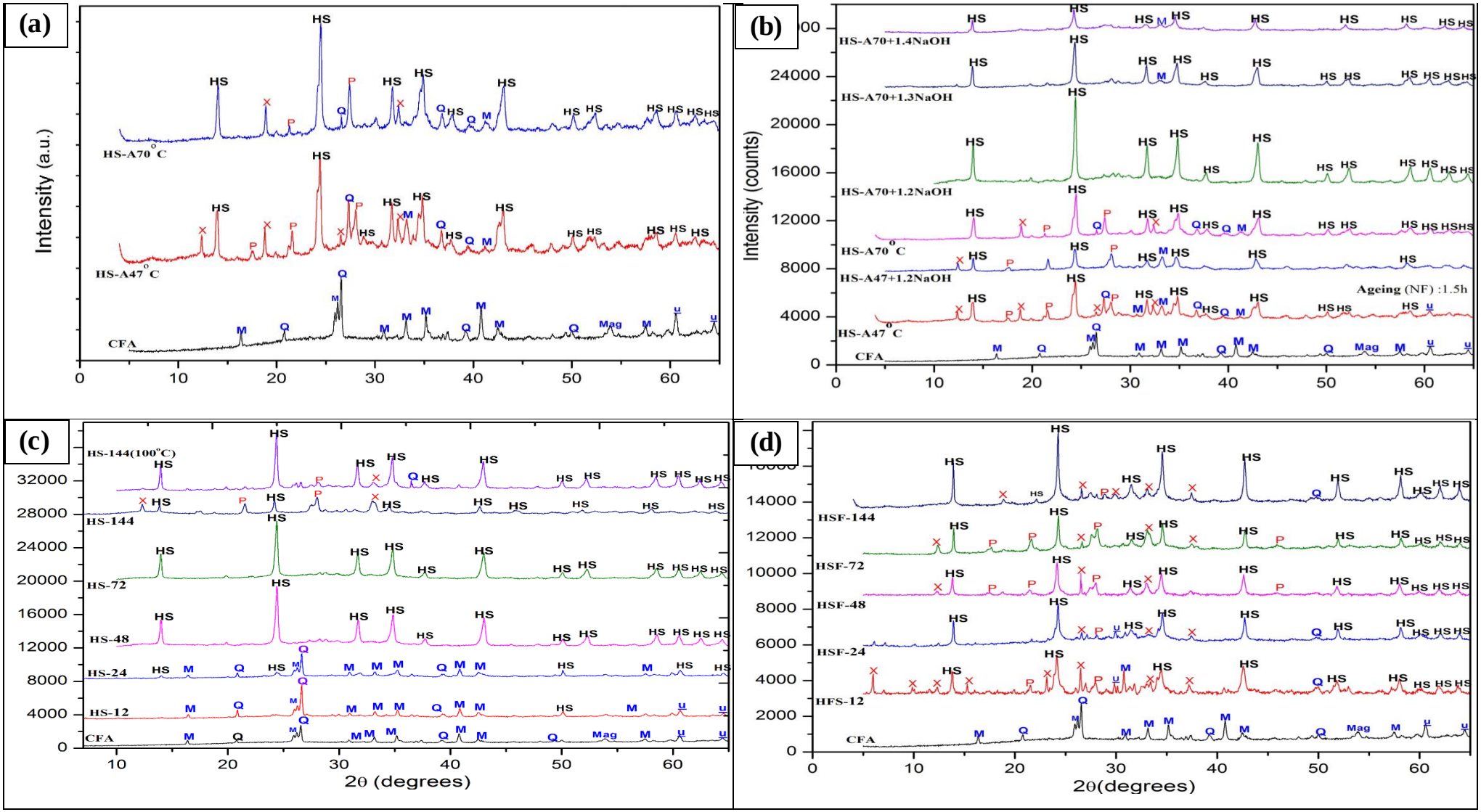

Figure 8.2. 2. XRD patterns illustrating formation of HS as a function of **(a)** varying ageing temperature at 1.5-hour optimised ageing time; **(b)** varying NaOH/CFA ratio at optimised ageing conditions (1.5h, 70°C); **(c)** direct hydrothermal synthesis crystallisation time at 140 °C and crystallisation temperature at 144-hour and **(d)** Fusion crystallisation time at 100 °C.

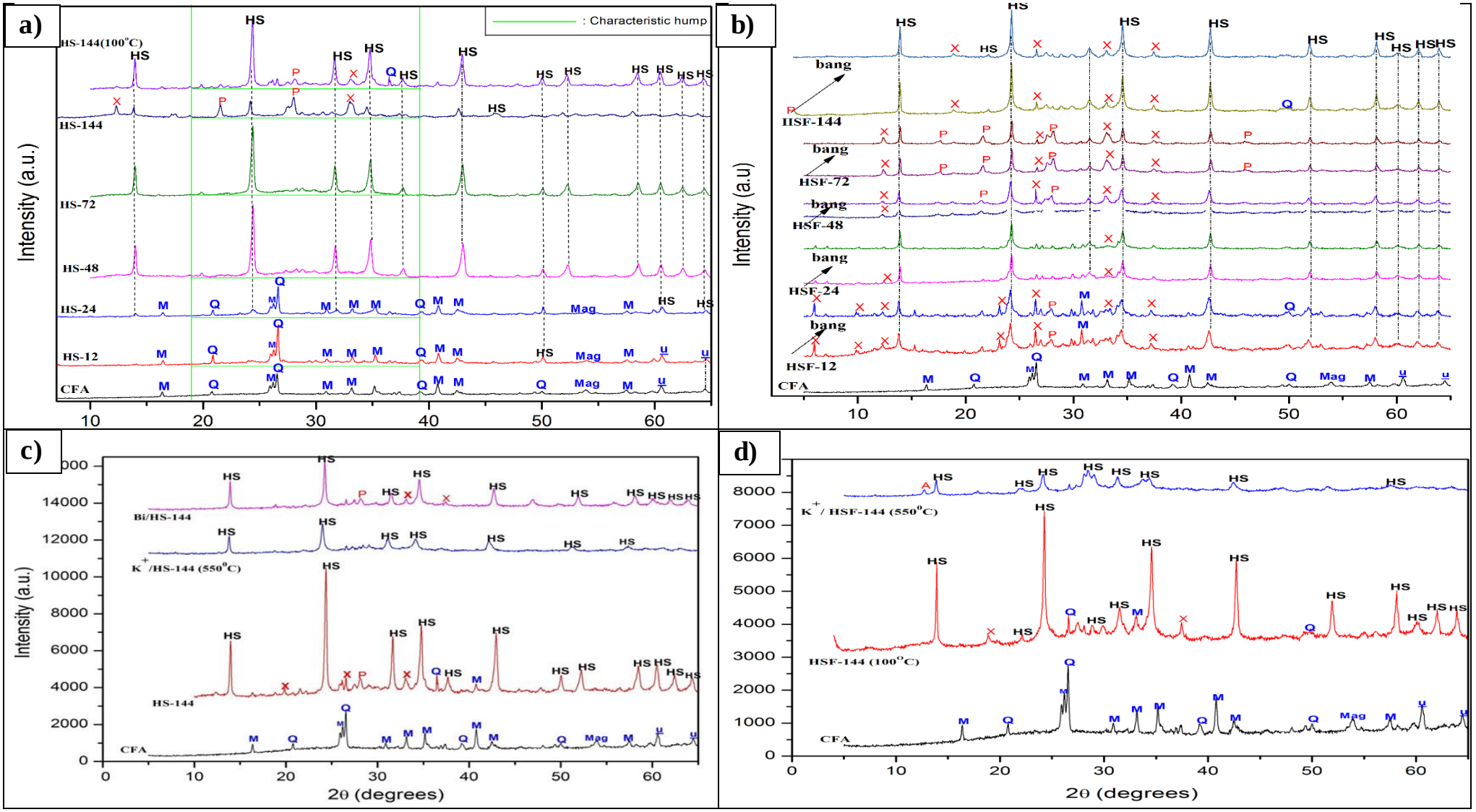

Figure 8.2. 3. XRD patterns illustrating: **(a)** Amorphous characterising humps of direct hydrothermal samples obtained with varying synthesis time and temperature, **(b)** Unprocessed and processed data of samples obtained via fusion-assisted with varying synthesis time, **(c)** Ion exchanged and bifunctional-modified direct hydrothermal HS and **(d)** Ion exchanged-modified fusion HS zeolite (Q = quartz; M = mullite; X = zeolite X; Mag = magnetite; P = zeolite P

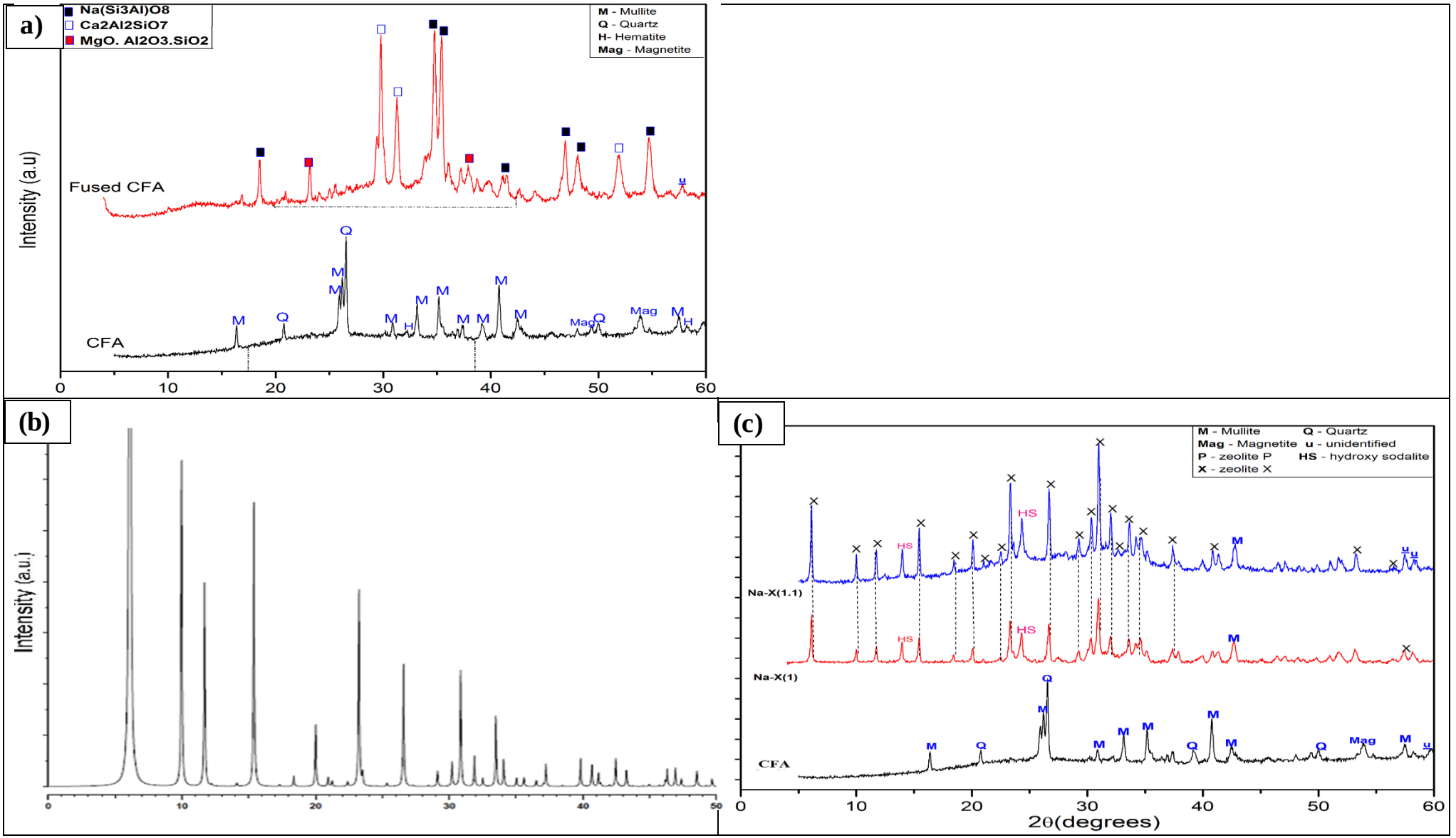

Figure 8.2. 4. XRD patterns: **(a)** CFA and fused fly ash (1.5h, 550°C), **(b)** of simulated zeolite Na-X as per IZA (Treacy and Higgins, 2007), **(c)** illustrating formation of zeolite Na-X with varying NaOH/CFA ratio.

8.2.1 Phase crystallinity, purity of synthesised HS zeolite samples at various conditions, synthesis method and modifications [Figure 8.2.5]

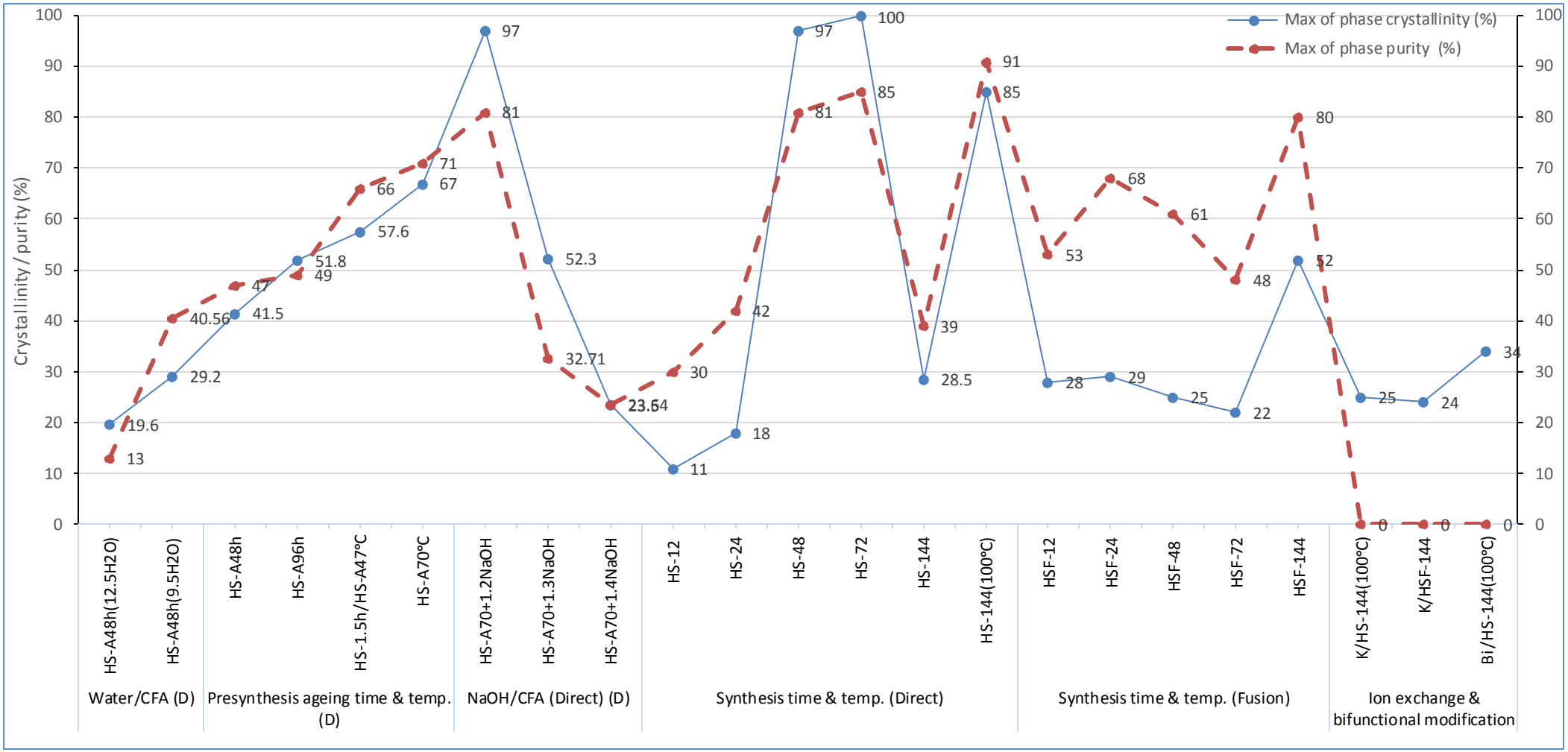

Figure 8.2. 5. Variation in phase crystallinity and purity of HS zeolite with variation in direct hydrothermal synthesis conditions, hydrothermal synthesis method and modification methods (D: Direct hydrothermal samples; Crystallinity: sample HS-72 reference material assigned as 100 %; Sample HS-A70+1.2NaOH = HS-48).

8.3 SEM micrographs of the synthesised samples at various synthesis conditions [Figure 8.3.1 – Figure 8.3.3]

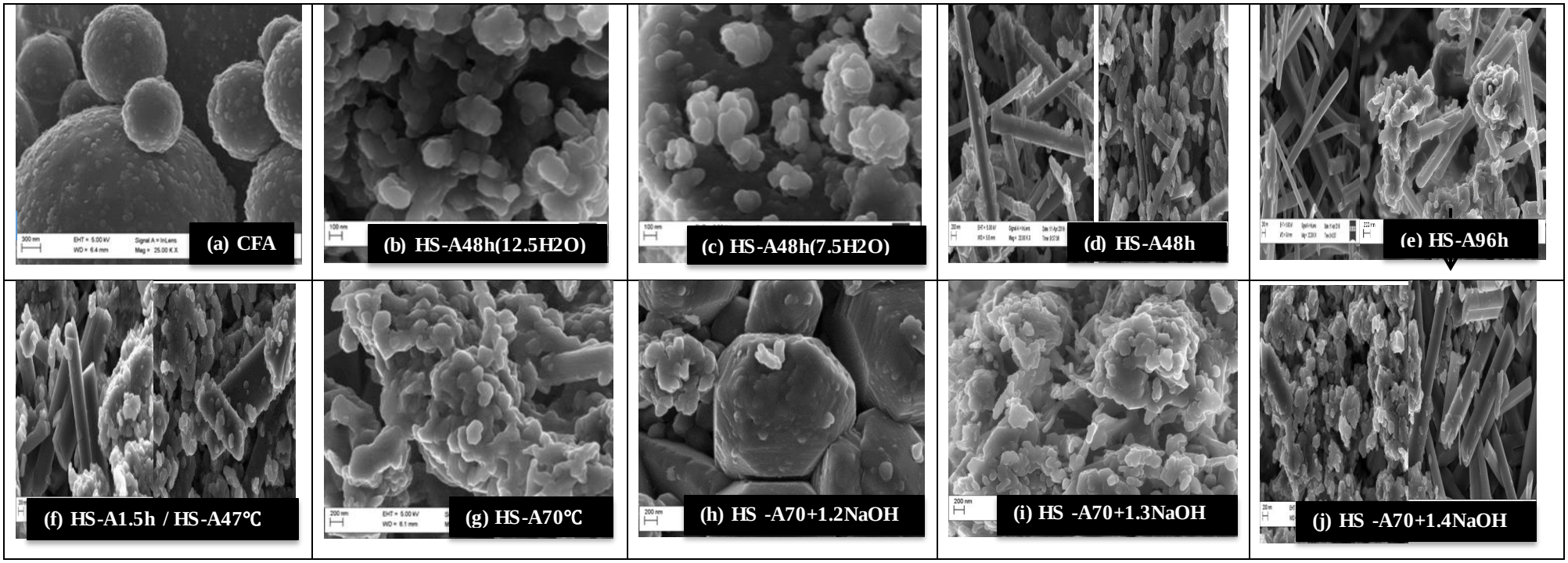

Figure 8.3. 1. SEM micrographs illustrating crystal morphology of synthesised HS samples as function of: **(a)** Arnot fly ash; **(b)-(d)** water/CFA ratio; **(d-f)** pre-synthesis ageing time; **(f-g)** Ageing temperature; **(g-j)** NaOH/CFA ratio in precursor feed mixtures

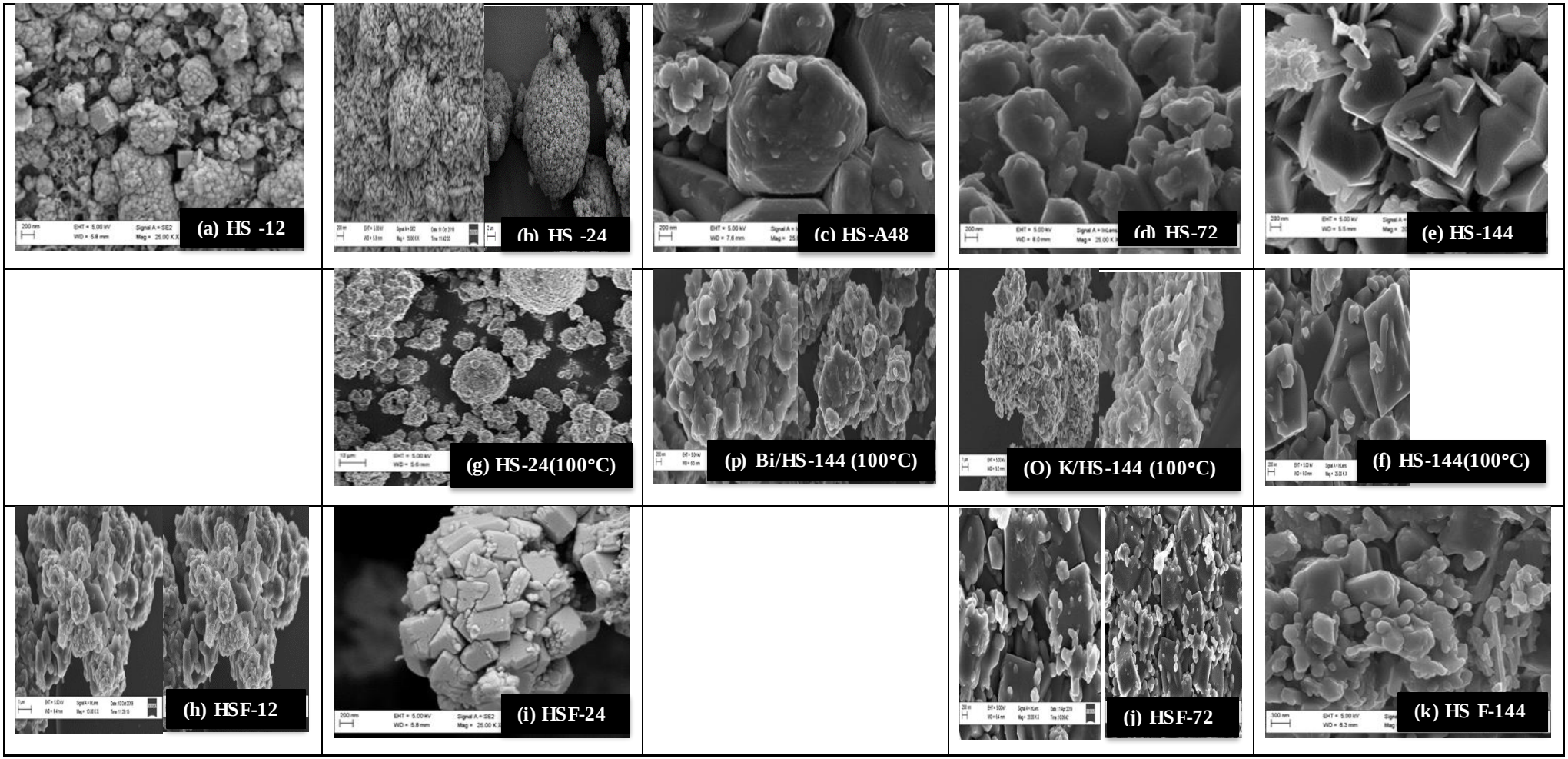

Figure 8.3. 2. SEM micrographs depicting crystal morphology of synthesised HS samples as function of: **(a-g)** Direct hydrothermal synthesis time; **(h-l)** Fusion-assisted synthesis method and time/temperature; and **(f, O, p)** Ion exchange & bifunctional modification

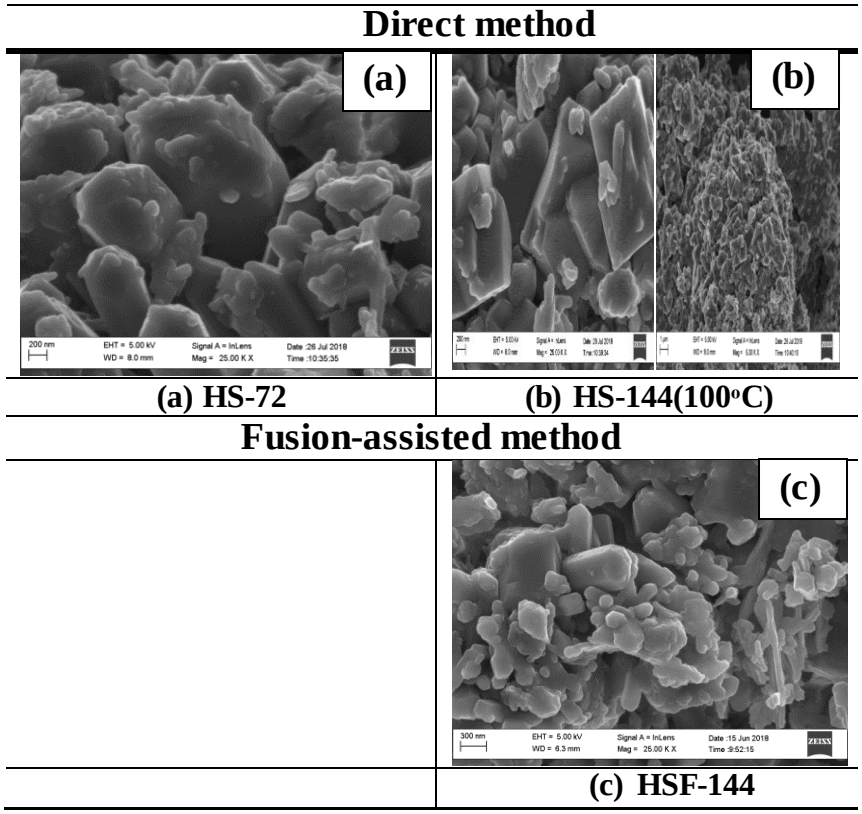

Figure 8.3. 3. SEM micrographs illustrating comparison between optimum HS zeolite obtained by **(a)-(b)** direct hydrothermal method and **(c)** by fusion method (HSF-144)

8.4 FT-IR spectra configuration of synthesised samples with varying synthesis conditions and method [Figure 8.4.1- Figure 8.4.2]

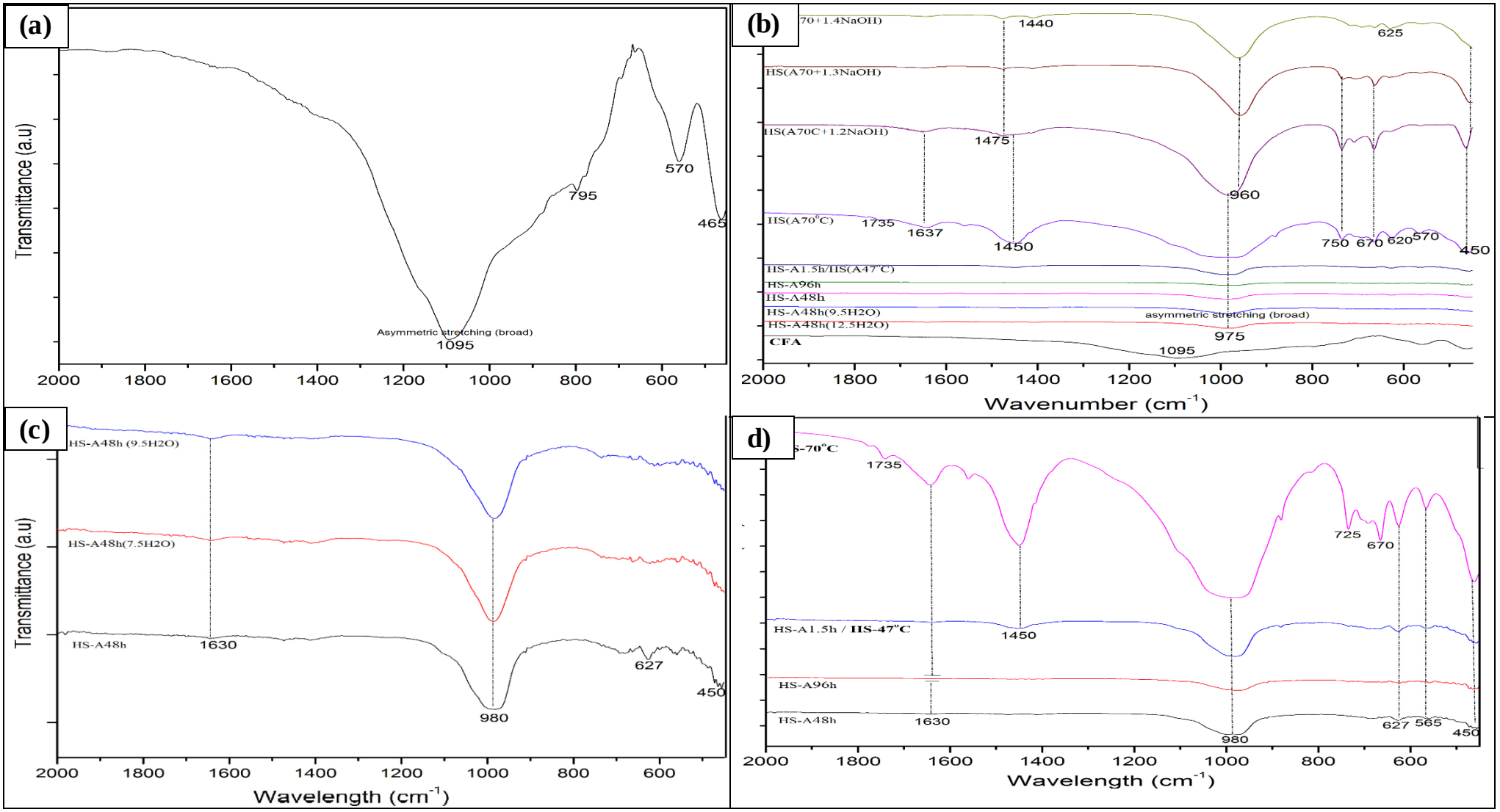

Figure 8.4. 1. FT-IR spectra of **(a)** Matla CFA, **(b)** HS samples obtained with varying water/CFA, ageing conditions and NaOH/CFA ratio; **(c)** HS samples obtained with varying water/CFA ratio; **(d)** HS samples obtained with varying ageing time (at 47°C ageing) and with varying ageing temperature (at 1.5-hour optimised ageing time).

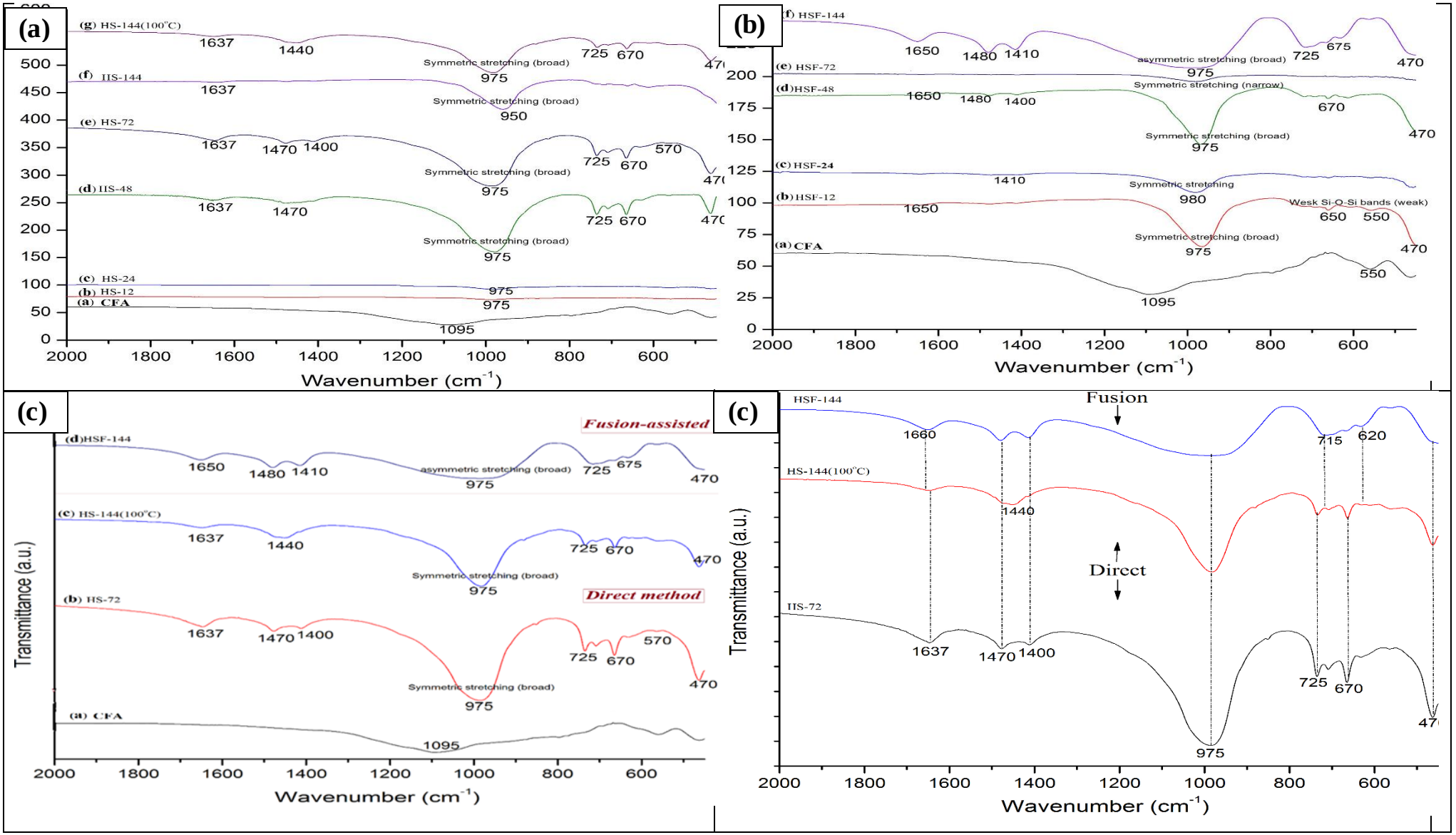

Figure 8.4. 2. FT-IR spectra of HS samples obtained with **(a)** varying synthesis crystallisation time and temperature via direct hydrothermal method; **(b)** with varying synthesis crystallisation time via fusion method, and **(c)** illustrating comparison between optimum HS zeolite obtained via direct hydrothermal method and via fusion-assisted method

8.5 Elemental composition of HS zeolite samples synthesised via direct and fusion hydrothermal method [Table 8.5.1 – Table 8.5.2]

Table 8.5. 1. Elemental composition of synthesised samples as a function of synthesis conditions: **(a-b)** water/CFA ratio; **(b-c)** Pre-synthesis ageing time; **(c-d)** Ageing temp.; **(c-e)** & **(d-e)** NaOH/CFA ratio; **(f)** direct hydrothermal synthesis time & temp.; **(g)** Fusion-assisted synthesis method & time; **(h)** Ion exchange & bifunctional modification

	Sample	O	Al	Si	Na	Mg	K	Ca	Ti	Fe	P	Total (%)	Si/Al ratio	Na/Al ratio
	CFA	43.92	7.57	10.02	-	1.04	0.15	2.92	0.20	0.76	0.84	100.00	1.32	-
(a)	HS-A48h(12.5H_2O)	45.54	15.50	21.53	7.44	0.69	-	3.28	0.85	2.71	-	99.5	1.39	0.48
	HS-A48h(9.5H_2O)	45.79	14.31	20.63	8.16	0.91	0.18	3.54	0.97	2.27	-	100.0	1.44	0.57
(b)	HS-A48h	46.48	13.46	19.94	9.69	0.76	-	3.35	0.94	2.36	-	100.00	1.48	0.72
	HS-A96h	46.64	13.73	19.48	11.95	0.57	0.22	2.85	0.79	1.23	-	100.00	1.42	0.87
(c)	HS-1.5h/HS-A47°C	44.38	14.04	20.38	13.34	0.79	-	3.86	1.17	2.04	-	100.00	1.45	0.95
(d)	HS-A**70°C**	51.12	13.61	13.52	**20.18**	0.31	0.06	0.75	0.19	0.26	-	100.00	**0.99**	**1.60**
(e)	HS-A70+1.2NaOH	45.09	14.32	19.5	14.62	0.65	-	3.57	0.93	1.33	-	100.0	1.36	1.02
	HS-A70+1.3NaOH*	-	-	-	-	-	-	-	-	-	-	-	-	-
	HS-A70+1.4NaOH	45.11	12.25	18.13	14.02	0.96	-	3.71	1.07	3.57	-	99	1.48	1.14
(f)	HS-12	58.63	17.08	17.49	3.04	0.58	0.37	1.30	0.90	0.62	-	100.0	1.02	0.18
	HS-24	59.35	16.50	13.33	4.89	0.99	0.38	2.69	0.78	1.09	-	81.4	0.81	0.30
	HS-48	45.09	14.32	19.5	14.62	0.65	-	3.57	0.93	1.33	-	100.0	1.36	1.02
	HS-72	44.77	13.97	19.07	15.24	0.96	-	3.78	0.79	1.43	-	100.0	1.37	1.09
	HS-144	43.96	13.91	19.96	12.4	0.84	0.83	4.01	2.64	1.44	-	100.0	1.43	0.89
	HS-144(**100°**C)	43.47	13.76	17.42	**20.67**	-	-	2.16	1.23	1.29	-	100.0	**1.27**	1.50
(g)	HSF-12	51.3	14.11	17.86	12.46	0.49	-	2.2	0.53	1.05	-	100	1.27	0.88
	HSF-24	61.28	10.90	13.11	12.31	-	-	1.35	0.26	0.79	-	100	1.20	1.13
	HSF-48*	-	-	-	-	-	-	-	-	-	-	-	-	-
	HSF-72	43.46	19.5	19.75	11.96	-	0.19	2.97	0.61	1.57	-	100.0	1.01	0.61
	HSF-144	65.35	12.42	14.65	**11.55**	0.39	-	1.18	0.29	0.57	-	100.0	1.18	**0.93**
(h)	K/HSF-14	59.75	10.1	13.67	8.17	0.8	3.77	1.97	0.44	1.13	-	100.0	1.35	0.81
	K/HS-144(100°C)	58.09	10.74	12.88	6.91	0.61	7.89	1.71	0.4	0.78	-	100.01	1.20	0.54
	Bi/HS-144(100°C)	40.5	16.1	20.67	11.42	1.91	-	3.77	1.37	3.05	-	99.99	1.28	0.71

Table 8.5. 2. Comparison between elemental composition of optimum direct hydrothermal and fusion HS zeolite

Sample	Element (atomic, w/w %)												
	O	**Al**	**Si**	**Na**	**Mg**	**K**	**Ca**	**Ti**	**Fe**	**P**	Total	**Si/Al**	**Na/Al**
CFA	65.15	11.23	14.86	-	1.54	0.23	4.32	0.30	1.13	1.25	100.0	**1.32**	-
Direct method													
HS-72	44.77	13.97	19.07	15.24	0.96	-	3.78	0.79	1.43	-	100.0	**1.37**	**1.09**
HS-144(100℃)	43.47	13.76	17.42	20.67	-	-	2.16	1.23	1.29	-	100.0	**1.27**	**1.50**
Fusion-assisted													
HSF-144	65.35	12.42	14.65	11.55	0.39	-	1.18	0.29	0.57	-	100.0	**1.18**	**0.93**

8.6 Textual properties of synthesised direct hydrothermal, fusion and ion exchanged HS zeolite [Table 8.6.1; Figure 8.6.1-8.6.2]

Table 8.6. 1. Textual properties of HS samples obtained via direct hydrothermal (varying ageing temperature, NaOH/CFA ratio, synthesis time/ temperature), fusion-assisted method and via ion exchange modification

Synthesis method	Sample	Surface area (m^2/ g)			Pore volume (cm^3/g)			Pore size (nm)
		Total[a]	Meso.[b]	Micro.[b]	Total[c]	Meso.[d]	Micro.[e]	
Direct	HS-A47℃	23.12	19.51	3.60	0.101		0.00172	19.24-21.98
	HS-A70℃	7.57	5.26	2.31	0.029		0.001003	21.58-22.85
	HS-72* (≈ HS-48)	17.60	15.75	1.85	0.089		0.00096	21.22-23.98
	HS-144 (100°C)	13.17	12.62	0.55	0.081		0.00042	22.24-27.58
Fusion	HSF-144	44.98	42.24	2.74	0.148		0.0018	12.99-15.31
Ion exchange	K/HS-144	< 13.17[g]	-	-	-		-	-
	K/HSF-144	25.78	25.03	0.75	0.0614[e]	-	0.00081	9.5-12.2

[a] Obtained by BET equation / method at $p/p_0 = 0.99$

[b] Measured by t-plot method

[c] Estimated at from adsorbed amount at $p/p_0 = 0.99$ or derived from BJH adsorption isotherms as "cumulative volume of pores"

[c] Derived from single point adsorption isotherms as "cumulative volume of pores"

[d] $V_{meso} = V_{ads.\frac{p}{po}=??} - V_{micro}$

[e] Measured by t-plot method

[f] Average pore diameters or width derived from adsorption isotherms using BJH method

[g] Assumingly less than 13.17 m^2/g due to pore blockages induced by ion exchange modification

* Since HS-48 (or HS-70+1.2NaOH) showed same characteristics as HS-72 and similar Na/Al and Si/Al ratio as HS-72, it is assumed that same applies with textual properties. i.e. $HS\text{-}72_{Surfacea\ area} = HS\text{-}48_{Surfacea\ area}$ or $HS\text{-}72_{Pore\ size} = HS\text{-}48_{Pore\ size}$

at P/P

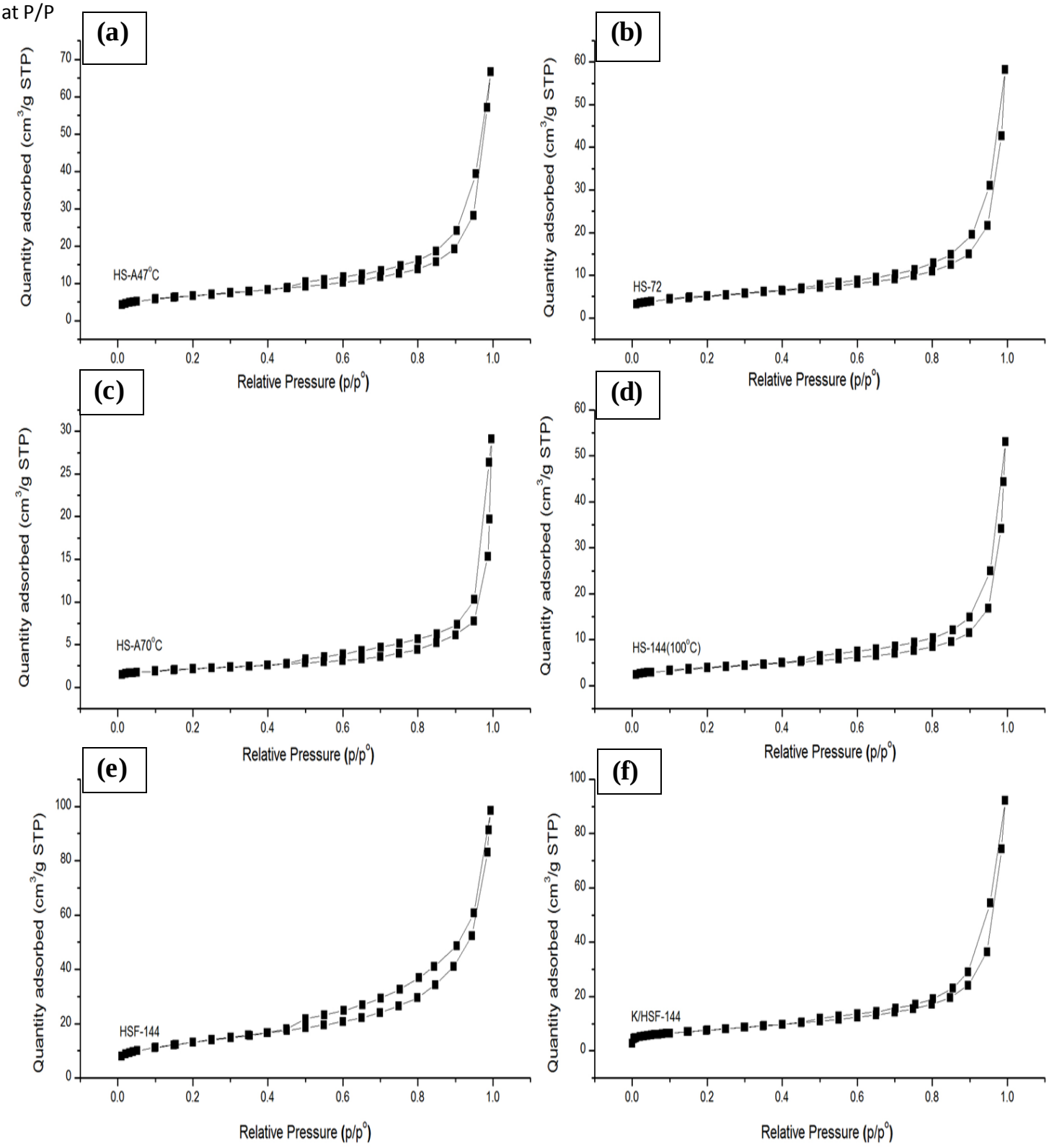

Figure 8.6. 1. N_2 adsorption-desorption isotherms of synthesised HS zeolite obtained by **(a)-(d)** direct hydrothermal, **(e)** fusion method and **(f)** ion exchange-modification

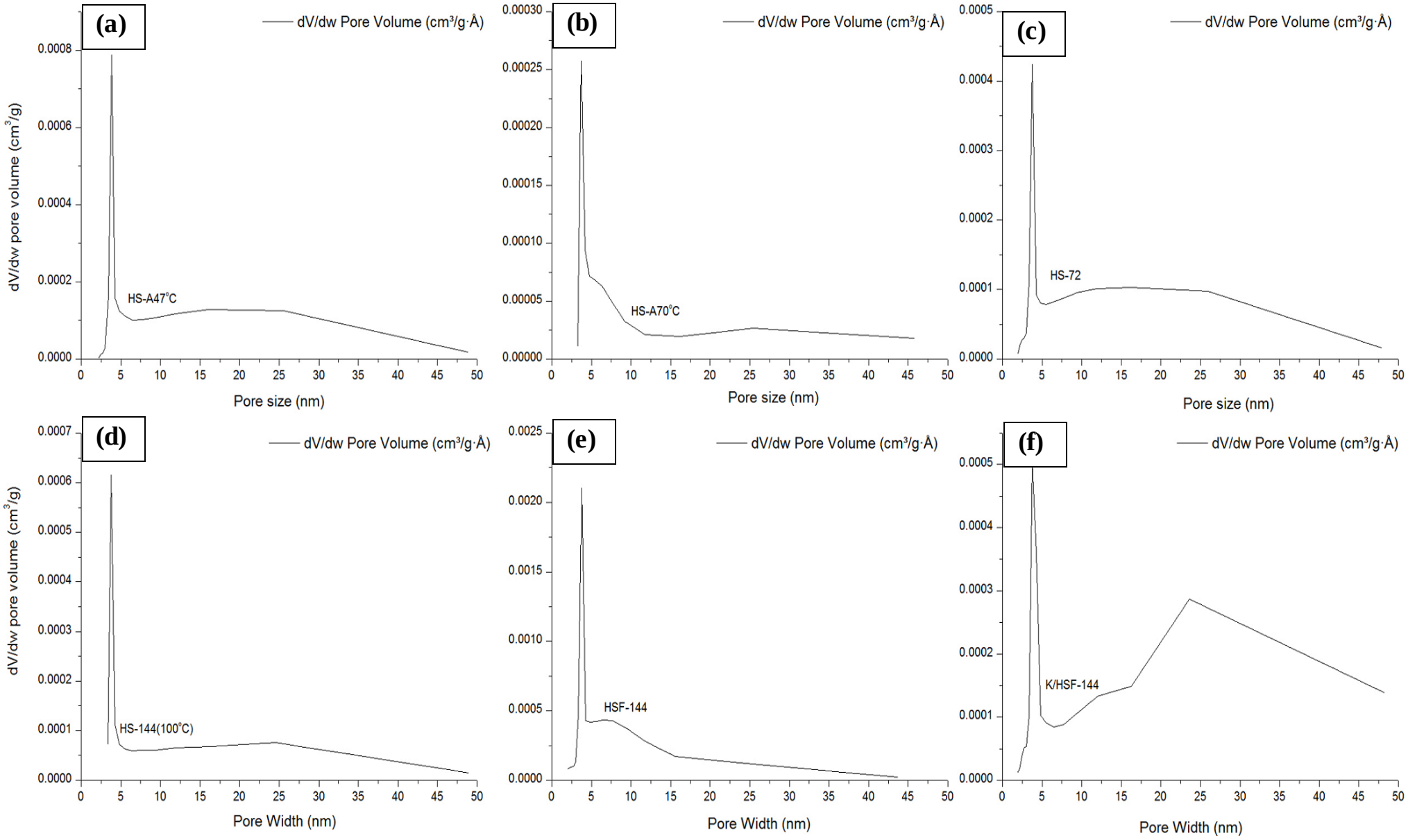

Figure 8.6. 2. Pore size distributions of synthesised HS zeolite obtained by **(a)-(d)** direct hydrothermal method, **(e)** fusion hydrothermal and **(f)** ion exchange-modification

8.7 Yield of HS zeolite, modified HS zeolite and Na-X zeolite products [Figure 8.7.1]

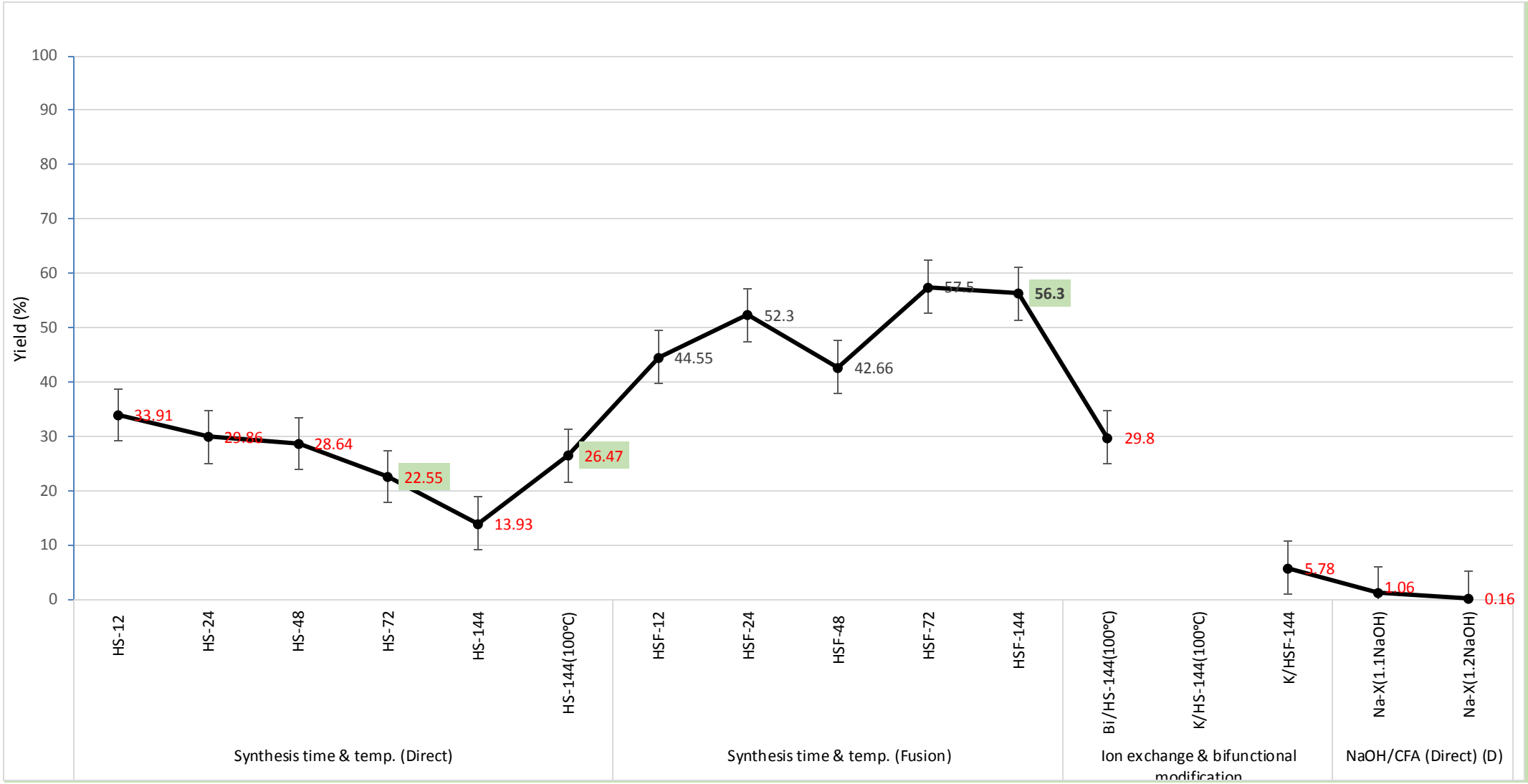

Figure 8.7. 1. Estimated yield of direct hydrothermal HS zeolite, fusion HS zeolite, modified HS zeolite and Na-X zeolite products from coal fly ash

8.7.1 Material balance for synthesis of HS zeolite via direct hydrothermal and fusion-assisted method [Figure 8.7.2]

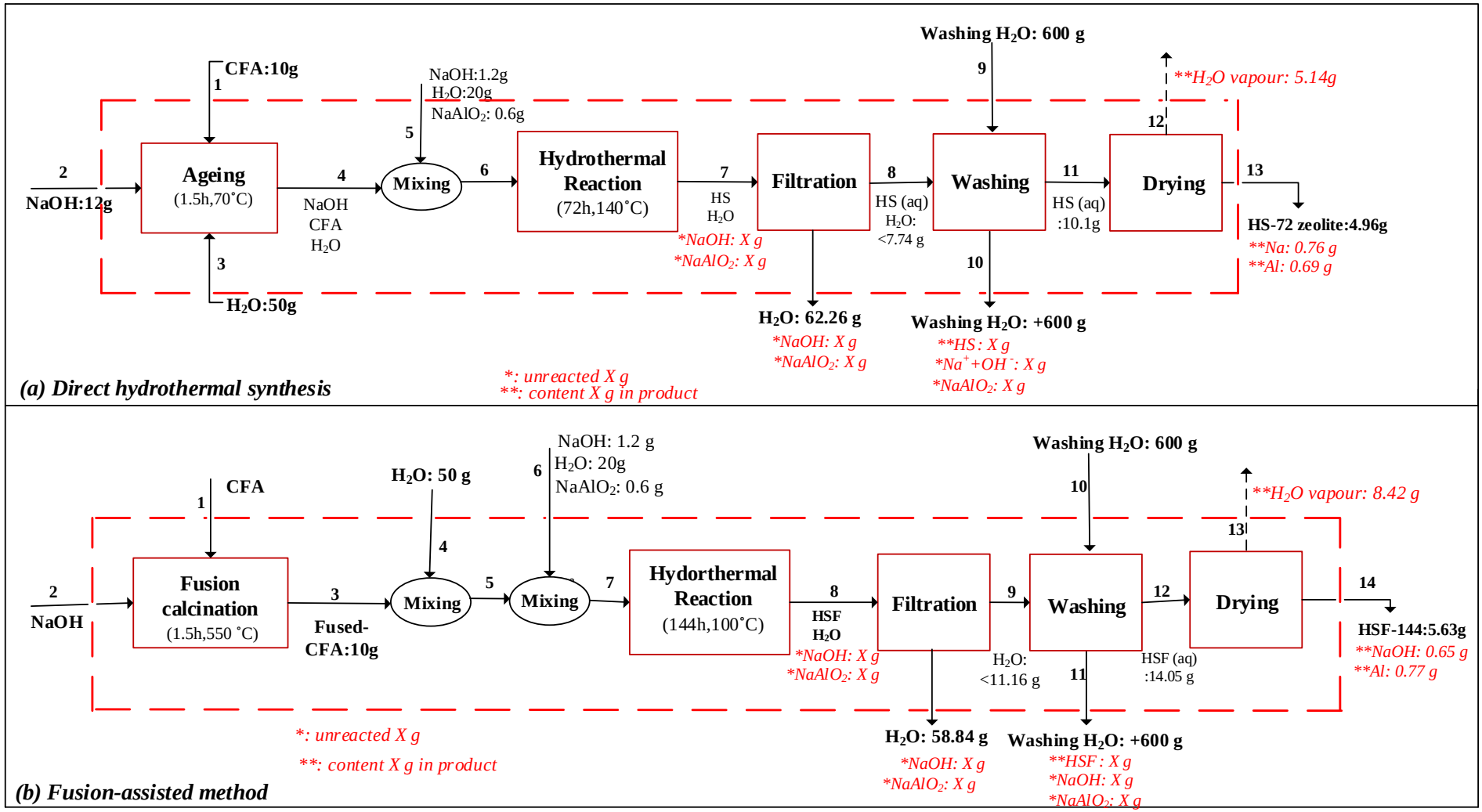

Figure 8.7. 2. Material balance for the synthesis of HS zeolite via direct and fusion process at respective optimal conditions (i.e. 72h, 140 °C for direct method, 144h,100 °C hydrothermal conditions for fusion method).

8.8 Comparison of the characteristic properties and yields of optimum HS zeolites obtained via direct and fusion hydrothermal synthesis [Figure 8.8.1 – Figure 8.8.2, Table 8.8.1]

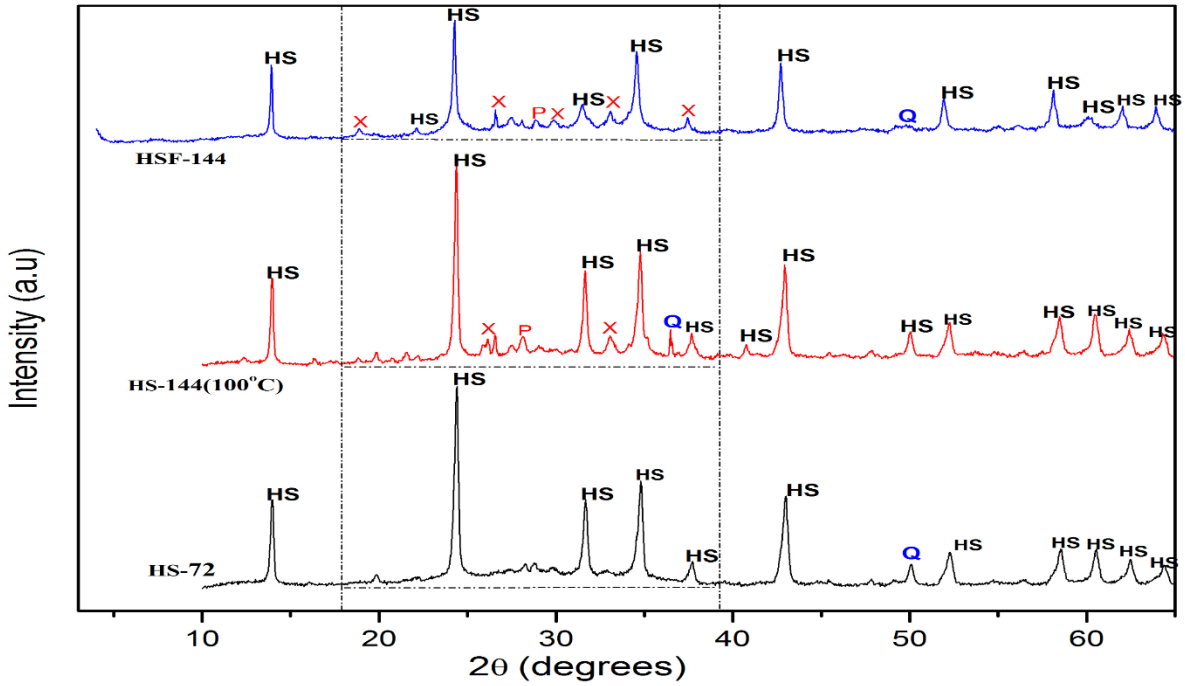

Figure 8.8. 1. Comparison between XRD patterns and amorphous characterising humps of optimum direct hydrothermal (HS-72, HS-144(100°C)) and fusion-assisted HS zeolite samples

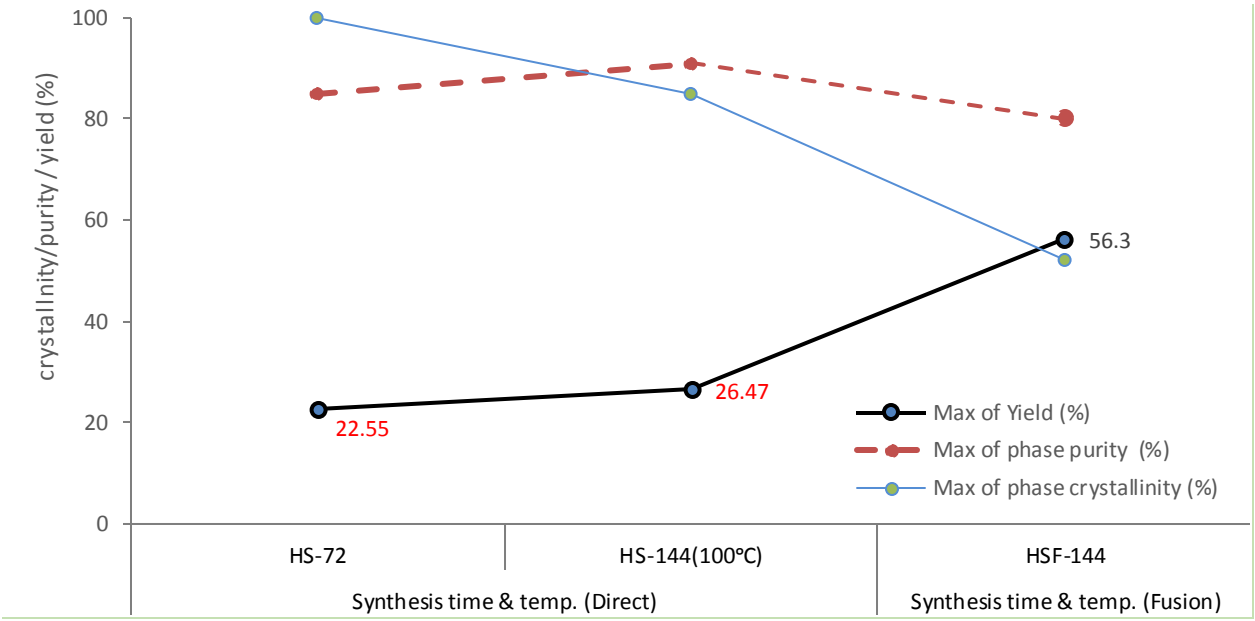

Figure 8.8. 2. Relative crystallinity, purity and estimated maximum yield of HS zeolite obtained at optimum conditions of direct hydrothermal and fusion-assisted method

Table 8.8. 1. Comparison of crystallinity, phase purity, crystal size, framework Si/Al ratio, Na/Al ratio and yields for optimum HS zeolites obtained via direct and fusion-assisted hydrothermal method

Synthesis method	**Samples**	Crystallinity (%)	Purity (%)	Crystal size[(a)] (nm)	Si/Al ratio	Na/Al ratio	Yields (%)
Direct method	HS-72	100*	85	31.90	1.37	1.09	22.55
	HS-144(100°C)	85	91	38.09	1.27	1.50	26.47
Fusion-assisted	HSF-144	52	80	37.39	1.18	0.93	56.3

* Assigned sample for relative crystallinity [(a)] Average crystal size obtained using scherrer equation

Appendix 2

8.9 Fatty acid profile of maggot oil and sunflower oil as biodiesel feedstocks [Figure 8.9.1 & Table 8.9.1]

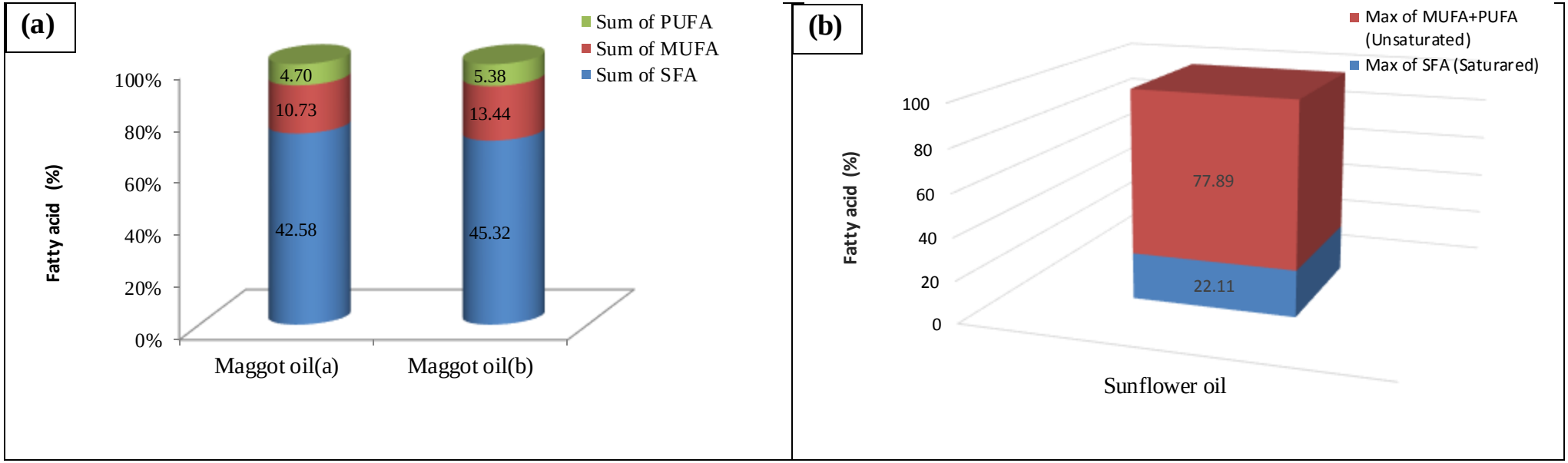

Figure 8.9. 1. Generated fatty acid profile of **(a)** waste-derived maggot oil [(a)Maggot oil in crude form, (b) Maggot oil in purified form], and **(b)** sunflower oil

Table 8.9. 1. Acid value and free fatty acid values of maggot and sunflower oil feedstock

Sample	**Acid value** ($mg\ KOH/$g oil)	% FFA[(a)]
Maggot oil	7.2 [(d)]	3.62
Sunflower oil	0.76	0.38

[(a)] Wt.% FFA $= \frac{\text{acid value in mg KOH/ g oil}}{1.99}$

8.10 Biodiesel obtained by transesterification of maggot oil using synthesized HS zeolite catalysts [Figure 8.10.1-5 & Table 8.10.1]

8.10.1 GC chromatogram illustrating Fatty acid methyl ester (FAME) of derived biodiesel from maggot oil [Figure 8.10.1-Figure 8.10.2]

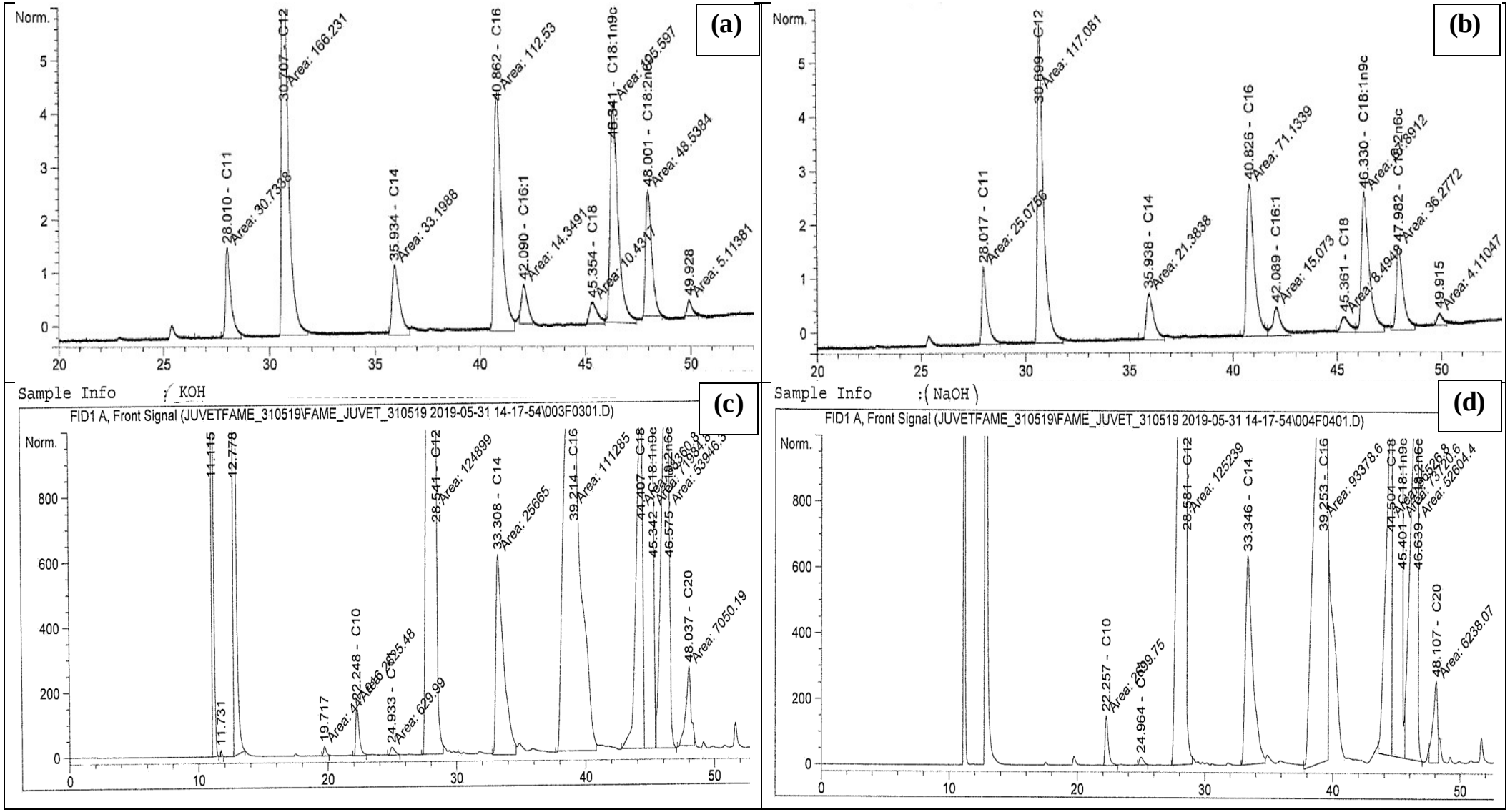

Figure 8.10.1. Fatty acid Methyl ester (FAME) profile of **(a-b)** maggot oil (magOil$_{(b)}$); **(c)** NaOH homogenous-catalysted maggot oil biodiesel; **(d)** KOH homogenous-catalysed maggot oil biodiesel

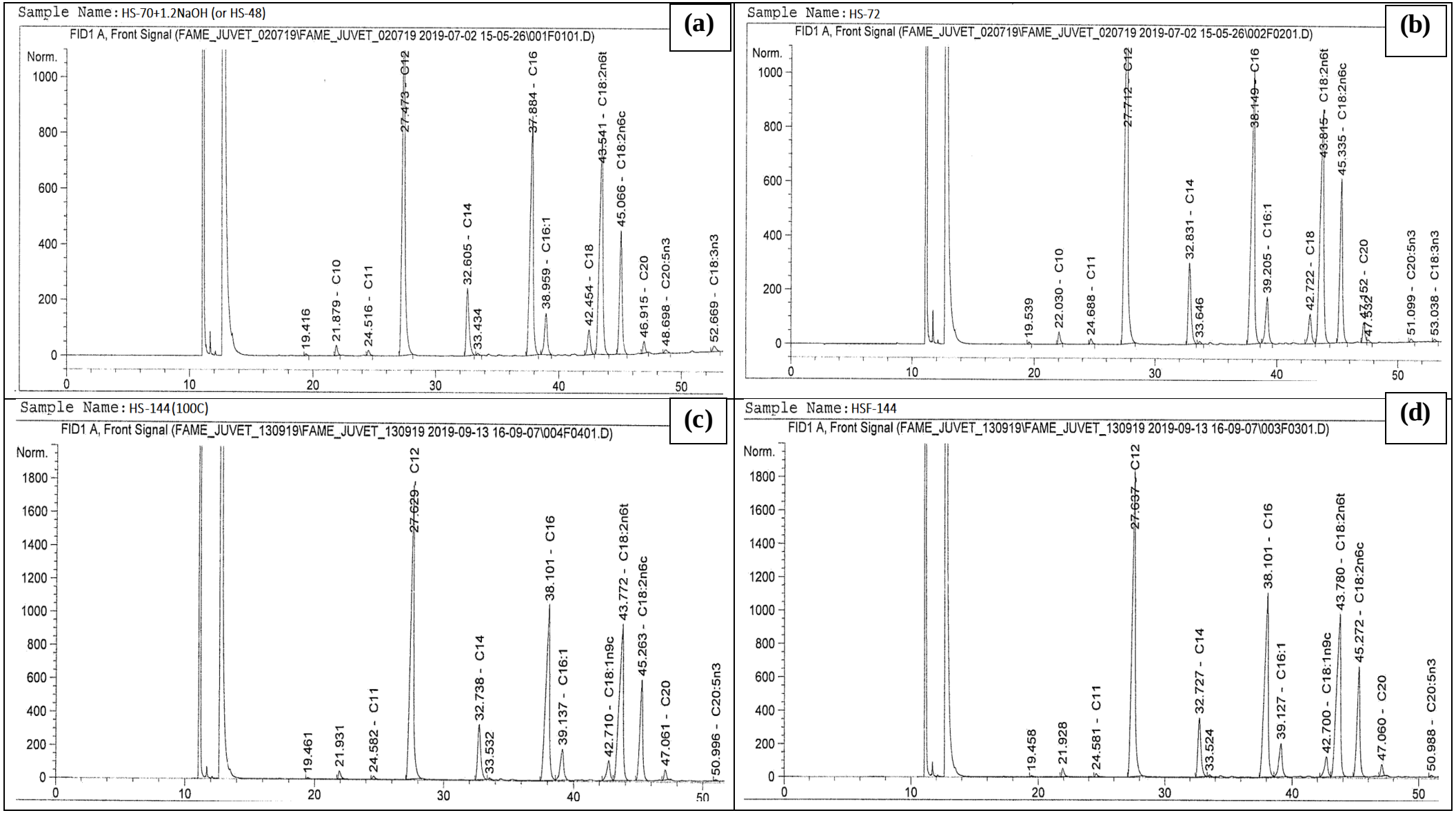

Figure 8.10. 2. Fatty acid methyl ester (FAME) profile of maggot oil-biodiesel obtained using direct method HS zeolite **(a)** HS-70°C, **(b)** HS-70+1.2NaOH (also coded as HS-48), **(c)** HS-72, (d) HS-144(100°C); and Fusion method HS zeolite **(e)** HSF-144 at optimised (single factor-based) transesterication conditions (catalyst wt. = 1.5 %, MeOH/oil ratio = 15:1; reaction temperature & time = 60°C, 1.5 h; and stirring rate = 600 rpm).

8.10.2 Yield and methyl ester content of biodiesel obtained using selected synthesized HS zeolite catalysts for transesterification of maggot/Sunflower oil [Figure 8.10.3 – Figure 8.10.4]

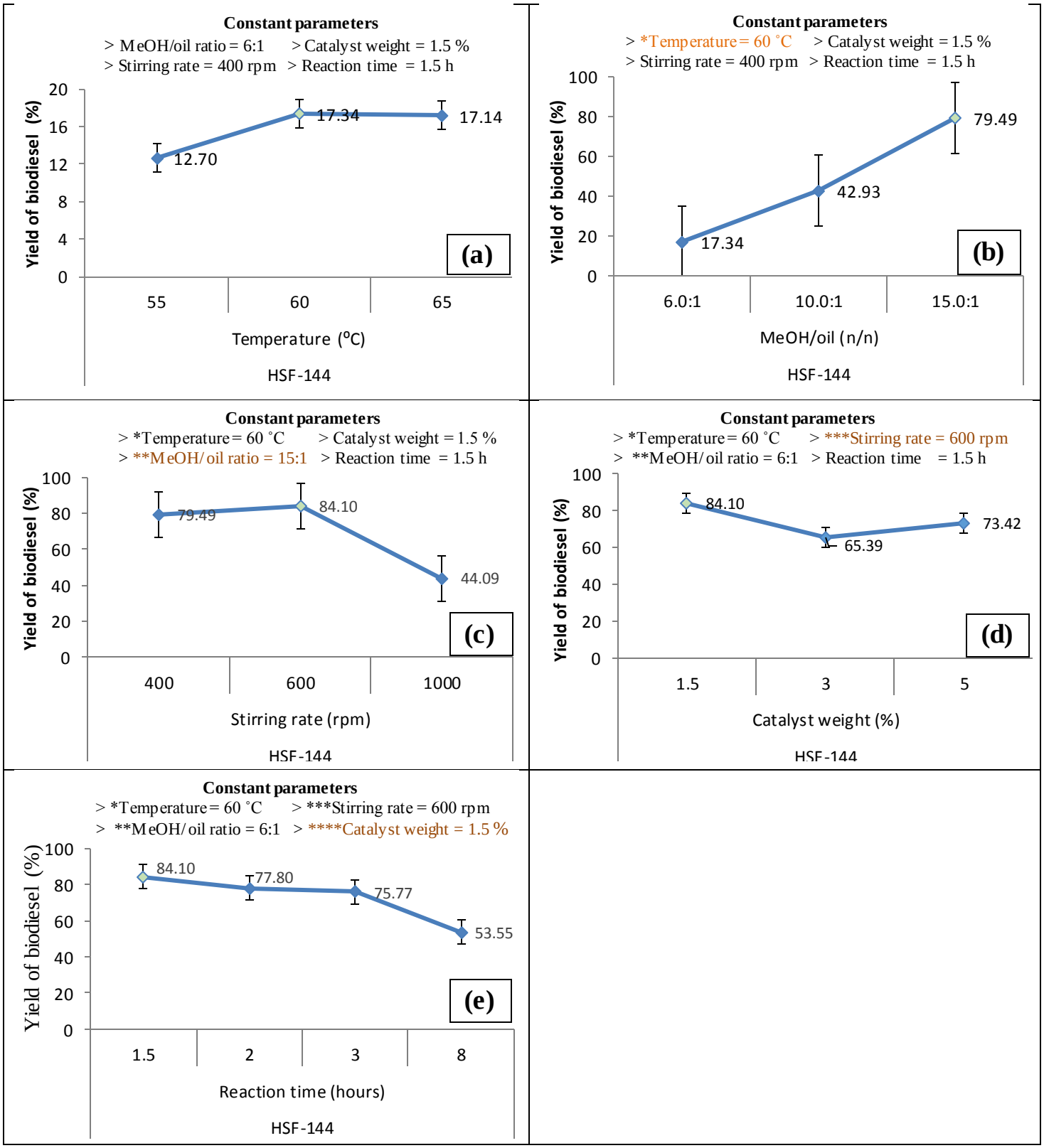

Figure 8.10. 3. Optimisation of biodiesel yield via single parameter approach: **(a)** Temperature, **(b)** MeOH/oil ratio, **(c)** Stirring rate, **(d)** catalyst weight, **(e)** Reaction time (baseline literature conditions: catalyst wt. = 1.5 %, MeOH/oil ratio = 6:1; reaction temperature & time = 60°C, 1.5 h; and stirring rate = 400 rpm.

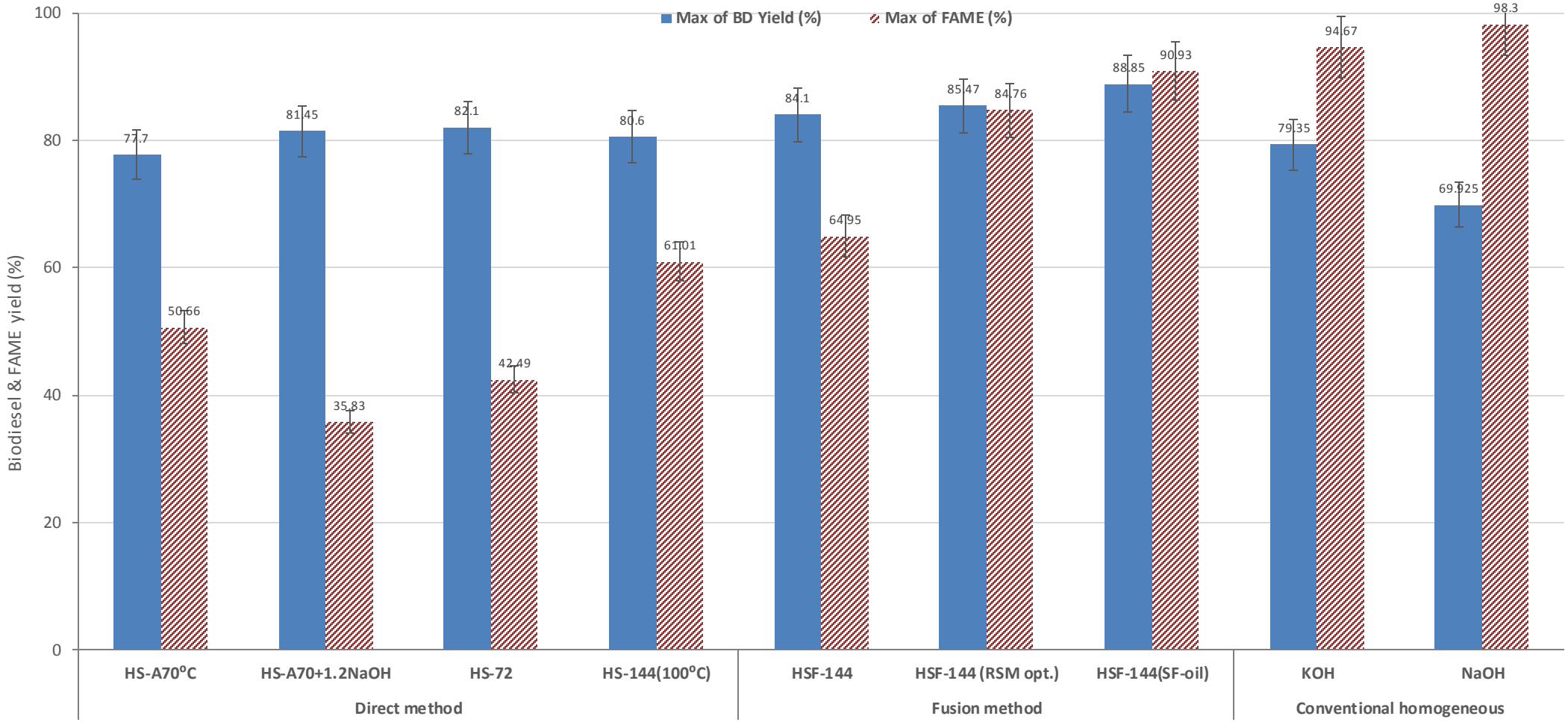

Figure 8.10.4. Yield and Fatty acid methyl ester (FAME) of biodiesel derived from maggot oil and sunflower oil using selected direct method HS zeolite; fusion HS zeolite and conventional homogeneous catalysts at optimised (single-parameter & RSM) transesterification conditions (catalyst wt. = 1.5 %, MeOH/oil ratio = 15:1; reaction temperature & time = 60°C, 1.5 h; and stirring rate = 600 rpm). NB: HS-70+1.2NaOH = HS-48

8.10.3 Physicochemical properties of biodiesel obtained by transesterification of maggot oil using synthesized HS zeolite and conventional homogenous catalysts [Table 8.10.1]

Table 8.10.1. Physical chemical properties of biodiesel obtained using synthesised HS catalyst samples

Catalyst synthesis method	Catalyst sample	Biodiesel properties							
		Acid value (mg KOH/g)	Saponification value (mg KOH/g)	Ester content[d] (% m/m)	Iodine value	Density at 40 °C (g/ml)	Kinematics viscosity at 40 °C (mm^2/s)	Refractive index[e]	Cetane number
Conv. homogenous catalyst	NaOH	0.28	124.33	98.3	69.02	0.862	3.8	1.4456	-
	KOH	0.35	146.64	94.67	82.63	0.874	4.39	1.4457	-
Direct method-derived HS zeolite (As per catalyst synthesis time & temperature.)	HS-70°C	0.53	145.53	**50.66**	49.38	0.914	5.82	1.4449	56.71
	HS-70+1.2NaOH or HS-48	0.53	145.37	35.83	59.02	0.907	5.73	1.4454	36.63
	HS-72	0.49	145.4	42.49	56.86	0.881	5.7	1.445	36.64
	HS-144 (100°C)	0.47	145.4	61.01	60.17	0.897	5.73	1.4461	36.6
Fusion method-derived HS zeolite (as per catalyst synthesis time	**HSF-144**	0.53	147.87	**64.95**	65.01	0.877	5.16	1.4455	36.63
	HSF (RSM opt.)	0.53	143.3	**84.76**	69.79	0.869	5.23	1.4443	35.5
	HSF(SF-oil)	0.53	161.66	**90.93**	68.56	0.864	4.19	1.4555	45.3
Ion exchange & bifunctional modified catalysts	K/HS-144	0.57	145.45	45.4	59.62	0.94	4.82	1.4451	36.67
	K/HSF-144	0.74	145.43	51.5	61.4	0.893	4.68	1.4435	36.66
	Bi/HS-144	0.53	145.64	51.08	54.74	0.91	5.25	1.4442	36.77
B-Standard[a]	**ENS[b] /ASTM[c]**	**0.5/0.8 Max**	**-**	**96.5**	**/120-130**	**0.86-0.90**	**3.5-5.0 /1.9-6.0**	**/1.479**	**51/47**

[a] Biodiesel Standard Specifications; [b] ENS14214 (European) and [c]ASTMD6751 (American for FAEE)
[d] Obtained from GC characterisation of respective biodiesel FAME samples – Also referred to as FAME content or yield

8.10.4 **Correlation of catalytic properties and activity in the transesterification of maggot oil** [Figure 8.10.5]

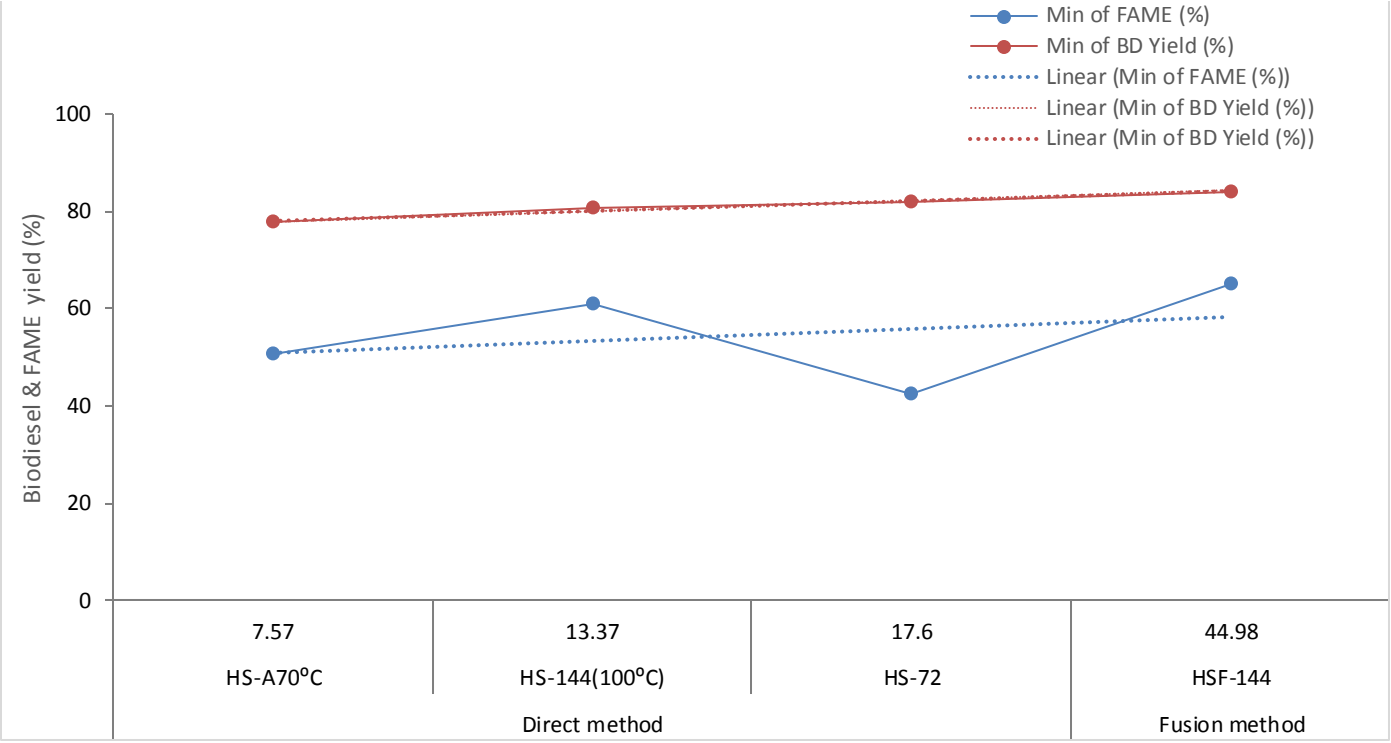

Figure 8.10.5. The effect of catalyst total surface area (7.57 → 44.98 m^2/g) on biodiesel and FAME yield from maggot oil

8.11 Analysis of optimization of transesterification of maggot oil using the response surface methodology (RSM) [Figure 8.11.1]

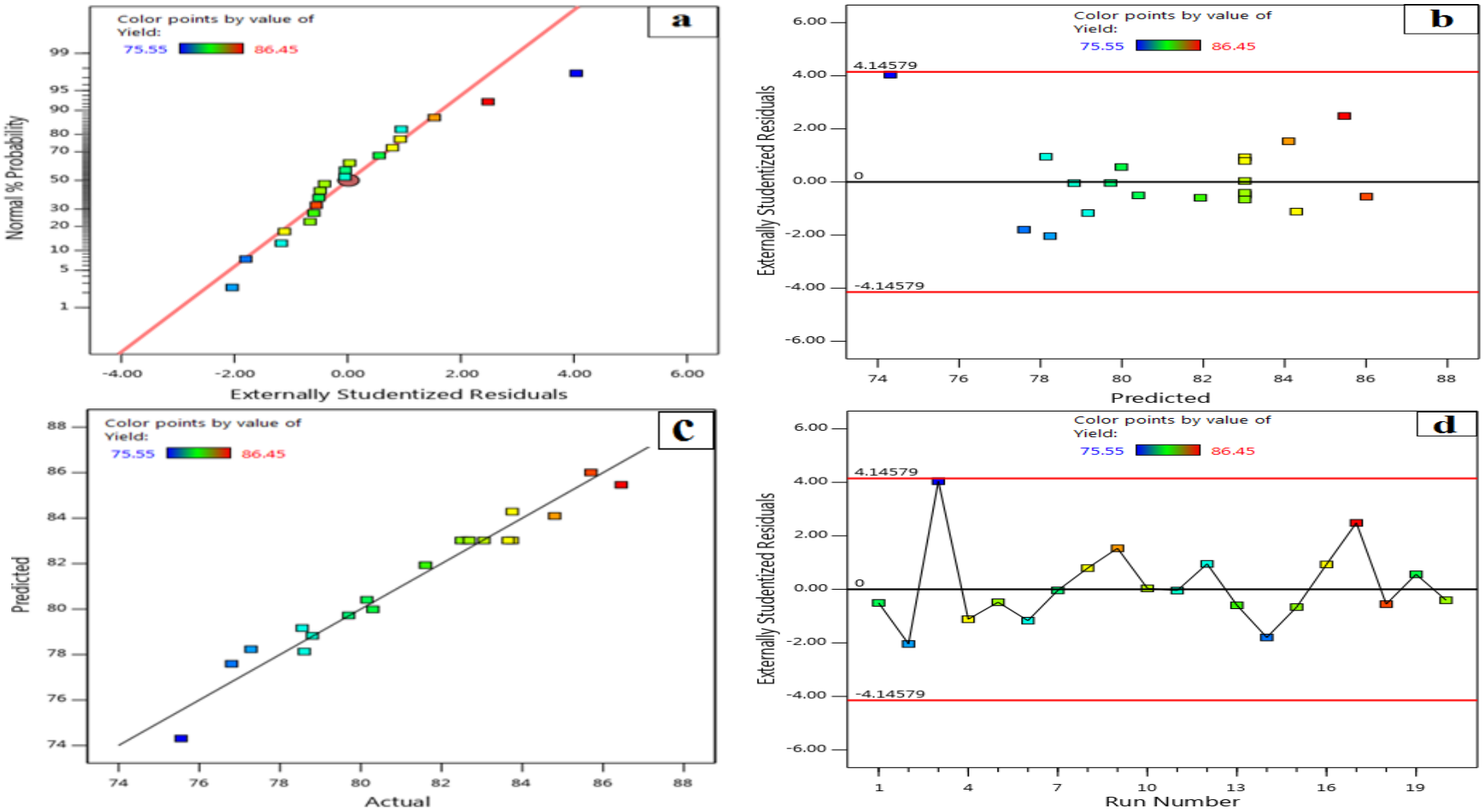

Figure 8.11. 1. Analysis of RSM-derived quadratic model, **(a)** Normal probability plots of residuals; **(b)** Residual vs. Predicted, **(c)** Predicted vs. Actual; and **(d)** Residuals vs. Run.

8.12 Kinetic data of transesterification of maggot oil using the synthesised HS zeolite [Figure 8.12.1 – Figure 8.12.2]

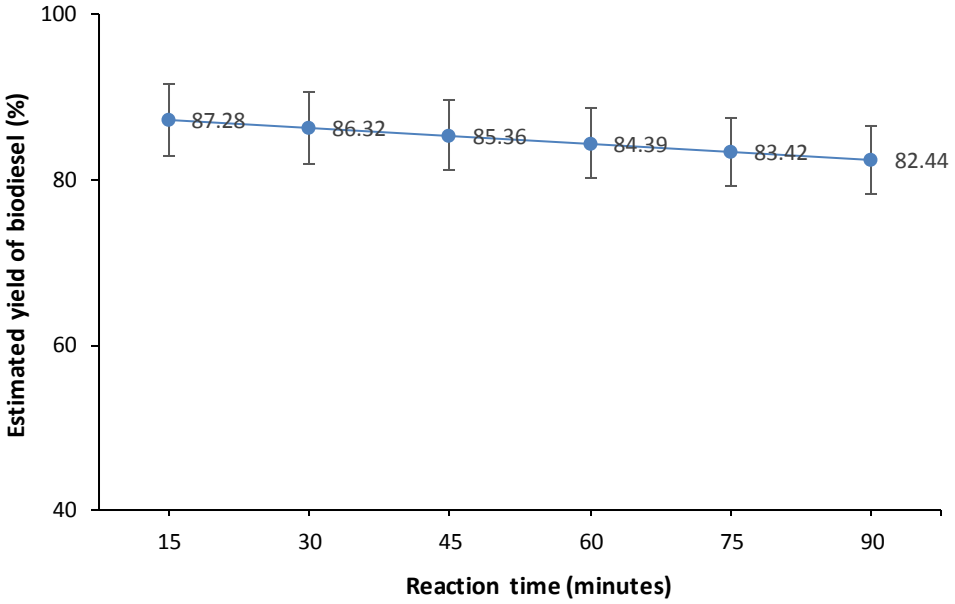

Figure 8.12. 1. Estimated yield biodiesel (FAME) with reaction time below 1.5 hour (estimated at optimised parameters: catalyst wt. = 1.5 %; MeOH/oil ratio = 15:1; reaction temperature = 60°C; and stirring rate = 600 rpm).

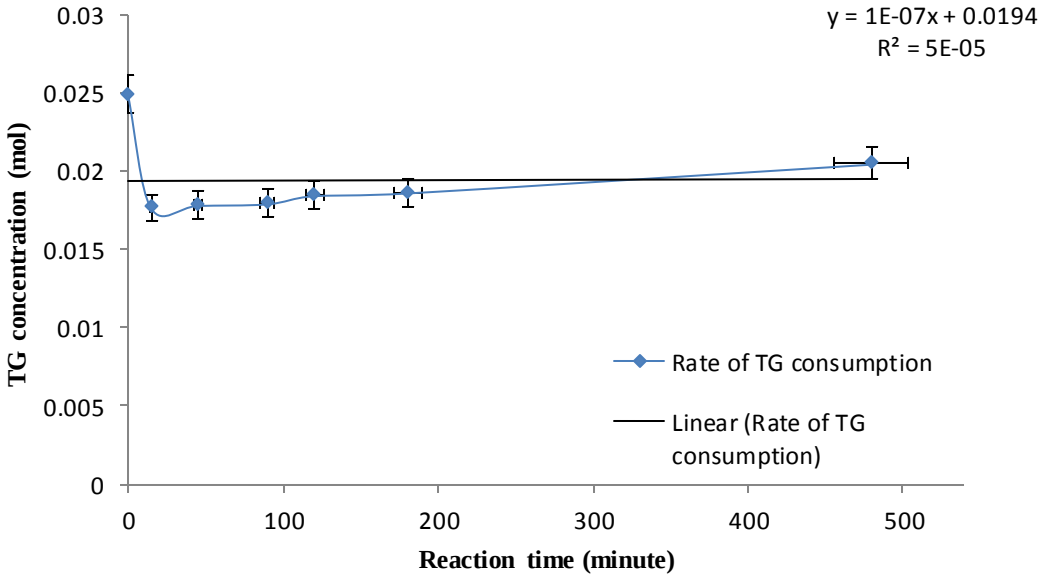

Figure 8.12. 2. Maggot oil triglyceride (TG) concentration with transesterification reaction time

8.13 Summary of the study novelty of the synthesis of fly-based zeolites for the transesterification of maggot oil [Table 8.13.1]

Table 8.13.1. Summary of the study novelty

	Study novelty
Feedstock	• Major **industrial** waste feedstock from lipid fraction of black soldier fly (organic waste-derived by-product) - Supplied by limited number of corporation worldwide • **Large**, continual availability and rising supply (due to demand for Magmeal) - Ascertains large scale and sustainable production of biodiesel
	• Potential conversion to biodiesel using conventional homogenous (NaOH and KOH) catalysts
Catalyst	• Major industrial waste feedstock (coal fly ash solid waste product) • Large and continual availability/supply of fly ash (due to coal burning in SA) - Guarantees scale up and sustainable production
	- Both low cost feedstocks and their successful beneficiation to high biodiesel yield and quality, guarantees the highest reduction in overall biodiesel production cost
Catalyst synthesis conditions	• HS zeolite **synthesis** and thorough **optimisation from fly ash** by two various synthesis methods o Direct method (1) o Fusion-assisted method (2) o Comparison of the methods for HS zeolite
	▪ Investigation and optimisation of direct hydrothermal presynthesis ageing and actual hydrothermal conditions (1) - novel ageing time (reduced) and temperature (1.5h, 70 °C) - Novel direct hydrothermal synthesis time and temperature conditions (72 h, 140°C ; 144 h, 100 °C) - Novel and established fusion-assisted hydrothermal synthesis time (144 h, 100°C) - Novel characteristics that best describe HS zeolite (morphologically, compositionally, etc.) via both methods - Direct hydrothermal method established to be the best for HS zeolite with regard to overall quality & energy efficiency, economic feasibility and up-scalability of the biodiesel heterogeneous (HS) catalyst synthesis process

Table 8.13.1 (*cont'd*). Summary of the study novelty

	Study novelty
HS zeolite (catalyst) modification	• Modification of HS (from fly ash) for biodiesel production o Ion exchange using KOH o Bifunctional modification - Both modification approaches resulted in poor overall characteristic of the products, however there is potential for better characteristics upon further studies
Catalyst activity tests	• HS (novel) heterogeneous catalyst **from fly ash** for biodiesel production o On both maggot oil and refined conventional vegetable oil feedstock - High catalytic performance of heterogeneous HS catalyst, resulting in high yield (80.6, 84.10 %) and quality compliant maggot oil-derived biodiesel (61.01 %, 64.95 % FAME) prior to RSM optimisation - HS zeolite showed better and competitive catalytic performance in the transformation of sunflower oil to biodiesel, giving an 88.85 % biodiesel yield and 90.93 % quality FAME yield.
	• Both synthesis and application of HS zeolite in a single study for biodiesel production
	• Optimisation of **maggot oil** conversion by one-factor approach and via RSM - High yield and quality biodiesel produced (85.47 % yield, 84.76 % FAME) at optimised conditions (6:1 meOH/oil, 400 rpm agitation rate, 1.5h reaction time), and which are considerably less energy requiring for an heterogeneous catalyst transesterification
	• Kinetic study of maggot oil transesterification using the produced HS zeolite - A moderately high reaction rate constant of 1.15×10^{-3} min^{-1} and a gradually increasing rate of reaction between 5.29×10^{-6} and 6.13×10^{-6} $mol/cm^3.min$ with an increase in reaction time.

9. References

<Nanganoa (2016) - Synthesis of Hydroxy-sodalite from Fine Fractions of Sandy.pdf>.

AGENCY, I. E. & BIROL, F. 2013. *World energy outlook 2013*, International Energy Agency Paris.

AGRIPROTEIN 2017. Our products.

ALAMU, O., WAHEED, M. & JEKAYINFA, S. 2008. Effect of ethanol–palm kernel oil ratio on alkali-catalyzed biodiesel yield. *Fuel,* 87**,** 1529-1533.

AMEH, A. E., EZE, C. P., ANTUNES, E., CORNELIUS, M.-L. U., MUSYOKA, N. M. & PETRIK, L. F. 2019. Stability of fly ash-based BEA-zeolite in hot liquid phase. *Catalysis Today*.

AMEH, A. E., FATOBA, O. O., MUSYOKA, N. M., LOUIS, B. & PETRIK, L. F. 2020. Transformation of fly ash based nanosilica extract to BEA zeolite and its durability in hot liquid. *Microporous and Mesoporous Materials,* 305**,** 110332.

AMEH, A. E., FATOBA, O. O., MUSYOKA, N. M. & PETRIK, L. F. 2017. Influence of aluminium source on the crystal structure and framework coordination of Al and Si in fly ash-based zeolite NaA. *Powder Technology,* 306**,** 17-25.

AQLILIRIANA, C., ERNEE, N. & IRMAWATI, R. 2015. Preparation and Characterization of Modified Calcium Oxide From Natural Sources and Their Application in The Transesterification of Palm Oil. *International Journal of Scientific and Technology Research,* 4**,** 168-175.

AUGHENBAUGH, K. L., STUTZMAN, P. & JUENGER, M. C. 2016. Identifying glass compositions in fly ash. *Frontiers in Materials,* 3**,** 1.

BABAJIDE, O., MUSYOKA, N., PETRIK, L. & AMEER, F. 2012. Novel zeolite Na-X synthesized from fly ash as a heterogeneous catalyst in biodiesel production. *Catalysis today,* 190**,** 54–60.

BABAJIDE, O. O. 2011. Optimisation of biodiesel production via different catalytic and process systems.

BAERLOCHER, C., MCCUSKER, L. B. & OLSON, D. H. 2007. *Atlas of zeolite framework types*, Elsevier.

BALDAN, A. 2002. Review progress in Ostwald ripening theories and their applications to nickel-base superalloys Part I: Ostwald ripening theories. *Journal of materials science,* 37**,** 2171-2202.

BALKUS, K. J. & LY, K. T. 1991. The preparation and characterization of an X-type zeolite: an experiment in solid-state chemistry. *Journal of Chemical Education,* 68**,** 875.

BAROUTIAN, S., AROUA, M. K., RAMAN, A. A. & SULAIMAN, N. M. 2009. RBD palm olein-based methyl/ethyl esters. *Journal of Oil Palm Research,* 21**,** 659–666.

BEHERA, S. K., MEENA, H., CHAKRABORTY, S. & MEIKAP, B. 2018. Application of response surface methodology (RSM) for optimization of leaching parameters for ash reduction from low-grade coal. *International Journal of Mining Science and Technology,* 28**,** 621-629.

BELVISO, C., CAVALCANTE, F. & FIORE, S. 2010. Synthesis of zeolite from Italian coal fly ash: differences in crystallization temperature using seawater instead of distilled water. *Waste management,* 30**,** 839-847.

BELVISO, C., CAVALCANTE, F., LETTINO, A. & FIORE, S. 2009. Zeolite Synthesized from Fused Coal Fly Ash at Low Temperature Using Seawater for Crystallization. Coal Combustion and Gasification Products 1, 8-13, doi: 10.4177. CCGP-D-09-0004.1.

BEZERRA, M. A., SANTELLI, R. E., OLIVEIRA, E. P., VILLAR, L. S. & ESCALEIRA, L. A. 2008. Response surface methodology (RSM) as a tool for optimization in analytical chemistry. *Talanta,* 76**,** 965-977.

BHUIYA, M. M. K., RASUL, M. G., KHAN, M. M. K., ASHWATH, N., AZAD, A. K. & HAZRAT, M. A. 2014. Second generation biodiesel: potential alternative to-edible oil-derived biodiesel. *Energy Procedia,* 61**,** 1969–1972.

BIODIESEL EDUCATION PROGRAM. 2017. *Triglyceride Molecular weight calculator* [Online]. Available: https://biodieseleducation.org/Production/MolecularweightCalculator.html February 26, 2019].

BORUGADDA, V. B. & GOUD, V. V. 2012. Biodiesel production from renewable feedstocks: Status and opportunities. *Renewable and Sustainable Energy Reviews,* 16**,** 4763-4784.
BOYCHEVA, S., ZGUREVA, D. & SHOUMKOVA, A. 2015. Recycling of lignite coal fly ash by its conversion into zeolites. *Coal Combustion and Gasification Products,* 7**,** 1-8.
BRASSELL, J. P. 2017. *Investigation of some scale-up conditions on the synthesis of faujasite zeolites from South African coal fly ash*. Cape Peninsula University of Technology.
BRECK, D. W. 1984. *Zeolite molecular sieves: structure, chemistry and use*, Krieger.
BRITO, A., BORGES, M. & OTERO, N. 2007. Zeolite Y as a heterogeneous catalyst in biodiesel fuel production from used vegetable oil. *Energy & Fuels,* 21**,** 3280-3283.
BUHL, J.-C., SCHUSTER, K. & ROBBEN, L. 2011. Nanocrystalline sodalite grown from superalkaline NaCl bearing gels at low temperature (333 K) and the influence of TEA on crystallization process. *Microporous and mesoporous materials,* 142**,** 666-671.
BUKHARI, S. S., BEHIN, J., KAZEMIAN, H. & ROHANI, S. 2014. A comparative study using direct hydrothermal and indirect fusion methods to produce zeolites from coal fly ash utilizing single-mode microwave energy. *Journal of materials science,* 49**,** 8261-8271.
CANAKCI, M. & VAN GERPEN, J. 1999. Biodiesel production viaacid catalysis. *Transactions of the ASAE,* 42**,** 1203.
CANESIN, E. A., DE OLIVEIRA, C. C., MATSUSHITA, M., DIAS, L. F., PEDRÃO, M. R. & DE SOUZA, N. E. 2014. Characterization of residual oils for biodiesel production. *Electronic Journal of Biotechnology,* 17**,** 39-45.
CHANTAWONG V., H., N.W. 2003. Synthesis of Zeolite from Thai Kaolin for Wastewater Treatment. *2nd Regional Conference on Energy Technology Towards a Clean Environment***,** 9-024.
CHANTAWONG, V. & HARVEY, N. Synthesis of zeolite from Thai Kaolin for wastewater treatment. Proceeding of the 2 nd Regional Conference on Energy Technology towards a Clean Environmental, 2003. 12-14.
CHERESOURCES.COM. 2011. *Green Chemistry with Zeolite Catalysts* [Online]. Available: http://www.cheresources.com/zeolitezz.shtml.
CHOUHAN, A. P. S. & SARMA, A. K. 2011. Modern heterogeneous catalysts for biodiesel production: A comprehensive review. *Renewable and Sustainable Energy Reviews,* 15**,** 4378-4399.
COOPERATION, A. P. E. 2009. Establishment of the guidelines for the development of biodiesel standards in the APEC region. *APEC: Singapore*.
CORMA, A., MENGUAL, J. & MIGUEL, P. J. 2012. Stabilization of ZSM-5 zeolite catalysts for steam catalytic cracking of naphtha for production of propene and ethene. *Applied Catalysis A: General,* 421-422**,** 121-134.
CUNDY, C. S. & COX, P. A. 2003. The Hydrothermal Synthesis of Zeolites: History and Development from the Earliest Days to the Present Time. *Chemical Reviews,* 103**,** 663-702.
DA CUNHA, M. E., KRAUSE, L. C., MORAES, M. S. A., FACCINI, C. S., JACQUES, R. A., ALMEIDA, S. R., RODRIGUES, M. R. A. & CARAMÃO, E. B. 2009. Beef tallow biodiesel produced in a pilot scale. *Fuel Processing Technology,* 90**,** 570–575.
DARNOKO, D. & CHERYAN, M. 2000. Kinetics of palm oil transesterification in a batch reactor. *Journal of the American Oil Chemists' Society,* 77**,** 1263–1267.
DEHKHODA, A. M. 2010. *Developing biochar-based catalyst for biodiesel production.* University of British Columbia.
DEMIRBAS, A. 2004. Pyrolysis of municipal plastic wastes for recovery of gasoline-range hydrocarbons. *Journal of Analytical and Applied Pyrolysis,* 72**,** 97-102.
DEMIRBAS, A. 2009. Progress and recent trends in biodiesel fuels. *Energy conversion and management,* 50**,** 14-34.
DENG, L., XU, Q. & WU, H. 2016. Synthesis of zeolite-like material by hydrothermal and fusion methods using municipal solid waste fly ash. *Procedia Environmental Sciences,* 31**,** 662-667.
DI SERIO, M., TESSER, R., PENGMEI, L. & SANTACESARIA, E. 2008. Heterogeneous Catalysts for Biodiesel Production. *Energy & Fuels,* 22**,** 207-217.

DIAS, J. M., ALVIM-FERRAZ, M. C. & ALMEIDA, M. F. 2009. Production of biodiesel from acid waste lard. *Bioresource technology,* 100**,** 6355–6361.
DO NASCIMENTO, L. A. S., ANGÉLICA, R. S., DA COSTA, C. E., ZAMIAN, J. R. & DA ROCHA FILHO, G. N. 2011. Comparative study between catalysts for esterification prepared from kaolins. *Applied Clay Science,* 51**,** 267-273.
DOS SANTOS, R. P., MARTINS, J., GADELHA, C., CAVADA, B., ALBERTINI, A. V., ARRUDA, F., VASCONCELOS, M., TEIXEIRA, E., ALVES, F. & LIMA FILHO, J. 2014. Coal fly ash ceramics: preparation, characterization, and use in the hydrolysis of sucrose. *The Scientific World Journal,* 2014.
DOUGLAS, K. 2012. *South African company finds economic value in flies and maggots* [Online]. How we made it in Africa. Available: https://www.howwemadeitinafrica.com/south-african-company-finds-economic-value-in-flies-and-maggots/.
DU PLESSIS, P. W. 2014. *Process design for the up-scale zeolite synthesis from South African coal fly ash*. Cape Peninsula University of Technology.
DWIVEDI, A. & JAIN, M. K. 2014. Fly ash â€"waste management and overview: A Review. *Recent Research in Science and Technology,* 6.
ECOSYSTEM 2010. Our product.
EL BANNA, S. & EL DEEN, O. 2004. Bio Diesel An Alternative Vehicles Fuel; Analytical View.
ENDALEW, A. K., KIROS, Y. & ZANZI, R. 2011. Inorganic heterogeneous catalysts for biodiesel production from vegetable oils. *Biomass and bioenergy,* 35**,** 3787-3809.
FAYYAZI, E., GHOBADIAN, B., VAN DE BOVENKAMP, H. H., NAJAFI, G., HOSSEINZADEHSAMANI, B., HEERES, H. J. & YUE, J. 2018. Optimization of biodiesel production over chicken eggshell-derived CaO catalyst in a continuous centrifugal contactor separator. *Industrial & engineering chemistry research,* 57**,** 12742-12755.
FERNANDES MACHADO, N. R. C., CALSAVARA, V., ASTRATH, N. G. C., NETO, A. M. & BAESSO, M. L. 2006. Hydrocarbons from ethanol using [Fe,Al]ZSM-5 zeolites obtained by direct synthesis. *Applied Catalysis A: General,* 311**,** 193-198.
FERNÁNDEZ-JIMÉNEZ, A. & PALOMO, A. 2005. Mid-infrared spectroscopic studies of alkali-activated fly ash structure. *Microporous and mesoporous materials,* 86**,** 207-214.
FERREIRA MADEIRA, F., BEN TAYEB, K., PINARD, L., VEZIN, H., MAURY, S. & CADRAN, N. 2012. Ethanol transformation into hydrocarbons on ZSM-5 zeolites: Influence of Si/Al ratio on catalytic performances and deactivation rate. Study of the radical species role. *Applied Catalysis A: General,* 443-444**,** 171-180.
FJERBAEK, L., CHRISTENSEN, K. V. & NORDDAHL, B. 2009. A review of the current state of biodiesel production using enzymatic transesterification. *Biotechnology and bioengineering,* 102**,** 1298-1315.
FREEDMAN, B., BUTTERFIELD, R. O. & PRYDE, E. H. 1986. Transesterification kinetics of soybean oil 1. *Journal of the American Oil Chemists' Society,* 63**,** 1375-1380.
FRISING, T. & LEFLAIVE, P. 2008. Extraframework cation distributions in X and Y faujasite zeolites: A review. *Microporous and Mesoporous Materials,* 114**,** 27-63.
GE, Q., HUANG, Y., QIU, F. & LI, S. 1998. Bifunctional catalysts for conversion of synthesis gas to dimethyl ether. *Applied Catalysis A: General,* 167**,** 23–30.
GOLBAD, S., KHOSHNOUD, P. & ABU-ZAHRA, N. 2017. Hydrothermal synthesis of hydroxy sodalite from fly ash for the removal of lead ions from water. *International Journal of Environmental Science and Technology,* 14**,** 135-142.
GONFA KENENI, Y., MARIO MARCHETTI, J. & FACULTY SCIENCES AND TECHNOLOGY, N. U. O. L. S., DRØBAKVEIEN 31, ÅS 1432, NORWAY 2017. Oil extraction from plant seeds for biodiesel production. *AIMS Energy,* 5**,** 316-340.
GOUGAZEH, M. & BUHL, J.-C. 2014. Synthesis and characterization of zeolite A by hydrothermal transformation of natural Jordanian kaolin. *Journal of the Association of Arab Universities for Basic and Applied Sciences,* 15**,** 35–42.

GUI, M. M., LEE, K. & BHATIA, S. 2008. Feasibility of edible oil vs. non-edible oil vs. waste edible oil as biodiesel feedstock. *Energy,* 33**,** 1646-1653.
GUO, F. & FANG, Z. 2011. Biodiesel production with solid catalysts. *Biodiesel, Feedstocks and Processing Technologies*.
HAAS, M. J., MCALOON, A. J., YEE, W. C. & FOGLIA, T. A. 2006. A process model to estimate biodiesel production costs. *Bioresource technology,* 97**,** 671-678.
HAJJARI, M., TABATABAEI, M., AGHBASHLO, M. & GHANAVATI, H. 2017. A review on the prospects of sustainable biodiesel production: A global scenario with an emphasis on waste-oil biodiesel utilization. *Renewable and Sustainable Energy Reviews,* 72**,** 445-464.
HALIM, R., GLADMAN, B., DANQUAH, M. K. & WEBLEY, P. A. 2011. Oil extraction from microalgae for biodiesel production. *Bioresource technology,* 102**,** 178-185.
HENMI, T. 1987. Synthesis of Hydroxy-Sodalite ("Zeolite") from Waste Coal Ash. *Soil Science and Plant Nutrition,* 33**,** 517-521.
HO, D. P., NGO, H. H. & GUO, W. 2014. A mini review on renewable sources for biofuel. *Bioresource technology,* 169**,** 742–749.
HOLLMAN, G., STEENBRUGGEN, G. & JANSSEN-JURKOVIČOVÁ, M. 1999. A two-step process for the synthesis of zeolites from coal fly ash. *Fuel,* 78**,** 1225-1230.
IEA. Key world energy statistics. 2006. IEA Paris.
INABA, M., MURATA, K., SAITO, M. & TAKAHARA, I. 2006. Ethanol conversion to aromatic hydrocarbons over several zeolite catalysts. *Reaction Kinetics and Catalysis Letters,* 88**,** 135–141.
INDEXMUNDI. 2019. *Commodities Prices* [Online]. Available: https://www.indexmundi.com/commodities/?commodity=soybean-oil.
JACOBSON, K., GOPINATH, R., MEHER, L. C. & DALAI, A. K. 2008. Solid acid catalyzed biodiesel production from waste cooking oil. *Applied Catalysis B: Environmental,* 85**,** 86-91.
JAHIRUL, M., KOH, W., BROWN, R., SENADEERA, W., O'HARA, I. & MOGHADDAM, L. 2014. Biodiesel Production from Non-Edible Beauty Leaf (Calophyllum inophyllum) Oil: Process Optimization Using Response Surface Methodology (RSM). *Energies,* 7**,** 5317-5331.
JAIMASITH, M. & PHIYANALINMAT, S. 2007. Biodiesel synthesis from transesterification by clay-based catalyst. *Chiang Mai J. Sci,* 34**,** 201-207.
JANOŠ, P., BUCHTOVÁ, H. & RÝZNAROVÁ, M. 2003. Sorption of dyes from aqueous solutions onto fly ash. *Water research,* 37**,** 4938-4944.
JAPIR, A. A.-W., SALIMON, J., DERAWI, D., BAHADI, M., AL-SHUJA'A, S. & YUSOP, M. R. 2017. Physicochemical characteristics of high free fatty acid crude palm oil. *OCL,* 24**,** D506.
JAYASINGHE, P. & HAWBOLDT, K. 2012. A review of bio-oils from waste biomass: Focus on fish processing waste. *Renewable and sustainable energy reviews,* 16**,** 798–821.
JENSEN, S. Ø., MARSZAL-POMIANOWSKA, A., LOLLINI, R., PASUT, W., KNOTZER, A., ENGELMANN, P., STAFFORD, A. & REYNDERS, G. 2017. IEA EBC annex 67 energy flexible buildings. *Energy and Buildings,* 155**,** 25-34.
JOHN, J. S. 2009. *Fly Larvae to Biofuel* [Online]. Greentech Media. Available: https://www.greentechmedia.com/articles/read/fly-larvae-to-biofuel-5923.
JUNAID, A. 2014. *Bio fuels, An alternative Fuel* [Online]. LinkedIn Corporation SlideShare: Science. Available: https://www.slideshare.net/appchem/biofuel-presentation-org 2019].
KARMAKAR, A., KARMAKAR, S. & MUKHERJEE, S. 2010. Properties of various plants and animals feedstocks for biodiesel production. *Bioresource Technology,* 101**,** 7201-7210.
KHATAMIAN, M. & IRANI, M. 2009. Preparation and characterization of nanosized ZSM-5 zeolite using kaolin and investigation of kaolin content, crystallization time and temperature changes on the size and crystallinity of products. *Journal of the Iranian Chemical Society,* 6**,** 187–194.

KIM, K. S., PARK, J. O. & NAM, S. C. 2013. Synthesis of Iron-loaded Zeolites for Removal of Ammonium and Phosphate from Aqueous Solutions. *Environmental Engineering Research,* 18**,** 267-276.

KRÜGER, J. 2003. South African fly ash: A cement extender. *A South Coal Fly Ash Association publication*.

KURNIASIH, E. & PARDI, P. Application of Response Surface Methodology for Biodiesel Synthesis Optimization Through Transesterification Reaction using h-zeolite/ki Heterogeneous Catalyst. IOP Conference Series: Materials Science and Engineering, 2019. IOP Publishing, 012033.

LAM, M. K., LEE, K. T. & MOHAMED, A. R. 2010. Homogeneous, heterogeneous and enzymatic catalysis for transesterification of high free fatty acid oil (waste cooking oil) to biodiesel: a review. *Biotechnology advances,* 28**,** 500–518.

LAM, M. K., TAN, K. T., LEE, K. T. & MOHAMED, A. R. 2009. Malaysian palm oil: Surviving the food versus fuel dispute for a sustainable future. *Renewable and Sustainable Energy Reviews,* 13**,** 1456-1464.

LEONG, S. Y., KUTTY, S. R. M., MALAKAHMAD, A. & TAN, C. K. 2016. Feasibility study of biodiesel production using lipids of Hermetia illucens larva fed with organic waste. *Waste Management,* 47**,** 84–90.

LEUNG, D. & GUO, Y. 2006. Transesterification of neat and used frying oil: optimization for biodiesel production. *Fuel processing technology,* 87**,** 883-890.

LEUNG, D. Y., WU, X. & LEUNG, M. K. H. 2010. A review on biodiesel production using catalyzed transesterification. *Applied energy,* 87**,** 1083–1095.

LI, Q., ZHENG, L., CAI, H., GARZA, E., YU, Z. & ZHOU, S. 2011. From organic waste to biodiesel: Black soldier fly, Hermetia illucens, makes it feasible. *Fuel,* 90**,** 1545-1548.

LI, Y. & YU, J. 2014. New stories of zeolite structures: their descriptions, determinations, predictions, and evaluations. *Chemical reviews,* 114**,** 7268-7316.

LUKIĆ, I., KESIĆ, Ž., MAKSIMOVIĆ, S., ZDUJIĆ, M., LIU, H., KRSTIĆ, J. & SKALA, D. 2013. Kinetics of sunflower and used vegetable oil methanolysis catalyzed by CaO· ZnO. *Fuel,* 113**,** 367-378.

LUO, J., ZHANG, H. & YANG, J. 2016. Hydrothermal Synthesis of Sodalite on Alkali-Activated Coal Fly Ash for Removal of Lead Ions. *Procedia Environmental Sciences,* 31**,** 605-614.

MA, F. & HANNA, M. A. 1999. Biodiesel production: a review. *Bioresource technology,* 70**,** 1-15.

MACHADO, N. R. C. F., CALSAVARA, V., ASTRATH, N. G. C., MATSUDA, C. K., JUNIOR, A. P. & BAESSO, M. L. 2005. Obtaining hydrocarbons from ethanol over iron-modified ZSM-5 zeolites. *Fuel,* 84**,** 2064-2070.

MAKGABA, C. P. & DARAMOLA, M. O. Transesterification of Waste Cooking Oil to Biodiesel over Calcined Hydroxy Sodalite (HS) Catalyst: A preliminary investigation. 2015 2015. Atlantis Press.

MALONDA SHABANI, J., BABAJIDE, O., OYEKOLA, O. & PETRIK, L. 2019. Synthesis of Hydroxy Sodalite from Coal Fly Ash for Biodiesel Production from Waste-Derived Maggot Oil. *Catalysts,* 9**,** 1052.

MANZANO-AGUGLIARO, F., SANCHEZ-MUROS, M. J., BARROSO, F. G., MARTÍNEZ-SÁNCHEZ, A., ROJO, S. & PÉREZ-BAÑÓN, C. 2012. Insects for biodiesel production. *Renewable and Sustainable Energy Reviews,* 16**,** 3744–3753.

MARCHETTI, J. M. 2012. A summary of the available technologies for biodiesel production based on a comparison of different feedstock's properties. *Process Safety and Environmental Protection,* 90**,** 157-163.

MARTINOT, E., DIENST, C., WEILIANG, L. & QIMIN, C. 2007. Renewable energy futures: Targets, scenarios, and pathways. *Annu. Rev. Environ. Resour.,* 32**,** 205-239.

MASHKOUR, A. P. D. M. A. & MOHAMMED, L. A. A. 2017. Impact of mixing speed & reaction time on the biodiesel production from sunflower oil. *Association of Arab Universities Journal of Engineering Sciences,* 24**,** 101-134.

MEHER, L. C., SAGAR, D. V. & NAIK, S. 2006. Technical aspects of biodiesel production by transesterification—a review. *Renewable and sustainable energy reviews,* 10**,** 248-268.
MEWA-NGONGANG, M., DU PLESSIS, H. W., HUTCHINSON, U. F., MEKUTO, L. & NTWAMPE, S. K. 2017. Kinetic modelling and optimisation of antimicrobial compound production by Candida pyralidae KU736785 for control of Candida guilliermondii. *Food Science and Technology International,* 23**,** 358-370.
MEZNI, M., HAMZAOUI, A., HAMDI, N. & SRASRA, E. 2011. Synthesis of zeolites from the low-grade Tunisian natural illite by two different methods. *Applied Clay Science,* 52**,** 209-218.
MINERALS, D. O. & ENERGY 2009. National energy efficiency strategy of the Republic of South Africa. Department of Minerals and Energy Pretoria.
MITTELBACH, M. & REMSCHMIDT, C. 2004. Biodiesel the Comprehensive handbook Martin Mittelbach. *Graz, Austria. Paperback,* 512.
MOLINA, A. & POOLE, C. 2004. A comparative study using two methods to produce zeolites from fly ash. *Minerals Engineering,* 17**,** 167-173.
MURAYAMA, N., YAMAMOTO, H. & SHIBATA, J. 2002. Mechanism of zeolite synthesis from coal fly ash by alkali hydrothermal reaction. *International Journal of Mineral Processing,* 64**,** 1–17.
MUSA, I. A. 2016. The effects of alcohol to oil molar ratios and the type of alcohol on biodiesel production using transesterification process. *Egyptian Journal of Petroleum,* 25**,** 21–31.
MUSYOKA, N. M. 2009. *Hydrothermal synthesis and optimisation of zeolite Na-P1 from South African coal fly ash.*
MUSYOKA, N. M. 2012. Zeolite A, X and Cancrinite from South African coal fly ash: mechanism of crystallization, routes to rapid synthesis and new morphology.
MUSYOKA, N. M., MISSENGUE, R., KUSISAKANA, M. & PETRIK, L. F. 2014. Conversion of South African clays into high quality zeolites. *Applied Clay Science,* 97-98**,** 182-186.
MUSYOKA, N. M., PETRIK, L. F., BALFOUR, G., GITARI, W. M. & HUMS, E. 2011. Synthesis of hydroxy sodalite from coal fly ash using waste industrial brine solution. *Journal of Environmental Science and Health, Part A,* 46**,** 1699–1707.
NABAVI, M. S., MOHAMMADI, T. & KAZEMIMOGHADAM, M. 2014. Hydrothermal synthesis of hydroxy sodalite zeolite membrane: Separation of H2/CH4. *Ceramics International,* 40**,** 5889-5896.
NANGANOA, L. T., MBADCAM, K. J. & KANG, S. 2016. Synthesis of Hydroxy-sodalite from Fine Fractions of Sandy Clay Loam Soil (Natural Aluminosilicate).
NASIR, N., DAUD, W., KAMARUDIN, S. & YAAKOB, Z. 2014. Methyl esters selectivity of transesterification reaction with homogenous alkaline catalyst to produce biodiesel in batch, plug flow, and continuous stirred tank reactors. *International Journal of Chemical Engineering,* 2014.
NAYLOR, R. L. & HIGGINS, M. M. 2017. The rise in global biodiesel production : Implications for food security. *Global Food Security*.
NELSON, L. A., FOGLIA, T. A. & MARMER, W. N. 1996. Lipase-catalyzed production of biodiesel. *Journal of the American Oil Chemists' Society,* 73**,** 1191-1195.
NOUREDDINI, H. & ZHU, D. 1997a. Kinetics of transesterification of soybean oil. *Journal of the American Oil Chemists' Society,* 74**,** 1457-1463.
NOUREDDINI, H. & ZHU, D. 1997b. Kinetics of transesterification of soybean oil. *Journal of the American Oil Chemists' Society,* 74**,** 1457–1463.
NYALE, S. M., EZE, C. P., AKINYEYE, R. O., GITARI, W. M., AKINYEMI, S. A., FATOBA, O. O. & PETRIK, L. F. 2014. The leaching behaviour and geochemical fractionation of trace elements in hydraulically disposed weathered coal fly ash. *Journal of Environmental Science and Health, Part A,* 49**,** 233-242.
OJHA, K., PRADHAN, N. C. & SAMANTA, A. N. 2004. Zeolite from fly ash: synthesis and characterization. *Bulletin of Materials Science,* 27**,** 555-564.

OLADIPO, B. & BETIKU, E. 2020. Optimization and kinetic studies on conversion of rubber seed (Hevea brasiliensis) oil to methyl esters over a green biowaste catalyst. *Journal of Environmental Management,* 268**,** 110705.
OONINCX, D., VAN HUIS, A. & VAN LOON, J. J. A. 2015. Nutrient utilisation by black soldier flies fed with chicken, pig, or cow manure. *Journal of Insects as Food and Feed,* 1**,** 131–139.
PANDIANGAN, K. D., ARIEF, S., JAMARUN, N. & SIMANJUNTAK, W. 2017. Synthesis of Zeolite-X from Rice Husk Silica and Aluminum Metal as a Catalyst for Transesterification of Palm Oil.
PETERNELE, W. S., MONGE FUENTES, V., FASCINELI, M. L., RODRIGUES DA SILVA, J., SILVA, R. C., LUCCI, C. M. & BENTES DE AZEVEDO, R. 2014. Experimental Investigation of the Coprecipitation Method: An Approach to Obtain Magnetite and Maghemite Nanoparticles with Improved Properties. *Journal of Nanomaterials,* 2014**,** 1-10.
PUPPE, L. & WEITKAMP, J. 1999. *Catalysis and zeolites: fundamentals and applications*, Springer.
PURWANTO, P., BUCHORI, L. & ISTADI, I. 2020. Reaction rate law model and reaction mechanism covering effect of plasma role on the transesterification of triglyceride and methanol to biodiesel over a continuous flow hybrid catalytic-plasma reactor. *Heliyon,* 6**,** e05164.
QUERALT, I., QUEROL, X., LÓPEZ-SOLER, A. & PLANA, F. 1997. Use of coal fly ash for ceramics: a case study for a large Spanish power station. *Fuel,* 76**,** 787-791.
QUEROL, X., MORENO, N., UMAÑA, J. T., ALASTUEY, A., HERNÁNDEZ, E., LOPEZ-SOLER, A. & PLANA, F. 2002. Synthesis of zeolites from coal fly ash: an overview. *International Journal of coal geology,* 50**,** 413–423.
RAMADHAS, A. S., JAYARAJ, S. & MURALEEDHARAN, C. 2005. Biodiesel production from high FFA rubber seed oil. *Fuel,* 84**,** 335-340.
RAMEZANI, K., ROWSHANZAMIR, S. & EIKANI, M. H. 2010. Castor oil transesterification reaction: a kinetic study and optimization of parameters. *Energy,* 35**,** 4142–4148.
RAMÍREZ-VERDUZCO, L. F., RODRÍGUEZ-RODRÍGUEZ, J. E. & DEL RAYO JARAMILLO-JACOB, A. 2012. Predicting cetane number, kinematic viscosity, density and higher heating value of biodiesel from its fatty acid methyl ester composition. *Fuel,* 91**,** 102-111.
RAMLI, A., FAROOQ, M., NAEEM, A., KHAN, S., HUMMAYUN, M., IQBAL, A., AHMED, S. & SHAH, L. A. 2017. Bifunctional Heterogeneous Catalysts for Biodiesel Production using Low Cost Feedstocks: A Future Perspective. *In:* JACOB-LOPES, E. & ZEPKA, L. Q. (eds.) *Frontiers in Bioenergy and Biofuels.* InTech.
RAMOS, M. J., CASAS, A., RODRÍGUEZ, L., ROMERO, R. & PÉREZ, Á. 2008. Transesterification of sunflower oil over zeolites using different metal loading: A case of leaching and agglomeration studies. *Applied Catalysis A: General,* 346**,** 79-85.
RATURI, A. K. 2016. Renewables 2016 Global status report.
RAYALU, S., MESHRAM, S. & HASAN, M. 2000. Highly crystalline faujasitic zeolites from flyash. *Journal of Hazardous Materials,* 77**,** 123-131.
REFAAT, A. 2011. Biodiesel production using solid metal oxide catalysts. *International Journal of Environmental Science & Technology,* 8**,** 203-221.
REYERO, I., ARZAMENDI, G., ZABALA, S. & GANDÍA, L. M. 2015. Kinetics of the NaOH-catalyzed transesterification of sunflower oil with ethanol to produce biodiesel. *Fuel Processing Technology,* 129**,** 147-155.
REYNOLDS-CLAUSEN, K. & SINGH, N. South Africa's power producer's revised coal ash strategy and implementation progress. Proceedings of the World of Coal Ash (WOCA) Conference, 2017. 9-11.
RIOS, C. A., WILLIAMS, C. D. & FULLEN, M. A. 2009. Nucleation and growth history of zeolite LTA synthesized from kaolinite by two different methods. *Applied Clay Science,* 42**,** 446-454.
ROWNAGHI, A. A., REZAEI, F. & HEDLUND, J. 2011. Yield of gasoline-range hydrocarbons as a function of uniform ZSM-5 crystal size. *Catalysis Communications,* 14**,** 37-41.
SAIFUDDIN, N., SAMIUDDIN, A. & KUMARAN, P. 2015. A review on processing technology for biodiesel production. *Trends in applied sciences research,* 10**,** 1.

SALVI, B. L. & PANWAR, N. L. 2012. Biodiesel resources and production technologies–A review. *Renewable and Sustainable Energy Reviews,* 16**,** 3680–3689.

SHARMA, Y. C., SINGH, B. & KORSTAD, J. 2011. Advancements in solid acid catalysts for ecofriendly and economically viable synthesis of biodiesel. *Biofuels, Bioproducts and Biorefining,* 5**,** 69-92.

SHEN, B., WU, C., WANG, R., GUO, B. & LIANG, C. 2006. Pyrolysis of scrap tyres with zeolite USY. *Journal of hazardous materials,* 137**,** 1065-1073.

SHEQAFRICA.COM 2018. Coal Fly Ash Holds African Opportunities.

SHIRANI LAPARI, S., RAMLI, Z. & TRIWAHYONO, S. 2015. Effect of Different Templates on the Synthesis of Mesoporous Sodalite. *Journal of Chemistry,* 2015**,** 1-6.

SHU, Q., YANG, B., YUAN, H., QING, S. & ZHU, G. 2007. Synthesis of biodiesel from soybean oil and methanol catalyzed by zeolite beta modified with La3+. *Catalysis Communications,* 8**,** 2159-2165.

SHUMBA, M., CHIGONDO, M., GUYO, U., CHIGONDO, F., MOYO, M., NHARINGO, T. & SEBATA, E. 2011. Synthesis of zeolites and their applications in heavy metals removal: a review.

SILITONGA, A., ATABANI, A., MAHLIA, T., MASJUKI, H., BADRUDDIN, I. A. & MEKHILEF, S. 2011. A review on prospect of Jatropha curcas for biodiesel in Indonesia. *Renewable and Sustainable Energy Reviews,* 15**,** 3733-3756.

SILVA, V. J., RODRIGUES, J. J., SOARES, R. R., NAPOLITANO, M. N. & RODRIGUES, M. G. F. 2013. COBALT SUPPORTED ON ZSM-5 ZEOLITE USING KAOLIN AS SILICON AND ALUMINUN SOURCES FOR FISCHER-TROPSCH SYNTHESIS. *Brazilian Journal of Petroleum and Gas,* 7**,** 83-94.

SIVASAMY, A., CHEAH, K. Y., FORNASIERO, P., KEMAUSUOR, F., ZINOVIEV, S. & MIERTUS, S. 2009. Catalytic Applications in the Production of Biodiesel from Vegetable Oils. *ChemSusChem,* 2**,** 278-300.

SOTOMAYOR, F. J., CYCHOSZ, K. A. & THOMMES, M. 2018. Characterization of micro/mesoporous materials by physisorption: concepts and case studies. *Acc. Mater. Surf. Res,* 3**,** 36-37.

STEENBRUGGEN, G. & HOLLMAN, G. 1998. The synthesis of zeolites from fly ash and the properties of the zeolite products. *Journal of geochemical exploration,* 62**,** 305-309.

STEPTO, R. & SZOSTAK, R. 1998. Molecular Sieves: principles of synthesis and identification. *Blackie Academic & Professional, London*.

SUN, K., LU, J., MA, L., HAN, Y., FU, Z. & DING, J. 2015. A comparative study on the catalytic performance of different types of zeolites for biodiesel production. *Fuel,* 158**,** 848-854.

SUN, Y.-Z., FU, K.-M., ZHU, H. & ZHU, T.-L. 2009. Silica-alumina molar ratio and some factors effect on the synthesis of zeolites from fly ash. *Journal of Coal Science and Engineering (China),* 15**,** 430–433.

SURENDRA, K. C., OLIVIER, R., TOMBERLIN, J. K., JHA, R. & KHANAL, S. K. 2016. Bioconversion of organic wastes into biodiesel and animal feed via insect farming. *Renewable Energy,* 98**,** 197–202.

SYAMSIRO, M., SAPTOADI, H., NORSUJIANTO, T., NOVIASRI, P., CHENG, S., ALIMUDDIN, Z. & YOSHIKAWA, K. 2014. Fuel oil production from municipal plastic wastes in sequential pyrolysis and catalytic reforming reactors. *Energy Procedia,* 47**,** 180-188.

THANGARAJ, B., SOLOMON, P. R., MUNIYANDI, B., RANGANATHAN, S. & LIN, L. 2019. Catalysis in biodiesel production—a review. *Clean Energy,* 3**,** 2-23.

THOMMES, M., KANEKO, K., NEIMARK, A. V., OLIVIER, J. P., RODRIGUEZ-REINOSO, F., ROUQUEROL, J. & SING, K. S. 2015. Physisorption of gases, with special reference to the evaluation of surface area and pore size distribution (IUPAC Technical Report). *Pure and Applied Chemistry,* 87**,** 1051-1069.

TONIOLO, N. 2018. Novel geopolymers incorporating silicate waste.

TREACY, M. M. & HIGGINS, J. B. 2007. *Collection of simulated XRD powder patterns for zeolites fifth (5th) revised edition*, Elsevier.

TSHIZANGA, N., ARANSIOLA, E. F. & OYEKOLA, O. 2017. Optimisation of biodiesel production from waste vegetable oil and eggshell ash. *South african journal of chemical engineering,* 23**,** 145-156.

USHAKOVA, N. A., BRODSKII, E. S., KOVALENKO, A. A., BASTRAKOV, A. I., KOZLOVA, A. A. & PAVLOV, D. S. Characteristics of lipid fractions of larvae of the black soldier fly Hermetia illucens. 2016 2016. Springer, 209–212.

USMAN, B. & GARBA, A. A. Application of Central Composite Design (CCD) in the Optimisation of Parameters for the Production of Biodiesel from Cattle Fat Using CaO as Solid Base Catalyst. A Conference paper presented at the Yusuf Maitama Sule University, Kano, Faculty of Science 3rd Annual International Conference at Kano, Nigeria, 2017.

USMANI, Z. & KUMAR, V. 2017. Characterization, partitioning, and potential ecological risk quantification of trace elements in coal fly ash. *Environmental Science and Pollution Research,* 24**,** 15547-15566.

UZOH, C. F., ONUKWULI, O. D. & NWABANNE, J. T. 2014. Characterization, kinetics and statistical screening analysis of gmelina seed oil extraction process. *Materials for Renewable and Sustainable Energy,* 3**,** 1-12.

VERMA, P. & SHARMA, M. 2016. Review of process parameters for biodiesel production from different feedstocks. *Renewable and Sustainable Energy Reviews,* 62**,** 1063-1071.

VIRIYA-EMPIKUL, N., KRASAE, P., PUTTASAWAT, B., YOOSUK, B., CHOLLACOOP, N. & FAUNGNAWAKIJ, K. 2010. Waste shells of mollusk and egg as biodiesel production catalysts. *Bioresource technology,* 101**,** 3765-3767.

VISWANADHAM, N., SAXENA, S. K., KUMAR, J., SREENIVASULU, P. & NANDAN, D. 2012. Catalytic performance of nano crystalline H-ZSM-5 in ethanol to gasoline (ETG) reaction. *Fuel,* 95**,** 298-304.

VOLLI, V. 2015. *Preparation and Characterization of Flyash Based Catalyst for Transesterification of Mustard Oil.* Indian Institute of Technology Guwahati.

VOLLI, V. & PURKAIT, M. K. 2015. Selective preparation of zeolite X and A from flyash and its use as catalyst for biodiesel production. *Journal of Hazardous Materials,* 297**,** 101-111.

VUJICIC, D., COMIC, D., ZARUBICA, A., MICIC, R. & BOSKOVIC, G. 2010. Kinetics of biodiesel synthesis from sunflower oil over CaO heterogeneous catalyst. *Fuel,* 89**,** 2054-2061.

WANG, C., QIAN, L., WANG, W., WANG, T., DENG, Z., YANG, F., XIONG, J. & FENG, W. 2017. Exploring the potential of lipids from black soldier fly: New paradigm for biodiesel production (I). *Renewable Energy,* 111**,** 749-756.

WANG, P., SHEN, B., SHEN, D., PENG, T. & GAO, J. 2007. Synthesis of ZSM-5 zeolite from expanded perlite/kaolin and its catalytic performance for FCC naphtha aromatization. *Catalysis Communications,* 8**,** 1452-1456.

WANG, Y.-S. & SHELOMI, M. 2017. Review of black soldier fly (Hermetia illucens) as animal feed and human food. *Foods,* 6**,** 91.

WANG, Y., OU, S., LIU, P., XUE, F. & TANG, S. 2006. Comparison of two different processes to synthesize biodiesel by waste cooking oil. *Journal of Molecular Catalysis A: Chemical,* 252**,** 107-112.

WEI, Z., XU, C. & LI, B. 2009. Application of waste eggshell as low-cost solid catalyst for biodiesel production. *Bioresource technology,* 100**,** 2883-2885.

WEITKAMP, J. 2000. Zeolites and catalysis. *Solid State Ionics,* 131**,** 175–188.

YANG, L., TAKASE, M., ZHANG, M., ZHAO, T. & WU, X. 2014. Potential non-edible oil feedstock for biodiesel production in Africa: a survey. *Renewable and Sustainable Energy Reviews,* 38**,** 461–477.

YUE, D., YOU, F. & SNYDER, S. W. 2014. Biomass-to-bioenergy and biofuel supply chain optimization: overview, key issues and challenges. *Computers & Chemical Engineering,* 66**,** 36–56.

YUNUS, R., FAKHRU'I-RAZI, A., OOI, T., BIAK, D. & IYUKE, S. 2004. Kinetics of transesterification of palm-based methyl esters with trimethylolpropane. *Journal of the American Oil Chemists' Society,* 81**,** 497-503.

ZHANG, J., CHEN, S., YANG, R. & YAN, Y. 2010. Biodiesel production from vegetable oil using heterogenous acid and alkali catalyst. *Fuel,* 89**,** 2939–2944.

ZHANG, R. 2010. The Elemental Composition of Atmospheric Particles at Beijing during Asian Dust Events in Spring 2004. *Aerosol and Air Quality Research*.

ZHANG, X., TANG, D., ZHANG, M. & YANG, R. 2013. Synthesis of NaX zeolite: Influence of crystallization time, temperature and batch molar ratio SiO2/Al2O3 on the particulate properties of zeolite crystals. *Powder Technology,* 235**,** 322-328.

ZHAO, X. Y., SHI, X., CHEN, L. D., ZHANG, W. Q., BAI, S. Q., PEI, Y. Z., LI, X. Y. & GOTO, T. 2006. Synthesis of Yb y Co 4 Sb 12/ Yb 2 O 3 composites and their thermoelectric properties. *Applied physics letters,* 89**,** 092121.

ZHENG, S., KATES, M., DUBÉ, M. & MCLEAN, D. 2006. Acid-catalyzed production of biodiesel from waste frying oil. *Biomass and bioenergy,* 30**,** 267-272.

ZHOU, A. & THOMSON, E. 2009. The development of biofuels in Asia. *Applied Energy,* 86**,** S11-S20.

ZIELKE-OLIVIER, J. & VERMEULEN, D. 2016. Fine Ash Leaching in Tailings Dams–An Impact on the Underlying Aquifers?

ZIOLKOWSKA, J. R. 2014. Prospective technologies, feedstocks and market innovations for ethanol and biodiesel production in the US. *Biotechnology Reports,* 4**,** 94–98.